(6)

THE BAROCLINIC INSTABILITY OF SIMPLE AND HIGHLY STRUCTURED ONE-DIMENSIONAL BASIC STATES

by

JAMES WILLIAM ANTHONY FULLMER

B.S., Drexel University
(1972)

SUBMITTED IN PARTIAL FULFILLMENT
OF THE REQUIREMENTS OF THE
DEGREE OF

DOCTOR OF PHILOSOPHY

at the

MASSACHUSETTS INSTITUTE OF TECHNOLOGY

MAY 1979

Signature of Author .....
Department of Meteorology, May 1, 1979

Certified by .....
Thesis Supervisor

Accepted by .....
Chairman, Departmental Committee
on Graduate Students

THIS THESIS

IS DEDICATED LOVINGLY

TO MY PARENTS

Mrs. Antonine H. Fullmer

Mr. James M. Fullmer

οὐ γὰρ ἄν ποτὲ
ἐξεῦρον ὀρθῶς τὰ μετέωρα πράγματα,
εἰ μὴ κρεμάσας τὸ νόημα καὶ τὴν φροντίδα
λεπτὴν καταμίξας εἰς τὸν ὅμοιον ἀέρα.

ARISTOPHANES *"The Clouds"* 423 B.C.

We shall not cease from exploration
And the end of all our exploring
Will be to arrive where we started
And know the place for the first time.

T.S. ELIOT *"Four Quartets"* 1943 A.D.

by
JAMES WILLIAM ANTHONY FULLMER

Submitted to the Department of Meteorology on 1 May 1979
in Partial Fulfillment of the Requirements for
the Degree of Doctor of Philosophy

ABSTRACT

The baroclinic instability of simple and highly structured one-dimensional basic states is studied using a frictionless, adiabatic, quasi-geostrophic model on a β-plane. Square-root-pressure coordinates are used at 48 levels in the vertical and calculations are made for the upper boundary conditions $\psi' = 0$ and $\omega' = 0$. Many properties of the unstable waves are considered: instability source, wavelength, growthrate, phase velocity, steering levels, and the vertical structure of their amplitude, phase, meridional entropy transport, and potential to kinetic energy conversion. First, simple basic states are assumed. Their shear and static stability each have a single value from 1000 to 250 mb, and another, independent value from 250 to 0 mb. These simple basic states are determined by 3 parameters: a shear ratio, a static stability ratio, and a generalized β parameter. A wide expanse of parameter space is considered. The highly structured basic states have zonal velocities and static stabilities obtained from one month averaged data for latitudes 25°N to 65°N and for months (January, April, July, and October), which represent seasonal extremes and transitions.

The longwave modes discovered by Green (1960) are shown to have several interesting properties. To exist, they require a non-zero value of $\bar{q}_y$ and are destabilized by the presence of a stratosphere or rigid lid. Doubling times are moderately short (about 1 week) and their meridional circulation in the lower stratosphere agrees with observations. Pressure amplitudes, kinetic energy destruction, and meridional entropy transport are particularly strong in the lower stratosphere (relative to other levels). Their kinetic energy is generated in the troposphere. Their entropy transports are countergradient in the lower stratosphere when a reversed shear exists in that region.

Quasi-geostrophic potential vorticity meridional gradient profiles ($\bar{q}_y$) for the one month averaged data possess a considerable number of zeros. These zeros and their associated negative $\bar{q}_y$ regions have a substantial effect on the unstable mode spectrum. Some modes' growthrates are drastically reduced when a particular negative $\bar{q}_y$ region is removed. New modes (distinct from those discovered by Eady, Charney, and Green) exist only when certain negative $\bar{q}_y$ regions are present. Some of the new modes are potentially important for the general circulation of specific regions of the atmosphere. In particular, longwave modes, in addition to those discovered by Green, could be important for the stratospheric circulation, and some are examples of in situ stratospheric baroclinic instability.

The unstable mode spectrum is also shown to be sensitive to small changes in the unperturbed state. It is shown that only those changes which drastically alter the negative regions and associated zeros of the $\bar{q}_y$ profile result in a substantial change in the unstable mode spectrum.

TABLE OF CONTENTS

CHAPTER I

INTRODUCTION

1.1 Background and Problems to be Addressed

One of the oldest and most interesting problems of dynamic meteorology is the stability of a horizontally uniform steady flow. The flow is said to be baroclinically unstable when there exist perturbations which grow exponentially with time, and which derive their energy from the available potential energy of the mean zonal flow. Investigation of the baroclinic instability problem began with the works of Charney (1947) and Eady (1949). Eady's model assumed a linear velocity profile, no variation of the coriolis parameter ($\beta = 0$), and rigid lids at the top and bottom. Unstable modes were found above a certain wavelength. Charney's model atmosphere had a rigid bottom but an unbounded top. A linear velocity profile was assumed (with the velocity constant above a certain height) and variation of the coriolis parameter was permitted. Charney found instability only for waves shorter than a certain wavelength which depended on the value of β (or on the value of the wind shear).

Burger (1962) established for a continuous model with constant $\beta \neq 0$ that all wavelengths have an exponentially unstable mode associated with them except for certain isolated wavelengths. Modes on the longwave side of these isolated wavelengths always grew more slowly than those on the shortwave side.

Green (1960) in a numerical model had also found that all resolved wavelengths were unstable (with the exception of isolated wavelengths) when $\beta \neq 0$. Green also extended Eady's and Charney's results to include a semi-

infinite "stratosphere" of increased constant static stability. The shear, however, was kept uniform throughout his atmosphere. The effect of the "stratosphere" was to make longer waves more unstable. His growth rate spectrum is similar to that for SR = 1 in Figure 3.4, given below. The shorter modes to the right of the cusp point in Figure 3.4 will be referred to as Charney or Eady modes. Those on the other, longwave side will be called Green modes.

Green showed that the fastest growing Eady mode did not have much vertical structure. However, Geisler and Garcia's (1977) numerical calculations found the Green modes to have streamfunction amplitudes in the stratosphere an order of magnitude larger than those in the troposphere. Geisler and Garcia assumed a reference state temperature characteristic of a mid- latitude winter, and both a linear and a mid-latitude winter mean zonal velocity profile. Both Green and Geisler and Garcia found growth rates of the Green modes to be much less than those of the Eady modes. However, there is no certainty that modes of largest growth rate must dominate. In fact, Gall (1976) and Staley and Gall (1977) have shown that the longer unstable waves can have a longer time to grow than the shorter waves because they extend higher into the atmosphere to regions where their growth is not halted as quickly by interactions with the mean flow (see also the discussion in Section IV-13). The Green modes, therefore, could be of great importance to the upper atmospheric circulation. Many of their properties remain uninvestigated; in particular, their kinetic energy release and entropy transport. Also uninvestigated is the dependence of the vertical structure of these waves on β, the shear of the mean zonal flow, and the static stability. The study of these properties of the Green modes is one major concern in this thesis.

One of the properties of the baroclinic modes which is essential to the atmospheric general circulation is their transport of heat. The transport is generally poleward and upwards, down the horizontal gradient of the mean temperature (Oort and Rasmusson, 1971), and accounts for a substantial part of the total heat flux at mid and high latitudes (Oort, 1971; Palmen and Newton, 1969, pp. 62-63). The eddy heat fluxes prevent the occurrence of very large meridional temperature gradients and associated intense westerlies. The theoretical study of Stone (1972) shows that the baroclinic eddies are essential to the determination of the atmospheric temperature structure. The studies of Phillips (1954) and Kuo (1956) show that the eddies help drive the mean meridional circulation. Models of the atmosphere, consequently, must include the effects of these baroclinic eddies.

The lower stratosphere (from the tropopause to 30 mb) presents a curious exception to the general description of atmospheric heat flux given above. Murgatroyd (1969) points out that the latitudinal heating gradient opposes the latitudinal temperature gradient in winter and summer and this requires a net countergradient meridional heat flux. The contribution of the mean meridional circulation to the horizontal flux has been calculated from observations of Oort and Rasmusson (1971) at 100 mb. At this level, the mean flux tends to be weaker (by a factor of 4 or more) than either the transient or stationary eddy flux and is generally equatorward. However, the observation of Oort and Rasmusson (1971) and Newell et al. (1974) show the eddy heat fluxes to be poleward up to 10 mb and countergradient between the tropopause and 30 mb. The transient eddy fluxes are about 1/2 to 2/3 as strong as those of the stationary eddies. Newell (1964a) has described

the lower stratosphere as a refrigerator which maintains the temperature minimum at the equator through countergradient eddy heat fluxes.

The origin of the observed lower stratosphere net countergradient heat flux has not been determined. The lone observations of Oort and Rasmusson at 100 mb are not strong enough to discount the mean meridional circulation from playing an important role in determining the net heat flux. The non-interaction theory begun by Charney and Drazin (1961) and extended by Holton (1974), Boyd (1976) and Andrews and McIntyre (1976) requires that, in the absence of diabatic effects and dissipation, the heat (and momentum) fluxes of stationary eddies (even if these eddies have harmonic time variations) are exactly balanced by transports of an induced mean meridional circulation. Thus, only transient eddy motion or a circulation in which diabatic or dissipative effects are important remain as candidates for producing the net countergradient heat flux in the lower stratosphere. Diabatic heating rates are small in the lower stratosphere ($< .5°K/day$; Newell et al. (1969), Murgatroyd (1969), Houghton (1978)) but still may be important to the heat budget (Vincent, 1968). Viscous dissipation is likely to be small compared to radiative damping (Holton, 1975). Although a circulation with diabaticity and possibly dissipation is a possible mechanism for generating the net countergradient heat flux, this mechanism is outside the scope of the current study.

The transient eddy component of the net countergradient heat flux is unlikely to come from in situ stratospheric baroclinic instability (Holton (1975), Simmons (1972)). Most of the transient eddy activity in the lower stratosphere, Holton claims, is probably due to the remnants of baroclinically unstable modes which originate in the troposphere. Green (1960) and

Peng (1965) have shown by numerical studies that the heat fluxes of the dominant Eady mode are very weak in the stratosphere. Green's (1960) fluxes for the dominant Eady mode were down gradient as he did not consider the reversed stratospheric temperature gradient. The strength of the Green mode amplitude in the stratosphere and the results of Gall (1976) mentioned above, indicate that these modes may possess strong stratospheric heat fluxes. The possibility that these fluxes may be significant and countergradient will be investigated, and implications for the parameterization of stratospheric eddy heat fluxes will be discussed.

Necessary conditions for baroclinic instability were derived by Charney and Stern (1962). They found that, in the absence of boundary temperature gradients, the quasi-geostrophic potential vorticity gradient ($\bar{q}_y$) profile must possess a zero for baroclinic instability to occur (for a more detailed discussion of this result, see section III-2). The calculations of Leovy in Charney and Stern (1962) show zeros in $\bar{q}_y$ above 100 mb for data of 14 October, 1957. Leovy and Webster (1976) also suggest that $\bar{q}_y$ may also have zeros on the tropical side of the stratospheric jet. Furthermore, Charney and Stern (1962) showed that such zeros are necessary conditions for an internal instability; they, as well as Green (1972), McIntyre (1972), Simmons (1972, 1974) and Dickinson (1973) have shown that a zero in $\bar{q}_y$ is a sufficient condition for instability in a number of special cases. Therefore, detailed profiles of $\bar{u}$ and $\bar{T}$, closer to those found in the atmosphere than the simple linear profiles studied by previous authors, may possess zeros in $\bar{q}_y$ which have associated unstable modes. Detailed profiles of $\bar{u}$ and $\bar{T}$ are also of interest because small variations in their detail have been shown to alter significantly the growth rate spectrum of the Eady modes (Gall and Blakeslee, 1977; Staley and Gall, 1977). In this thesis, the

effect of the structure of the $\bar{u}$ and $\bar{T}$ profiles on the baroclinic instability problem will be considered along with the sensitivity of the results to small variations in these profiles.

1.2 Outline of the thesis

The problems raised in the discussion above will be addressed through a comprehensive study of the baroclinic instability of both simple and highly structured one-dimensional basic states.* Many properties of the unstable waves are considered: instability source, wavelength, growth rate, phase velocity, steering levels, and the vertical structure of their pressure amplitude, phase, meridional entropy transport and kinetic energy generation. The model used is the quasi-geostrophic β-plane model of Green (1960) written in square-root-pressure coordinates. This choice of vertical coordinate gives an equal number of levels in the upper layer (stratosphere) and lower layer (troposphere). The upper layer is thereby given sufficient resolution without having an unnecessary number of levels in regions of very little mass. In Chapter II the mathematics of the model are developed and the numerical accuracy of the integration scheme is checked.

This study first extends Green's results by a "two-layer multi-level model" (Chapter III). Within each layer, the shear, $\bar{u}_p$, and static stability, $\sigma_\rho \equiv -\frac{1}{\rho}\frac{d \ln \theta}{dp}$, are constant but can have independent values. A 3-parameter family results. In addition to Green's generalized β-parameter, $\gamma_T \equiv \frac{\beta\sigma\, p_{oo}^2}{f^2 u_0}$, there is a shear ratio $SR \equiv \frac{u_p \text{ (upper layer)}}{u_p \text{ (lower layer)}}$ and static stability ratio $\sigma_\rho \equiv \frac{\sigma \text{ (upper layer)}}{\sigma \text{ (lower layer)}}$. Green's assumption of the same shear in both layers has been relaxed. A wide expanse of the three-dimensional

---

* Klein (1974) addressed the same baroclinic stability problem, but confined himself to profiles of zonal wind and temperature which are characteristic of a mid-latitude winter. In addition, he was restricted by his method of analysis to only the most unstable mode at each wavelength.

parameter space is explored. The dependence of the Eady and Green mode's properties on the parameter values is studied in detail. In particular, it is shown that the Green modes do have strong countergradient heat fluxes in the lower stratosphere although nearly all of their kinetic energy is drawn from the troposphere.

Chapter IV presents a further extension of Green's model to more realistic $\overline{u}$ and $\overline{T}$ profiles for the basic state. The profiles are obtained from monthly averaged data at different latitudes and are one-dimensional. One cannot rigorously justify using monthly averaged data for the unperturbed state, since the $\overline{u}$ and $\overline{T}$ profiles from monthly averaged data do contain the effects of atmospheric eddies, and the unperturbed flow does not vary on a much slower time scale than the eddies. Nevertheless, the use of monthly averaged data for the unperturbed state can be viewed as a reasonable way of relaxing the simplified representation of $\overline{u}$ and $\overline{T}$ in previous baroclinic instability studies. It is a reasonable "next step" which allows one to see how the unstable modes are affected by detail in the structure of the basic state.

The one-dimensionality of the basic state is justified partly by the work of Moura and Stone (1976). They found that if the unperturbed state is locally unstable, it is globally unstable. Local conditions (e.g. at a single latitude) are important in determining instability even if meridional variations are included and if the unstable modes have large meridional scales. The one-dimensional basic state is also justified by the secondary role that the meridional variations are found to have in determining the depth and location of regions of negative $\overline{q}_y$. Calculations in Chapter IV

will show that vertical variations alone represent well the features of the $\bar{q}_y$ profile which are important in determining stability properties.

As in Chapter III, the Green and Eady modes are studied in detail, and the Green mode is again shown to possess strong countergradient heat fluxes in the lower stratosphere. In addition to the Green and Eady modes, other long and short wave modes are shown to exist for the more detailed $\bar{u}$ and $\bar{T}$ profiles. This reveals an advantage of the eigenvalue approach over the numerical time integration approach. The latter gives only the most unstable eigenvalue at each wavelength; the former gives all the unstable modes. Many of the new long and short wave modes are shown to exist only when certain negative $\bar{q}_y$ regions exist. The existence of negative $\bar{q}_y$ regions is shown to be very sensitive to small variations in the basic state. Indeed, small variations in the basic state are shown to affect the unstable mode spectra significantly only when they result in changes in the depth and location of negative $\bar{q}_y$ regions.

Most of the model calculations were done with the upper boundary condition $\psi' = 0$ at $p = 0$ (ψ' is the perturbation stream function). However, to allow for a possible source of instability at $p = 0$, results assuming $\omega' = 0$ at $p = 0$ are presented and explained whenever these differ significantly from those assuming $\psi' = 0$ at $p = 0$. Chapter II discusses the choice of the upper boundary condition in more detail.

CHAPTER II

THE MODEL

2.1 The Model Eigenvalue Equation

The quasi-geostrophic model on a β-plane is well-suited for the purposes of this study. It is simple enough to allow a detailed parameter study of large-scale motions and it still provides a good approximation to the properties of such motion. The equations for such a model, written in $\pi = \pi(p)$ coordinates, π being an arbitrary function of pressure, are:

$$\frac{D}{Dt}(f + \zeta) = f_o \frac{\partial w}{\partial \pi} \pi' \tag{1}$$

$$\pi' \frac{D}{Dt} \frac{\partial \psi}{\partial \pi} = - \frac{\sigma}{f_o} \omega \tag{2}$$

where x, y, t are the eastward, northward, and time coordinates, ψ is the horizontal streamfunction, $f = f_o + \beta y$ is the Coriolis parameter, $\sigma = \frac{1}{\rho} \frac{d \ln \theta_s}{dp}$ is the reference state static stability, $\omega = \frac{dp}{dt}$ is the vertical velocity, $\pi' \equiv \frac{d\pi}{dp}$, $\zeta \equiv \frac{\partial^2 \psi}{\partial x^2} + \frac{\partial^2 \psi}{\partial y^2}$ is the vorticity, and $\frac{D}{Dt} = \frac{\partial}{\partial t} - \frac{\partial \psi}{\partial y} \frac{d}{dx} + \frac{\partial \psi}{\partial x} \frac{d}{dy}$.

One next non-dimentionalizes with scales $p \sim p_{oo}$ $x,y \sim L$, $\psi \sim Lu_o$ $t \sim \frac{L}{u_o}$, $\omega \sim \frac{p_{oo} u_o}{L}$. Then, following Phillips (1954), one defines:

$$\psi = \bar{\psi} + \psi'$$

$$\psi' = \Psi(\pi) \cos \mu y \, e^{ik(x-ct)}$$

$$\bar{\psi}_x \equiv \bar{\psi}_{yy} \equiv 0$$

The time variation of the mean flow, $\bar{\psi}_t$ is then of order $|\psi'|^2$. With the

above substitutions, the differential equations become:*

$$(\gamma_T - (u-c)\,\underline{P}^2)\,\Psi = \left[\frac{1}{ik}\,\frac{\sigma_T p_{oo}^2}{fL^2 u_o}\right]\pi'\,\frac{d\omega}{d\pi} \tag{3}$$

$$(u-c)\,\Psi_\pi - u_\pi \Psi = -\left[\frac{1}{ik}\,\frac{\sigma_T p_{oo}^2}{fL^2 u_o}\right]\frac{1}{\pi'}\,\omega \tag{4}$$

where all quantities except those in brackets [ ] are non-dimensional and $\gamma_T \equiv \dfrac{\beta\sigma_T p_{oo}^2}{f^2 u_o}$ is the generalized β parameter, and $\underline{P}^2 \equiv \dfrac{(k^2+\mu^2)\sigma_T p_{oo}^2}{f^2}$ is the non-dimensional wavenumber. Using Phillips' 1954 grid, one writes the vorticity equation at odd levels and the thermodynamic equation at even levels. Combining these finite difference equations as Phillips did results in:

$$\begin{aligned} 0 = &\left[\gamma_T - (u_n-c)\,\underline{P}^2) - \Sigma_n^- \Pi_n^- (u_{n-2}-c) - \Sigma_n^+ \Pi_n^+ (u_{n+2}-c)\right]\Psi_n \\ &+ \Sigma_n^- \Pi_n^- (u_n-c)\Psi_{n-2} + \Sigma_n^+ \Pi_n^+ (u_n-c)\Psi_{n+2} \end{aligned} \tag{5}$$

where n is odd and runs from 1 to N-1 = 97 (N is defined as the value of n at the ground level and equals twice the number of levels at which ψ is written), $(\ )_n$ means the value of $(\ )$ at level n,

$$\Pi_n^+ \equiv \frac{\pi'_n\,\pi'_{n+1}}{(\Delta\pi)^2},\quad \Pi_n^- \equiv \frac{\pi'_n\,\pi'_{n-1}}{(\Delta\pi)^2},\quad \text{and}\quad \Sigma_n^\pm \equiv \sigma_T/\sigma_{n\pm1}$$

With appropriate boundary conditions (discussed below), eigenvalues of this system of equations are found by the QR algorithm. The algorithm is one of the most efficient methods known for solving the complete eigenvalue problem for symmetric or non-symmetric matrices (Dahlquist and Björck, 1969). It is most efficient if the matrix value whose eigenvalues are desired is in Hessenberg form. The eigenvalue matrix is balanced, and put into Hessenberg form and solved for its eigenvalues by EISPACK subroutines

---

*In the equations and symbols below σ_T is the nominal tropospheric value of σ given in Section 3.3.

provided by the MIT Information Processing Service (IPS). The IPS publication AP-42 describes these subroutines.

Eigenfunctions are obtained by assuming Real$\{\Psi_1\}$ = Real$\{\Psi_2\}$ = 1 if the boundary condition is $\omega' = 0$ at the top, or by assuming Real$\{\Psi_3\}$ = Im$\{\Psi_3\}$ = 1 if the condition is $\Psi' = 0$ at the top. The eigenvalue equation is then used to integrate downwards. The homogeneity of the eigenvalue equation justifies the arbitrary choice for Ψ_1 or Ψ_3.

2.2 Boundary Conditions

At the bottom $\omega \equiv 0$. This is justified because in the first approximation for quasi-geostrophic motions $\omega \cong -gpw$. In the atmosphere for motions of synoptic or larger scale, the other terms in the ω - w equation are smaller by an order of magnitude or more. The $\omega = 0$ lower boundary condition also filters out horizontally propagating acoustic waves. The lower boundary condition is applied at level N. It results in an equation relating Ψ_{N-1} to Ψ_{N-3}. This relation between Ψ_{N-1} and Ψ_{N-3} is obtained by writing the eigenvalue equation (Eq. 5) at level N with $\pi^+_{N-1} \equiv 0$.

At p = 0, the top of the model atmosphere, both the author and Holton (1975) have found that only the $\omega = 0$ boundary condition has been used in the literature for quasi-geostrophic models. While being exact in theory, this condition can act as a rigid lid. It can introduce spurious free oscillations which may be unstable, and cause reflections of vertically propagating modes (Lindzen, *et al.*, 1968; Cardelino, 1978).

Geisler and Garcia (1977) assumed $\Psi' = 0$ at a level "(typically 100 km) where solutions of interest have already decayed to a negligible value",

their model is in geometric coordinates. Indeed, asymptotic solutions of the quasi-geostrophic equations for $\bar{U}$ profiles linear with height show that $|\psi'|$ grows or decays exponentially. Assuming $\psi' = 0$ in a geometric coordinate model retains only the realistic decaying solution. Charney in Morel et al. (1973) requires that the upward energy flux $\rho_s \overline{\psi'w'}$ is zero at $z = \infty$. This is satisfied if the decaying solution is selected because $\lim_{z \to \infty} \rho_s \psi^* \psi_z = \lim_{z \to \infty} \rho_s \overline{\psi'w'}$. The assumption behind the upper boundary condition $\lim_{z \to \infty} |\psi| = \lim_{z \to \infty} \rho_s \overline{\psi'w'} = 0$ is that one's solution should decay away from energy sources which are at finite heights.

For the model used here, problems with $\bar{u}_p$ constant have $\bar{u}_z \sim \rho u_p \longrightarrow 0$ as $z \to \infty$, so that the available potential energy goes to zero as $z \to \infty$. For this case, which has no energy source near the top, Charney and Pedlosky (1963) have shown that the energy flux of the disturbance will decay at least exponentially with height. The disturbance will then decay to zero amplitude at the top. Thus, $\Psi' = 0$ is a realistic boundary condition.

Consideration of energy sources above the stratosphere is not within the scope of the current study. Calculations, therefore, are presented primarily with $\Psi' = 0$ as the upper boundary condition. However, comparisons will be made with calculations which have $\omega' = 0$ as the upper boundary condition. Important differences in the calculations resulting from the different boundary conditions will be pointed out and their physics will be discussed. In particular, it will be seen that the long wave Green mode experiences a behavior analogous to reflection when $\omega' = 0$ is used.

Implementation of upper boundary conditions in the reduction of the number of model levels from 49 to 48 (Figure 2.1 shows the height and pressure of model levels). The condition $\omega_0 = 0$ is replaced by $\Psi_1' = 0$ and

the remaining 48 equations at levels 3 to 97 are solved for their eigenvalues.

2.3 Fluxes and Energetics

To obtain the horizontal entropy fluxes, one first uses the hydrostatic and Poisson relations: $\frac{\partial\psi}{\partial p} = -\frac{1}{f_o\rho}$ (6); $\theta = (\frac{p_{oo}}{p})^{\kappa} T$ (7); and the ideal gas law $P = \rho RT$ (8); to relate θ to the streamfunction:

$$\theta = -\frac{f_o}{R}\, p\,(\frac{p_{oo}}{p})^{\kappa}\,\frac{\partial\psi}{\partial p} \qquad (9)$$

The meridional velocity is simply $v' = \psi_x'$ and the vertical velocity is related to ψ through the thermodynamic equation. With the additional assumption that $\psi_{m=\text{even}} = \frac{1}{2}(\psi_{m+1} + \psi_{m-1})$, one multiplies the expressions for v and θ, ω and θ, and ω and ψ. Then averaging zonally and simplifying results in:

$$(\overline{v'\theta'})_\ell = \Pi_\ell'\, P_\ell^{1-\kappa}\, km\varepsilon\, \frac{1}{2\Delta\pi}\left[\text{Real}\,\{i\,\Psi^*_{\ell-1}\,\Psi_{\ell+1}\}\right]$$

$$(\overline{\omega'\theta'})_\ell = (\frac{\sigma_T}{\sigma_\ell})\,\Pi_\ell'^{\,2}\, P_\ell^{1-\kappa}\, km\varepsilon\, \frac{1}{(\Delta\pi)^2}\left[(\frac{\Delta\pi}{\pi'}\,P_\ell^{\kappa-1}\,\bar{\theta}_\ell\,\tan\mu y + u_{\ell-1} - u_{\ell+1})\right.$$

$$\cdot\ \text{Real}\,\{i\,\Psi_{\ell-1}\,\Psi^*_{\ell+1}\} - 2c_i\,\text{Real}\,\{\Psi_{\ell-1}\,\Psi^*_{\ell+1}\}$$

$$\left. +\ c_i\left[\bar{\Psi}_{\ell-1}\,\Psi^*_{\ell-1} + \Psi_{\ell+1}\,\Psi^*_{\ell+1}\right]\right]$$

$$(\overline{\omega'\psi'})_\ell = -\frac{\sigma_T}{\sigma_\ell}\,\Pi_\ell'\, km\varepsilon\, \frac{1}{4\Delta\pi}\left[c_i\left[\Psi_{\ell+1}\,\Psi^*_{\ell+1} - \Psi_{\ell-1}\,\Psi^*_{\ell-1}\right]\right.$$

$$\left. -\ (u_{\ell+1} + u_{\ell-1} - 2c_r)\,\text{Real}\,\{i\,\Psi_{\ell-1}\,\Psi^*_{\ell+1}\}\right]$$

where $m = \cos^2 \mu y$, $\varepsilon = e^{k|c_i|t}$, c_r and c_i are the real and imaginary parts of the phase speed and ℓ is even. Given eigenvalues and eigenfunctions, the above non-dimensional correlations are then computed. The last correlation is often called the "pressure work term" for reasons given below.

The quasi-geostrophic energy equations have been derived by Charney (in Morel, 1973) for geometric corrdinates. Their counterparts for pressure coordinates are:*

$$\frac{d\mathcal{K}}{dt} = -\iint \overline{u'v'}\,\bar{u}_y \, dy\, dp - \frac{1}{R_o}\iint \overline{\omega'\theta'}\left(\frac{p}{p_{oo}}\right)^{K} \frac{1}{p}\, dy\, dp$$

$$- \frac{1}{R_o}\int \overline{\psi'\omega'}\, dy\Big|_{p_1}^{p_2} = CK + CE + BE$$

$$\frac{d\mathcal{E}}{dt} = \iint \overline{u'v'}\,\bar{u}_y \, dy\, dp - \iint \frac{1}{\Sigma\Lambda}\,\overline{v'\theta'}\,\bar{\theta}_y \left(\frac{p}{p_{oo}}\right)^{2K} \frac{1}{p^2}\, dy\, dp$$

$$- \frac{1}{R_o}\int \overline{\psi'\omega'}\Big|_{p_1}^{p_2} dy = CK + CA + BE$$

$$\frac{d\mathcal{A}}{dt} = \frac{1}{R_o}\iint \overline{\omega'\theta'}\left(\frac{p}{p_{oo}}\right)^{K} \frac{1}{p}\, dy\, dp - \iint \frac{1}{\Sigma\Lambda}\,\overline{v'\theta'}\,\bar{\theta}_y \left(\frac{p}{p_{oo}}\right)^{2K} \frac{1}{p^2}\, dy\, dp = -CE + CA$$

where $\Sigma = \frac{\sigma_T}{\sigma}$, $\Lambda = L^2/L_r^2$, ($L_r = \frac{\sigma_T p_{oo}^2}{f_o^2}$ is the radius of deformation)

$$\mathcal{K} = \frac{1}{2}\overline{|\nabla\psi'|^2}$$

$$\mathcal{E} = \frac{1}{2}\left[\overline{|\nabla\psi'|^2} + \frac{1}{\Sigma\Lambda}\overline{(\psi'_p)^2}\right] = \mathcal{K} + \mathcal{A}$$

$$\mathcal{A} = \frac{1}{2\Sigma\Lambda}\overline{(\psi'_p)^2}\,.$$

---

*Note: Once $\pi(p)$ is known, writing the energy equations in π coordinates requires only a very simple transformation.

$\mathcal{K}$, $\mathcal{E}$, and $\mathcal{A}$ are the Eddy Kinetic Energy, Total Eddy Energy, and Eddy Available Potential Energy, respectively (Lorenz, 1967). The power integral CK, which represents transfer of kinetic energy between zonal mean and eddy flow, is not present for this one-dimensional model since $\bar{u}_y = 0$. The power integral CA, which represents the transfer of available potential energy between zonal mean and eddy flows is studied by presenting profiles of the horizontal heat flux. The horizontal heat flux has the more direct effect on temperatures. Profiles of the full power integral CE are presented because CE describes the source regions for Eddy Kinetic Energy. The last term, BE, describes the transfer of eddy kinetic energy into or out of a given pressure layer P_1 to P_2. Since Ψ is always -90° out of phase with v, the $\overline{\psi'\omega'}$ correlation reveals the relation of poleward to downward velocities throughout the atmosphere. It will be used to relate model eddy motions to observations.

2.4 Numerical Accuracy

The numerical method described above is a second order scheme, and numerical experiments did show the error in growth rates varying inversely with the square of the number of levels when $\pi = \sqrt{\frac{p}{p_{00}}}$ is the coordinate. For nominal values of the stratosphere/troposphere shear ratio, SR = -1.5, and static stability ratio $\sigma_\rho = 50$ (see Chapter III for the calculation of these values), Figure 2.2 illustrates the Eady mode's growth rate accuracy as a function of γ_T ($\gamma_T = 2$ is nominal). Note that many more levels are needed to obtain accurate growth rates for higher γ_T because the most unstable wavelength becomes shorter, and the associated vertical structure becomes finer.

The model resolution of 48 levels is of good accuracy at least to wavenumber $\underline{P}$ = 6 or wavelength = 1.8 x 10^3 km. In low latitudes γ_T can be large and one would need 15 or more levels to even detect instability if γ_T = 10.

The results in Figure 2.2 are identical for both upper boundary conditions. The Green mode, however, which has the longer wavelength of 8.3 x 10^3 km ($\underline{P}$ = 1.3) for nominal parameter values, is resolved much better when $\psi'_{(p=0)}$ = 0 is the upper boundary condition. In this case, the doubling time is determined to within 2% of its 48 level value (6.1 days) when only 13 levels are used. However, when $\omega'_{(p=0)}$ is the upper boundary condition, 37 levels are required for the doubling time to be within 2% of its 49 level value (14.7 days) (the marked differences between these estimates of the Green mode doubling time is discussed with the Chapter III $\omega'|_{(p=0)}$ = 0 calculations). The above and additional calculations showed that when doubling times of long-wave modes were calculated, calculations using $\psi'|_{(p=0)}$ = 0 converged more rapidly than those using the more common $\omega'|_{(p=0)}$ = 0 upper boundary condition.

The ability of the model to converge over the entire range of the vertical coordinate is illustrated in Figure 2.3, which shows results valid for both upper boundary conditions. For the meridional entropy flux of the Eady mode, good convergence is obtained for the model resolution of 48 levels (49 levels, for the $\omega'_{(p=0)}$ = 0 boundary condition).

For entropy fluxes of the Eady mode at higher γ_T values and shorter wave lengths, Figures 2.4 and 2.5 show model convergence (their results are identical for both upper boundary conditions). The quantities $\overline{v'\theta'}_T$ and $\overline{v'\theta'}_s$ are the mass weighted zonally averaged meridional entropy fluxes for

the troposphere and stratosphere, respectively. Each profile of $\overline{v'\theta'}$ has been normalized, i.e. the maximum value for all levels in the profiles has been set equal to 1. Good convergence on values of $\overline{v'\theta'}_T$ and $\overline{v'\theta'}_S$ exists for modes with zonal wavelengths as small as 1.8×10^3 km.

Three additional checks were made on model accuracy. The first is a check for satisfaction (numerically) of the lower boundary condition. Both upper and lower boundary conditions were, of course, used to determine the eigenvalues. Determination of the eigenfunctions, however, started with the upper boundary equation $\Psi_1 = 0$ and assumed an amplitude and phase for Ψ_3 (see the earlier discussion in this chapter for a justification of this assumption). Then the model eigenvalue equation (Eq. 5) is used to determine values of Ψ at lower levels. The value of Ψ at the lowest level, Ψ_{N-1}, is obtained from the eigenvalue equation written at level N-3, which relates Ψ_{N-1} to Ψ_{N-3} and Ψ_{N-5}. The remaining Ψ equation, written at level N-1 contains the lower boundary condition. It must be satisfied by the Ψ_{N-1} and Ψ_{N-3} values, which were determined by the eigenvalue equation written at higher levels. Satisfaction of this lower boundary equation was checked for all model results.

A second check is satisfaction of Howard's Semicircle Theorem Test (see Pedlosky (1964) for application of this theorem to quasi-geostrophic models). All values of the eigenvalues were found to be within the theoretical limits of the test.

A final check on the model's validity is its ability to reproduce previous results. A plot of growth rate contours vs γ_T^{-1} and wavelength $\frac{2\pi}{P}$ for Green's linear $\bar{u}$ profile reproduces his Figure 3 exactly (see Figure

2.6 and Green (1960), Figure 3). Both calculations used a rigid lid (w' or $\omega' = 0$) at the top.

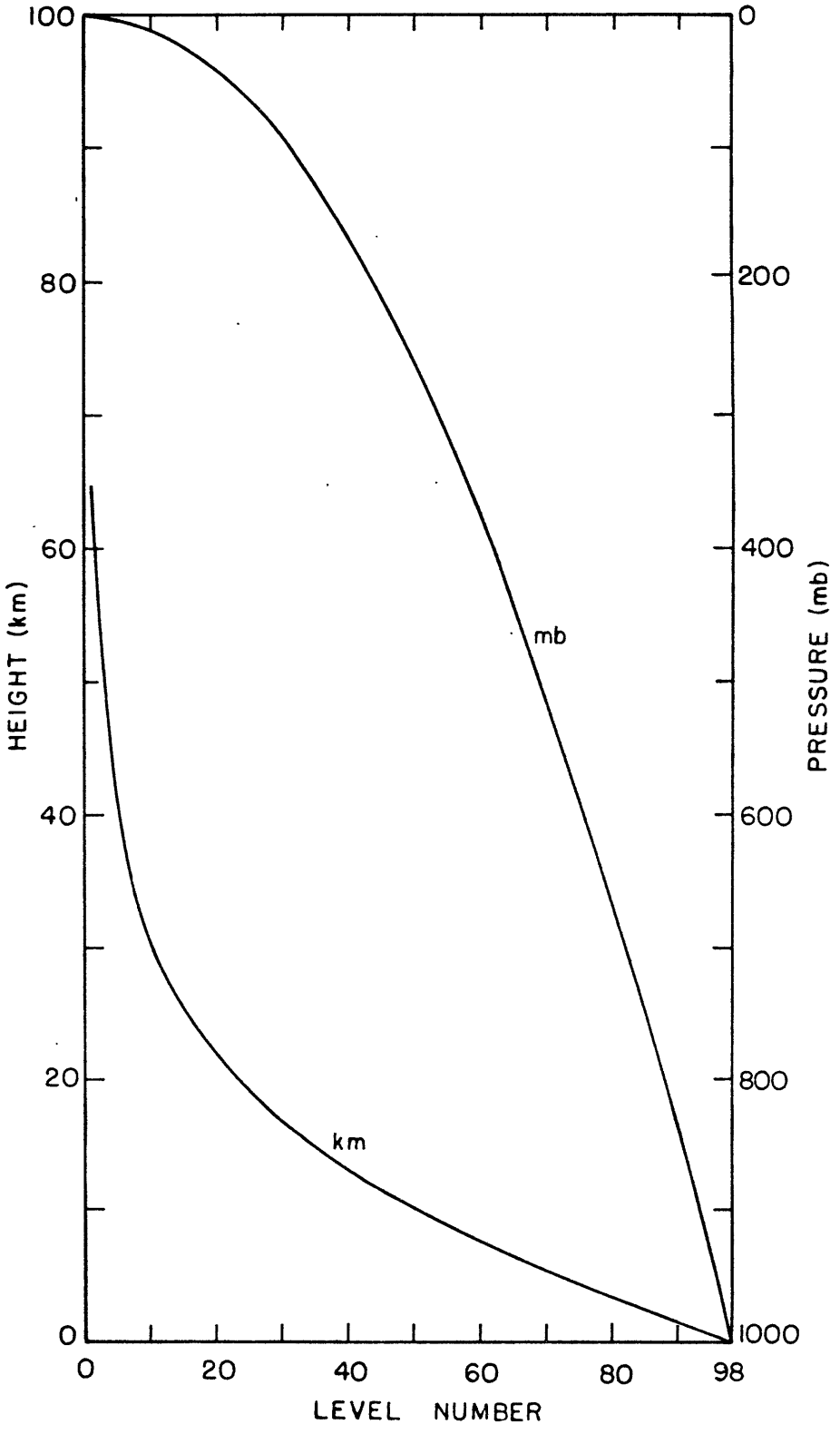

Figure 2.1. Height and pressure of model levels.

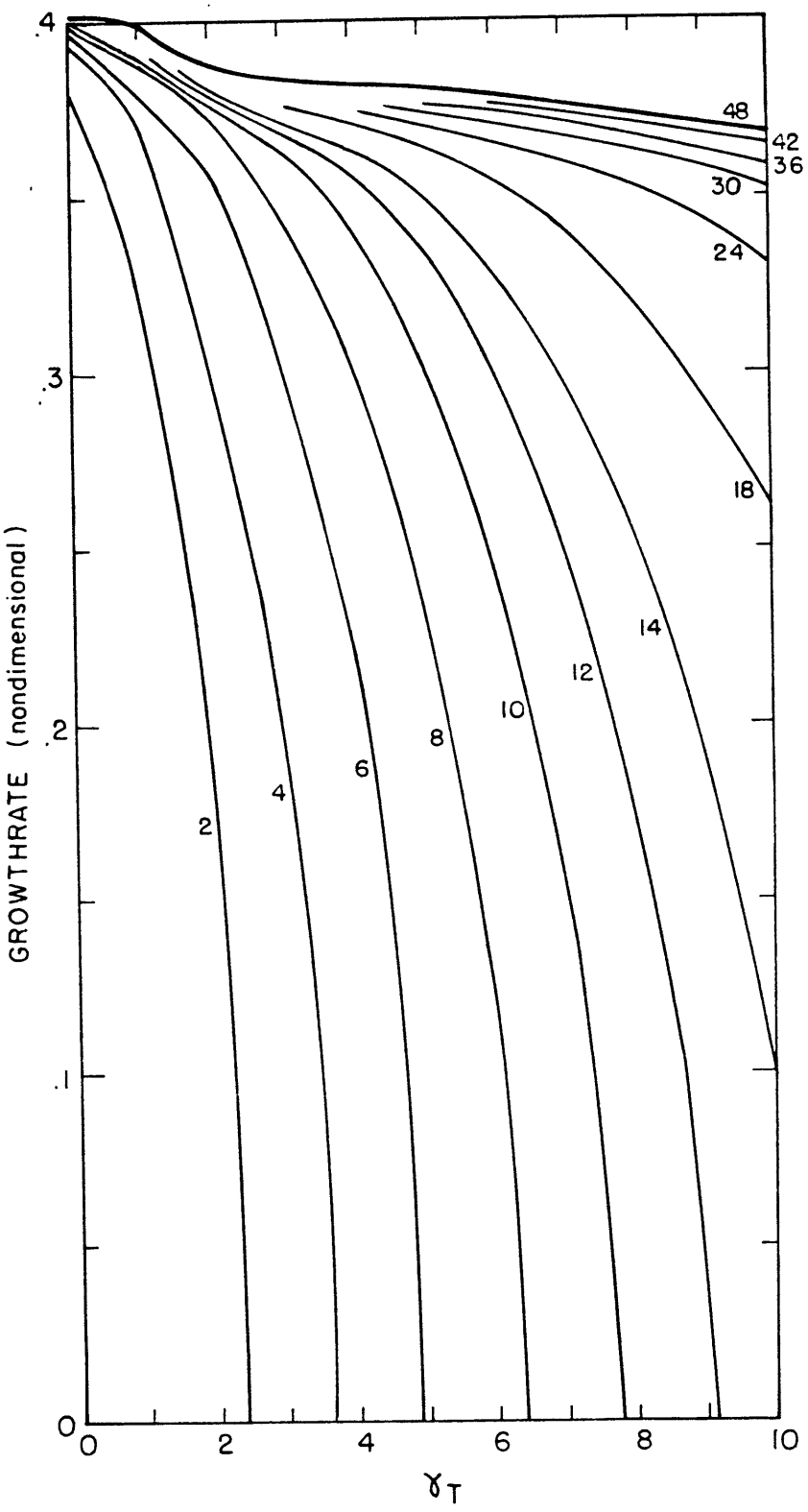

Figure 2.2. Growthrate vs. γ_T of the fastest growing Eady mode for models with indicated numbers of levels for which ψ is written; SR = -1.5, $\sigma_\rho = 50$.

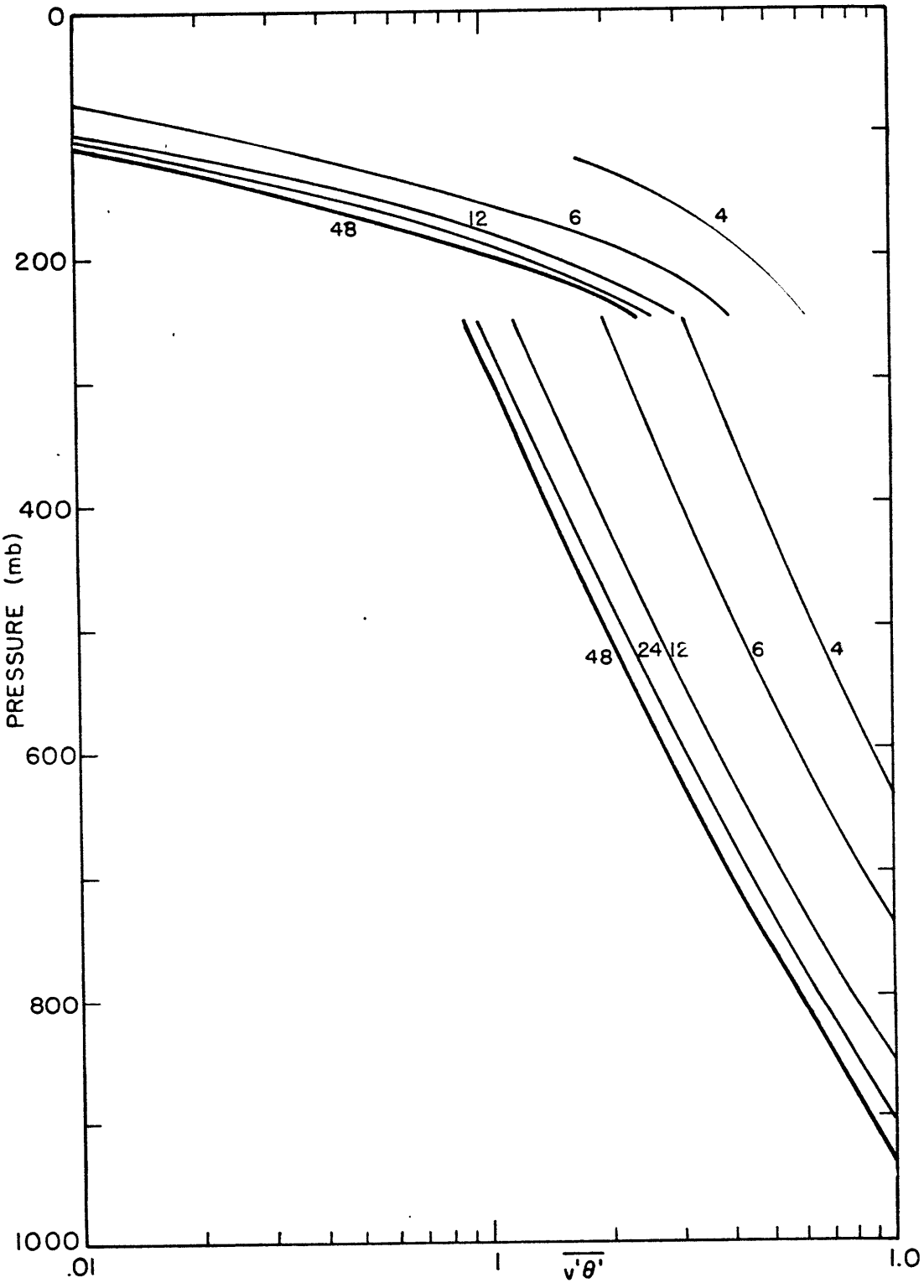

Figure 2.3. Vertical structure of the meridional heat flux of the fastest growing Eady mode for $\gamma_T = 2$, SR = -1.5, $\sigma_\rho = 50$.

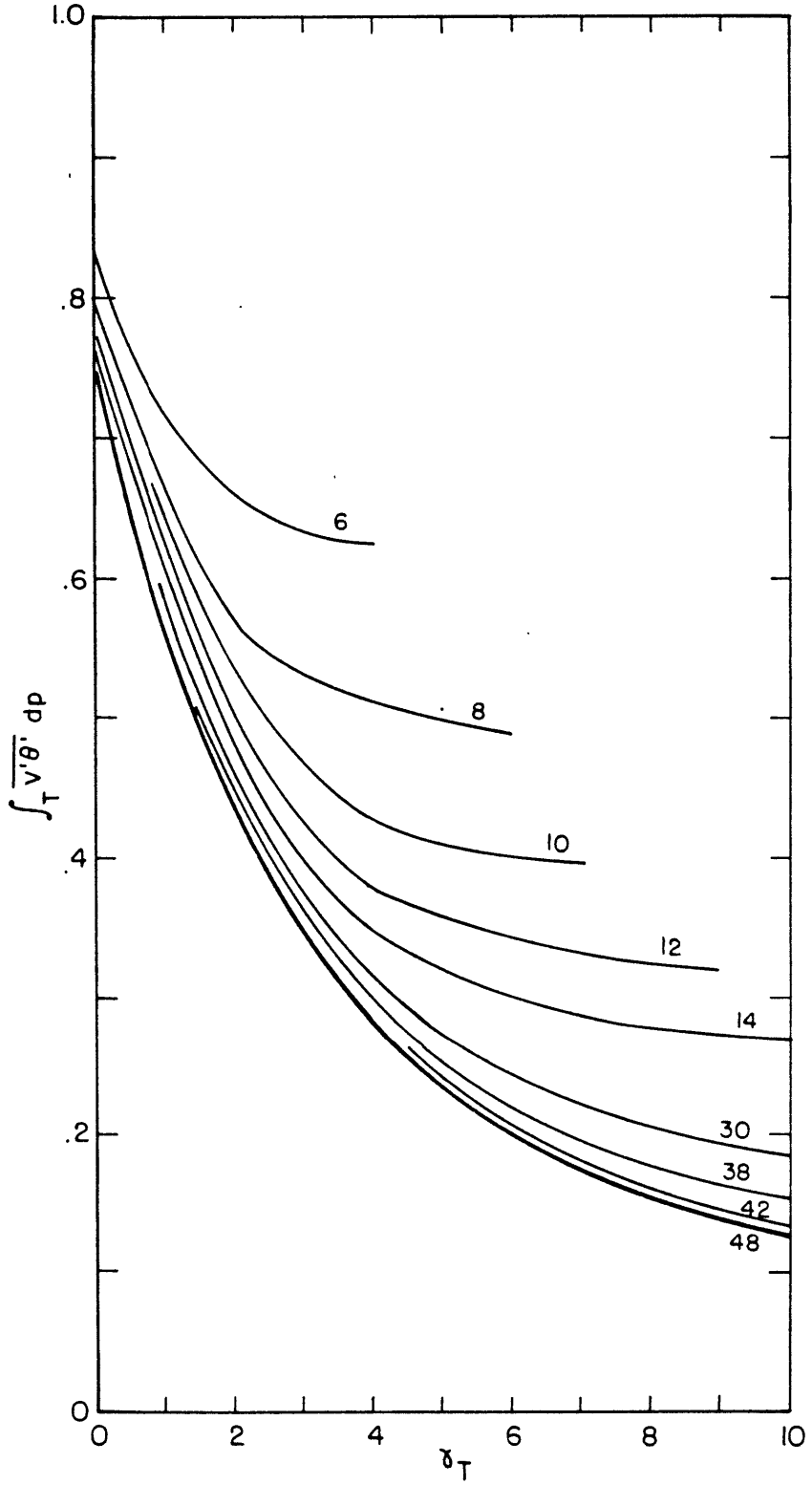

Figure 2.4. As in Figure 2.2, except for the tropospherically integrated meridional heat flux.

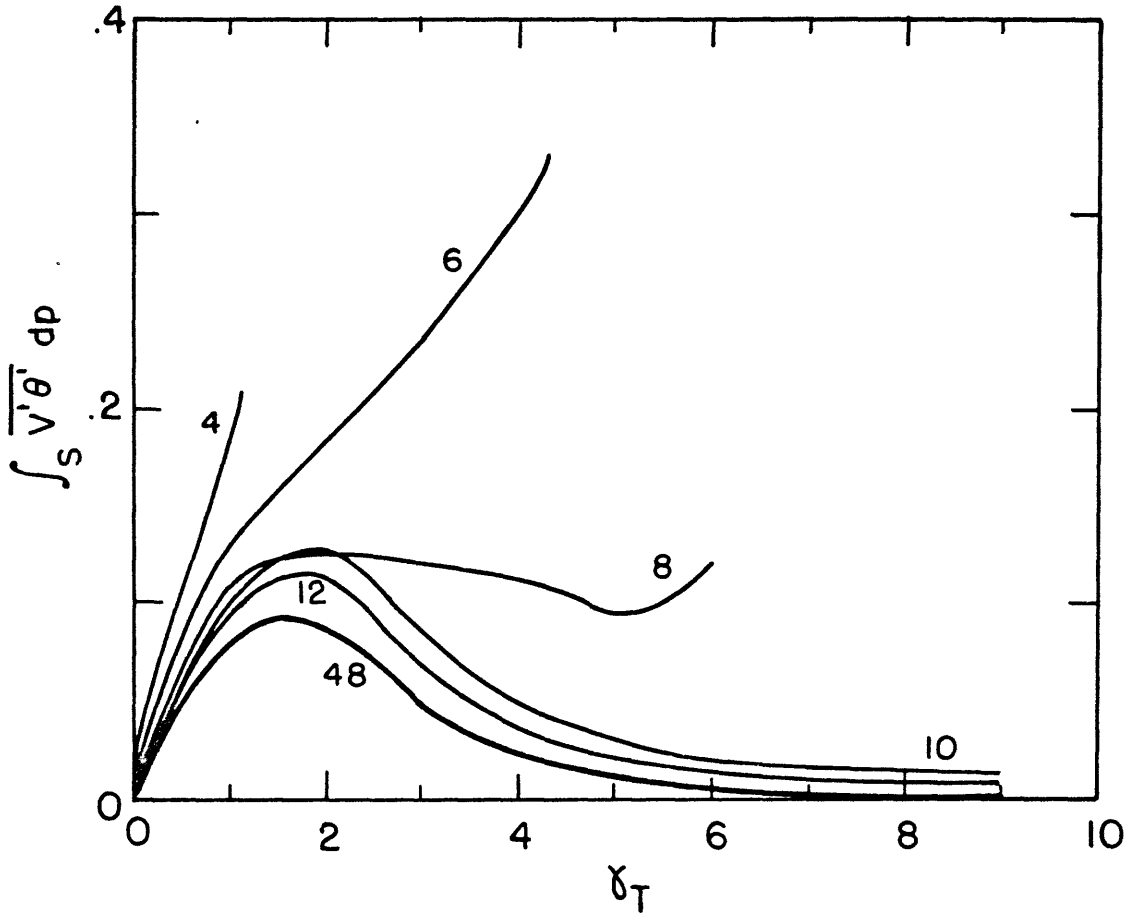

Figure 2.5. As in Figure 2.2, except for the stratospherically integrated meridional heat flux.

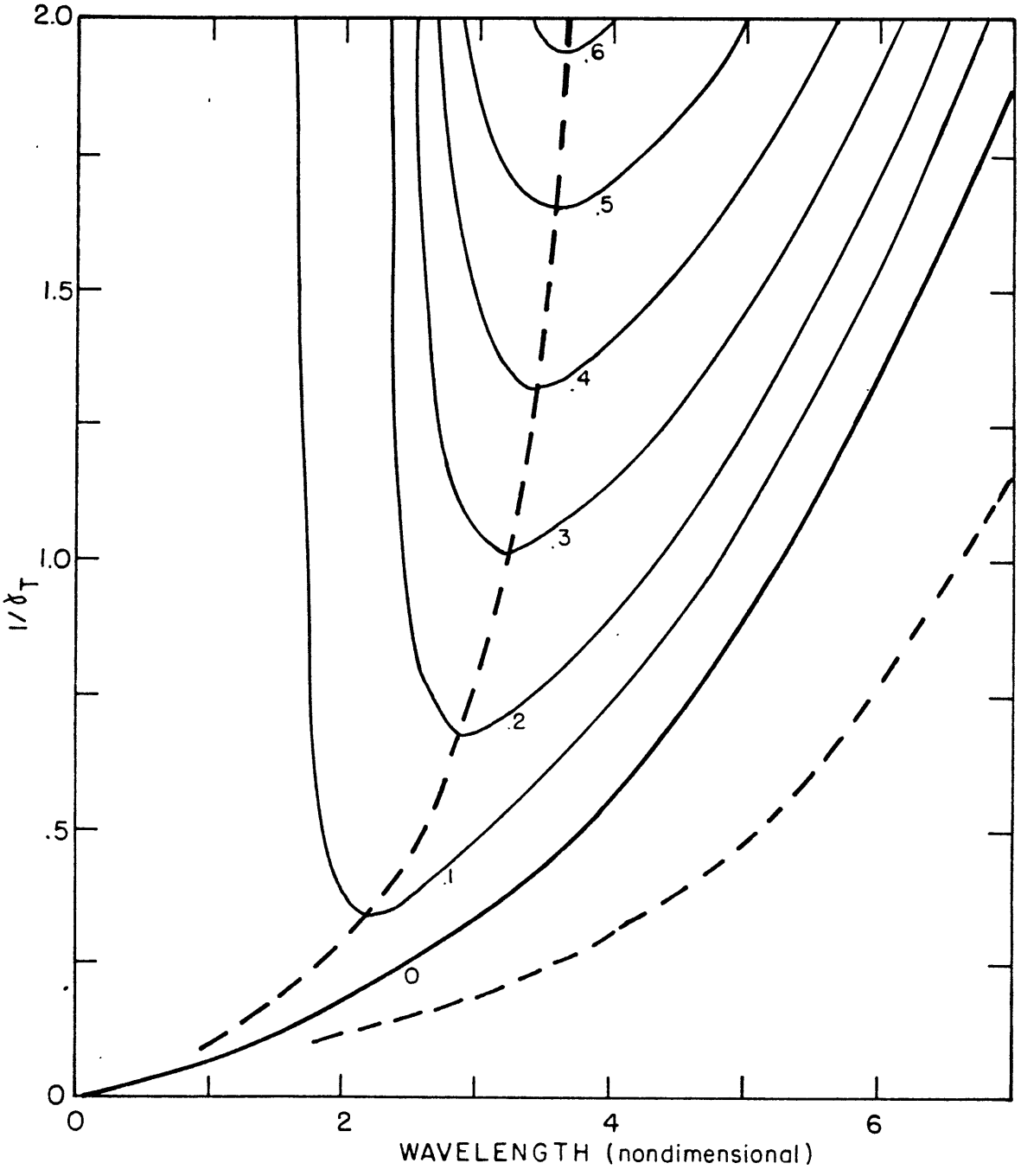

Figure 2.6. Non-dimensional growthrate ~~(R)~~ P_{c_r} divided by γ_T, as a function of γ_T^{-1} and wavelength; $\sigma_\rho = 1$, SR = 1, $u(p=0) = 1$, and $\bar{\omega}' = 0$ at p = 0. Neutral modes are shown by the heavy zero curve.

$\frac{2\pi}{P}$

CHAPTER III

TWO-LAYER MULTI-LEVEL MODEL RESULTS

3.1 Introduction and Overview

This chapter treats the atmosphere as a 2-layer system having a troposphere and stratosphere. Each layer has an independent shear and static stability, and these unperturbed flow parameters are constant within each layer. This approach simplifies the parametric study of how the unperturbed state affects the perturbations. Within each layer are 24 levels so that the vertical structure of the perturbations can be studied in fine detail.

Three parameters completely determine the unperturbed state: γ_T, the generalized β-parameter, defined in chapter II; SR, the shear ratio $\equiv (\frac{du}{dp})_{\text{stratosphere}} / (\frac{du}{dp})_{\text{troposphere}}$; and σ_ρ, the static stability ratio $\sigma_{\text{stratosphere}}/\sigma_{\text{troposphere}}$. The velocity field, $u_n = \frac{U_n}{u_o}$ ranges from 0 to 1 between ground and tropopause $(\frac{p}{p_{oo}} = \frac{1}{4})$ and from 1 to $1 + \frac{1}{3}$ SR between tropopause and p = 0:

$$u = \begin{cases} 1 - \frac{4}{3}\,SR\,p + \frac{1}{3}\,SR & \text{stratosphere} \\ \frac{4}{3}\,(1-p) & \text{troposphere} \end{cases}$$

The static stability parameter, $\Sigma_m = 1$ for $m > 49$ and $\Sigma_{m,} = \frac{1}{\sigma_\rho}$, for $m < 49$ (note: $m \neq 49$, as m is even). When values for γ_T, SR, and σ_ρ are chosen, the model eigenvalue equation is ready to be solved to any specified non-dimensional wavenumber P.

Solutions will first be obtained for combinations of special and nominal values of the parameters. "Nominal" values are defined as those

appropriate for mid-latitude winter conditions: $\gamma_T = 2$, SR = -1.5, and $\sigma_\rho = 50$ (these values are calculated below). Special values used are $\gamma_T = 0$ (no β-effect), SR = 1 (uniform shear throughout the atmosphere), SR = 0 (no shear above $p/p_{oo} = 1/4$), and $\sigma_\rho = 1$ (no stratosphere, uniform static stability throughout the atmosphere). Every combination of these parameter values will be studied. This will enable one to see the effects of: uniform shear, zero shear above $p/p_{oo} = 1/4$, and nominal shear above $p/p_{oo} = 1/4$, both with and without a stratosphere, and with and without the β-effect.

The second part of this parameter study will use the nominal parameter values to define an origin in parameter space. The study will include parameter values on axes through the origin along each of which only one parameter varies. Both the first and second parts of the parameter study will treat in detail mode growth rates and phase speeds, and the vertical structures of streamfunction amplitude and phase, of meridional heat transport and of eddy kinetic energy generation. This will be done for both the Eady and Green modes.

The third part of the parameter study will discuss growth rates of the Eady and Green modes on γ_T = constant planes in parameter space. Interesting vertical structure properties will be noted.

Finally, calculations will be presented to point out how changing the upper boundary condition from $\psi' = 0$ to $\omega' = 0$ affects the perturbations.

3.2 Necessary Conditions for Baroclinic Instability

An important part of this study will be the relation of unstable modes to the necessary conditions for baroclinic instability, given by the

Charney-Stern theorem. Charney (in Morel, 1973) derives the theorem for geometric coordinates with a zero energy flux condition at the upper boundary ($\lim_{z\to\infty} \overline{\psi'w'} = \lim_{z\to\infty} \overline{\psi'\psi'^*_z} = 0$), $z = \infty$. The derivation in pressure coordinates for $\omega' = 0$ at $p = 0$ is similar and results in the equation (analogous to Charney's equation 9.18):

$$c_i\left[\int \left(\frac{f_o^2}{\sigma}\frac{|\psi'|^2}{|\bar{u}-c|^2}\bar{u}_p\right)_{p=0} dy - \int \left(\frac{f_o^2}{\sigma}\frac{|\psi'|^2}{|\bar{u}-c|^2}\bar{u}_p\right)_{p=1} dy + \int_1^0\int \frac{|\psi'|^2}{|\bar{u}-c|^2}\bar{q}_y\, dy\, dp\right] = 0 \qquad (1)$$

$$\bar{q}_y \equiv \beta - \bar{u}_{yy} - f_o^2\left(\frac{1}{\sigma}\bar{u}_p\right)_p - f_o^2\left(\frac{\sigma_y}{\sigma}\bar{\psi}_p\right)_p \qquad (2)^*$$

For the profiles of this section (linear $\bar{u}$, constant σ), $\psi' = 0$ at $p = 0$ forces $\lim_{p\to 0} \overline{\psi'^*\psi'_p} = 0$. This (for any $\bar{u}$ and σ) results in $\lim_{p\to 0} \overline{\psi'\omega'} = 0$, i.e. no energy flux at $p = 0$. Also, $\psi' = 0$ at $p = 0$ results (for any $\bar{u}$ and σ) in the disappearance of the first integral in the above equation. The upper boundary condition $\omega' = 0$ would allow this integral to remain. Thus the upper boundary condition $\psi' = 0$ has as necessary conditions for baroclinic instability:

(1) $\bar{q}_y = 0$ in the fluid in the absence of a temperature gradient $\bar{\theta}_y$ α $\bar{u}_p$ at the lower boundary, or

(2) a balance between the lower boundary integral and the $\bar{q}_y$ integral.

The $\omega' = 0$ upper boundary condition would have as necessary conditions for baroclinic instability:

(1) $\bar{q}_y = 0$ in the fluid in the absence of temperature gradients at both boundaries, or

(2) a balance between upper boundary, lower boundary, and $\bar{q}_y$ integrals.

---

* It is not consistent to use the σ_y term in quasi-geostrophic models. Calculations show that this term is small. It is used only in the calculations of Tables 4.1 to 4.4.

The $\omega' = 0$ case has the distinction that a temperature gradient at the upper boundary as well as a temperature gradient at the lower boundary and an internal zero of $\overline{q_y}$ is a potential source for baroclinic instability. Indeed, later calculations show that there are modes which depend on a non-zero value of $\bar{\theta}_y$ at p = 0 for their existence, that there are other modes which depend on specific zeros of $\bar{q}_y$ for their existence, and that there are still other modes which exist when $\bar{\theta}_y \neq 0$ at the ground. The modes which exist only for $\bar{\theta}_y \neq 0$ at p = 0 may not be realistic for the atmosphere; however, they may play a role in laboratory experiments or oceanic flows. They will be discussed with the $\omega'\big|_{p=0} = 0$ calculations.

3.3 Nominal Parameter Values

The origin or "nominal" point is chosen to approximate a winter stratosphere and troposphere at 45°N. Using U.S. Standard Atmospheric values for January 45°N at 1000, 250, and 28 mb one has:

$$\sigma_T \approx g\left(\frac{\Delta Z}{\Delta p}\right)^2 \frac{\Delta \ell n\ \theta}{\Delta Z} \approx 9.81 \frac{m}{sec^2} \left(\frac{10200\ m}{75000\ nt/m^2}\right)^2 \frac{\ln 327 - \ln 273}{10200\ m} = .321 \times 10^{-5} \frac{}{m^4\ sec^2\ kg^{-2}}$$

$$\sigma_S \approx 9.81 \frac{m}{sec} \left(\frac{14000\ m}{23200\ nt/m^2}\right)^2 \frac{\ln 599 - \ln 327}{14000\ m} = .169 \times 10^{-3} \frac{}{m^4 sec^2\ kg^{-2}}$$

thus:

$\sigma_\rho = 52.5$; $u_{28} = 13$ m/sec, $u_{250} = 24$ m/sec, and $u_{1000} = 0$ give for the shear ratio: SR = -1.55 and 24 m/sec for U_o.

$\beta = 1.64 \times 10^{-11}\ m^{-1}\ sec^{-1}$, $P_{oo} = 10^5 nt/m^2$, $f = 10^{-4} sec^{-1}$ and u_0 and σ_T from above give: $\gamma_T = 2.19$.

The winter values of $\gamma_T = 2.19$, SR = -1.55, $\sigma\rho = 52.5$ are rounded to the nominal values $\gamma_T = 2$, SR = -1.5, $\sigma\rho = 50$. It should be noted that γ_T and $\underline{P}$ are analogous to the γ and P parameters of Green (1960), and, as in Green, $\mu \equiv 0$ for all calculations. Since μ appears only in the combination $k^2+\mu^2$, the results for any value of μ can be recovered by a reinterpretation of the value of k. In this chapter, k represents the number of waves in a latitude circle at 45°.

It is also interesting to note that the value of γ_T corresponding to the critical shear of the Phillips (1954) 2-level model is: $\gamma_T = \frac{\beta \sigma_T P_{00}^2}{2f^2 u_c} = 2.06$ where $u_c \simeq \frac{\beta R(\theta_{250}-\theta_{1000})}{2f^2}$ (R is the gas constant, see Stone (1978). The winter value of $\gamma_T = 2.19$ is very close to Phillips' critical value. This shows again that the mid-latitude troposphere is remarkably close to two-level neutral stability for time averages of over a few (3) months (see also Moura and Stone (1974) and Stone (1978)).

3.4 Results for Special and Nominal Parameter Values

Figures 3.1 to 3.4 present the doubling times and phase velocities of the unstable modes for special and nominal parameter values. It is immediately apparent that the presence or absence of a stratosphere or of the β-effect affects the results much more than variation of the upper layer's shear. The presence of a greater static stability in the upper layer, not surprisingly, lessens further the influence of upper layer shear variation. Eady modes grow faster for a reversed upper layer shear if no stratosphere is present and very slightly more slowly if there is a stratosphere. The overall shape of the doubling time curves is little affected

by variation of SR. This is not the case for γ_T. As pointed out by Green (1960), zero β-effect stabilizes short waves. Also, when SR = 1 and there is no stratosphere in addition to no β-effect, all modes are stable; this differs from Green's results for a rigid lid (see discussion of $\omega' = 0$ at $p = 0$ calculations). As γ_T increases, short waves become more unstable (see Figures 3.17 and 3.18). The presence of a stratosphere lessens doubling times of the Eady mode for all values of SR and γ_T from about 2 1/2 to 1 1/2 days. When both the stratosphere and β-effect are present, the long wave "Green Mode" appears and has its fastest doubling time (6 days) for the nominal, reversed stratospheric shear. The doubling time and wave number of the most unstable Green and Eady modes for the parameter values γ_T, SR, σ_p = 2, 1, 50 compare well with those calculated by Geisler and Garcia (1977) for a constant shear and more realistic temperature profile. Differences are less than 10%.

Phase velocities calculated by Geisler and Garcia are almost twice as large as this model's values for γ_T, SR, σ_p = 2, 1, 50. The difference is due to the much larger $\bar{u}$ values in the former model. A fairer comparison between this model and that of Geisler and Garcia will be made in the next chapter. For zero β-effect, phase velocities are very large at long wavelengths (note the change of scale in Figures 3.1 and 3.2). When there is both a β-effect and a stratosphere present, the phase velocity goes to zero with the growth rate at a "critical" wavelength which defines the separation between the Eady and Green modes. The existence of neutral waves stationary relative to the surface wind at this critical wavelength was discovered by Green (1960). Steering levels, as in Green's study are below the mid level ($p/p_{oo} = 1/2$) for all wavelengths.

Streamfunction amplitudes and phases are presented for the most unstable Eady and Green Modes in Figures 3.5 to 3.8. For the Eady mode, the presence of a stratosphere causes a sharp peak in $|\Psi|$ at the tropopause independent of β-effect and shear variation. This peak is approximately equal to the peak at the ground. The latter is narrower for $\gamma_T \neq 0$; this also was observed by Green (1960). Variation in SR has negligible effect when $\sigma_\rho = 50$, but when $\sigma_\rho = 1$, larger values of $|\Psi|$ occur around the tropopause as SR goes to negative values (Figures 3.6 and 3.7). The Green mode, existing only for $\gamma_T \neq 0$, $\sigma_\rho \neq 1$ has a strong peak in the stratosphere which moves up from 180 mb to 120 mb as the stratospheric shear reverses.

Streamfunction phases are constant throughout the upper layer when $\gamma_T = 0$ or $\sigma_\rho = 1$. When there is both a β-effect and a stratosphere, the pressure wave tilts westward with height in the stratosphere for both Eady and Green modes, the Green mode having a much greater tilt. In the troposphere the Green mode also has a greater westward tilt.

For quasi-geostrophic disturbances, a westward tilt of the wave with height means entropy is transported poleward (Lorenz, 1951). The model calculations of $\overline{v'\theta'}$, Figures 3.9 to 3.12, illustrate this property for the fastest growing Eady and Green modes: all tilts are westward and all $\overline{v'\theta'}$ values are positive. When there is no β-effect $\overline{v'\theta'}$ is independent of σ_ρ and SR values and is zero in the upper layer, reflecting the constancy of phase there. In the presence of both a stratosphere and a β-effect, entropy transports are significant in the stratosphere, for both modes. The Green mode has a much stronger stratospheric transport. It peaks at the tropopause and remains large in the lower stratosphere. The

flux is strongest for the case of reversed shear. Thus, nominal conditions produce modes which have larger stratospheric heat transports than all the other cases considered.

A local maximum in the entropy flux in the lower stratosphere is observed (Oort and Rasmusson, 1971; Newell et al., 1974). Thus, the Green mode could be very important for lower stratospheric dynamics. This problem will be addressed in more detail in the next chapter.

Except for the Green mode with uniform shear (SR = 1), no modes have kinetic energy generated in the upper layer (see Figures 3.13 to 3.16). Only this Green mode and an Eady mode with no stratosphere and SR = 1 have their kinetic energy destroyed in any region of the lower layer. In all cases there is, of course, a net generation of mode kinetic energy when the entire model atmosphere is considered. And in all cases, there is a net mode kinetic energy generation in the troposphere and net loss in the stratosphere. The maximum mode kinetic energy generation is in the mid to low troposphere for all cases except the Green mode with reversed stratospheric shear. This latter mode has its strongest kinetic energy generation in the upper troposphere.

Earlier discussion pointed out that for no stratosphere and uniform shear there was apparently no Green mode for $\gamma_T = 0$ or 2, and there were no unstable modes for SR = 1, $\sigma_\rho = 1$ and $\gamma_T = 0$. Is there a Green mode for a stronger β effect? What happens to it for small β? These questions are answered by a graph (Figure 3.17) similar to Green's (1960) figure 3 with the difference that Green's rigid lid is replaced by $\psi' = 0$ at $p = 0$.*

---

* Differences between this graph and Green's Figure 3 are discussed with the $\omega' = 0$ at $p = 0$ calculation later in this chapter.

The Green mode is seen to exist for large β-effect (or small tropospheric shear, u_0) but is very weak, and its wavelength becomes infinite as γ_T or $\bar{q}_y = \beta$ goes to zero. Also, as γ_T or $\bar{q}_y$ goes to zero, growth rate per unit γ_T remains constant so that the growth rate approaches zero with γ_T or $\bar{q}_y$.

When SR and σ_p have their nominal values, and γ_T varies, the situation is much different (see Figure 3.18). The fastest growing Eady mode growth rate changes little as $\gamma_T \propto \bar{q}_y$ goes to zero, and the Green mode is much stronger and is at a shorter wavelength for $\gamma_T < 10$.

3.5 Results for variation of one parameter with others fixed at nominal values

In this section two parameters are held at their nominal values and the third varies over a wide range of parameter space. Doubling times and phase velocities are obtained for zonal wave numbers 0 to 15, and vertical structures of wave properties are presented for the fastest growing Green and Eady modes. Shorter modes are trapped near the ground and are outside the stratospheric focus of this thesis (Chapter IV illustrates properties of these waves for realistic $\bar{T}$ and $\bar{U}$ profiles).

Figures 3.19 to 3.21 show that the doubling time of the fastest growing Green mode is much more sensitive to parameter variation than is the doubling time of the fastest growing Eady mode. The wave numbers of the most unstable Green and Eady modes are not very sensitive to the variation of SR and σ_p but increase markedly as γ_T increases. This increase of most unstable mode wavenumber with γ_T was pointed out earlier (see Figures 3.17 and 3.18). As SR takes on values from -12 to 4, the Green mode remains constant in strength for reversed shear in the stratosphere but be-

comes much weaker for large positive SR. The Eady mode, however, becomes slightly stronger and the wavelength for which it is most unstable slightly increases with SR throughout its range. For values of σ_ρ between 1 and 1000, the Green mode has its fastest doubling time, 6 days, near the nominal value, $\sigma_\rho = 50$ (intermediate calculations, not shown, refines this value of σ_ρ to be 60). As γ_T varies from 0 to 10 there is a dramatic decrease in the Green mode's fastest doubling time - from 12 days ($\gamma_T = 1$) to 3 days ($\gamma_T = 10$). The wavenumber of the fastest growing Green mode increases from 2.0 to 7.5. Thus, at high γ_T the Green mode is no longer long-wave. Green (1960) has shown that longer waves are expected to have longer doubling times because they only weakly satisfy the necessary condition for instability, viz., that particle paths have an average slope between that of the isentropes and the horizontal. Green's heuristic argument was for rigid lids at top and bottom. To the extent that a 50-fold increase in the static stability approximates a rigid lid, one can say that the Green mode grows slower at lower γ_T when $\Psi' = 0$ in the upper boundary conditions because it is at a longer wavelength.

The phase velocities, shown in Figures 3.22 to 3.24, all have a sharp minimum at the wavenumber which, by definition, separates the Green and Eady modes. The Green mode is defined to include all wavenumbers less than that of the sharp minimum in the phase velocity. There are other, weaker minima in some of the phase velocity curves. These are found to be associated with weak minima (which may not be resolved) in the doubling time curves. Phase velocities are most strongly influenced by changes in γ_T. For all wavelengths, phase velocities decrease with increasing γ_T. And, for all wavenumbers and parameter combinations of this section (except SR

< -2), the unstable modes have a single steering level in the lower troposphere. For a strongly reversed stratospheric shear (SR < -2) some modes have an additional steering level in the stratosphere.

Streamfunction amplitudes and phases for the fastest growing Eady and Green modes are presented in Figures 3.25 to 3.36. The structure of the Eady mode amplitude in the troposphere is little affected by varying SR and σ_ρ (except when $\sigma_\rho \cong 1$). Peaks of the pressure amplitude occur at the ground and tropopause. The peaks are of approximately equal value and the one at the tropopause decays less rapidly into the stratosphere for small σ_ρ, when $\sigma_\rho \geq 10$. When γ_T begins to increase beyond 3, the tropopause peak begins to weaken substantially. Stratospheric Eady mode pressure amplitudes are largest when γ_T is near its nominal value.

The Green mode has larger streamfunction amplitudes in the stratosphere than the Eady mode for all parameter combinations of this section. Figures 3.8 and 3.28 through 3.30 show that the Green mode's amplitude peaks higher in the stratosphere, and has larger values there (relative to those of other levels) when the parameters are near their nominal values. The peak, for near nominal parameter values, occurs at 120 mb, and the amplitude remains greater than half the peak value from below the tropopause to 30 mb. For $\gamma_T \geq 7$, there are pressure amplitude peaks at the tropopause and 75 mb which are separated by a sharp minimum at 140 mb (see Figure 3.30). The upper peak is weaker and has a value of .7 times the tropopause peak value. The Green mode also has a peak at the ground which is as strong as the peak in the stratosphere when $\sigma_\rho \leq 10$ or SR ≤ -4. In comparison with that of the Eady mode, the vertical structure of the Green mode's pressure

amplitude is much more sensitive to variations of SR or σ_p . The same was seen to be true regarding the doubling times of the Eady and Green modes, and, as subsequent figures illustrate, the same is also true for the vertical structure of mode phase, meridional entropy transport and kinetic energy generation. The larger amplitude of the Green mode at stratospheric levels renders it more sensitive to variations of SR and σ_p , which are really variations in the stratospheric shear and static stability because γ_T is held constant.

The phase of the Eady mode streamfunction varies much less with height than does the phase of the Green mode (Figures 3.31 to 3.36). Except for the case of a very stable stratosphere, $\sigma_p \geq 1000$, the Eady mode pressure wave has only a slight westward tilt with height. The tilt of the Green mode is very strongly westward with height and is most strongly westward when γ_T or σ_p are large or when SR $\cong$ -4. The Green mode has its most rapid vertical phase variation concentrated in a region just above the tropopause (100-250 mb) and in the lower troposphere (550-750 mb). The phase can change 180° in these regions. The Green mode and, at a slower rate, the Eady mode vertical wavelength approaches zero in the stratosphere as $\sigma_p \longrightarrow \infty$. Amplitudes of both modes also approach zero in the stratosphere as $\sigma_p \longrightarrow \infty$ and are negligible for $\sigma_p > 1000$.

The meridional entropy transports, $\overline{v'\theta'}$, of both modes (Figures 3.37 to 3.42) are all poleward, as expected for quasi-geostrophic waves which tilt westward with height. The stratospheric transports are generally very weak for the Eady mode (in comparison to the tropospheric transports) except when the stratospheric shear is easterly (SR < 0), but even these

transports are far shallower than those of the Green mode in the lower stratosphere. Tropospheric Eady mode $\overline{v'\theta'}$ values are little affected by changes in SR and σ_ρ, but as γ_T increases, they decrease rapidly at all levels except near the ground. The entropy transports of the Green mode in the lower stratosphere are generally stronger than those in the troposphere except for transports near the ground when SR is positive, $\sigma_\rho \leq 10$, or $\gamma_T \geq 7$. The stratospheric Green mode fluxes are countergradient and are strongest when the parameters are near their normal values. They have their strongest peak at the tropopause and remain at greater than half the peak value up to 130 mb. Stratospheric Green mode $\overline{v'\theta'}$ values are weakest for SR positive or $\sigma_\rho \leq 10$.

The generation of mode kinetic energy for both Eady and Green modes occurs only in the troposphere except for the Green mode when SR > 0 (see Figures 3.43 to 3.48). In this unique case there is a weak, shallow region above the tropopause where Green mode kinetic energy is generated. The generation of Eady mode kinetic energy is stronger in the lower and mid-troposphere (except for $\gamma_T = 10$; in this case alone there is a weak destruction of mode kinetic energy in a region of the troposphere). The generation of Eady mode kinetic energy is affected only slightly by variations of SR or σ_ρ; however, the generation decreases rapidly as γ_T increases. The generation of Green mode kinetic energy when SR $\leq$ 0, $\sigma_\rho \neq 10$, or $\gamma_T < 7$ is nearly constant throughout the troposphere except near the ground where it goes to zero with ω; when SR > 0, $\sigma_\rho = 10$, or $\gamma_T \geq 7$, there is a mid-tropospheric destruction of Green mode kinetic energy. The strongest Green mode kinetic energy generation is always in the lower troposphere. In summary, the strongest generation of both Eady and Green mode kinetic energy

is in the troposphere. Therefore, both modes are tropospheric in origin. They drive the stratosphere, i.e. they lose kinetic energy in that region and build up zonal available potential energy there with counter-gradient entropy fluxes when SR < 0. The Green mode has much stronger and deeper stratospheric entropy transports and kinetic energy losses in comparison to its tropospheric values of these quantities than does the Eady mode. It is also a (zonally) longer wave mode and can, according to Gall (1976) more easily penetrate into the stratosphere. Therefore, the Green mode could be of much greater importance to lower stratospheric dynamics than the Eady mode.

3.6 Results for constant γ_T planes in parameter space

This section explores a much wider expanse of parameter space. It focuses on the growth rate of the most unstable Eady and Green modes and discusses properties of their vertical structure which may be of importance to the general circulation at specific levels of the atmosphere. It also ascertains whether any new modes appear in the range of parameter space which it covers. Parameter space of this model has 4 dimensions represented by γ_T, SR, σ_ρ, and P. The value of the wavenumber P is always chosen to be that of a local maximum in the curve of growth rate vs P. The remaining 3 dimensions are sampled by examining planes of constant γ_T at γ_T = .5, 2, and 6. On these planes, σ_ρ varies from 1 to 1000 and SR varies from 14 or 0 to -14, depending on the value of γ_T and the mode presented.

The doubling time of the fastest growing Eady mode is contoured on the constant γ_T planes in Figures 3.49 to 3.51. On all planes there is only a slight variation of doubling time with SR and σ_ρ when $\sigma_\rho > 20$; and

the variation is even slighter for larger γ_T. Most doubling times are between 1.5 and 2.0 days. There is a lengthening of doubling time to 3 or 4 days for small σ_ρ and $|SR| > 10$. As seen in the previous section, wavenumbers of the most unstable Eady mode increase with γ_T. When γ_T is not large, they also increase as σ_ρ approaches 1 and SR becomes large and negative. When $\sigma_\rho > 20$ they vary little with SR and σ_ρ. The wavenumber will typically double from SR = -2 to SR = -10 ($\sigma_\rho = 2$, $\gamma_T = .5$ or 2); it will also double from $\sigma_\rho = 50$ to $\sigma_\rho = 2$ (SR = -14, $\gamma_T = .5$ or 2) with the most rapid increase at the smallest values of σ_ρ. On the $\gamma_T = 2$ plane, the most unstable wavenumber is between 6 and 7 for $\sigma_\rho > 20$ and is near 15 for SR < -8 and $\sigma_\rho \leq 2$.

The fastest-growing Green mode undergoes a much less smooth variation of doubling time with SR and σ_ρ (Figures 3.52 to 3.54). It is much shorter for higher γ_T, independent of the values of SR and σ_ρ. On all the γ_T planes, the fastest doubling times are when σ_ρ is small and SR is large and negative; this is the same region where the Eady mode is weakest. The longest doubling times occur for small σ_ρ and SR going positive. For $\gamma_T = .5$ or 2 there is a region of shorter doubling times for nominal and larger values of σ_ρ and SR near -2. The nominal point (SR = -1.5, $\sigma_\rho = 50$, $\gamma_T = 2$) occurs in a local region of shorter doubling times whose values are about 6 days. The $\gamma_T = 2$ plane shows the most complicated variation of Green mode doubling time with SR and σ_ρ. This, in part, could be due to the difficulty in defining a fastest growing Green mode when there is no minimum of growth rate between the Green and Eady modes (see the SR = -4 curve in Figure 3.19). In this case, a point .6 zonal wavenumbers to the left of the point of greatest curvature was chosen to be the wavenumber of the fastest growing Green mode (e.g. 3.6 was chosen as the wavenumber of the fastest growing Green mode on the SR = -4 curve of Figure

3.19). In all cases there was a minimum in the phase velocity curve which separated the Green and Eady modes, and the point of greatest curvature of the doubling time curves was always on the long-wave (Green mode) side of this minimum. The wavenumber of the most unstable Green mode varies with the parameters in a manner similar to that of the Eady mode. On the $\gamma_T = 2$ plane the wavenumber is between 3 and 4 when $\sigma_\rho > 20$ and is near 8 when SR < -10 and $\sigma_\rho < 5$.

Much of what was discussed in the previous section about the Eady and Green mode vertical structure also holds true for the much larger expanse of parameter space considered in this section. Exceptions are presented below.

Stratospheric Green mode $|\psi|$ values are weaker when $\gamma_T < 2$. The Eady mode peak values of $|\psi|$ at the ground and tropopause are equal except when $\sigma_\rho < 10$ or $\gamma_T > 3$; then the tropopause peak becomes weaker. The peaks of the Green mode streamfunction amplitude are at the ground and in the lower stratosphere with the latter being much stronger except (1) when $\sigma_\rho < 15$ and SR < 0, and (2) when $\gamma_T = .5$ and SR is large and negative. The stratospheric peak of the Green mode amplitude is strongest when parameters are all near their nominal values, and when $\gamma_T = 6$ with SR and σ_ρ near their nominal values.

The streamfunction phases of the Eady mode and Green mode behave as described in the previous section, except when $\gamma_T = 6$ and $-8 < SR < -2$. In this case the phase varies about twice as rapidly for both modes.

The stratospheric $\overline{v'\theta'}$ peak of the Green modes is weak when $\sigma_\rho < 20$. It is strongest when parameters are near their nominal values and also when $\gamma_T = .5$ or 6; SR is near its nominal value, and $\sigma_\rho \geq 30$.

The previous discussion of this section has centered on the Eady and Green modes. For the parameter value combinations considered in earlier sections of this chapter, there was only one conjugate unstable eigenvalue for each wavenumber; this contained the Eady and Green modes. The mean flow in all previous sections possessed no zeros of $\overline{q}_y$. Therefore, the unstable eigenvalue containing the Eady and Green modes owed its existence to a temperature gradient at the ground.

In this section one has the possibility of an internal zero of $\overline{q}_y$ helping to satisfy the necessary condition for instability. This zero may occur only at the boundary between the two layers ($p = \frac{1}{4}$). The value of $\overline{q}_y$ for the simple profiles of this chapter is easily obtained, as $\overline{u}_{pp}$, σ_y, σ_p are all zero except at the internal boundary where there is a jump in $\overline{u}_p$ and σ. Thus, everywhere except at $p = \frac{1}{4}$, $\overline{q}_y = \beta$. There is a δ-function in $\overline{q}_y$ at $p = \frac{1}{4}$, so $\overline{q}_y$ goes through a zero at $p = \frac{1}{4}$ if

$$\left[\frac{1}{\sigma}\overline{u}_p\right]_{\frac{1}{4}=p} > 0$$

where $[\quad]_{1/4}$ denotes the jump in $\frac{1}{\sigma}\overline{u}_p$ across $p = \frac{1}{4}$. In terms of the parameters describing the profiles, this means:

$$SR < \sigma_p \quad \text{if } \overline{u}_p > 0 \text{ for } p > \tfrac{1}{4}$$

$$\overline{u}_p \Big|_{p<\frac{1}{4}} < 0 \quad \text{if } \overline{u}_p = 0 \text{ for } p > \tfrac{1}{4}$$

$$SR > \sigma_p \quad \text{if } \overline{u}_p < 0 \text{ for } p > \tfrac{1}{4}$$

The case with $\overline{u}_p = 0$ in the lower layer was applied to the underside of the polar night jet by Murray (1960) and Simmons (1972). The condition $SR > \sigma_p$ is applicable to the profiles of the present model. Since the upper layer

of the present model is assumed to be more stable than the lower layer, ($\sigma_\rho > 1$), for there to be an internal zero of $\overline{q}_y$, the shear in the upper layer must therefore be more westerly than that of the lower layer (SR $>$ 1). This does not represent the situation at the earth's tropopause but does approximate conditions just beneath the polar night jet.

Both Simmons and the author find that an unstable conjugate eigenvalue is associated with the zero of $\overline{q}_y$ caused by discontinuities in $\overline{u}_p$ and σ. It occurs only when SR $> \sigma_\rho$ for all values of γ_T. For the present model the eigenvalue is not well determined, even for 48 levels. The difficulty is in resolving a mode whose strongest amplitude and $\overline{v'\theta'}$ values are concentrated in a very shallow region around the internal boundary. Results for 48 levels when γ_T = 2, SR = 10, σ_ρ = 5 give doubling times of about one week for wavenumber 8, and a vertical decay scale (from the internal boundary) of about 40 mb. The phase speed is westerly at 30 m/sec which places the steering level at 225 mb. Simmons' doubling times are slightly longer than a week and his vertical decay scale is only a few kilometers. The pressure wave of the mode tilts very slightly westward with height; the total phase change from p = 0 to the ground is .1 radians. Essentially all of the mode's kinetic energy is generated at the internal boundary. This mode will be referred to as the "internal boundary mode".

3.7 Calculations for $\omega' = 0$ at P = 0

In the discussion of numerical accuracy (Chapter II), it was pointed out that the fastest growing Eady mode growth rate and vertical structure was not affected by changing the upper boundary condition from $\Psi' = 0$ to

$\omega' = 0$ if a nominal stratosphere was present. A comparison of Figures 2.6 and 3.17 shows that this is far from the case if there is no stratosphere (SR = 1, $\sigma_p = 1$). These two figures' results are calculated from identical assumptions, except for the upper boundary condition. The Eady mode, instead of changing little with γ_T (for $\omega' = 0$ at $p = 0$), becomes stable as $\gamma_T \longrightarrow 0$ when $\psi' = 0$ at $p = 0$. Also, when $\psi' = 0$ at $p = 0$, the Green mode's wavenumber approaches zero as γ_T decreases below 3, and the mode becomes very weak (the doubling time is longer than 60 days). This compares with a zonal wavenumber of 2.5 for small γ_T and a doubling time of 20 days for the $\omega' = 0$ at $p = 0$ calculations. When nominal values of the parameters are assumed, the fastest growing Green mode's doubling time is twice as long when $\omega' = 0$ at the top. This contrasts with the small effect on the Eady mode when the upper boundary condition is changed and a nominal stratosphere is present.

The streamfunction amplitude of the Eady and Green mode for the case of no stratosphere, SR = 1, and $\omega'|_{p=0} = 0$, both had peak values at the bottom and top of the model atmosphere; the peaks were of equal value (see Green, 1960, Figures 5 and 6). Forcing $\psi' = 0$ at the top placed a severe constraint on these modes, causing their growth rates to be much smaller.

On the other hand, for nominal values of σ_p and γ_T, and SR = -1.5, 0, or 1, the fastest growing Eady mode streamfunction amplitude went to zero at the top for both upper boundary conditions, and the mode's growth rate was unchanged (to within 2%). For the same parameter values, however, the fastest growing Green mode amplitude peaks, which occur in the lower stratosphere (Figure 3.8), are replaced by a node in that region and 2 peaks near

the top and at the tropopause when the upper boundary condition is changed to $\omega' = 0$ (see Figure 3.55). The effect is analogous to what happens when one gets spurious reflections; the effect results in the doubling of the Green modes' doubling time (sic.). For the case using $\omega' = 0$ at P = 0, the fastest growing Green mode has a weak region of kinetic energy generation within 15 mb of the top.

When $\omega' = 0$ at p = 0 and one parameter value is varied and the others are held at their nominal value, one finds that for $\gamma_T = 3$, $\sigma_p > 40$, or $-3 < SR < -1$ the same behavior analogous to reflection and destructive interference occurs. For the Green modes at other parameter values, the change in the upper boundary condition from $\omega' = 0$ to $\Psi' = 0$ lowers the level of the $|\Psi|$ peak from the top down to the mid stratosphere; the growth rate of these Green modes are substantially reduced.

For all parameter combinations where $\gamma_T \neq o$ and $\sigma_p > 10$, the meridional entropy transport for the Green and Eady modes is not strongly affected by changing the upper boundary condition. The transports are very weak near p = 0 for both modes and both boundary conditions.

The kinetic energy loss in the upper stratosphere for the Green mode is smaller when $\omega' = 0$ at p = 0. Green mode kinetic energy loss or generation is little affected at other levels. The kinetic energy loss or generation for the Eady mode is unaffected by changing the upper boundary condition.

A new type of mode appears for $\omega'|_{p=0}$ when there is a stratosphere and when SR > the nominal value (compare Figures 3.19 and 3.56). The wavenumber of its growth rate peak for γ_T and σ_p nominal varies from zonal wavenumber 4 to wavenumber 1 as SR increases from -1 to 30; the value of the

fastest doubling time remains constant at $4\frac{1}{2}$ days, as does the steering level (800 mb). The streamfunction amplitude peaks at the top and decreases as a linear function of pressure to about 10% as much at the tropopause. It remains close to this value below the topopause. The wave tilts westward with height. Entropy transports are everywhere poleward and are especially strong in the lower stratosphere; the peak flux is at the tropopause. Mode kinetic energy is destroyed in the lower stratosphere but is generated everywhere else with greatest generation in the troposphere. The mode is only present when the temperature gradient at the upper boundary is able to play a role in fulfilling the necessary condition for instability.

A second conjugate pair of eigenvalues (one eigenvalue of each pair represents an unstable mode) exists when $SR < 0$ and $\omega' = 0$ at $p = 0$ (see Figure 3.57). When $\psi' = 0$ was the upper boundary condition, there was only one conjugate unstable eigenvalue solution to the model's differential equation except for the internal boundary mode which exists when $SR > \sigma_\rho$. This new solution for $\omega' = 0$ at $p = 0$ exists only when the temperature gradient at the top boundary is positive (warmer toward the poles). The new solution has growth rates which exceed those of the other solution (which contains the Eady and Green modes) when the Richardson number of the upper layer is less than that of the lower layer. The ratio of the two Richardson numbers (upper/lower) equals σ_ρ / SR^2. Thus, $\sigma_\rho < SR^2$ is the condition for dominance of the new solution; as illustrated by Figure 3.58. It can also be seen from Figure 3.58 that the doubling times of the fastest growing mode of the new solution decreases quickly with R_i of the upper layer. The zonal wavenumber of the fastest growing mode ranges from 3 when $SR = -14$, $\sigma_\rho > 40$, and $\gamma_T = 2$ to 9 when $SR < -3$, $\sigma_\rho = 2$, $\gamma_T = 2$. Phase velocities

are large and easterly; at $\gamma_T = 2$, SR = -8 and $\sigma_p = 50$, the phase velocity of the most unstable mode is -28 m/sec. The phase velocity becomes more negative as SR becomes more negative so that steering levels remain around 50 mb. Streamfunction amplitudes peak at the top and decrease rapidly toward the tropopause where they are approximately 30% as large. In the troposphere, the amplitude gradually decreases to a value of 20% (of the peak value) at the ground. The phases show a strong eastward tilt of the pressure wave with height in the stratosphere, a very slight eastward tilt just below the tropopause and a slight westward tilt in the troposphere. The phase change in the stratosphere is about $\pi/2$ radians. Correspondingly the entropy transports are strong and equatorward in the stratosphere, weak and equatorward in the upper troposphere, and weak and poleward in the lower troposphere. There is a strong generation of mode kinetic energy in the stratosphere with the greatest generation being at the steering level. Mode kinetic energy is lost in the troposphere but in a smaller amount.

The picture of this new conjugate eigenvalue that emerges is one of a mode which is generated in the stratosphere and "drives" the upper troposphere (through a loss of its kinetic energy) with weak counter-gradient entropy fluxes. In a general sense, its properties mirror those of the Eady mode: It is destabilized by a temperature gradient at the opposite boundary and drives the upper troposphere instead of the lower stratosphere.

The internal boundary mode described earlier undergoes substantial changes in growth rate and vertical structure when the upper boundary condition changes to $\omega' = 0$. Its doubling time for the most unstable mode is extremely short when $\omega' = 0$ at p = 0, and becomes much shorter when SR $\gg \sigma_p$. When γ_T, SR, σ_p = 2, 10, 5, the doubling time is only 3/4 of a day and the

zonal wavenumber is 5. Unlike the situation when $\psi' = 0$ at p = 0, the eigenvalue is well resolved for the $\omega' = 0$ upper boundary condition. The difficulty of resolving a mode whose pressure amplitude has a single very sharp peak has been removed; the pressure amplitude now peaks at the top and decreases only gradually to a value of 30% (of the peak value) at the 250 mb internal boundary. The amplitude in the lower layer gradually decreases to a value of .15 (of the peak value) near the ground. The phase speed and steering level are about the same as for the $\Psi' = 0$ upper boundary condition: 30 m/sec and 225 mb, respectively. The entropy transports are strongest in the bottom of the upper layer, peaking at the internal boundary; they are poleward (down gradient) and do not decrease to half the peak value until 120 mb. There are weak equatorward transports in the upper part of the lower layer, and weak poleward transports near the ground. The eddy kinetic energy is generated in a region just above the internal boundary and destroyed in a region just below it, just like the new conjugate mode described above.

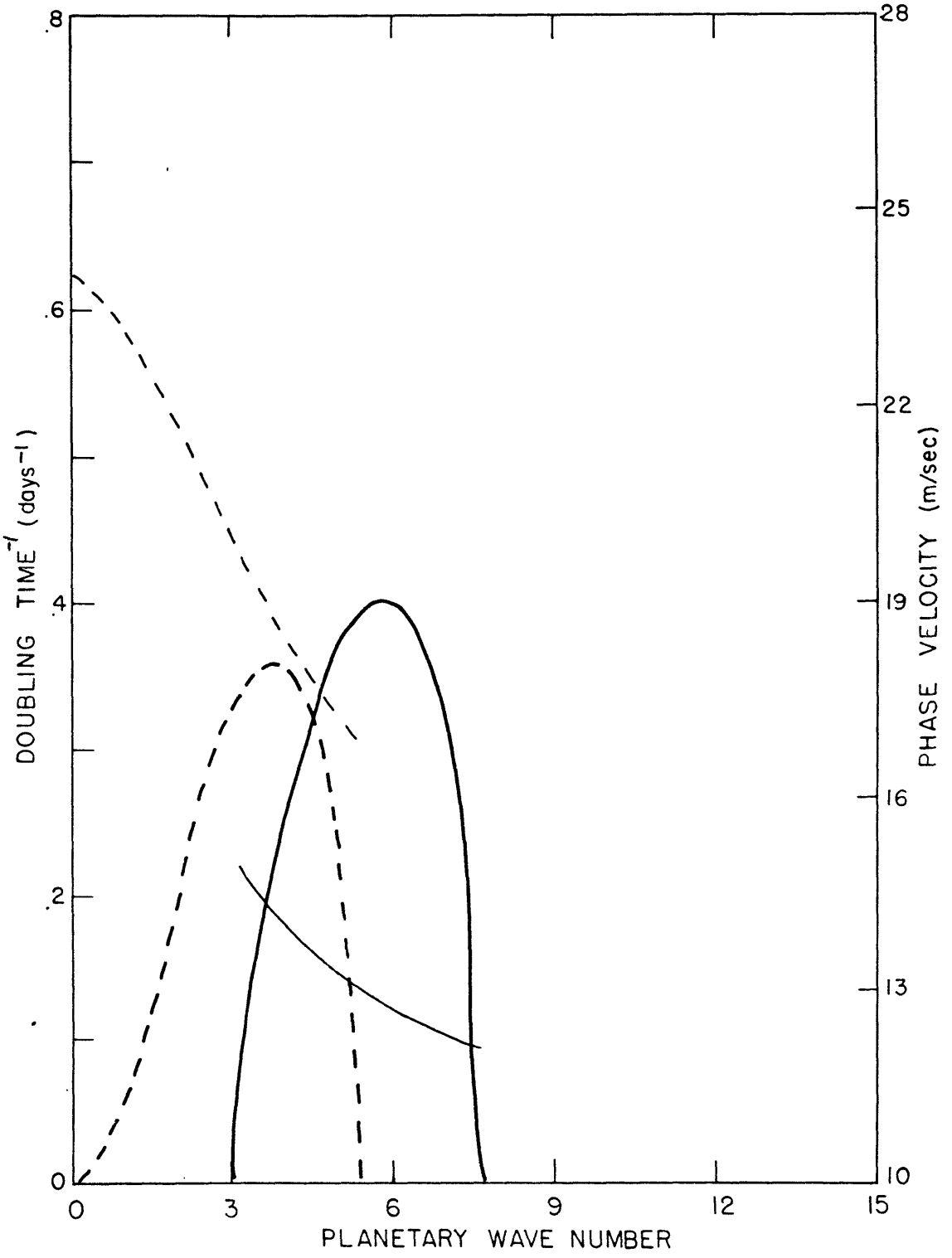

Figure 3.1. Doubling time^{-1} (thick lines) and phase velocity (thin lines) vs. wavenumber for $\gamma_T = 0$, $\sigma_0 = 1$, and SR = 0 (dash), and SR = -1.5 (solid).

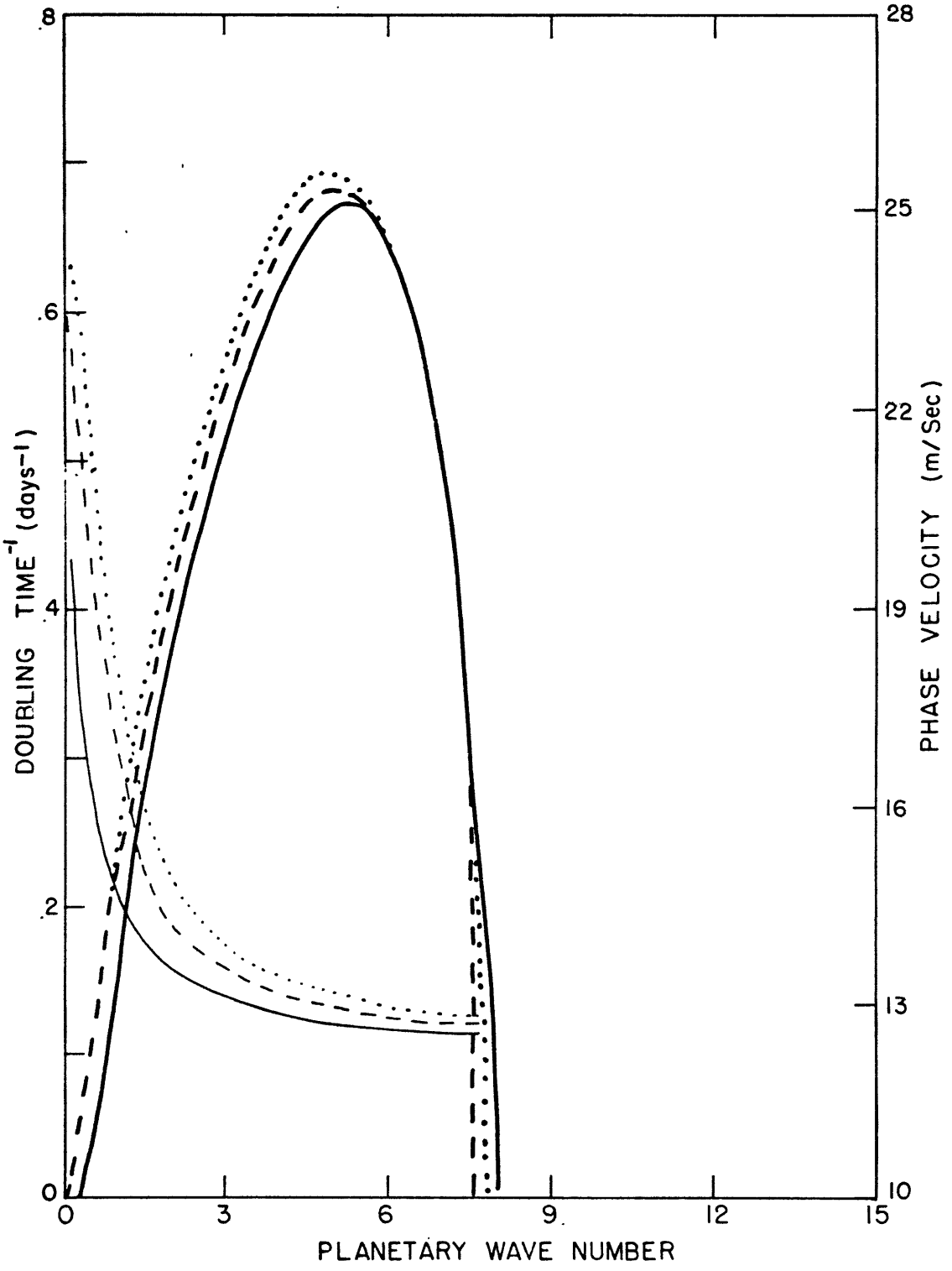

Figure 3.2. As in Figure 3.1, for $\gamma_T = 0$, $\sigma_\rho = 50$, and SR = -1.5 (solid), 0 (dash), and 1 (dot).

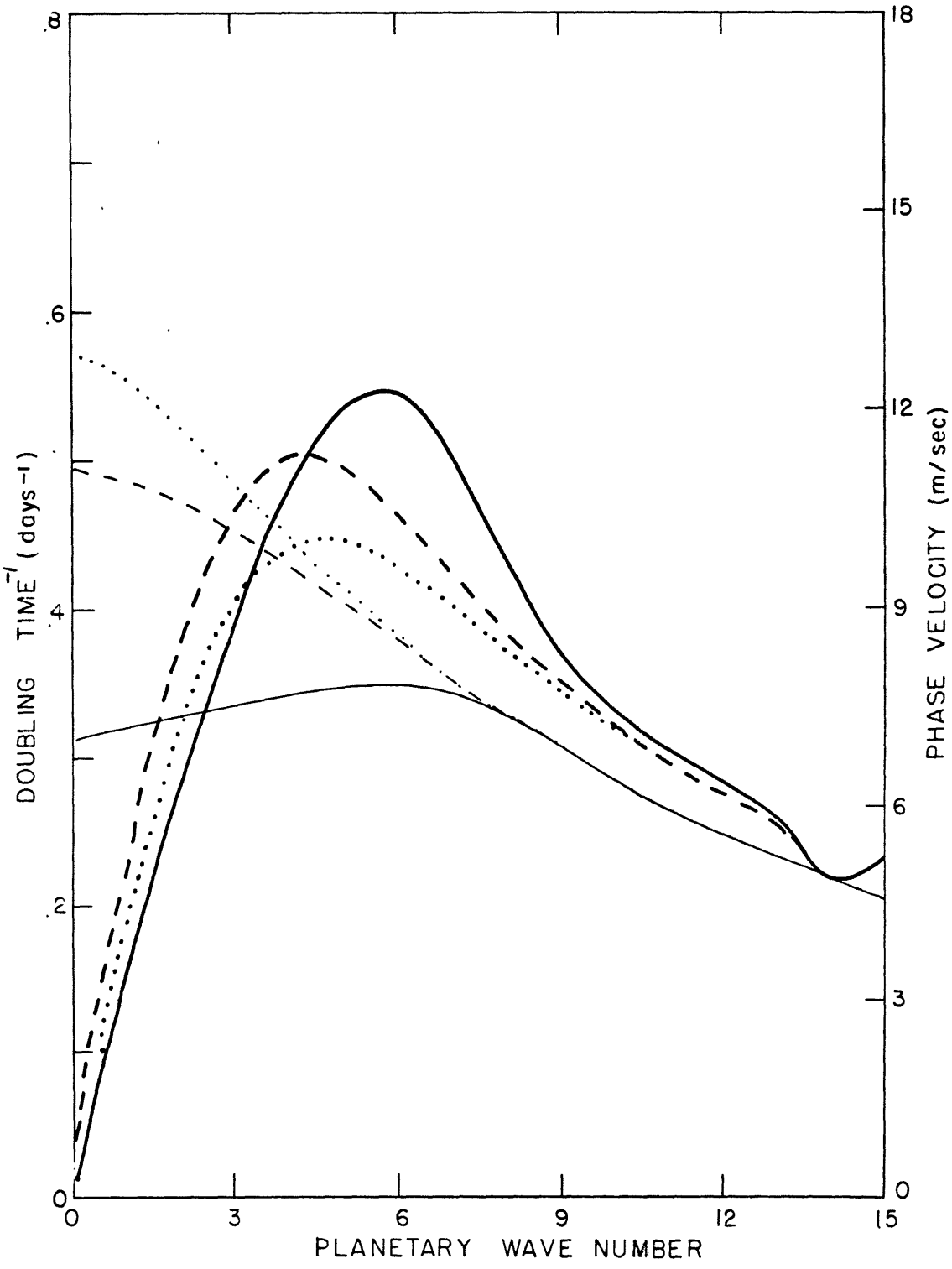

Figure 3.3. As in Figure 3.1, except: $\gamma_T = 2$, $\sigma_\rho = 1$, and SR = -1.5 (solid), 0 (dash), and 1 (dot).

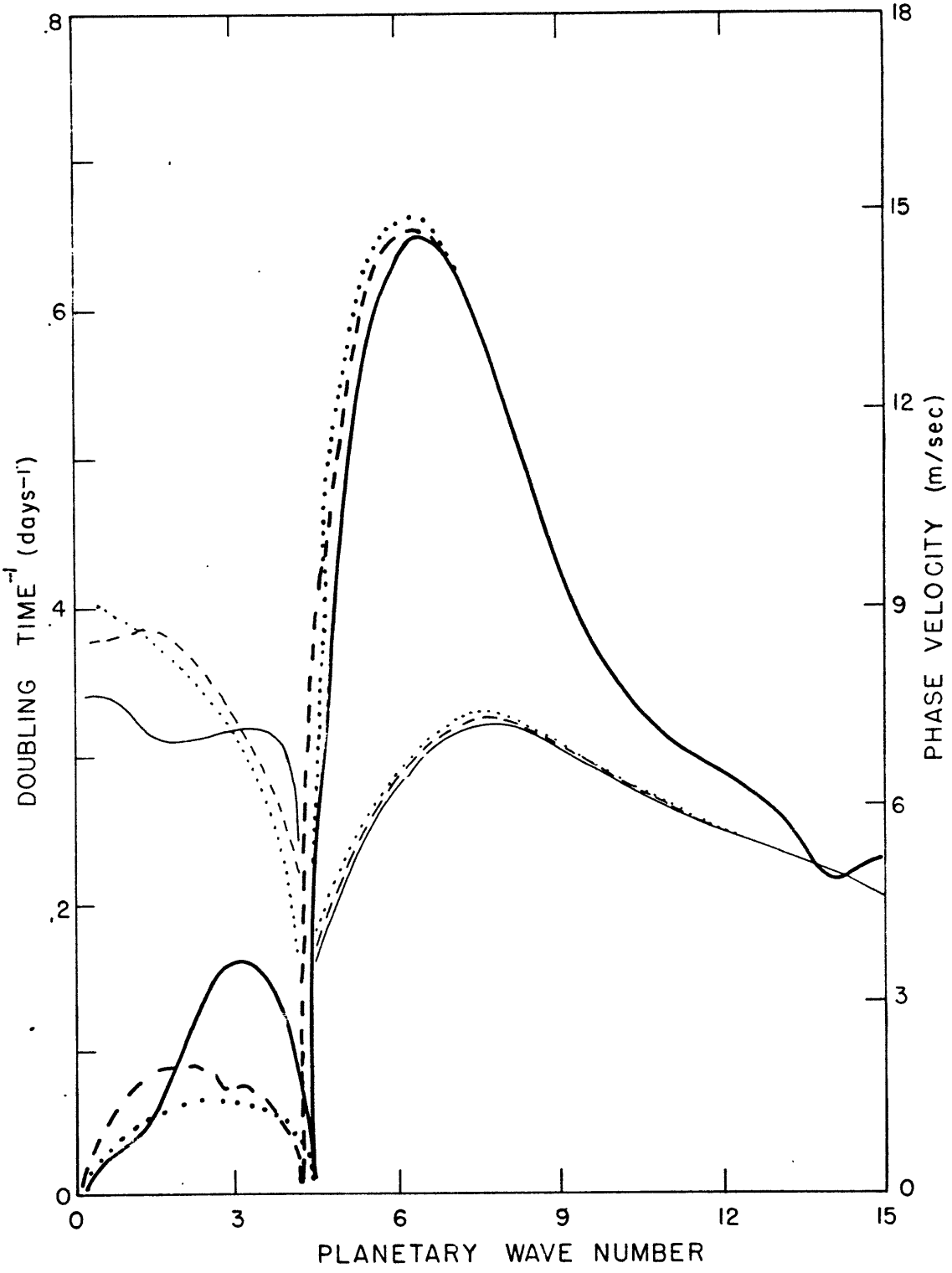

Figure 3.4. As in Figure 3.1, except: $\gamma_T = 2$, $\sigma_\rho = 50$, and SR = -1.5 (solid), 0 (dash), and 1 (dot).

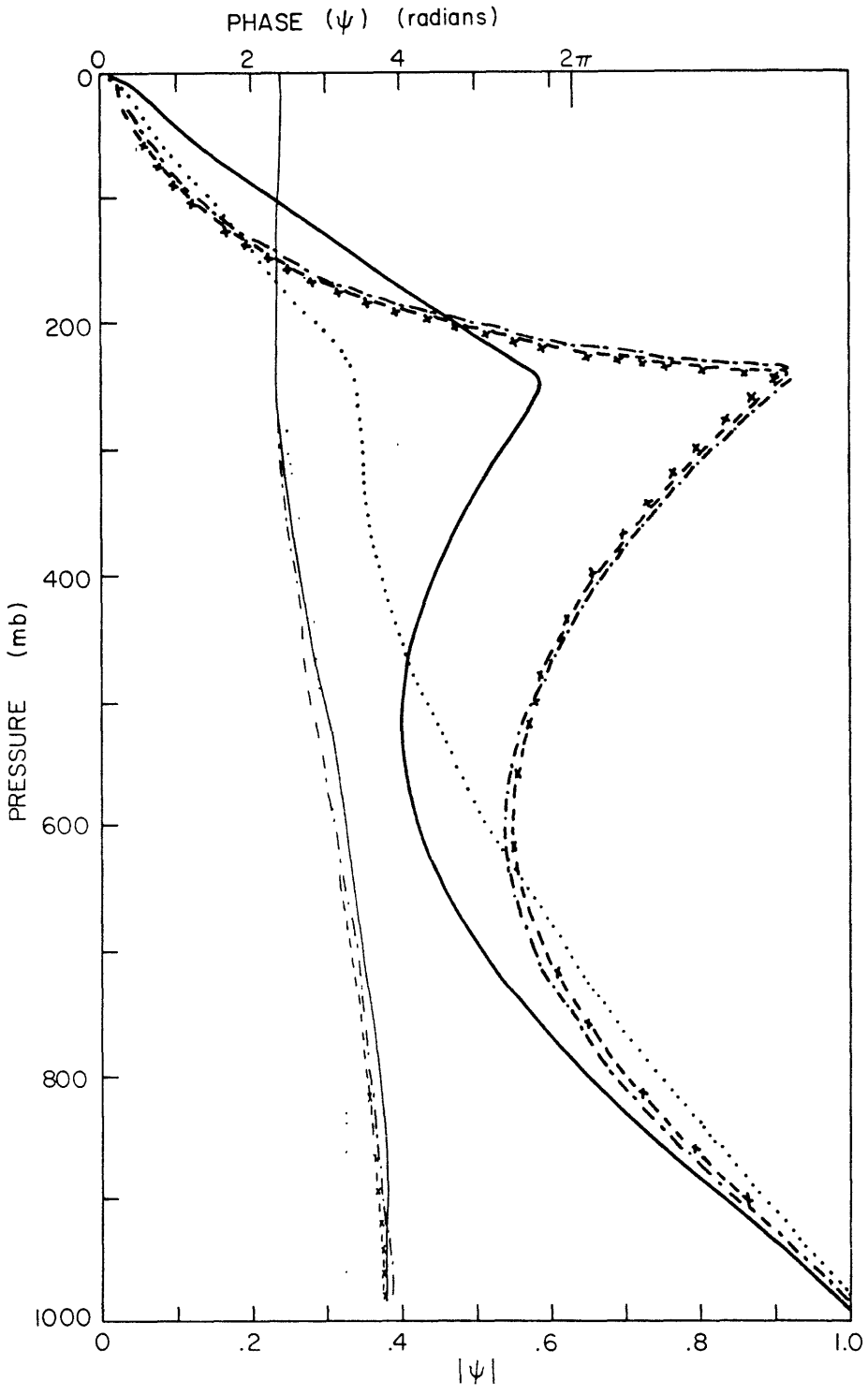

Figure 3.5. Vertical structure of the streamfunction amplitude (thick lines) and phase (thin lines) for the fastest growing Eady mode, $\gamma_T = 0$, and: $\sigma_\rho = 1$, SR = -1.5 (solid); $\sigma_\rho = 1$, SR = 0 (dot); $\sigma_\rho = 50$, SR = -1.5 (dash dot); $\sigma_\rho = 50$, SR = 0 (dash); and $\sigma_\rho = 50$, SR = 1 (cross).

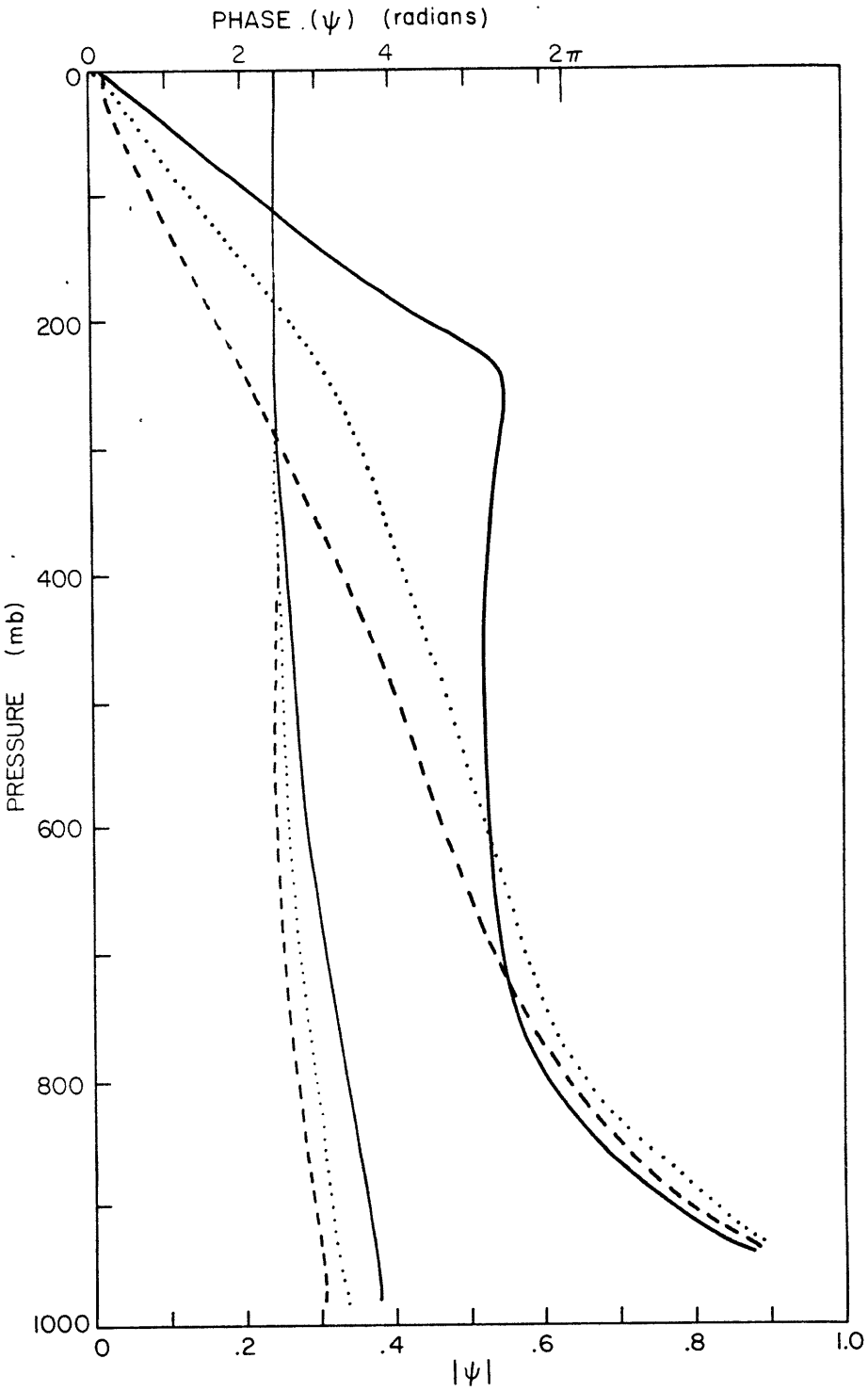

Figure 3.6. As in Figure 3.5, for γ_T = 2, and SR = -1.5 (solid), 0 (dot), and 1 (dash)

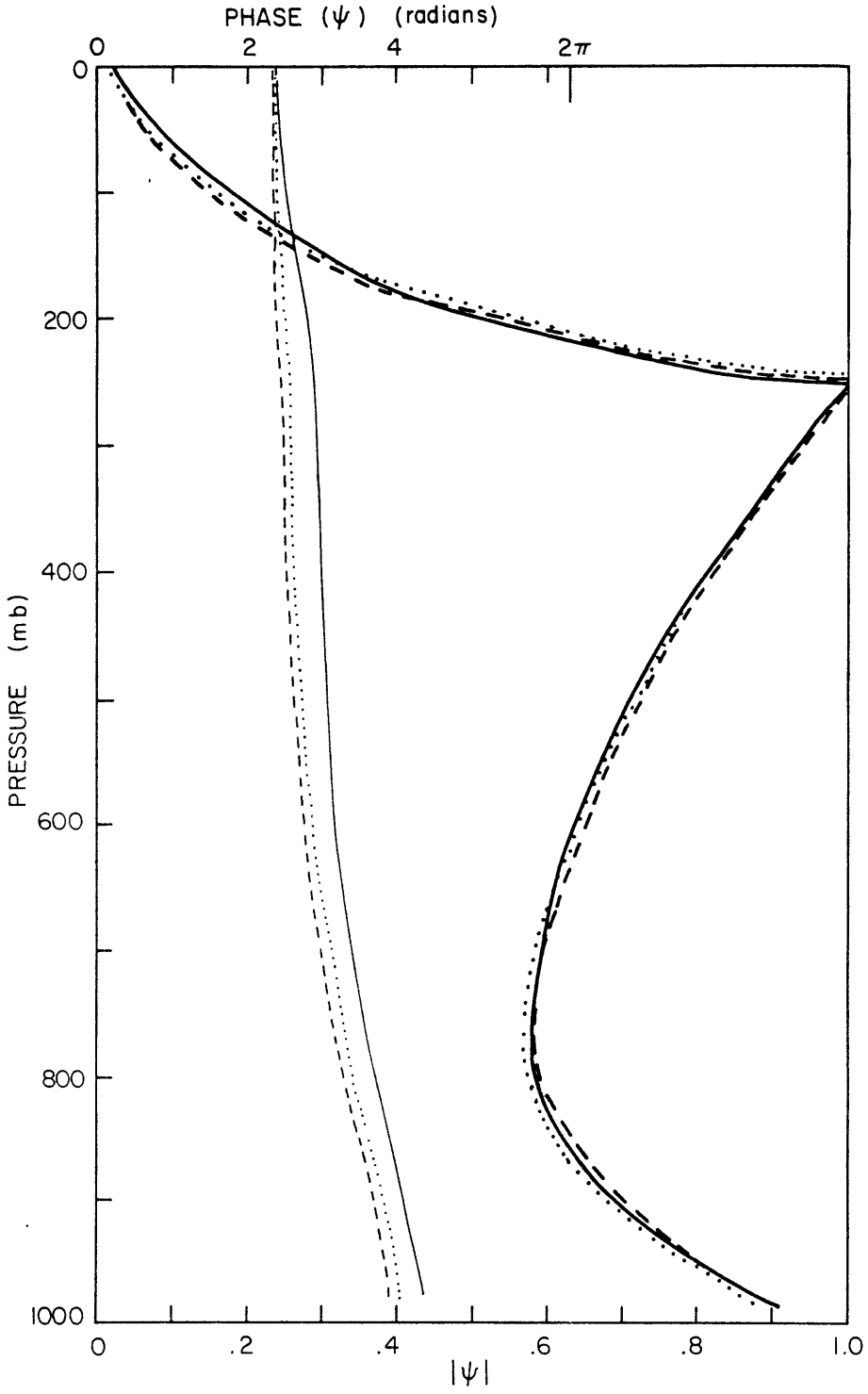

Figure 3.7. As in Figure 3.5, for $\gamma_T = 2$, $\sigma_\rho = 50$, and SR = -1.5 (solid), 0 (dot), and 1 (dash).

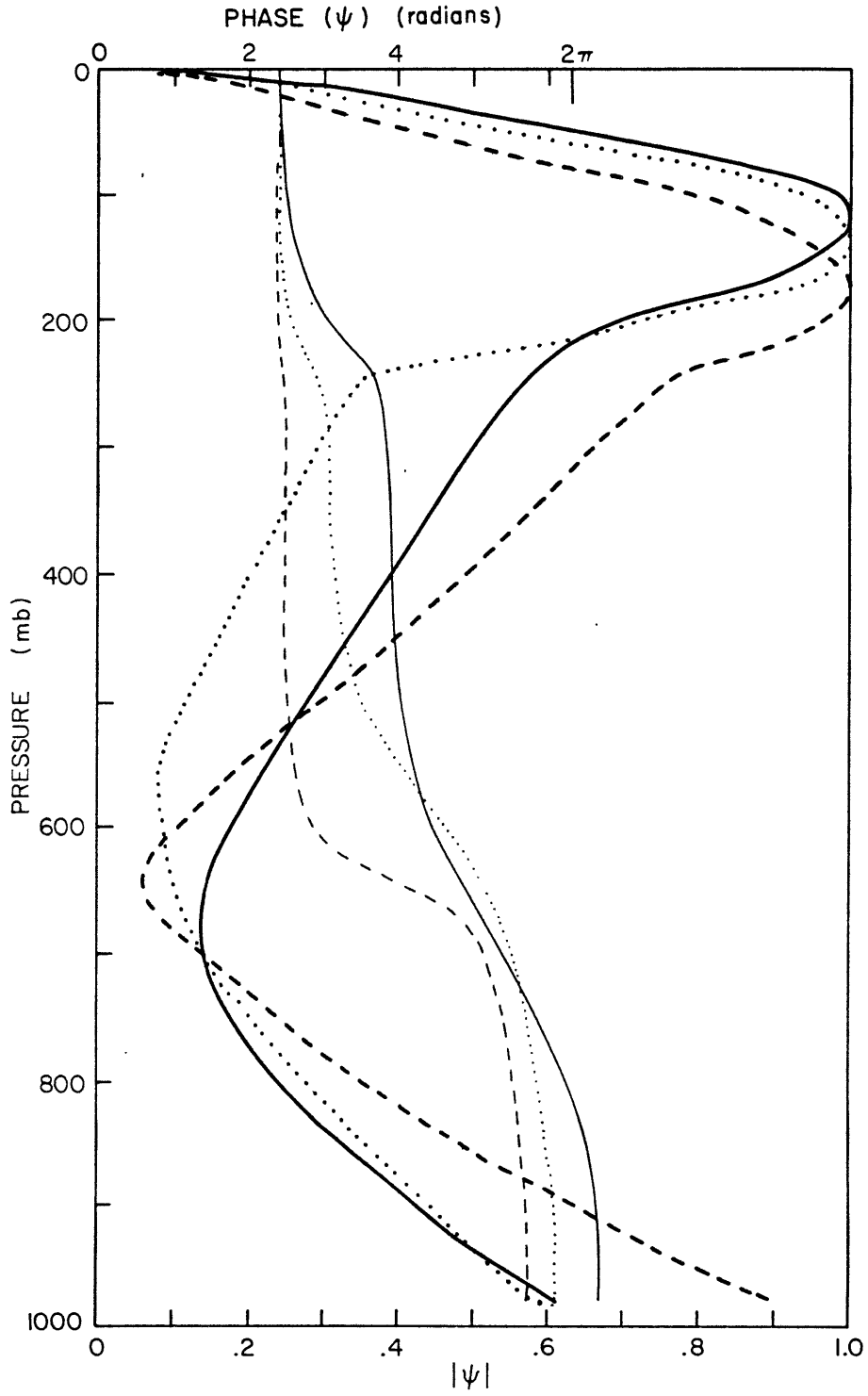

Figure 3.8. Vertical structure of the streamfunction amplitude (thick lines) and phase (thin lines) for the fastest growing Green mode, $\gamma_T = 2$, $\sigma_0 = 50$, and SR = -1.5 (solid), 0 (dot), and 1 (dash).

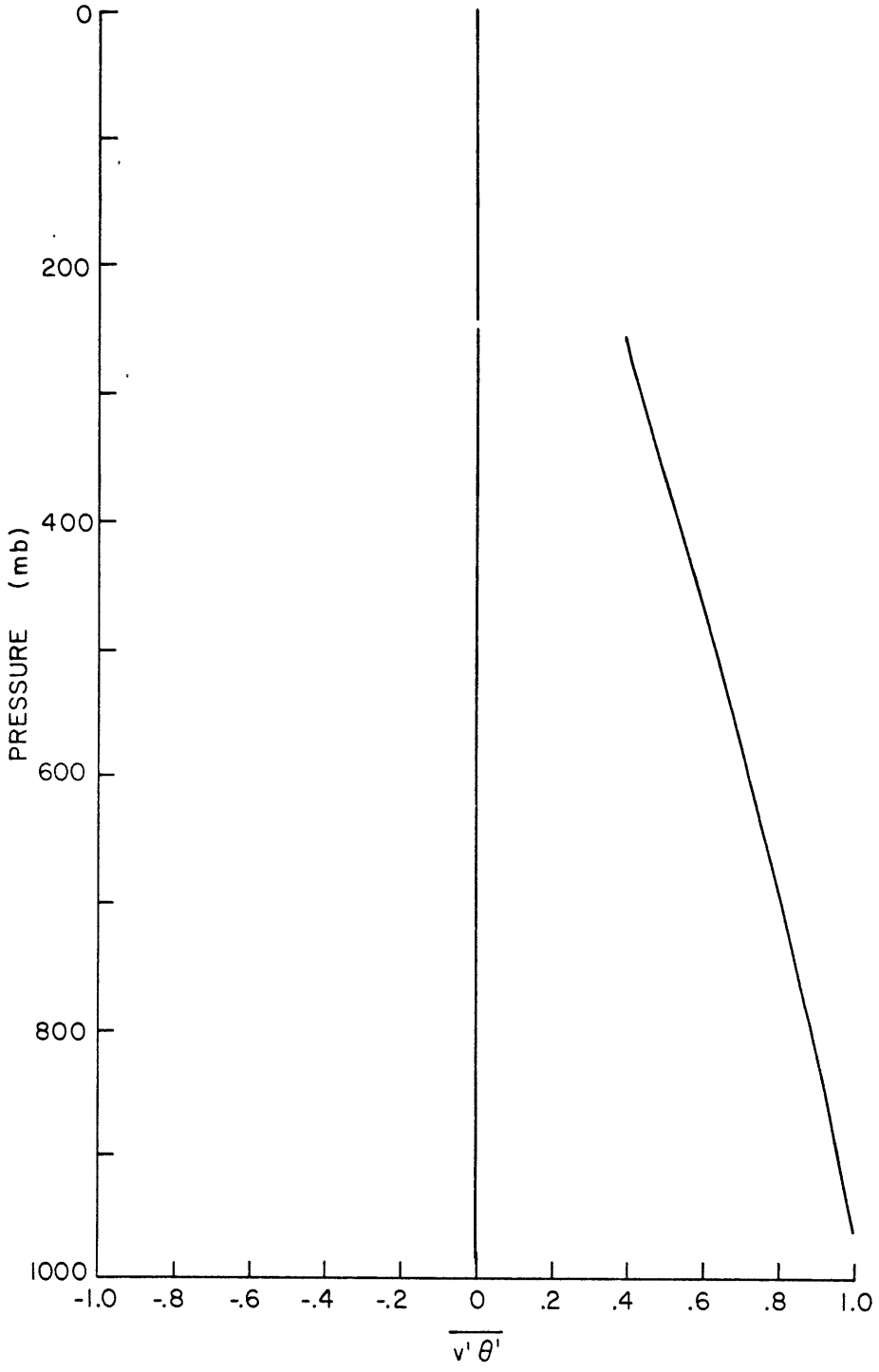

Figure 3.9. Vertical structure of the meridional entropy transport for the fastest growing Eady mode for the same cases as in Figure 3.5. Note, all curves are identical.

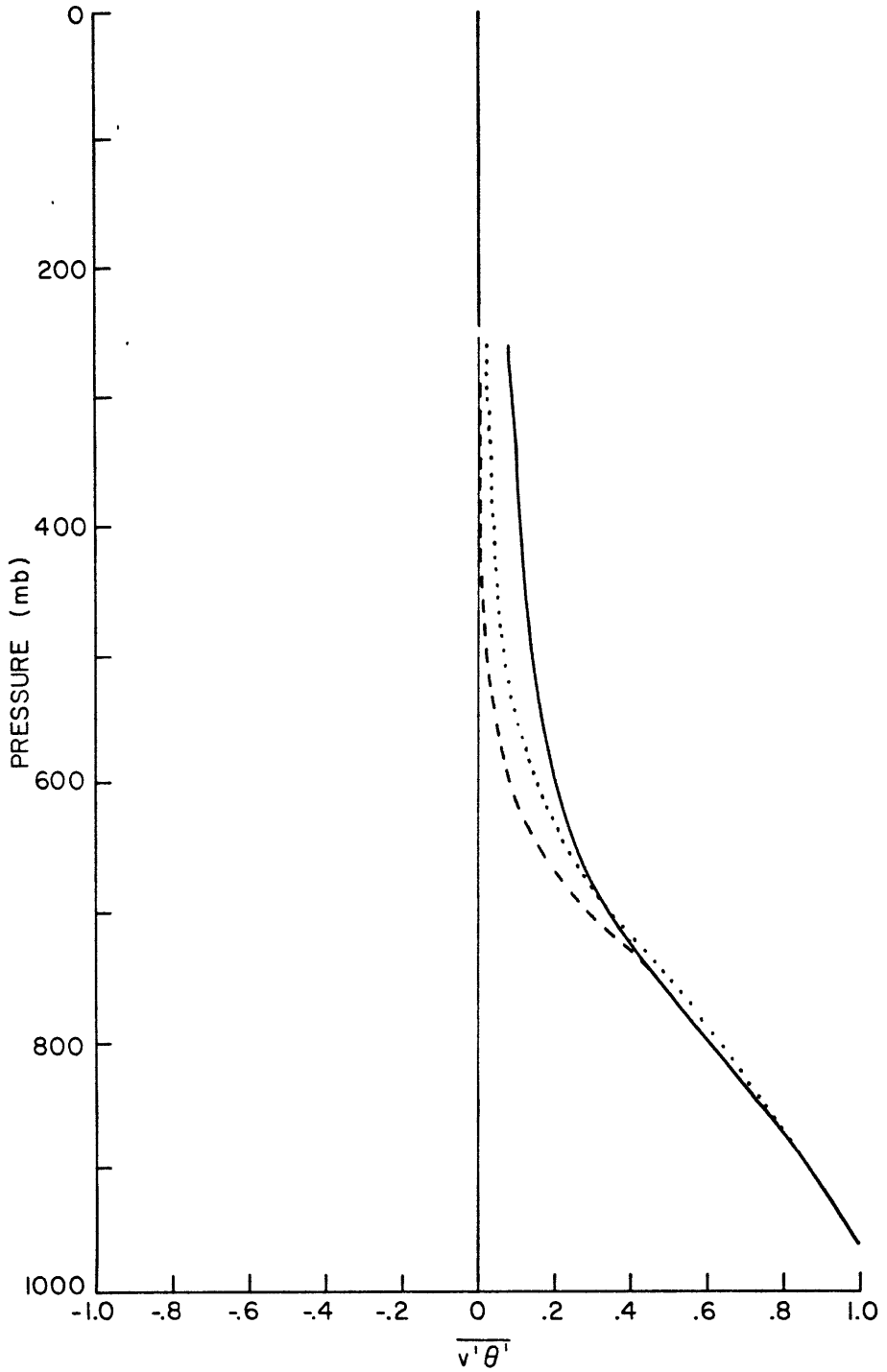

Figure 3.10. As in Figure 3.9, for the cases: $\gamma_T = 2$, $\sigma_\rho = 1$, and SR = -1.5 (solid), 0 (dot), and 1 (dash). All curves are zero above 250 mb.

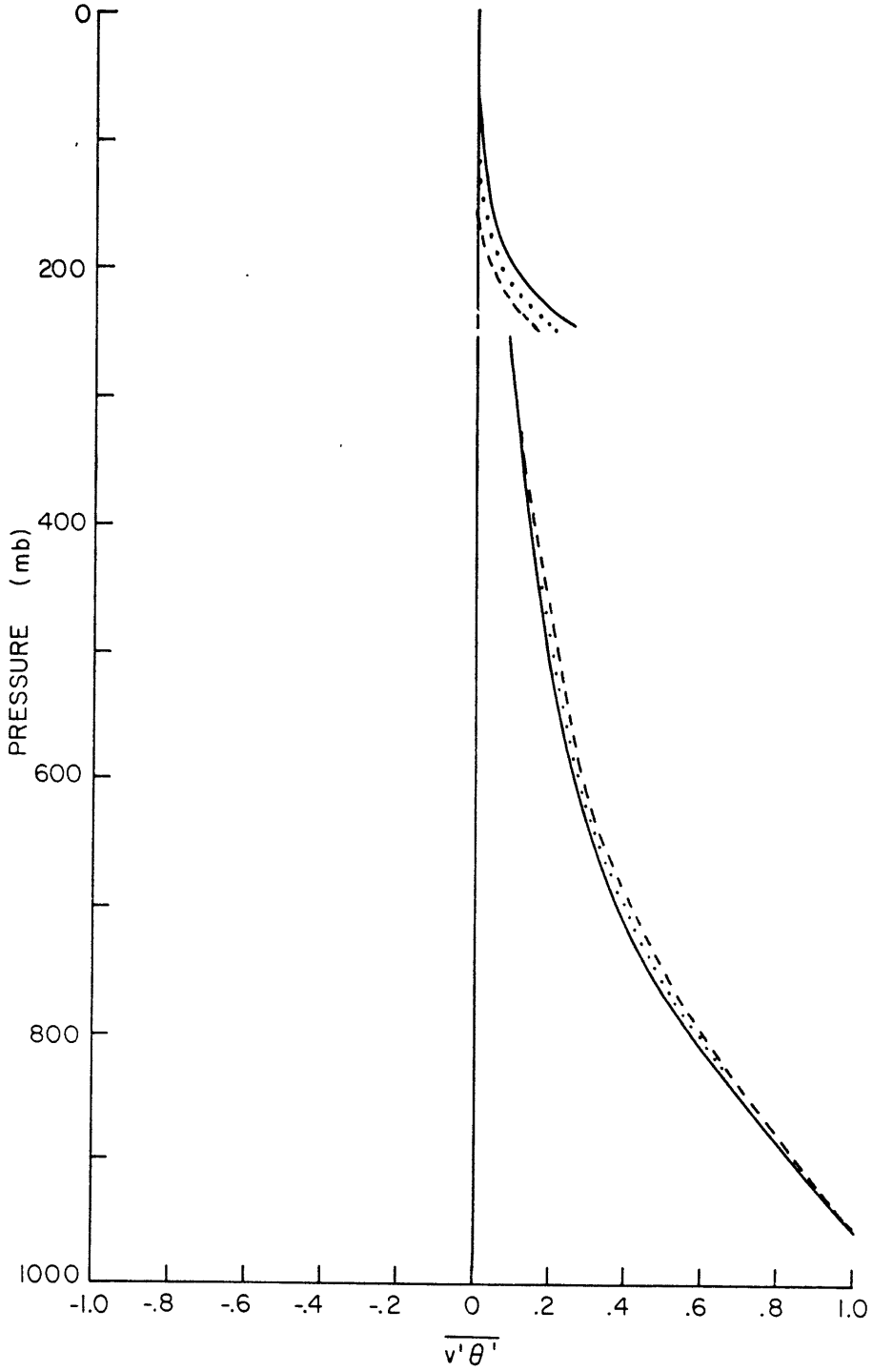

Figure 3.11. As in Figure 3.9, for $\gamma_T = 2$, $\sigma_\rho = 50$, and SR = -1.5 (solid), 0 (dot), and 1 (dash).

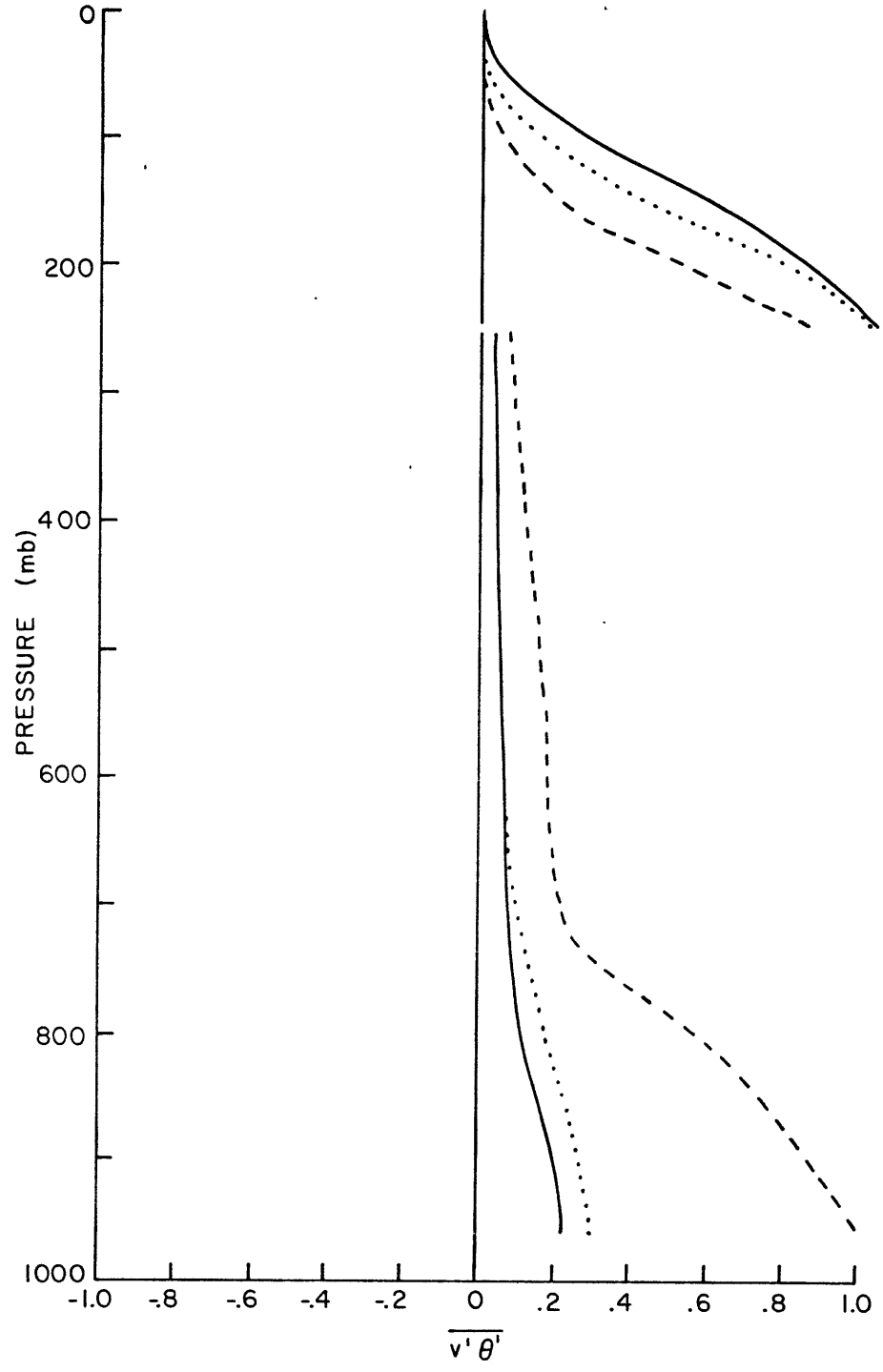

Figure 3.12. Vertical structure of the meridional entropy transport for the fastest growing Green mode for same cases as in Figure 3.8.

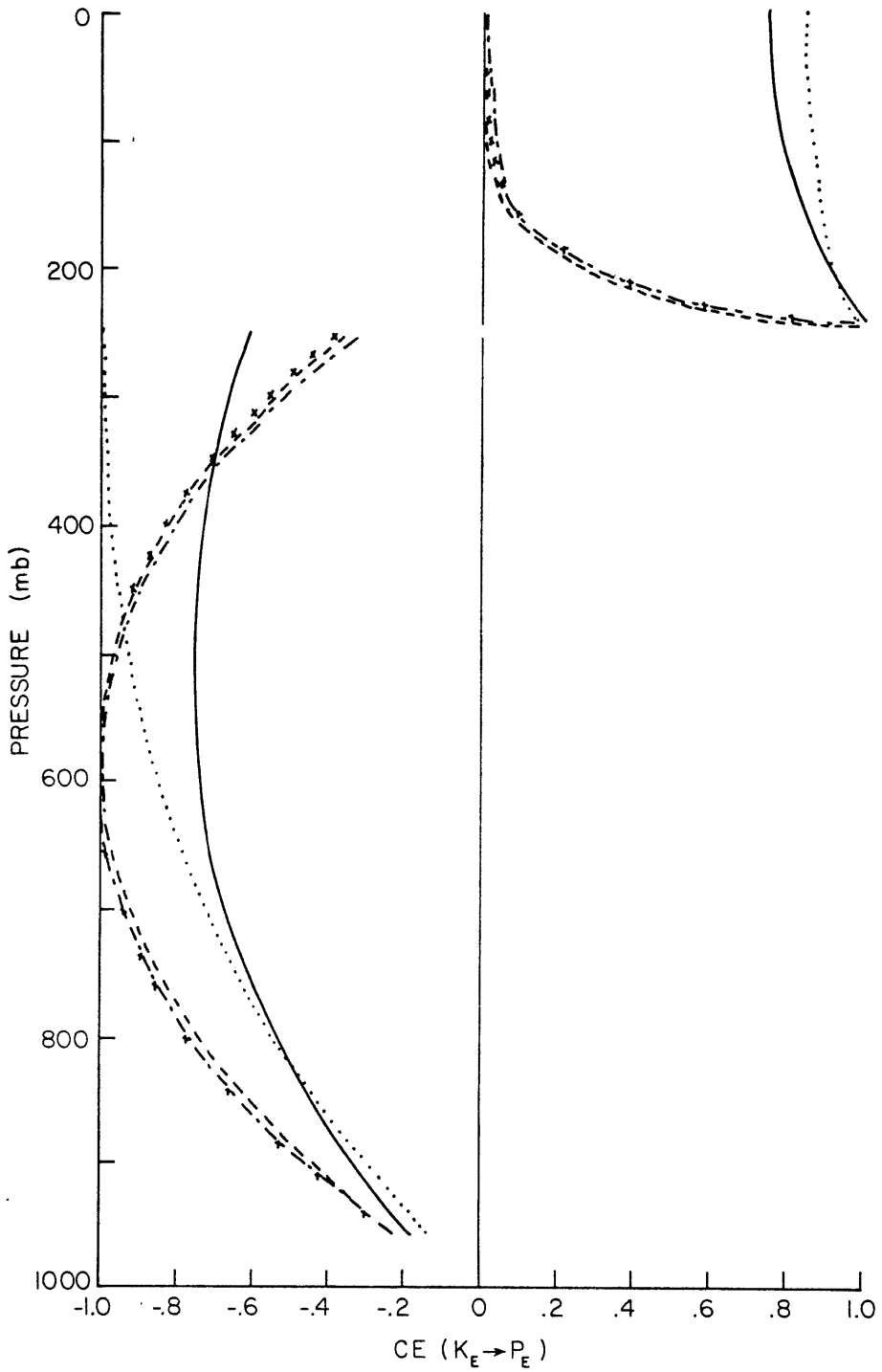

Figure 3.13. Vertical structure of the transfer of eddy kinetic to eddy available potential energy ($K_E \rightarrow P_E$ is positive), for the fastest growing Wady mode for the same cases as in Figure 3.5.

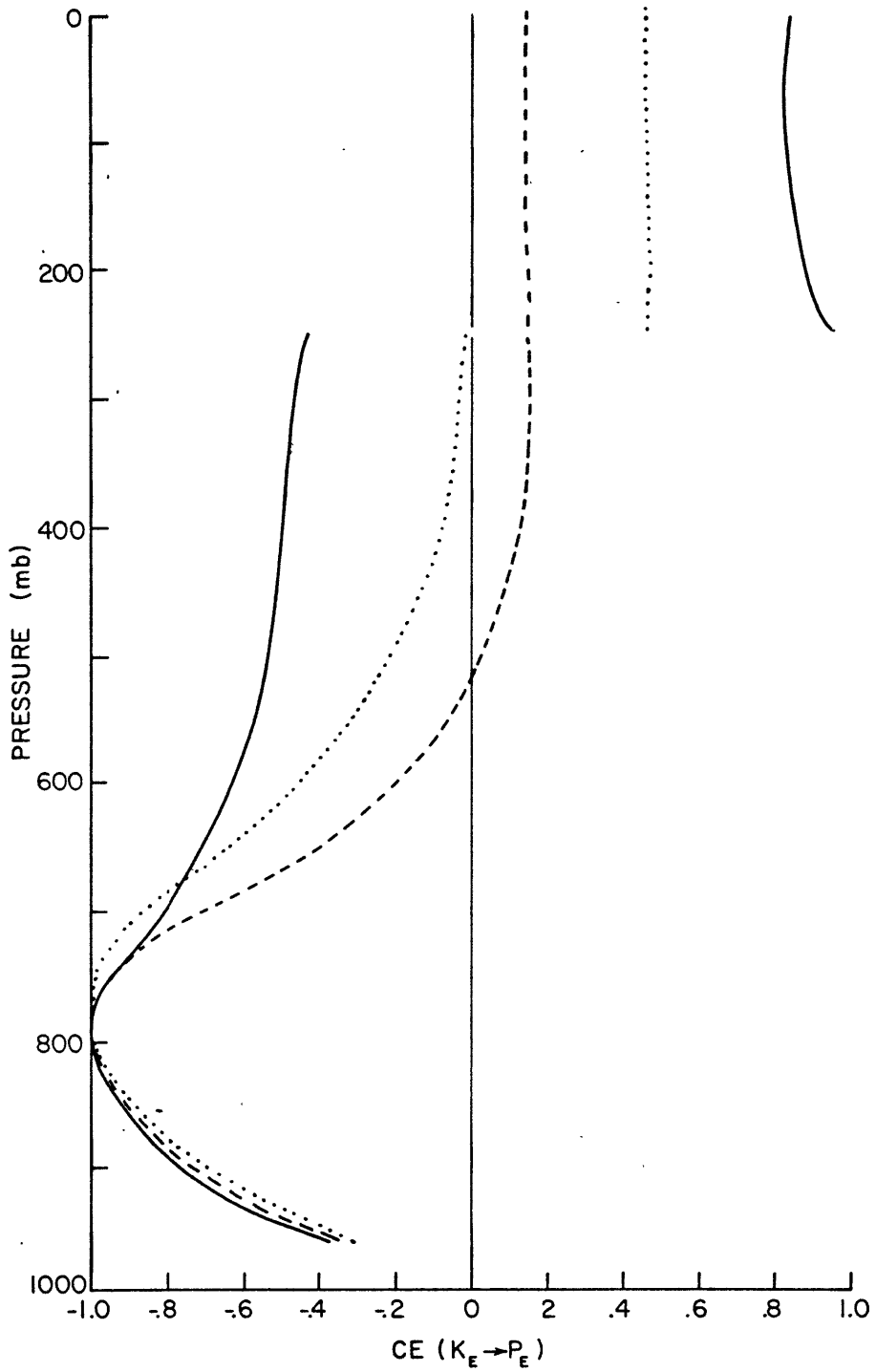

Figure 3.14. As in Figure 3.13, for the cases $\gamma_T = 2$, $\sigma_\rho = 1$, and SR = -1.5 (solid), 0 (dot), and 1 (dash).

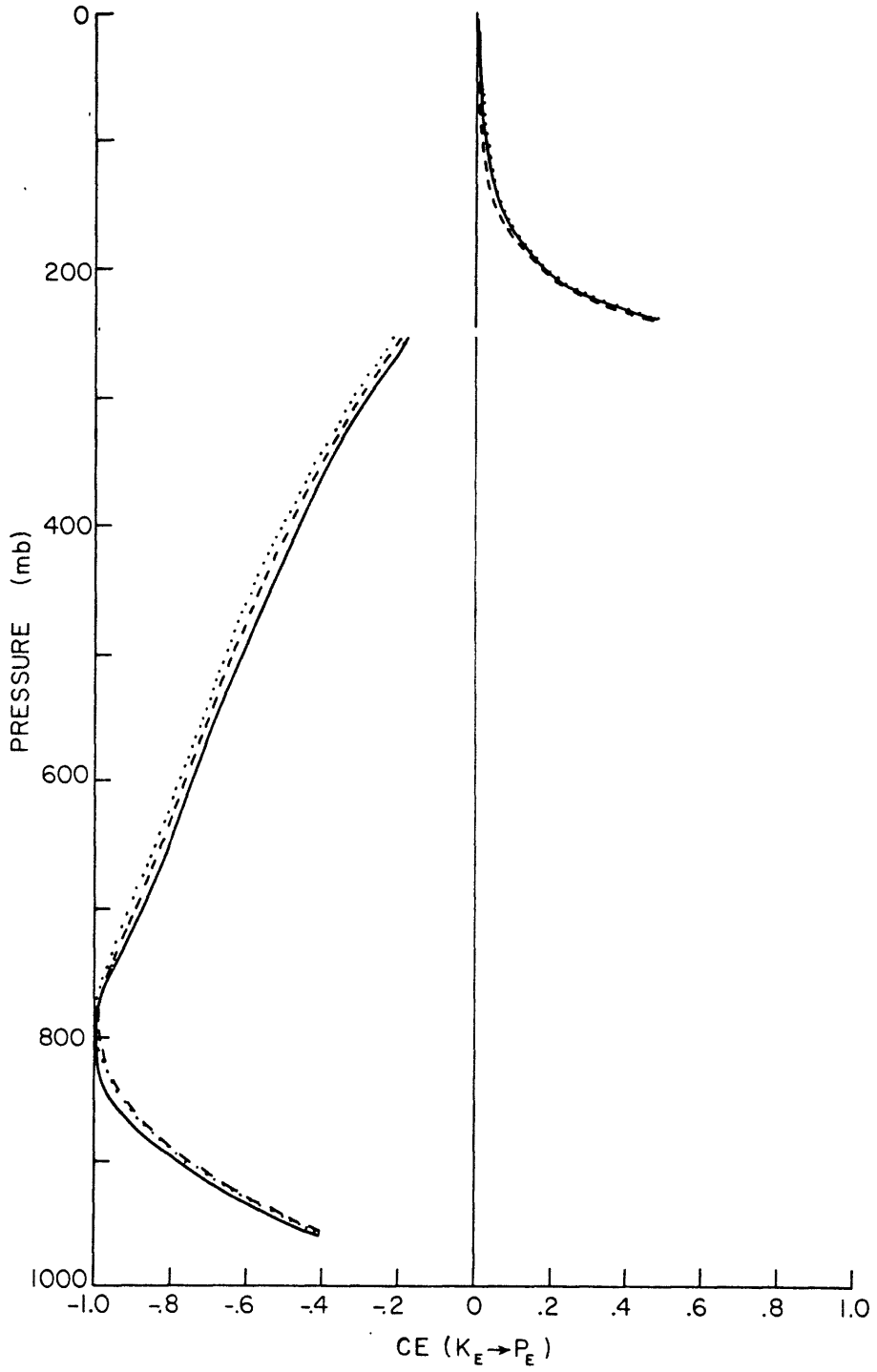

Figure 3.15. As in Figure 3.13, for the cases γ_T = 2, σ_ρ = 50, and SR = -1.5 (solid), 0 (dot), and 1 (dash).

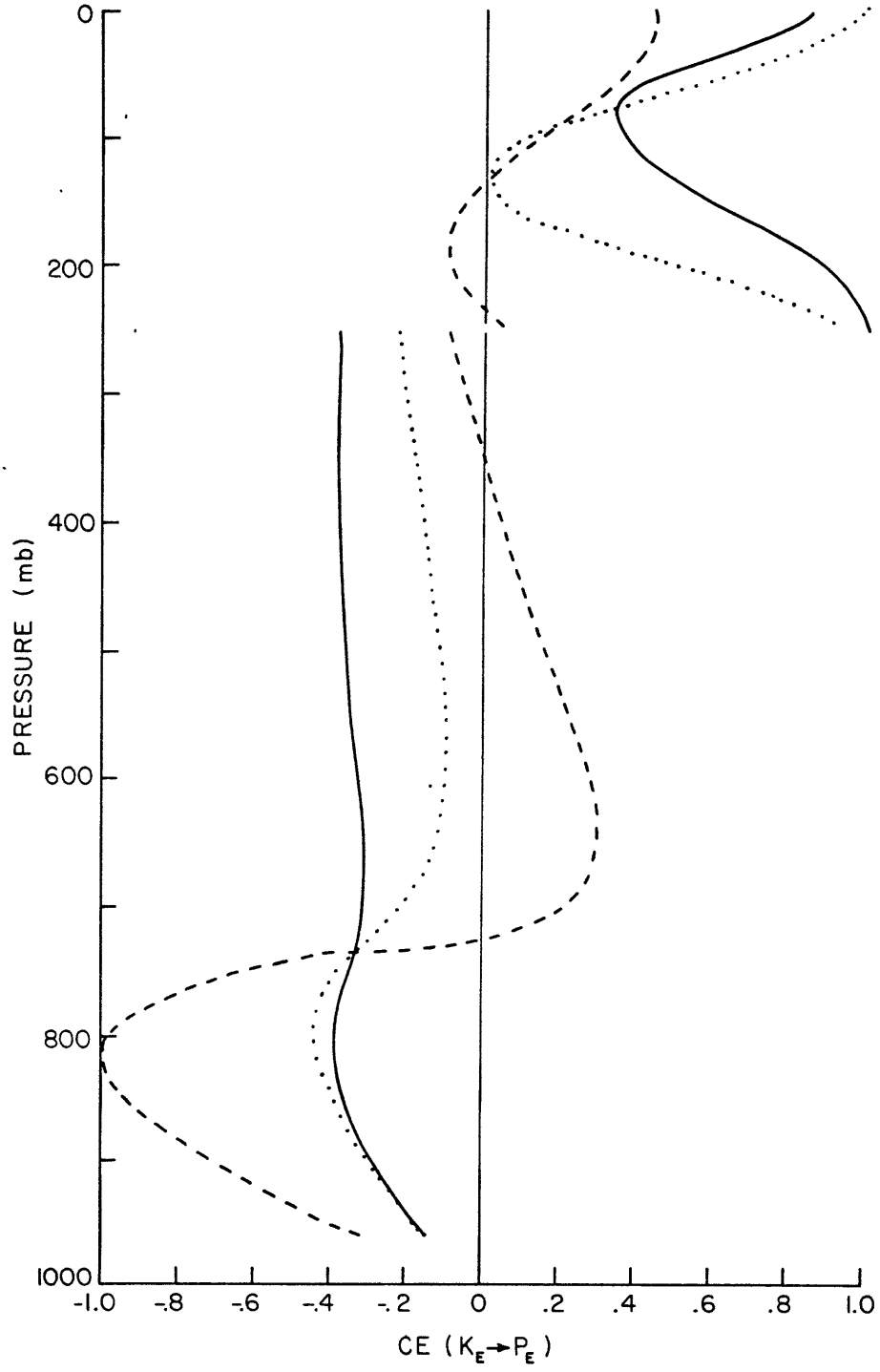

Figure 3.16. As in Figure 3.13, except for the fastest growing Green mode for cases γ_T = 2, σ_o = 50, and SR = -1.5 (solid), 0 (dot), and 1 (dash).

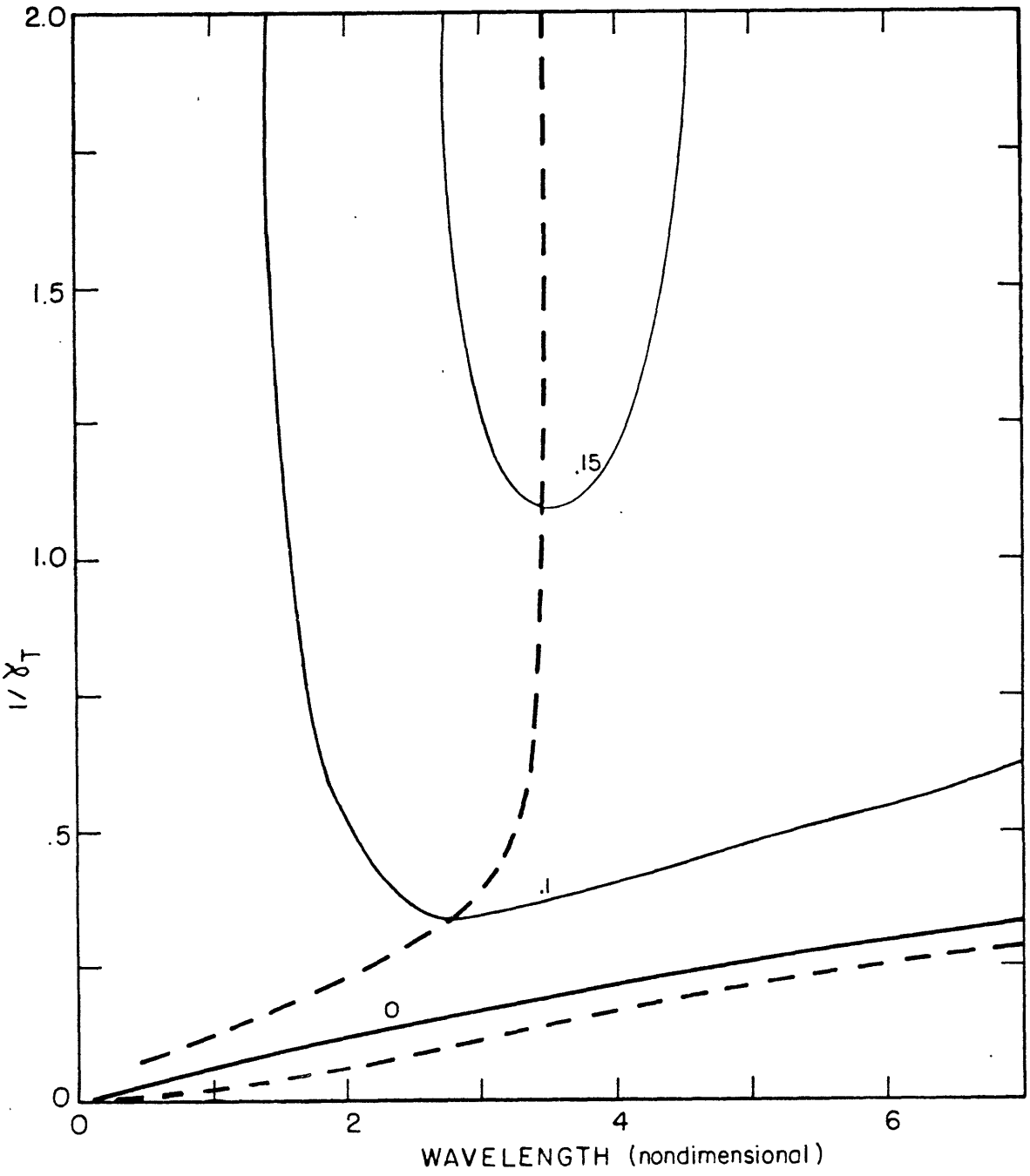

Figure 3.17. Non-dimensional growthrate $\frac{\ell_{c,i}}{R}$ divided by γ_T vs γ_T^{-1} and wavelength $\frac{\lambda}{2\pi/\ell}$, $\sigma_o = 1$, SR = 1, $u(p=\frac{1}{4}) = 1$, and $\psi' = 0$ at p = 0. Compare Figure 2.6.

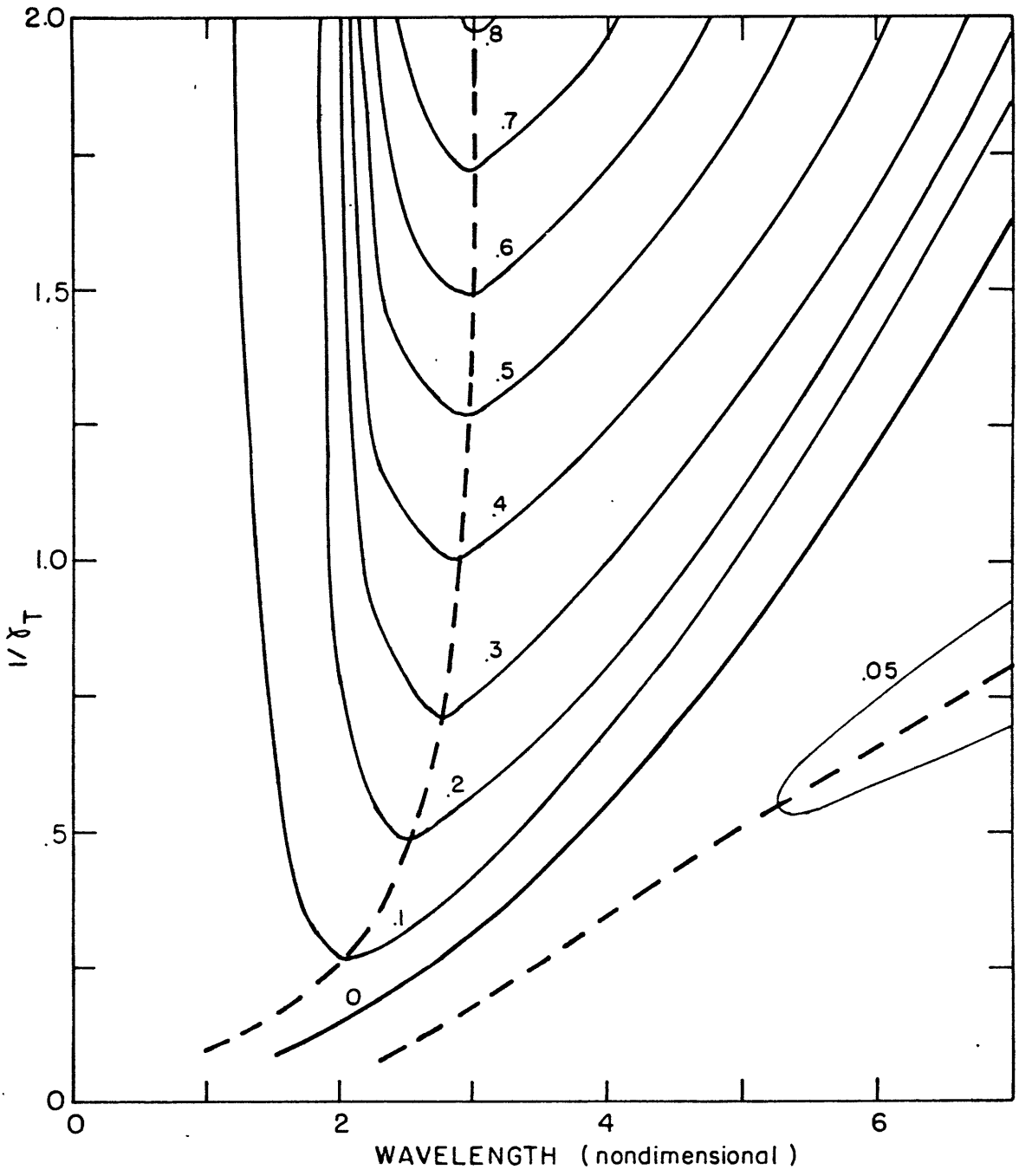

Figure 3.18. Non-dimensional growthrate $\frac{\rho_{c2}}{2\pi}$ divided by γ_T vs γ_T^{-1} and wavelength: σ_ρ = 50. SR = -1.5, $u(p=\frac{1}{4})$ = 1, and ψ' = 0 at p = 0.

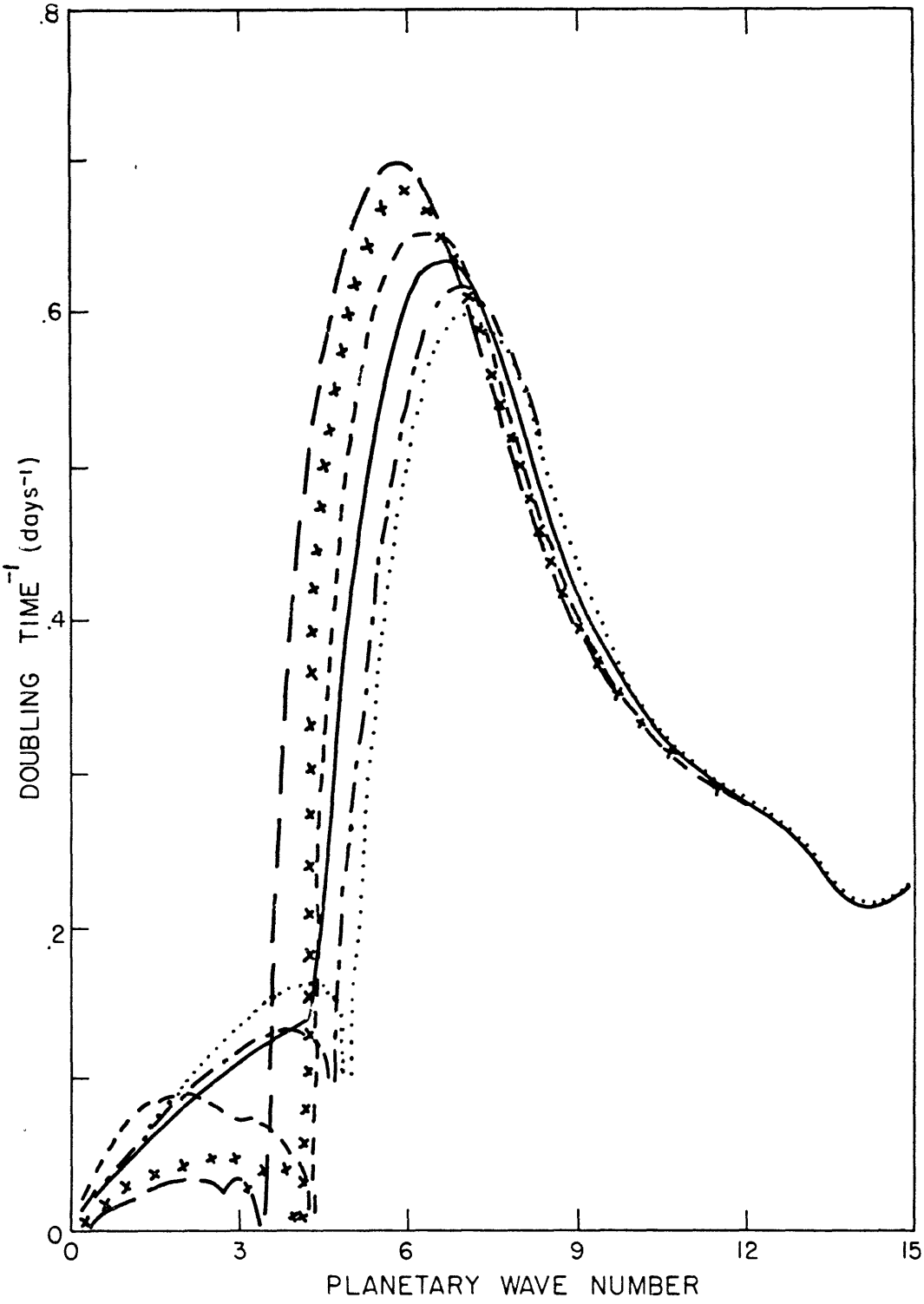

Figure 3.19. Doubling time^{-1} vs. wavenumber for γ_T = 2, σ_0 = 50, and SR = -12 (dot), -8 (dash dot), -4 (solid), 0 (dash), 4 (cross), and 8 (long dash).

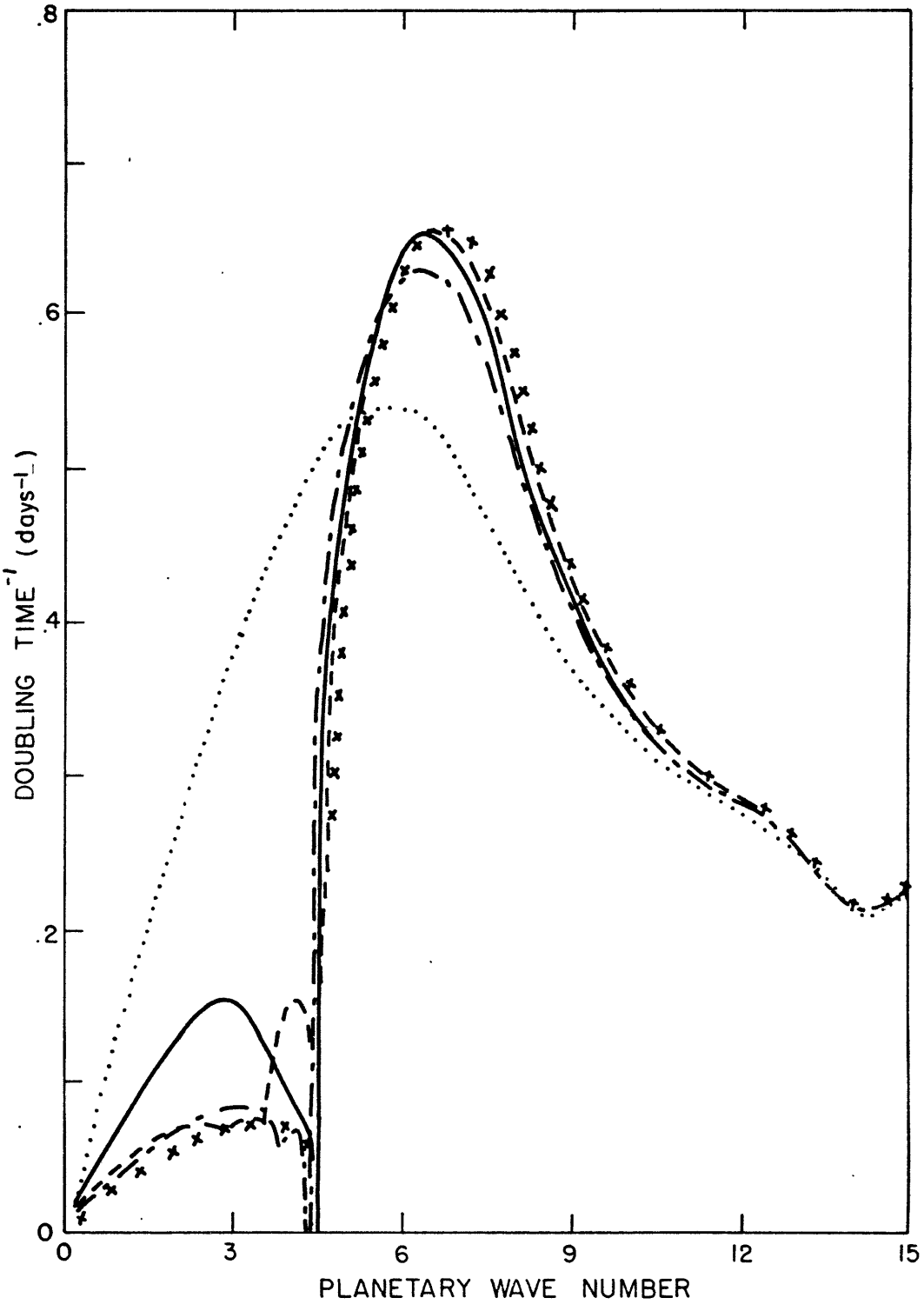

Figure 3.20. As in Figure 3.19, for the cases: γ_T = 2, SR = -1.5, and σ_ρ = 1 (dot), 10 (dash dot), 40 (solid), 100 (dash), and 1000 (cross).

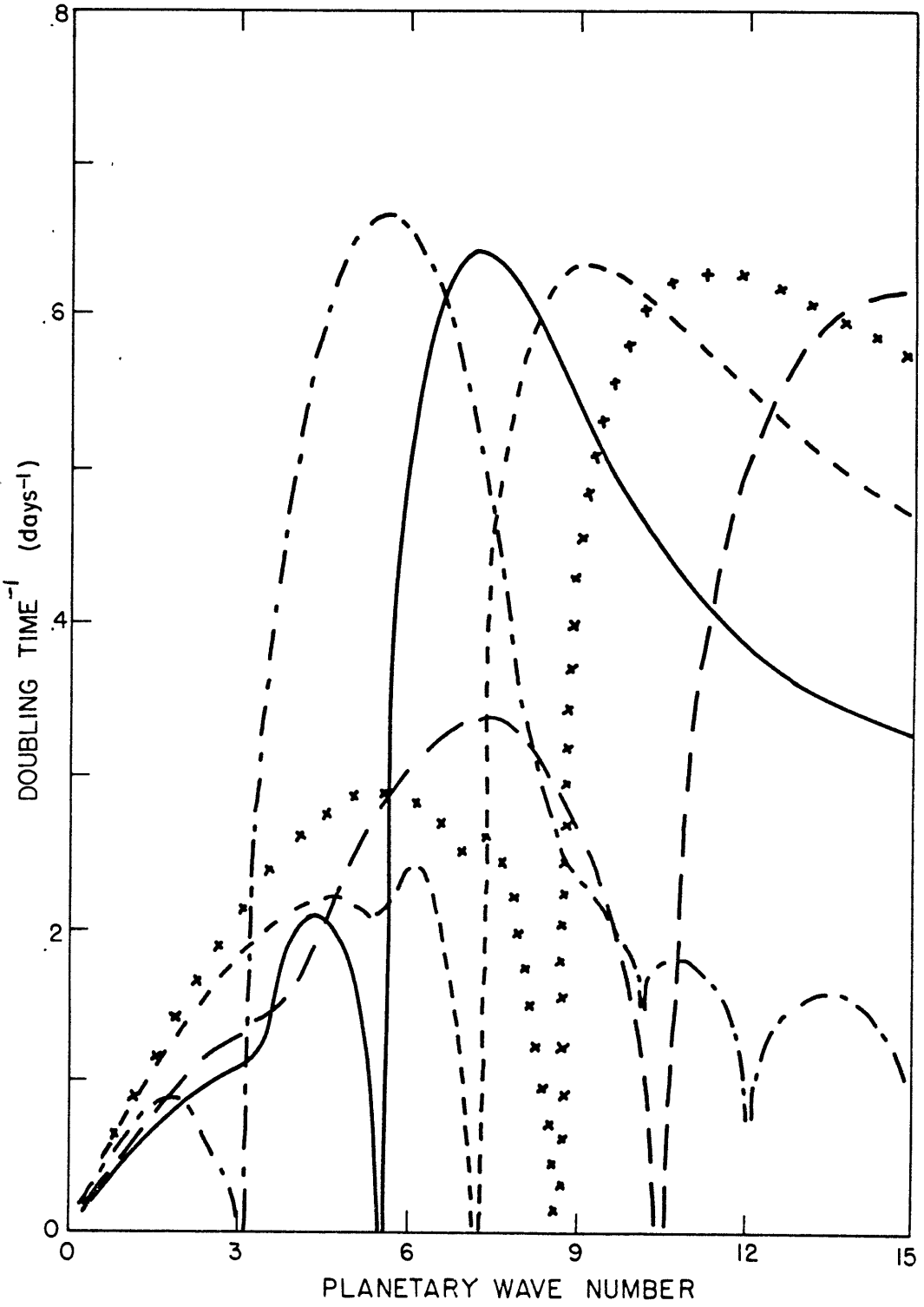

Figure 3.21. As in Figure 3.19, for the cases SR = -1.5, σ_0 = 50, and γ_T = 1 (dash dot), 3 (solid), 5 (dash), 7 (cross), and 10 (long dash).

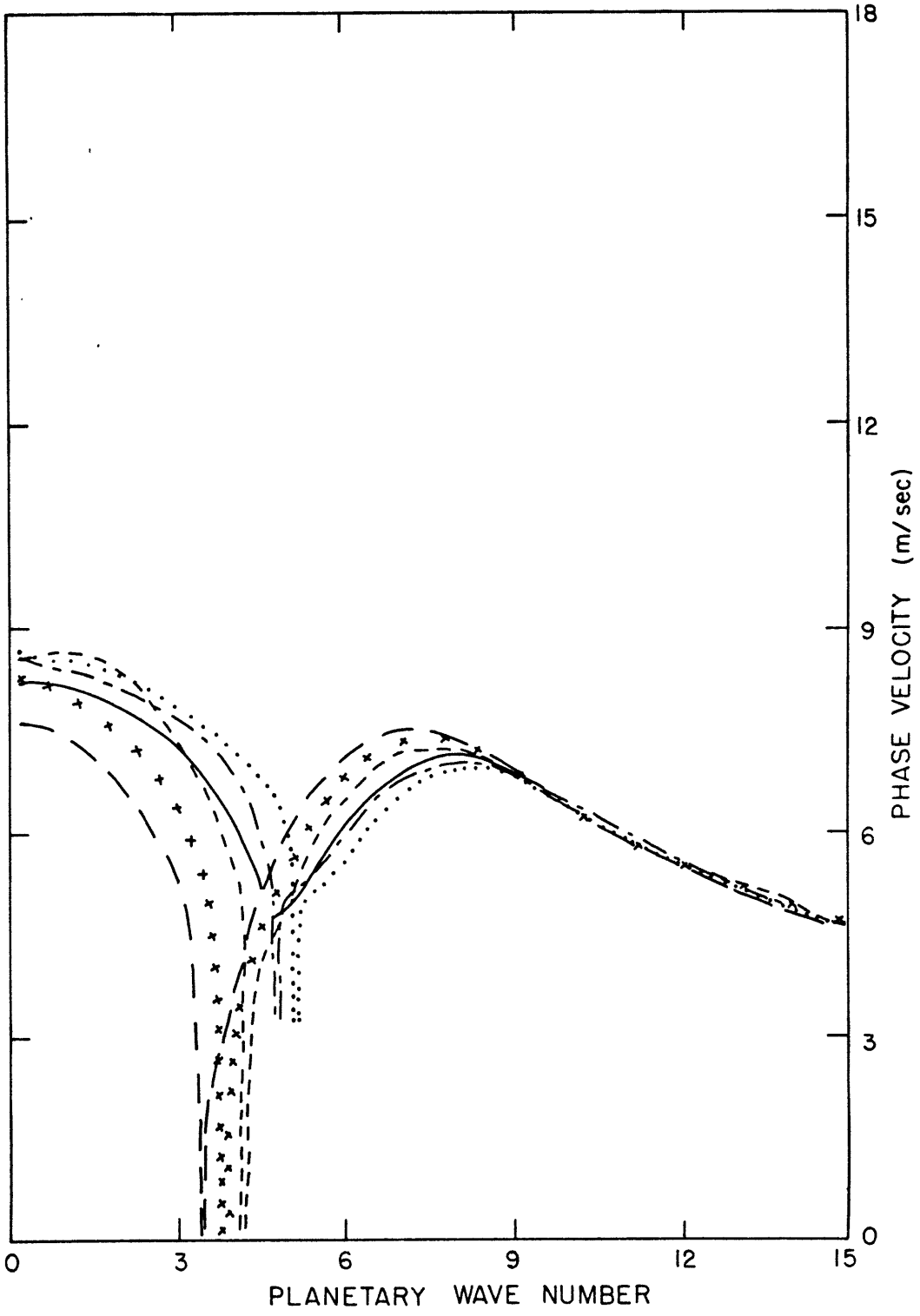

Figure 3.22. Phase velocity vs. wavenumber for the same cases as in Figure 3.19.

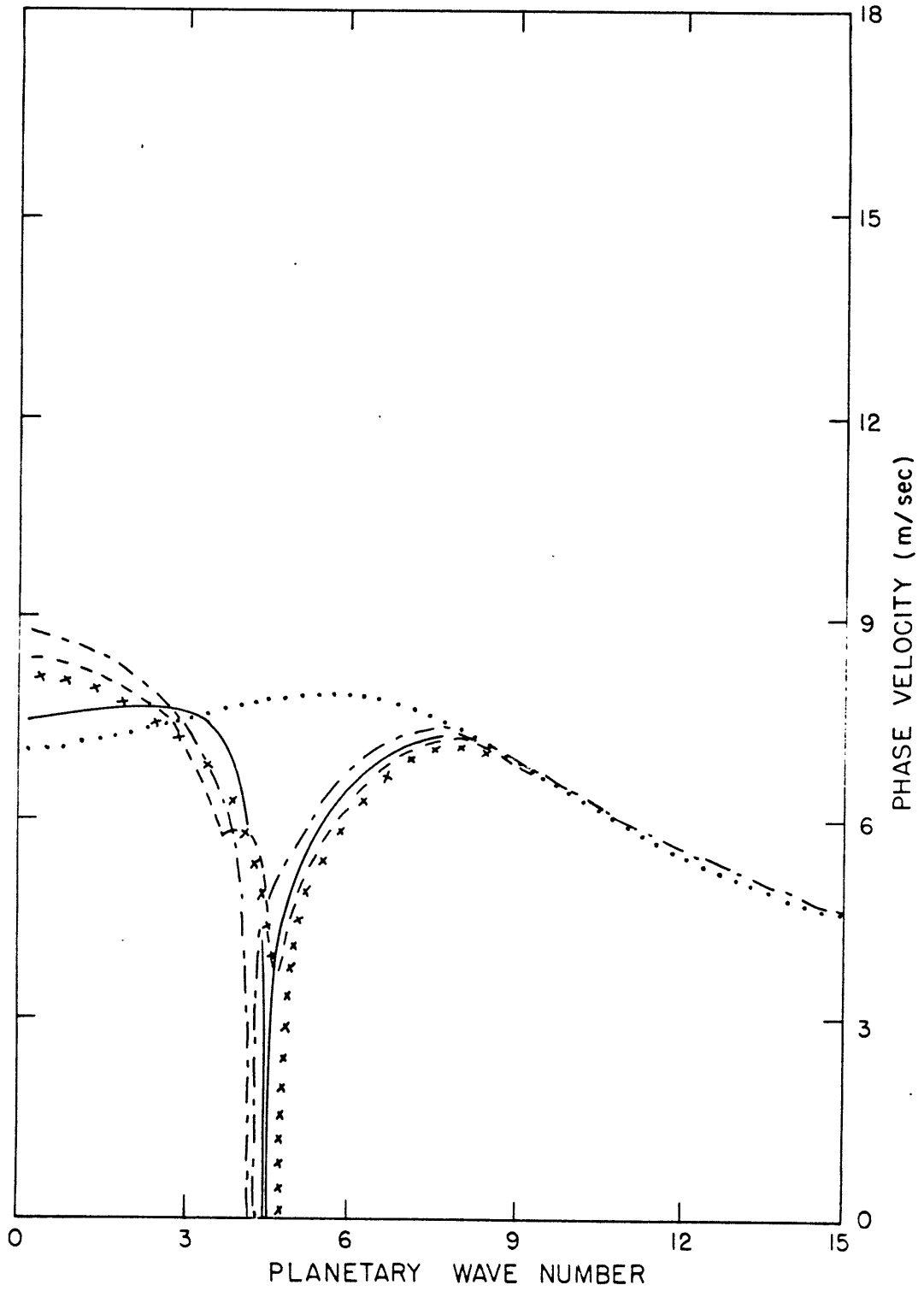

Figure 3.23. Phase velocity vs. wavenumber for the same cases as in Figure 3.20.

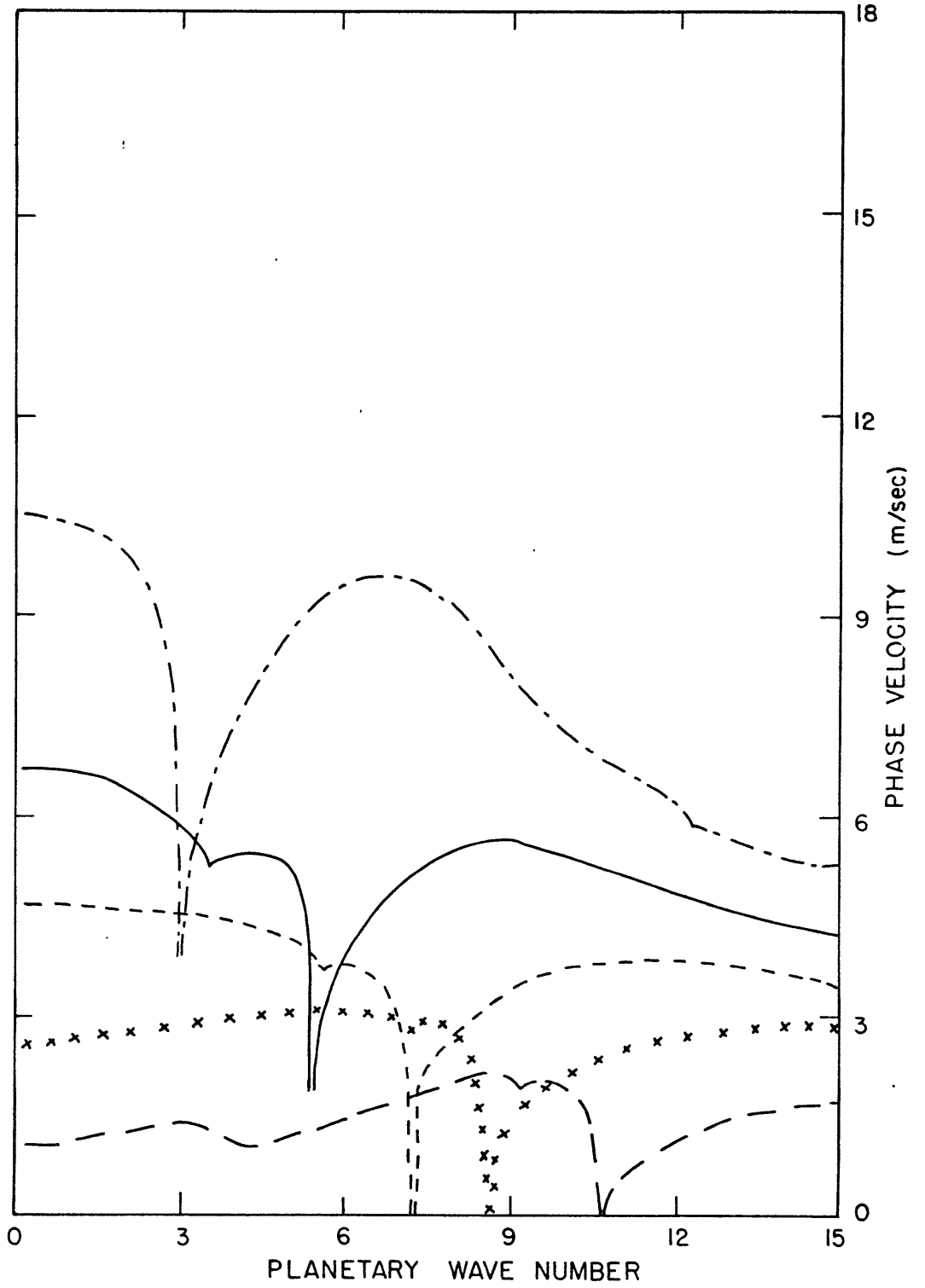

Figure 3.24. Phase velocity vs. wavenumber for the same cases as in Figure 3.21.

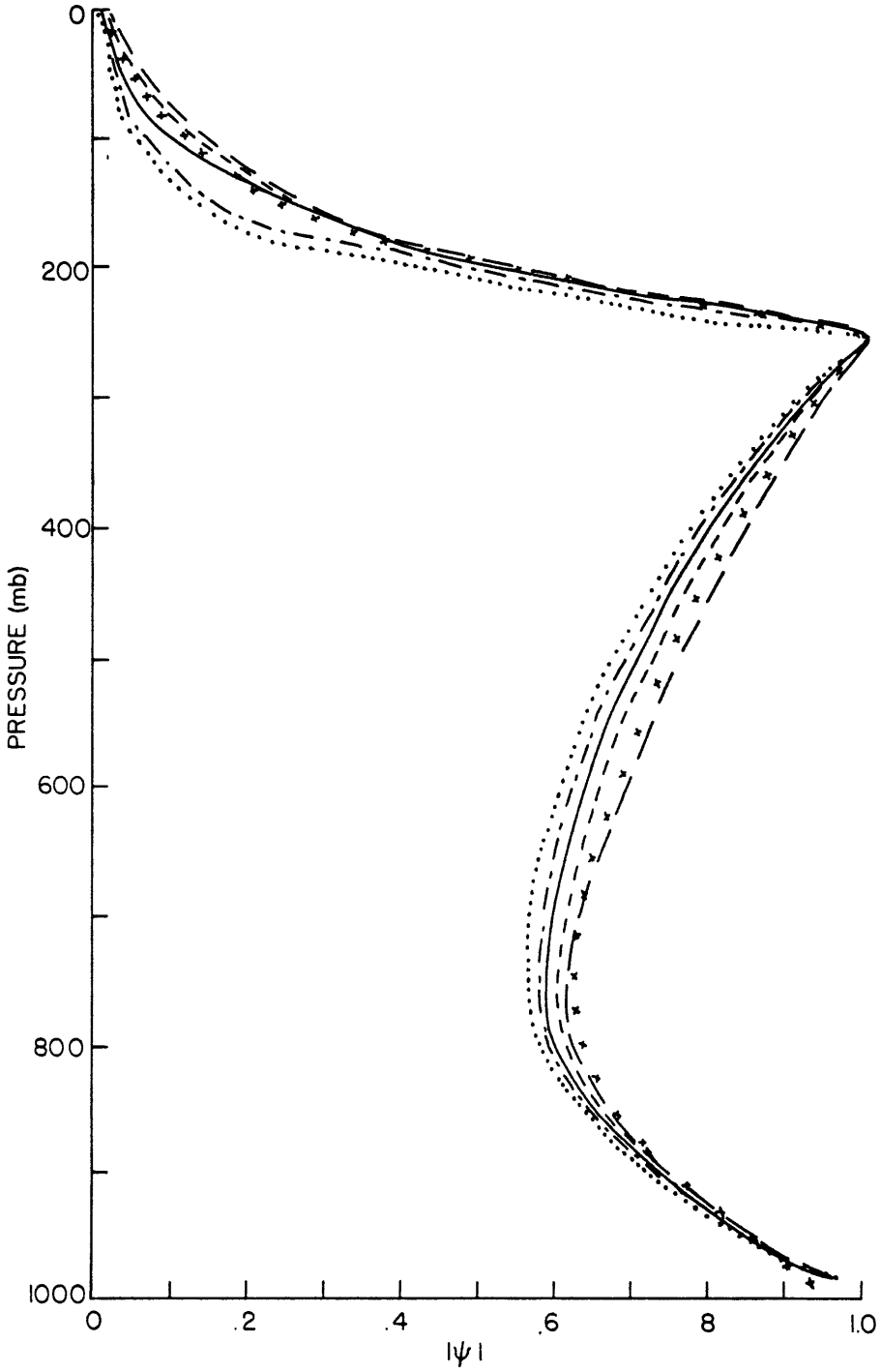

Figure 3.25. Vertical structure of the streamfunction amplitude for the fastest growing Eady mode for the same cases as in Figure 3.19.

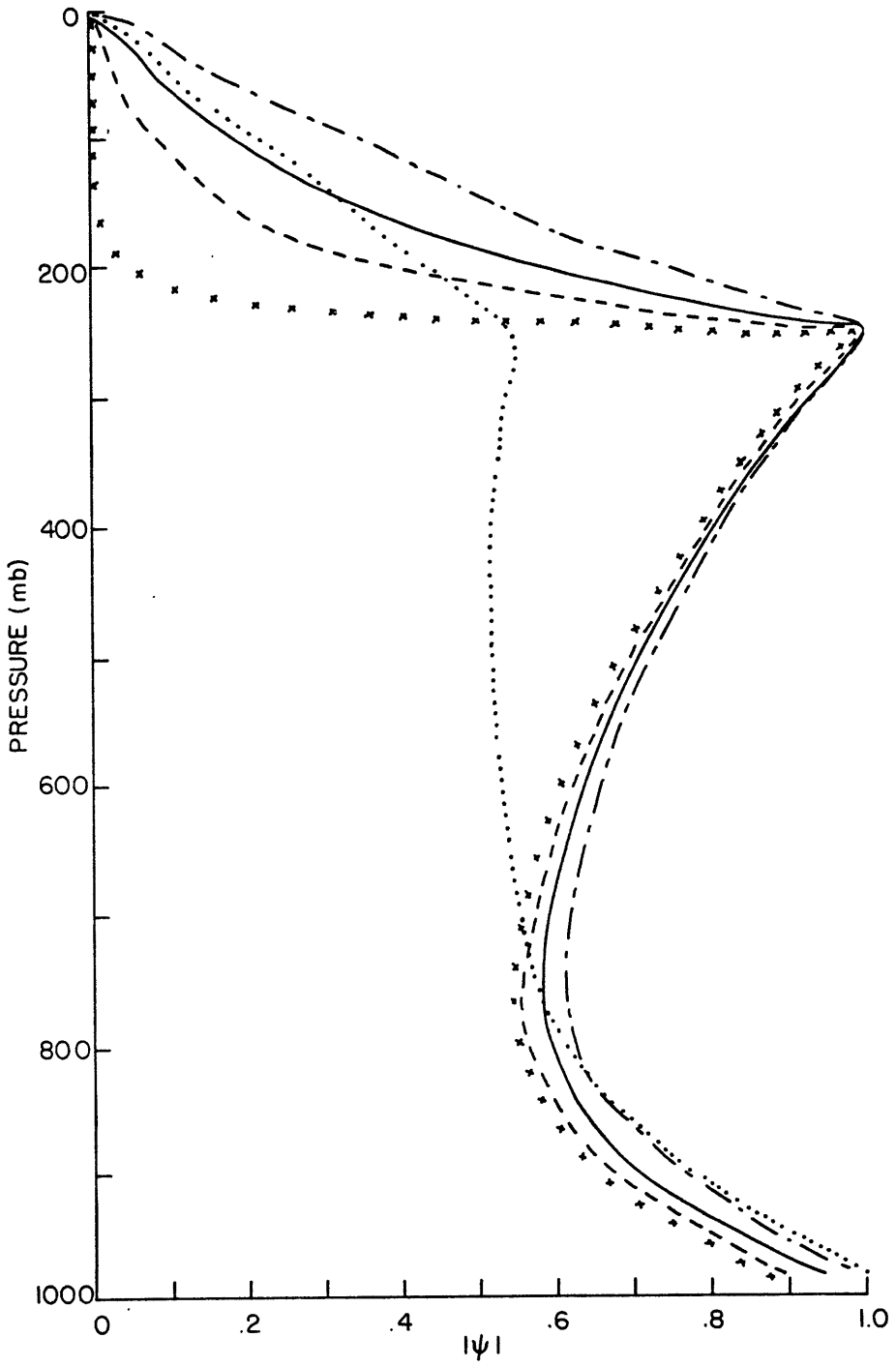

Figure 3.26. As in Figure 3.25, for the cases γ_T = 2, SR = -1.5, and σ_p = 1 (dot), 10 (dash dot), 40 (solid), 100 (dash), and 1000 (cross).

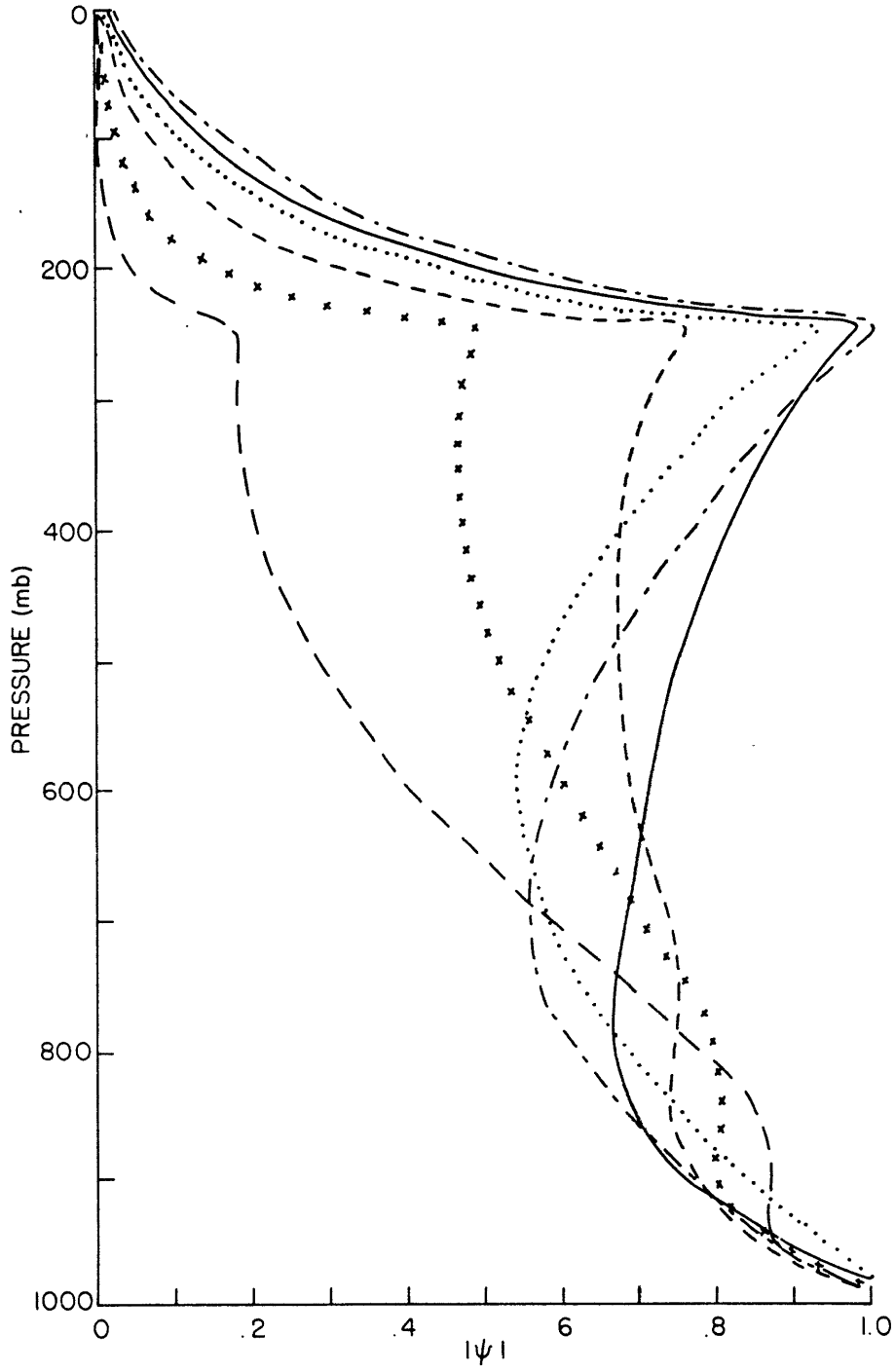

Figure 3.27. As in Figure 3.25, for the cases SR = -1.5, σ_ρ = 50, and γ_T = 0 (dot), 1 (dash dot), 3 (solid), 5 (dash), 7 (cross), and 10 (long dash).

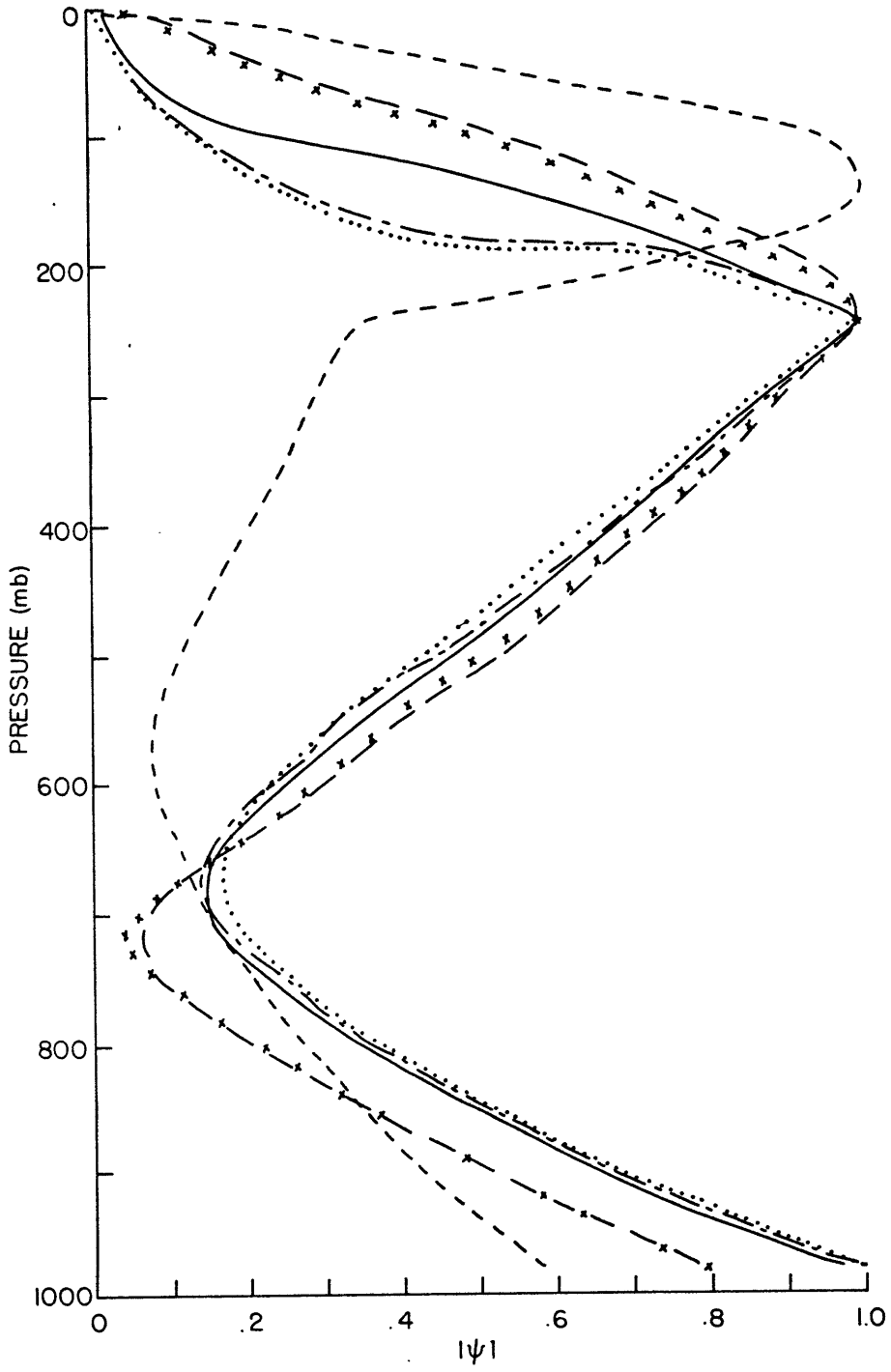

Figure 3.28. Vertical structure of the streamfunction amplitude for the fastest growing Green mode, for the same cases as in Figure 3.19.

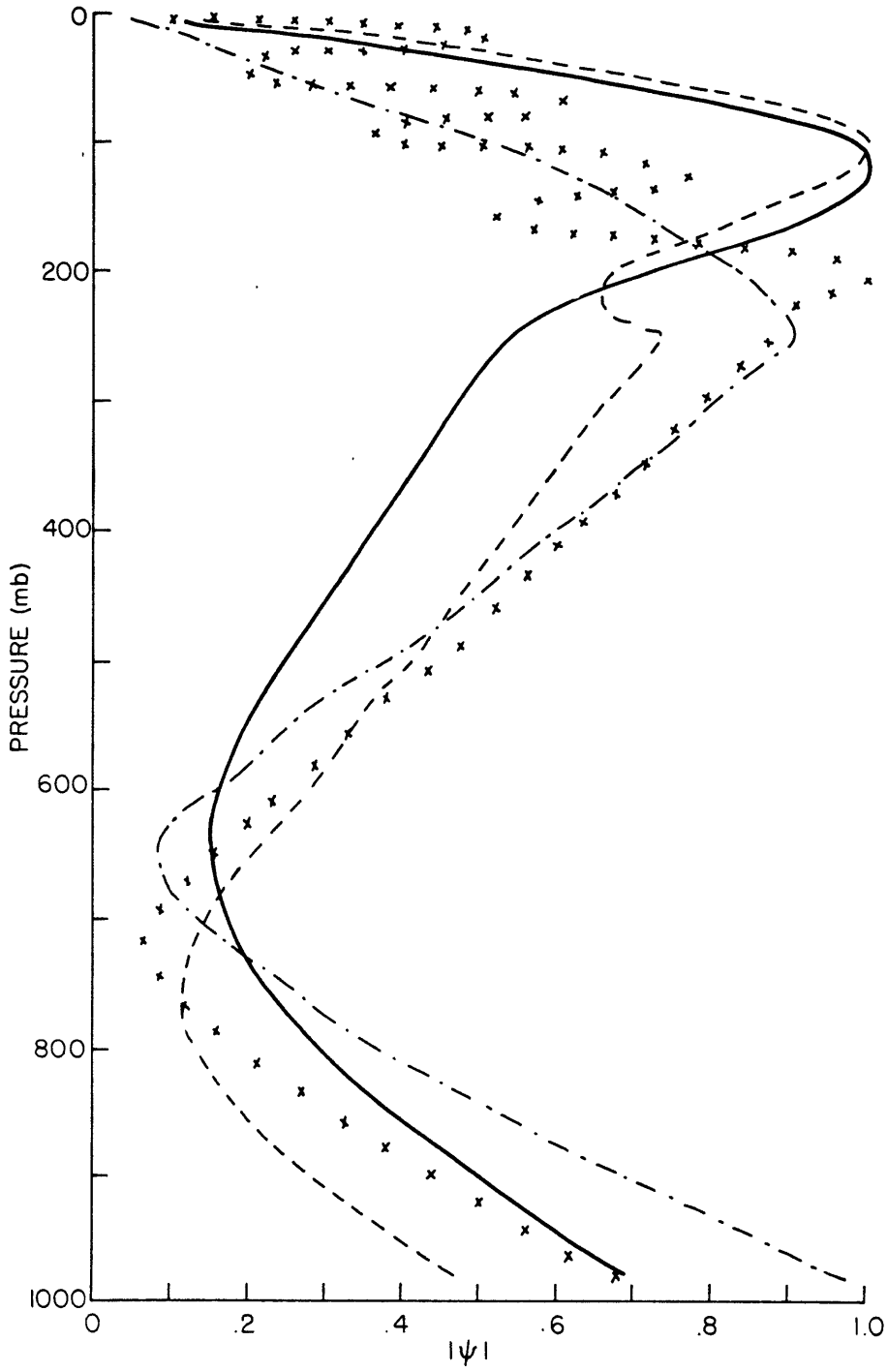

Figure 3.29. As in Figure 3.28, for the cases γ_T = 2, SR = -1.5, and σ_ρ = 10 (dash dot), 40 (solid), 100 (dash), and 1000 (cross).

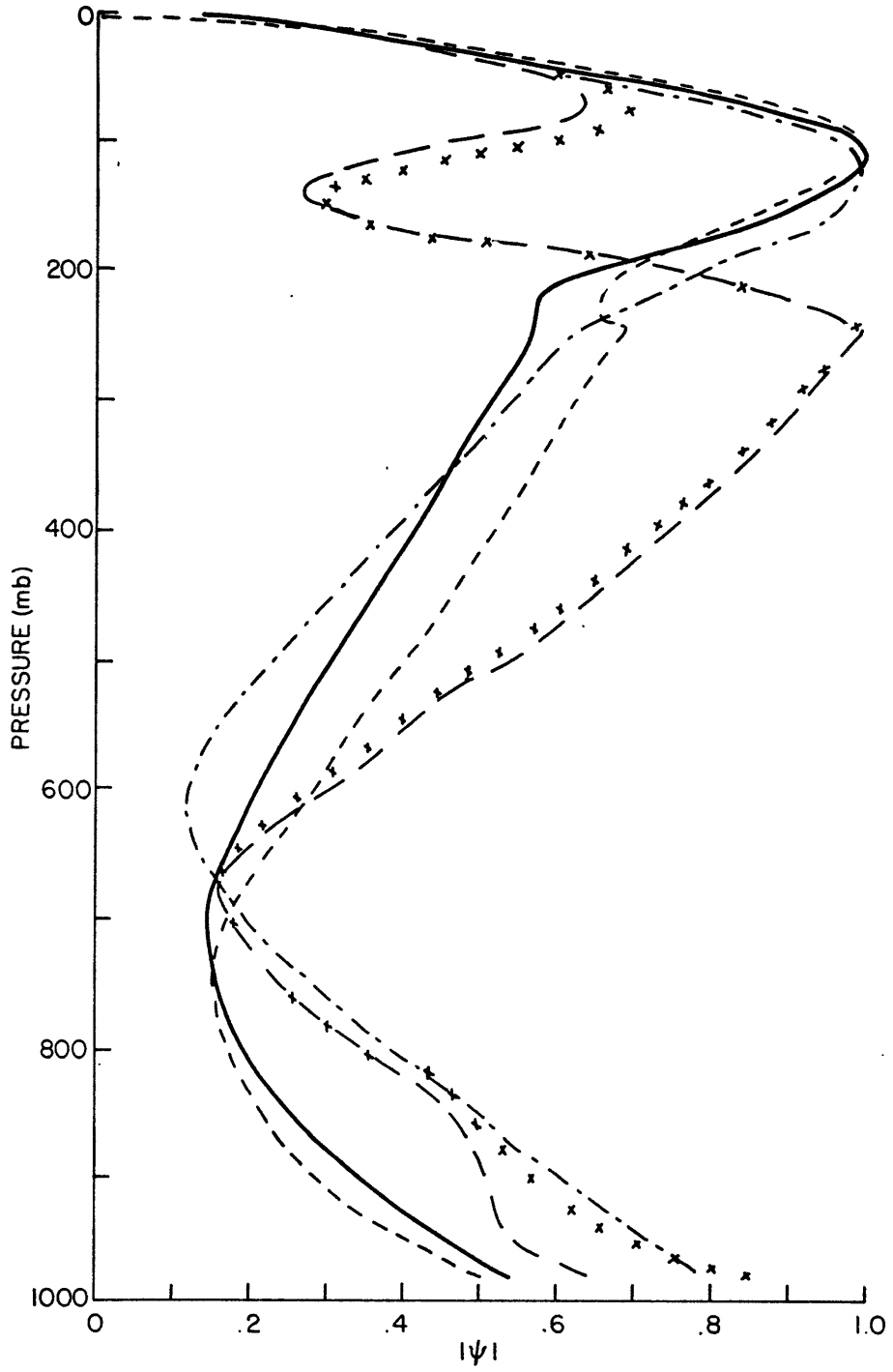

Figure 3.30. As in Figure 3.28, for the cases SR = -1.5, σ_ρ = 50, and γ_T = 1 (dash dot), 3 (solid), 5 (dash), 7 (cross), and 10 (long dash).

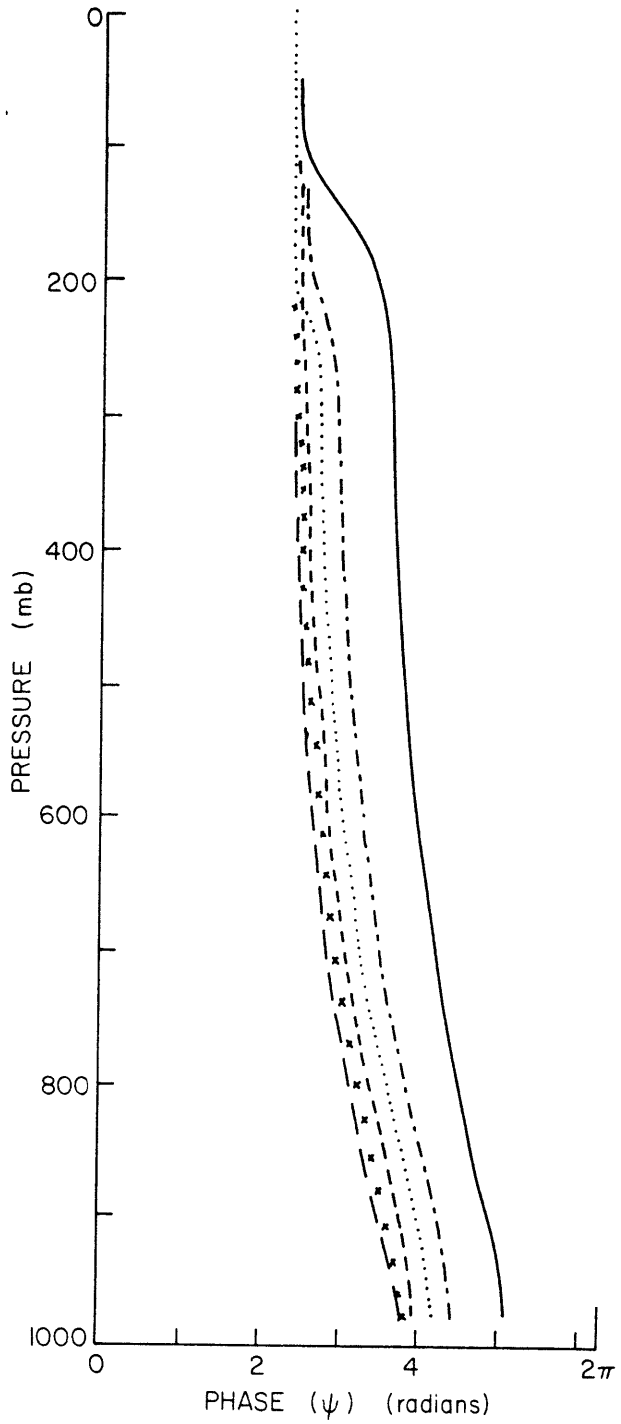

Figure 3.31. Vertical structure of the streamfunction phase for the fastest growing Eady mode, for the same cases as in Figure 3.19.

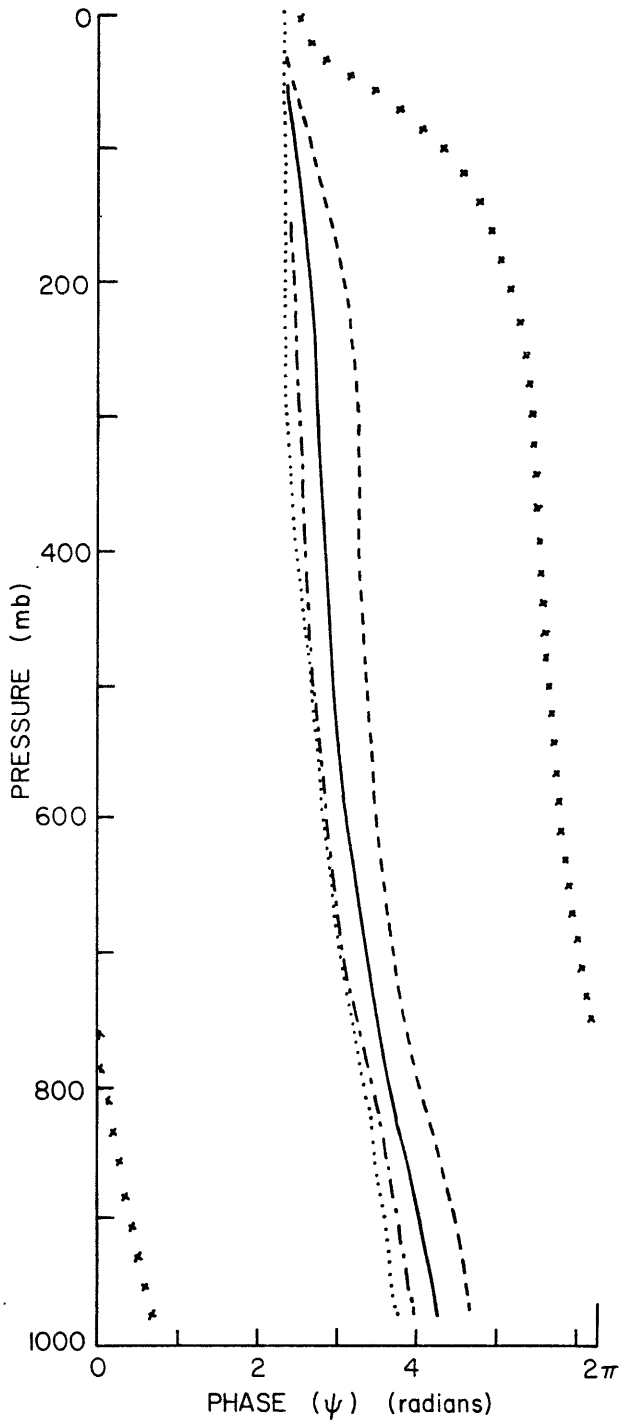

Figure 3.32. As in Figure 3.31, for the cases $\gamma_T = 2$, SR = -1.5, and σ_ρ = 1 (dot), 10 (dash dot), 40 (solid), 100 (dash), and 1000 (cross).

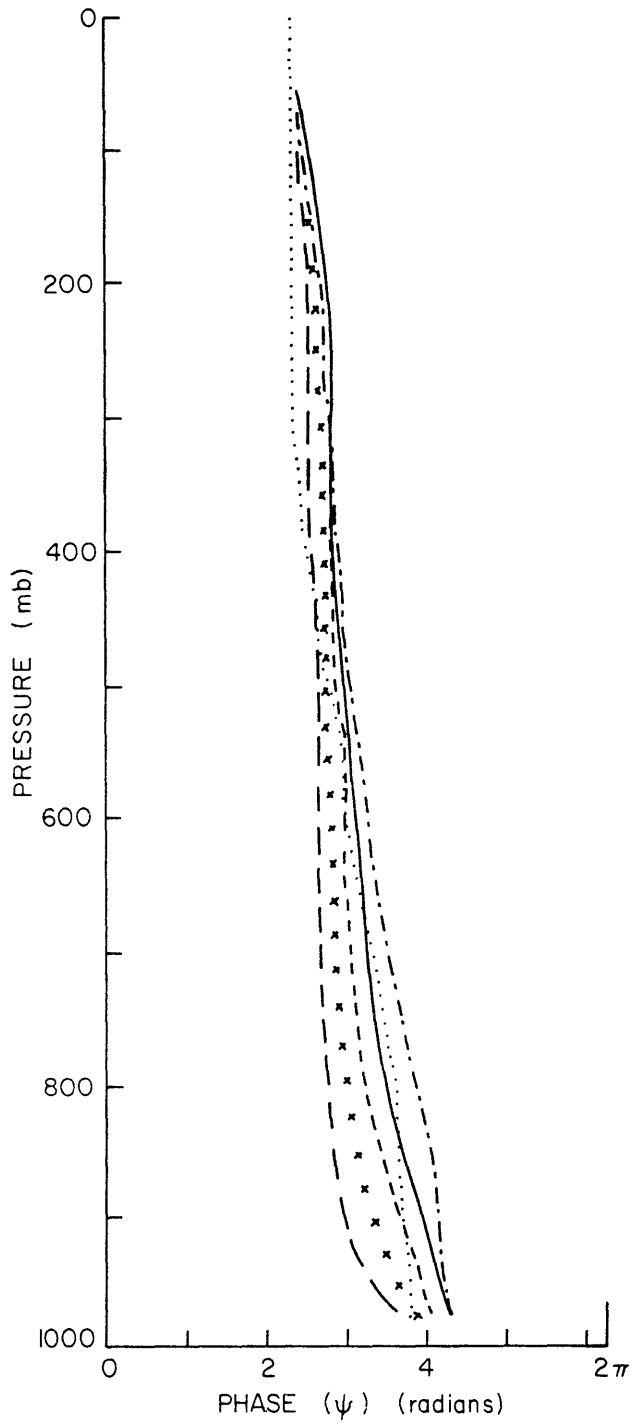

Figure 3.33. As in Figure 3.31, for the cases SR = -1.5, σ_ρ = 50, and γ_T = 1 (dash dot), 3 (solid), 5 (dash), 7 (cross), and 10 (long dash).

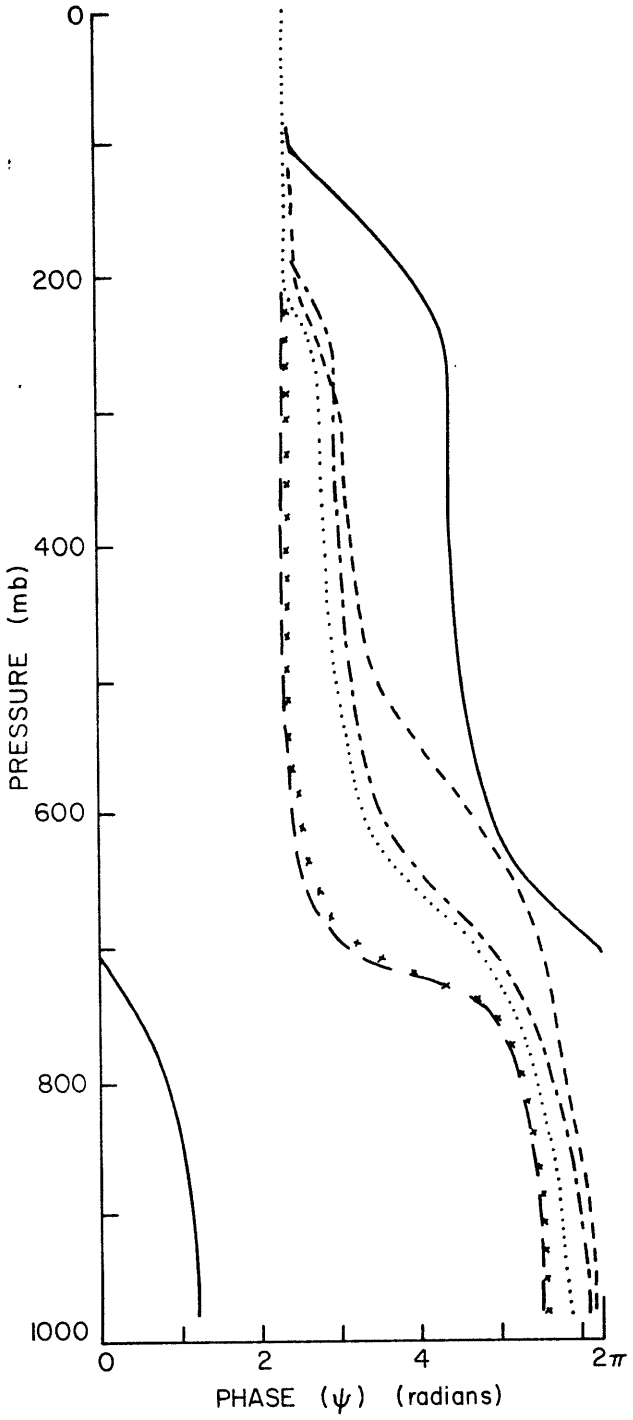

Figure 3.34. Vertical structure of the streamfunction phases for the fastest growing Green mode, for the same cases as in Figure 3.19.

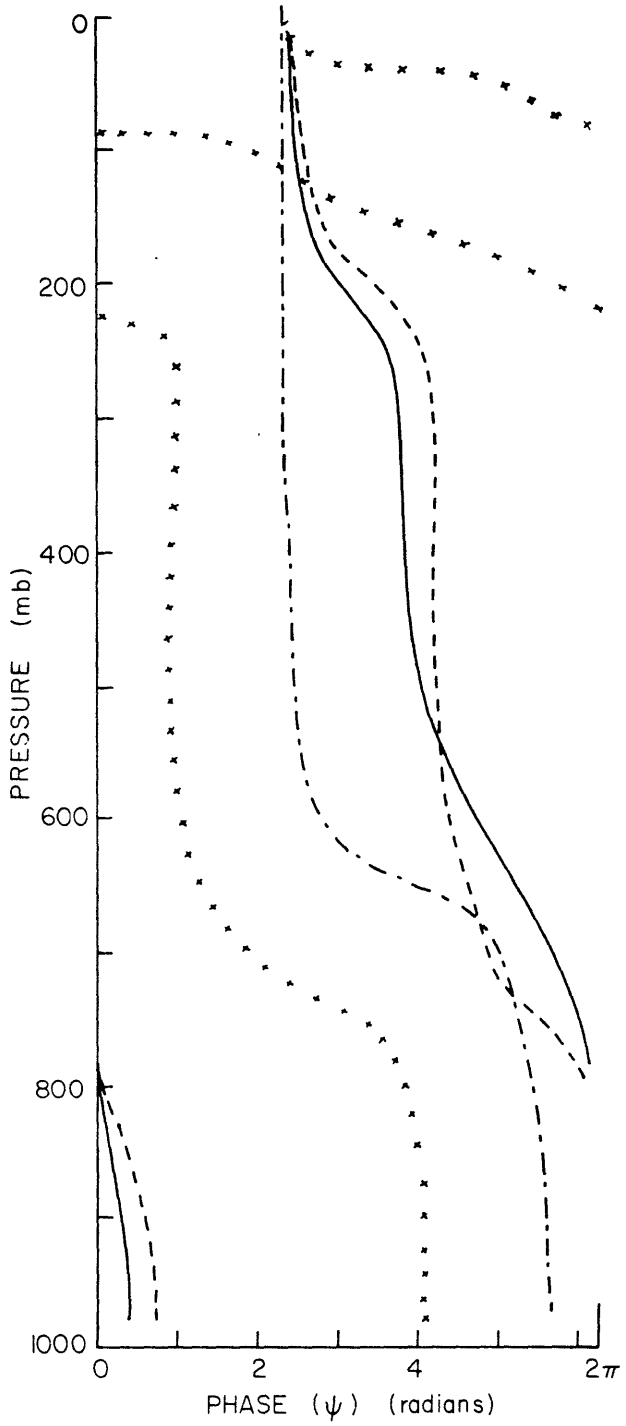

Figure 3.35. As in Figure 3.34, for the cases γ_T = 2, SR = -1.5, and σ_ρ = 10 (dash dot), 40 (solid), 100 (dash), and 1000 (cross).

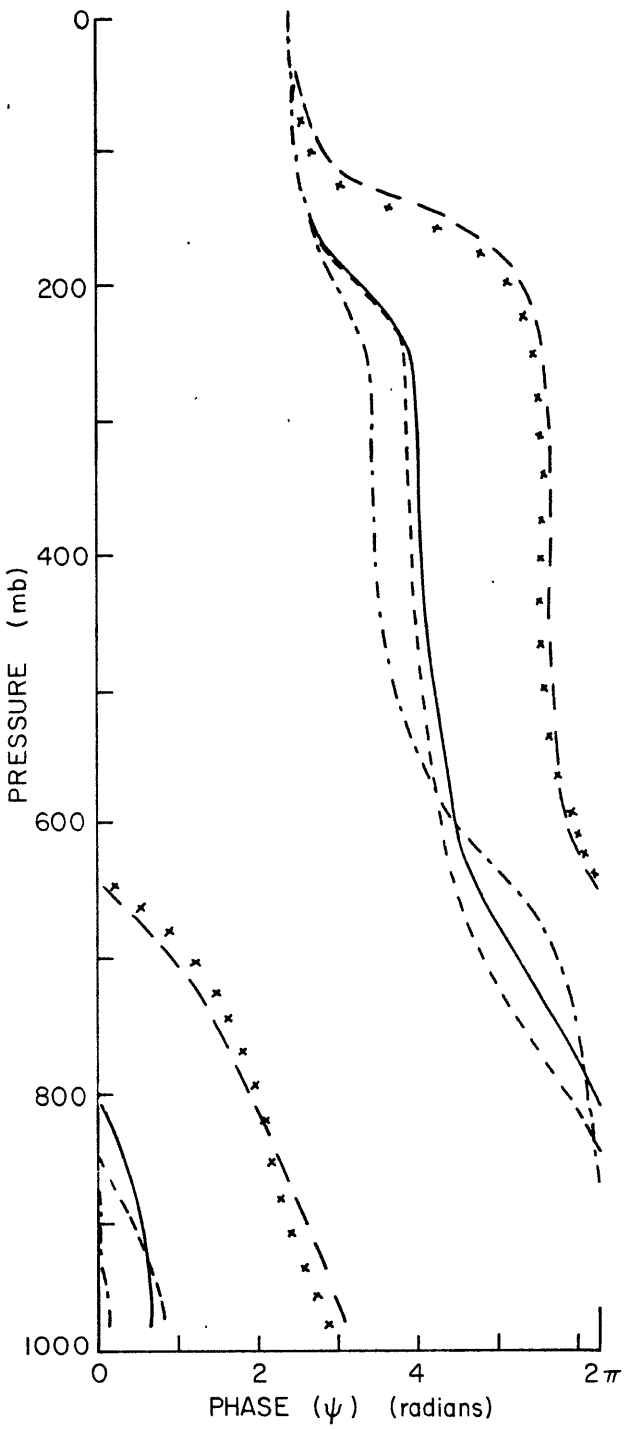

Figure 3.36. As in Figure 3.34, for the cases SR = -1.5, σ_ρ = 50, and γ_T = 1 (dash dot), 3 (solid), 5 (dash), 7 (cross), and 10 (long dash).

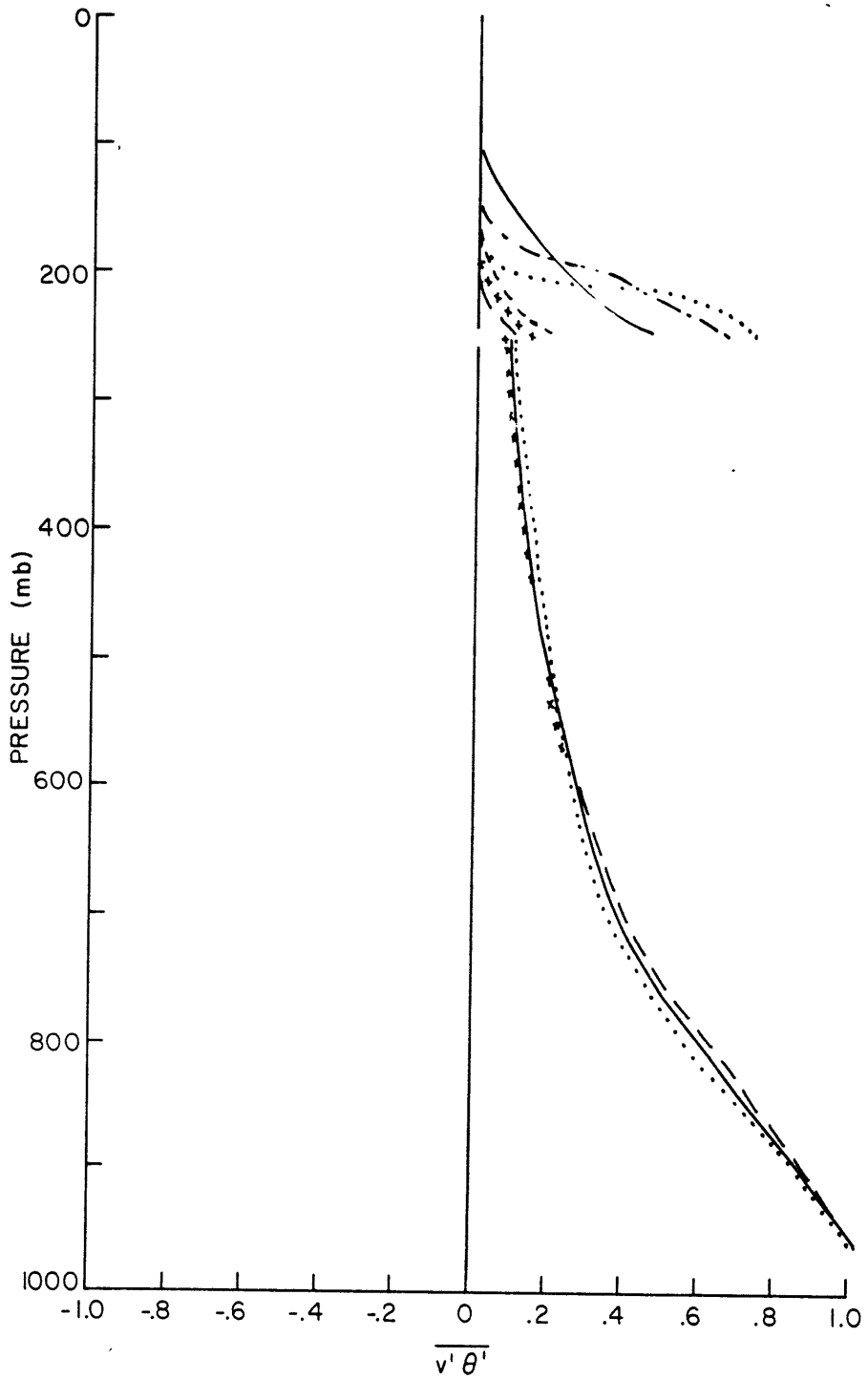

Figure 3.37. Vertical structure of the meridional entropy transport for the fastest growing Eady mode, for the same cases as in figure 3.19. Where cases are not shown, they coincide with those presented: the curve for SR = -8 coincides with that of SR = -12 at some levels; the curves of SR = 0 and SR = +4 coincide with that of SR = -4 at some levels.

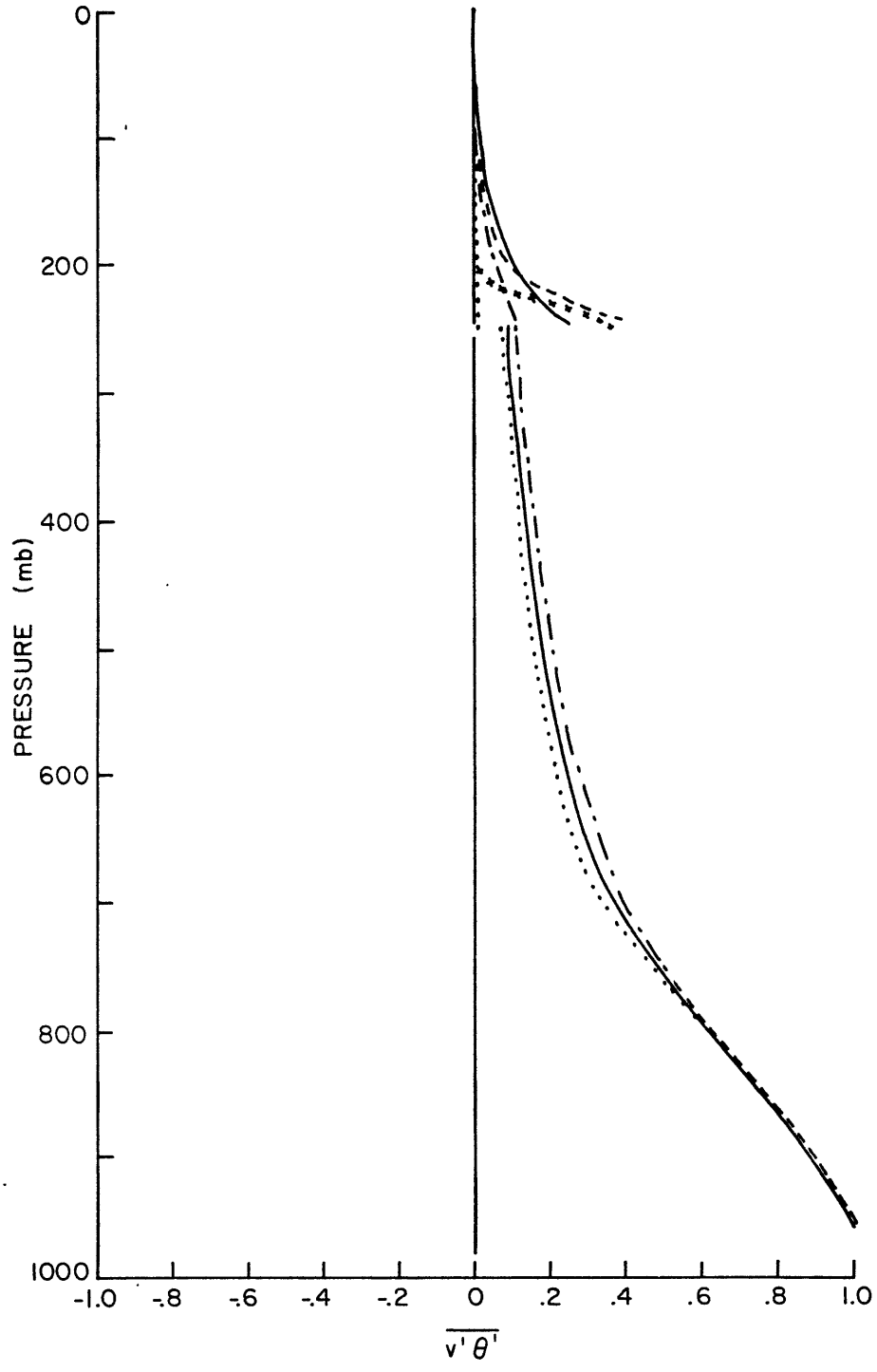

Figure 3.38. As in Figure 3.37, except for the cases γ_T = 2, SR = -1.5, and σ_ρ = 1 (dot), 10 (dash dot),40 (solid), 100 (dash), and 1000 (cross). Where cases are not shown, they coincide with those presented: below 250 mb, the σ_ρ = 40. 100, and 1000 coincide.

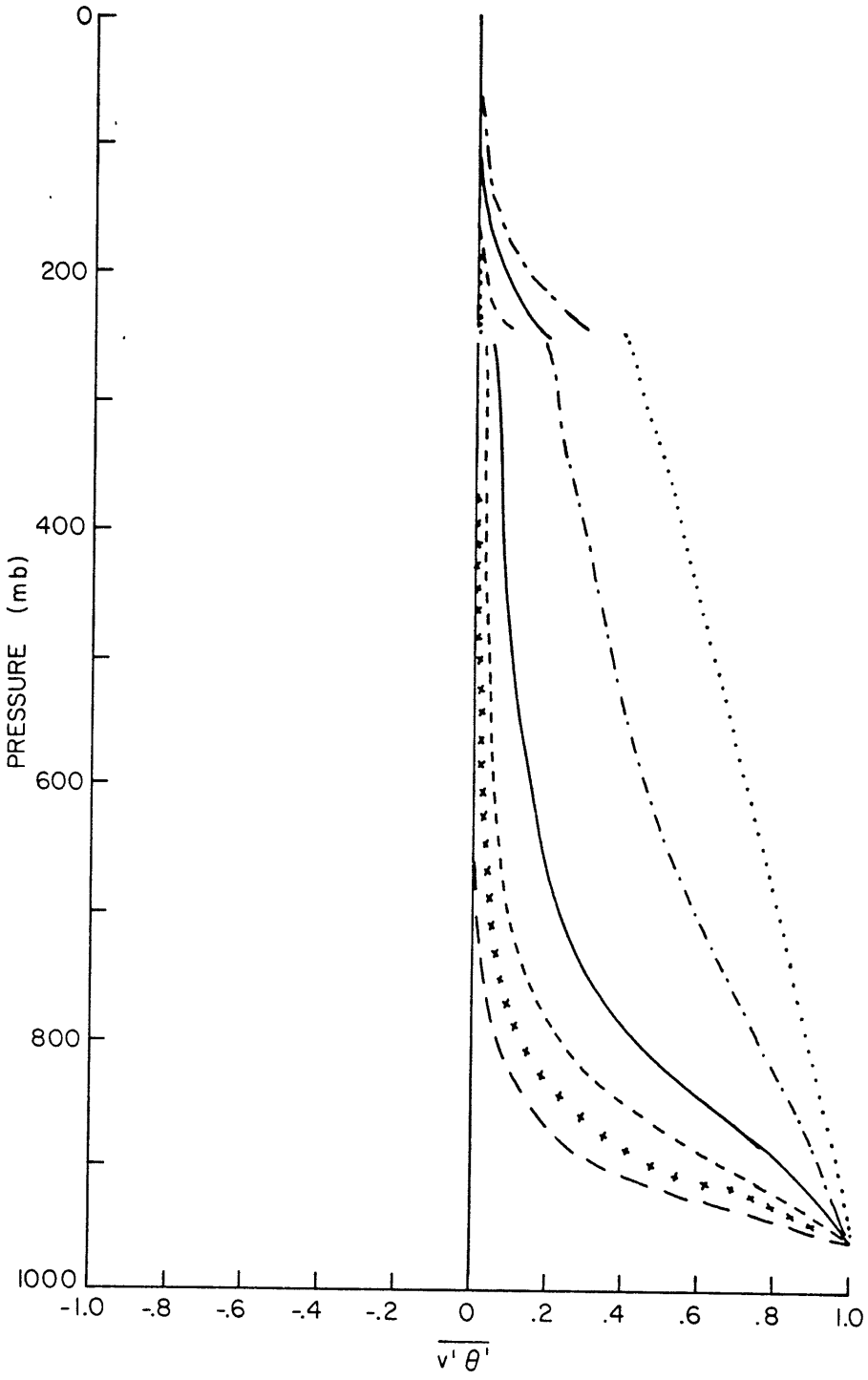

Figure 3.39. As in Figure 3.37, except for the cases SR = -1.5, σ_D = 50, and γ_T = 0 (dot), 1 (dash dot), 3 (solid), 5 (dash), 7 (cross), and 10 (long dash).

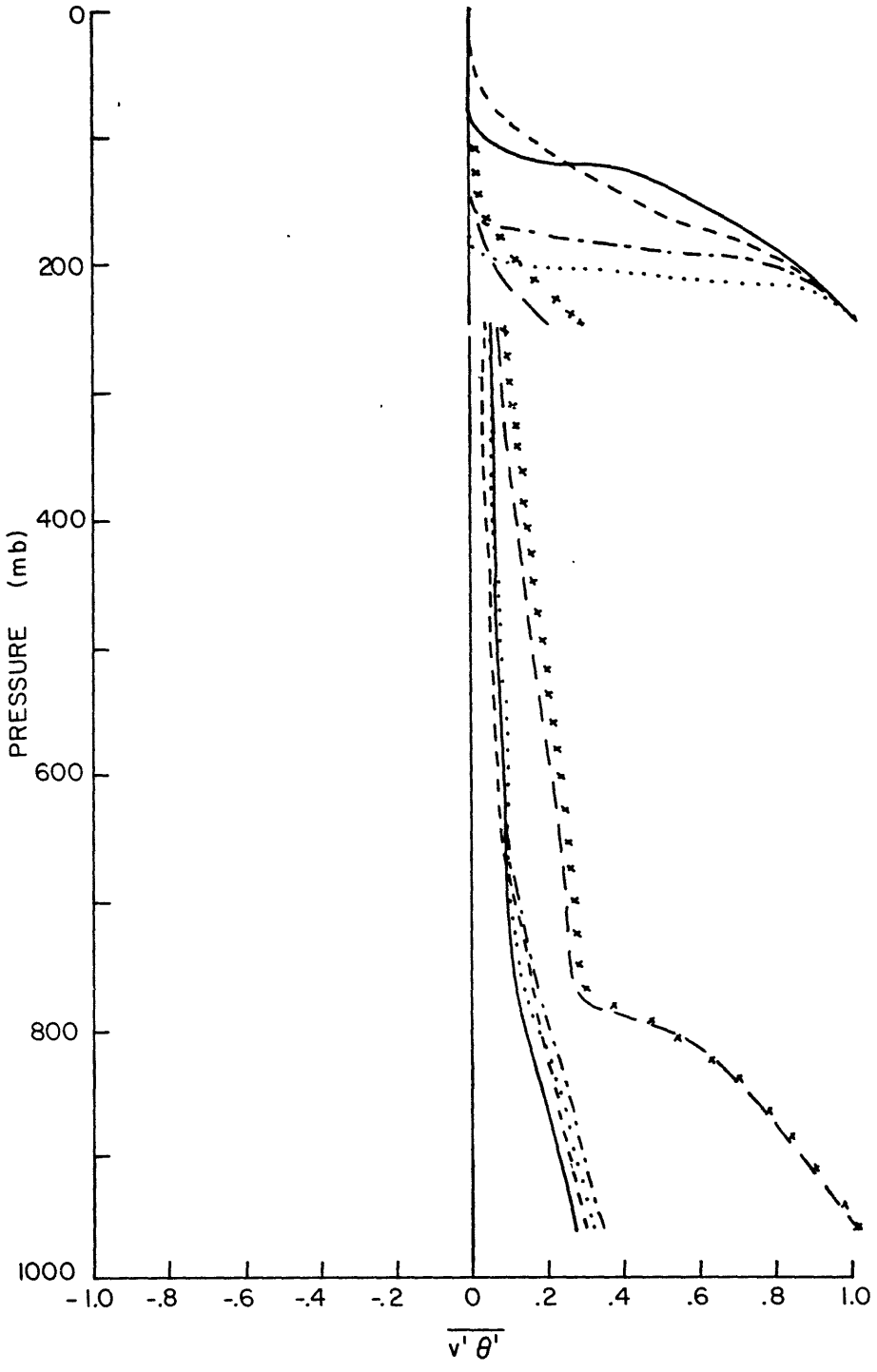

Figure 3.40. Vertical structure of the meridional entropy transport for the fastest growing Green mode, for the same cases as in Figure 3.19.

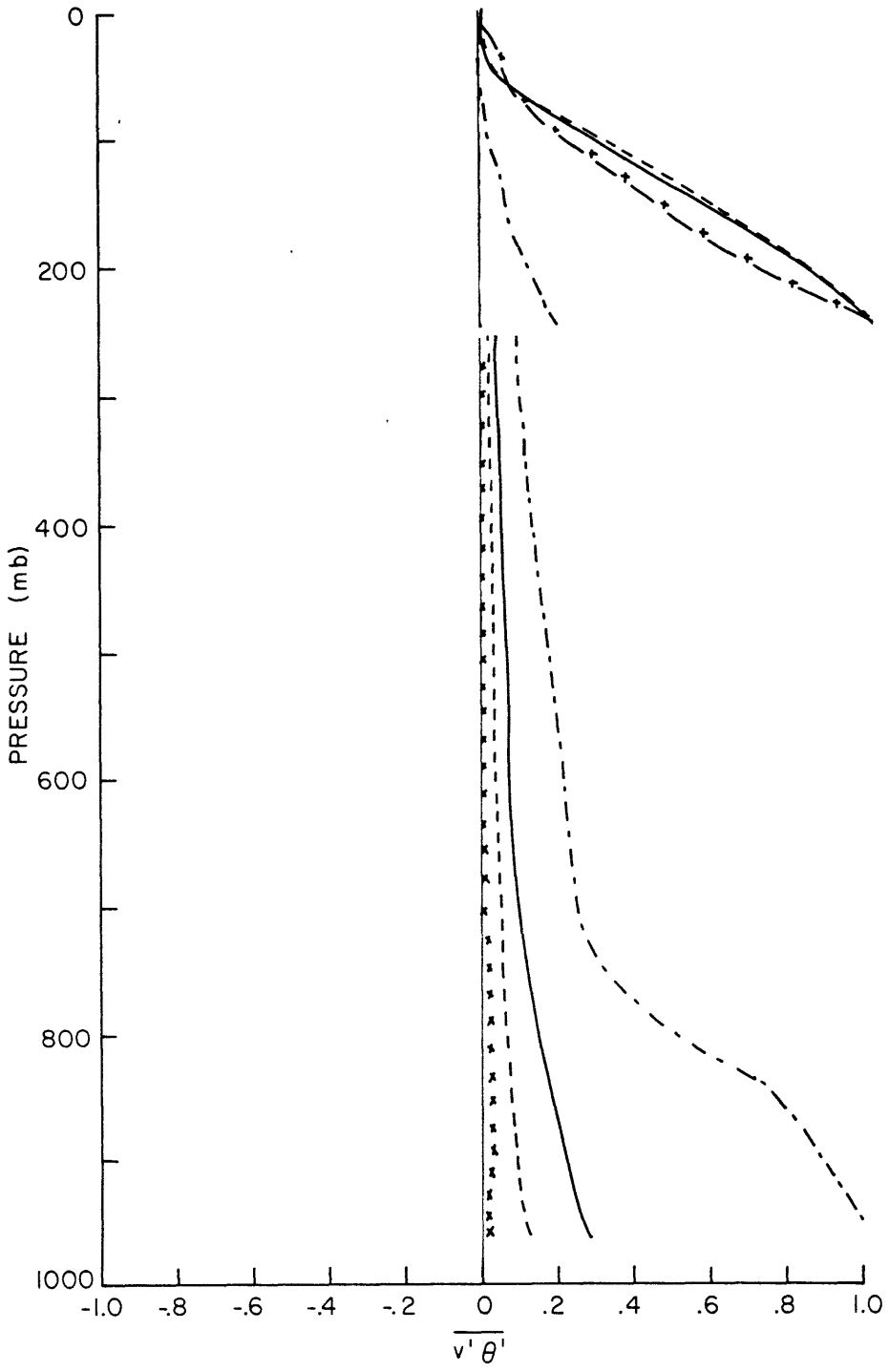

Figure 3.41. As in Figure 3.40, except for the cases γ_I = 2, SR = -1.5, and σ_ρ = 10 (dash dot), 40 (solid), 100 (dash), and 1000 (cross).

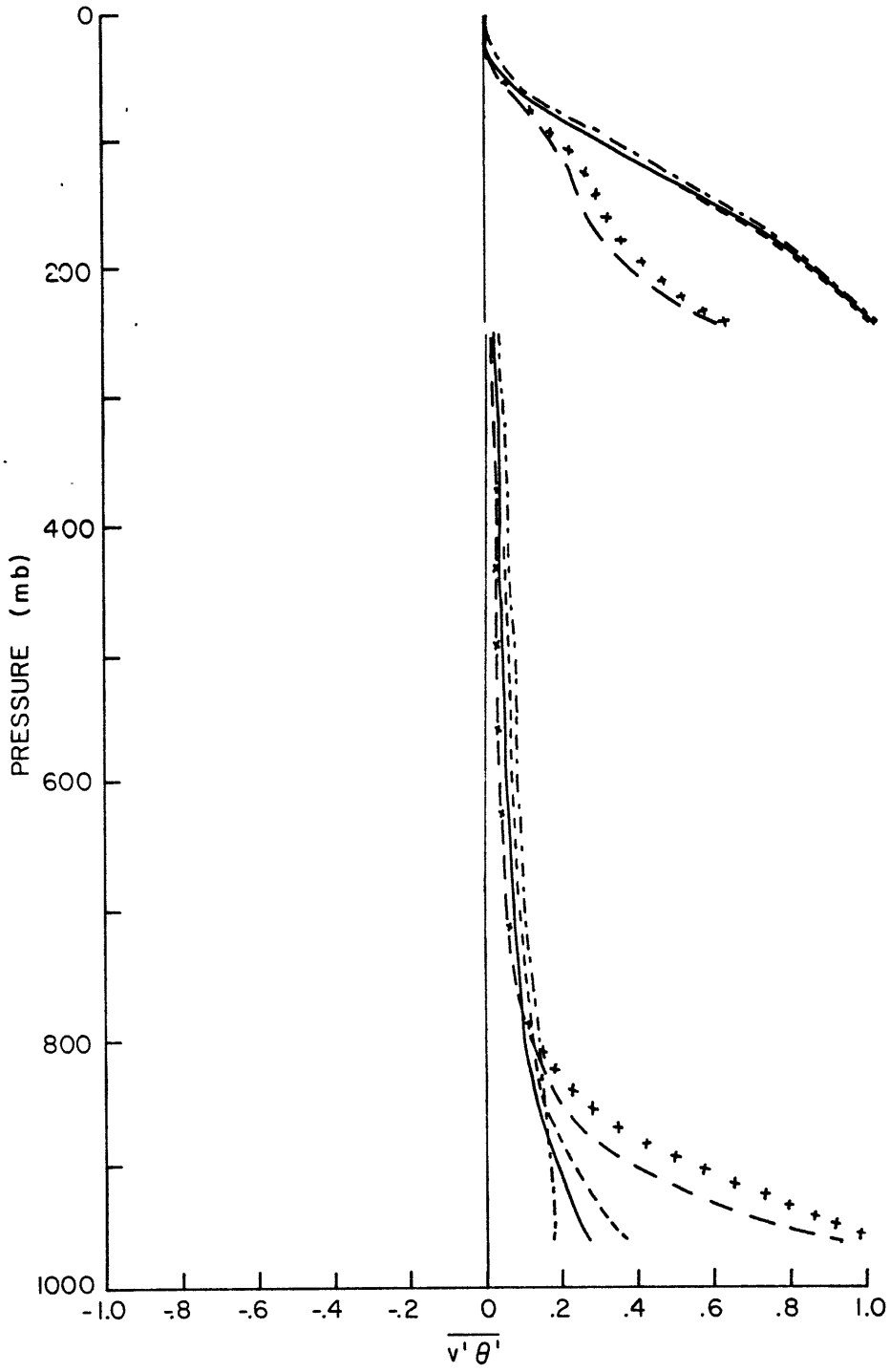

Figure 3.42. As in Figure 3.40, except for the cases SR = -1.5, σ_ρ = 50, and γ_T = 1 (dash dot), 3 (solid), 5 (dash), 7 (cross), and 10 (long dash).

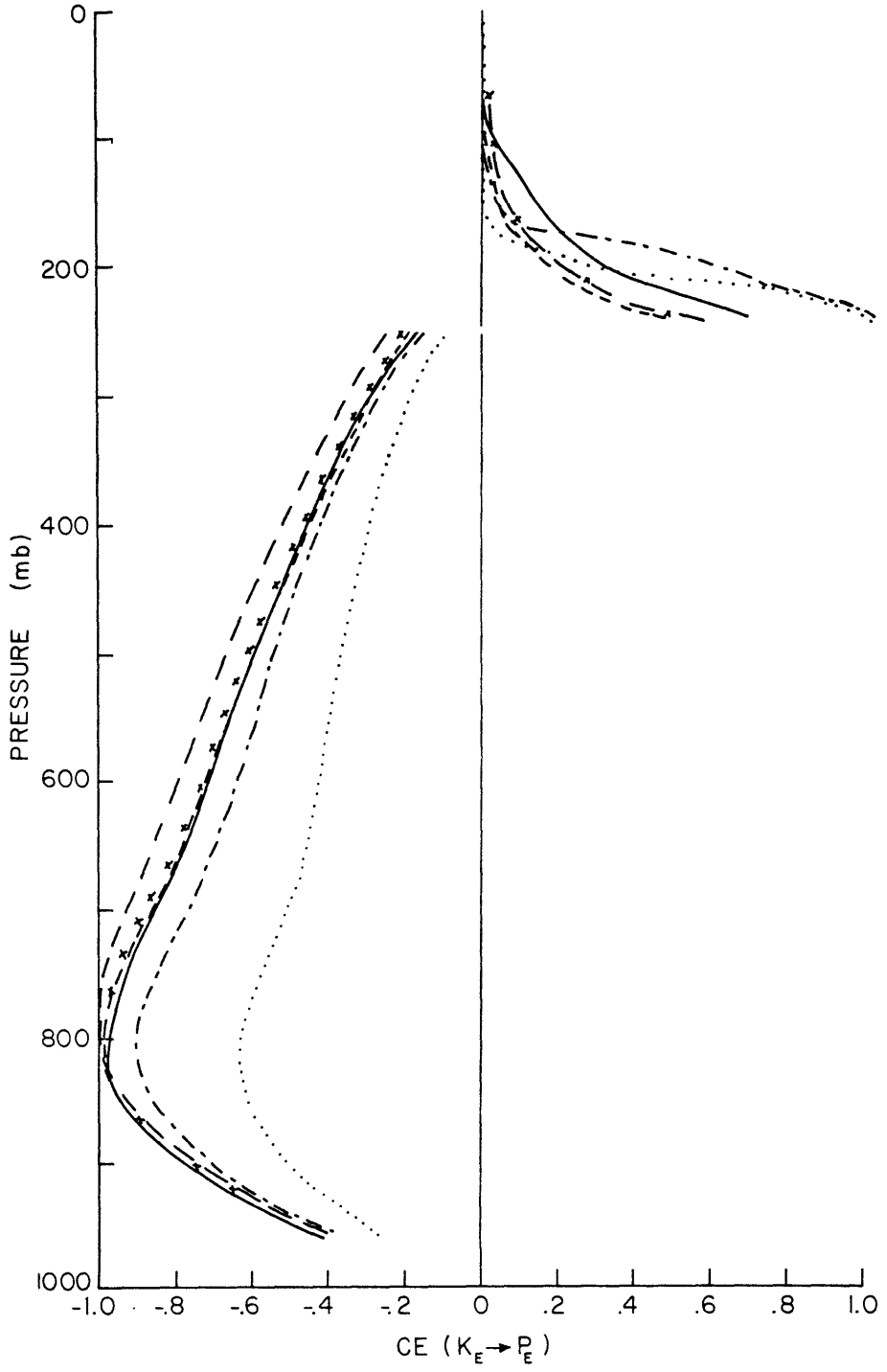

Figure 3.43. Vertical structure of the transfer of eddy kinetic to eddy available potential energy ($K_E \rightarrow P_E$ is positive) for the fastest growing Eady mode, for the same cases as in Figure 3.19.

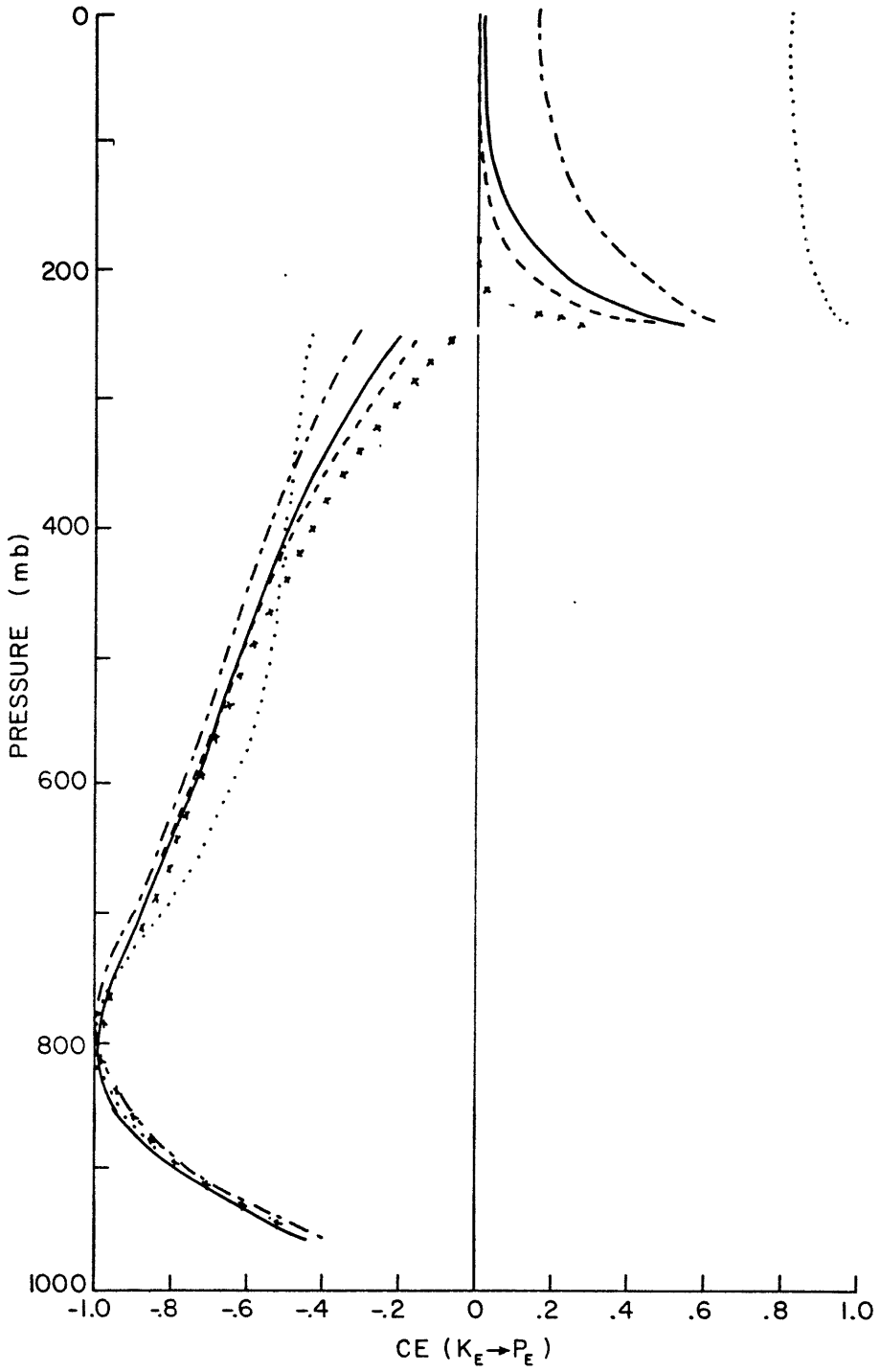

Figure 3.44. As in Figure 3.43, except for the cases γ_T = 2, SR = -1.5, σ_ρ = 1 (dot), 10 (dash dot), 40 (solid), 100 (dash), and 1000 (cross).

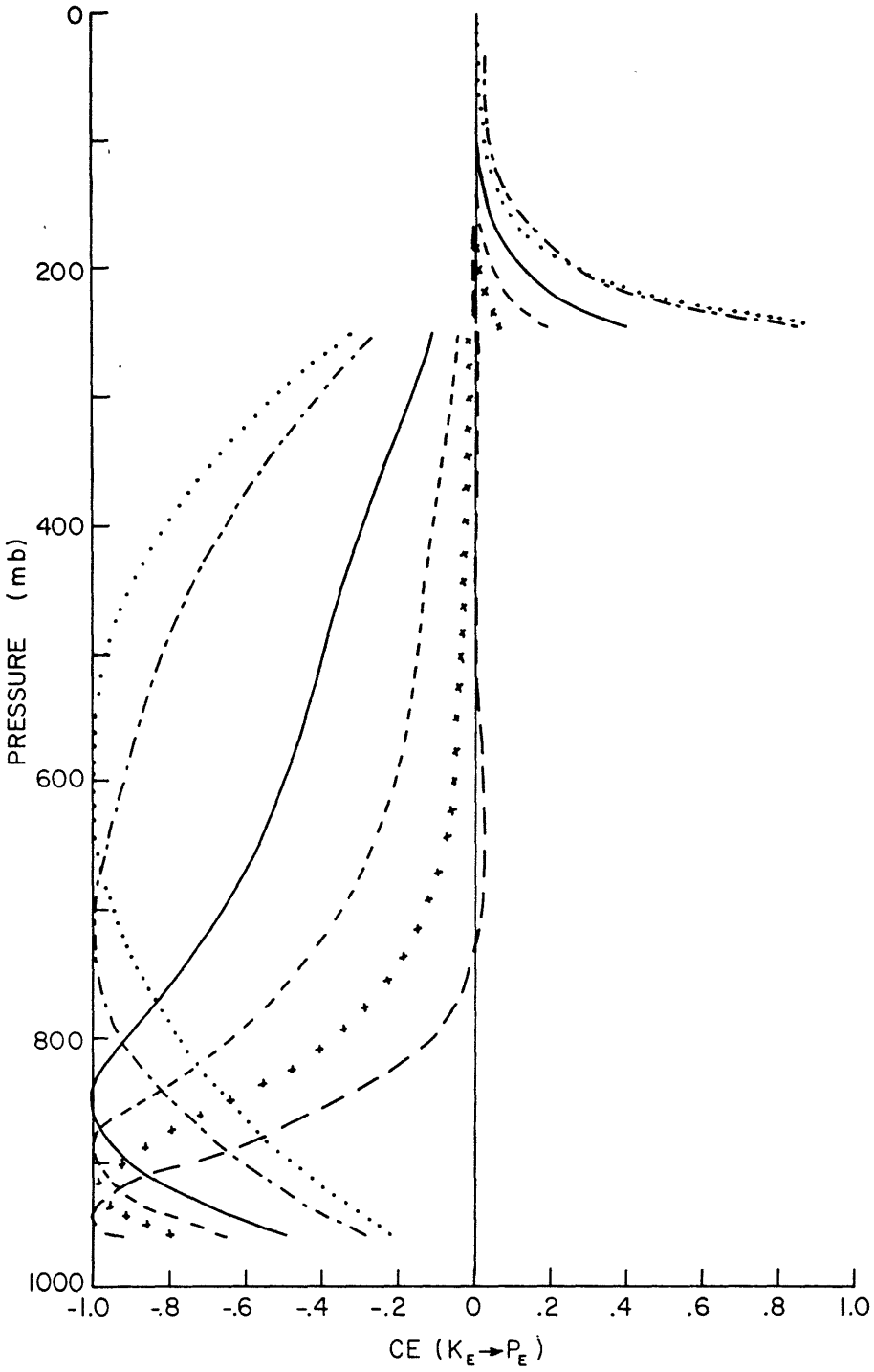

Figure 3.45. As in Figure 3.43, except for the cases SR = -1.5, σ_ρ = 50, and γ_T = 0 (dot), 1 (dash dot), 3 (solid), 5 (dash), 7 (cross), and 10 (long dash).

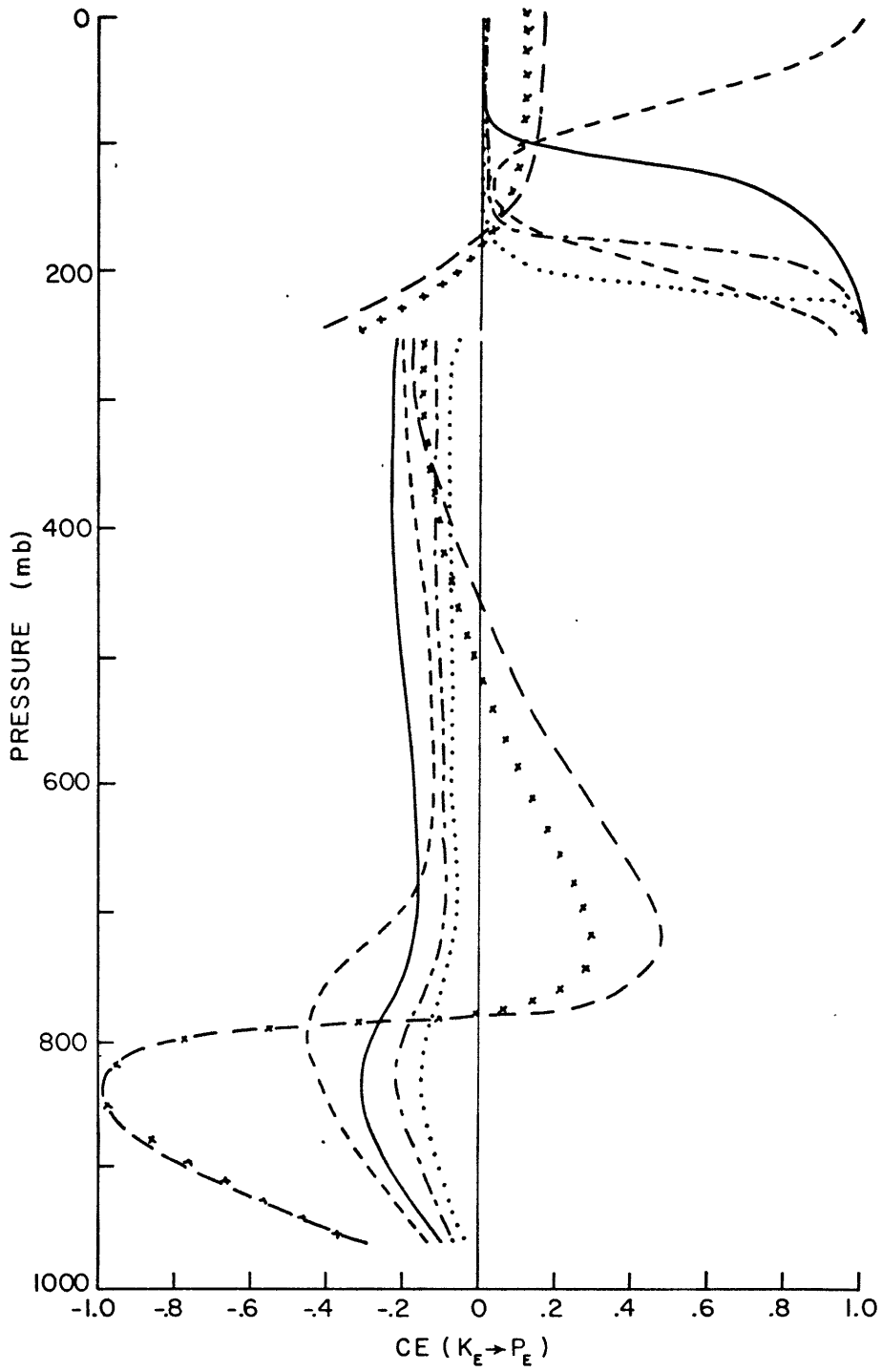

Figure 3.46. Vertical structure of the transfer of eddy kinetic to eddy available potential energy ($K_E \rightarrow P_E$ is positive) for the fastest growing Green mode, for the same cases as in Figure 3.19.

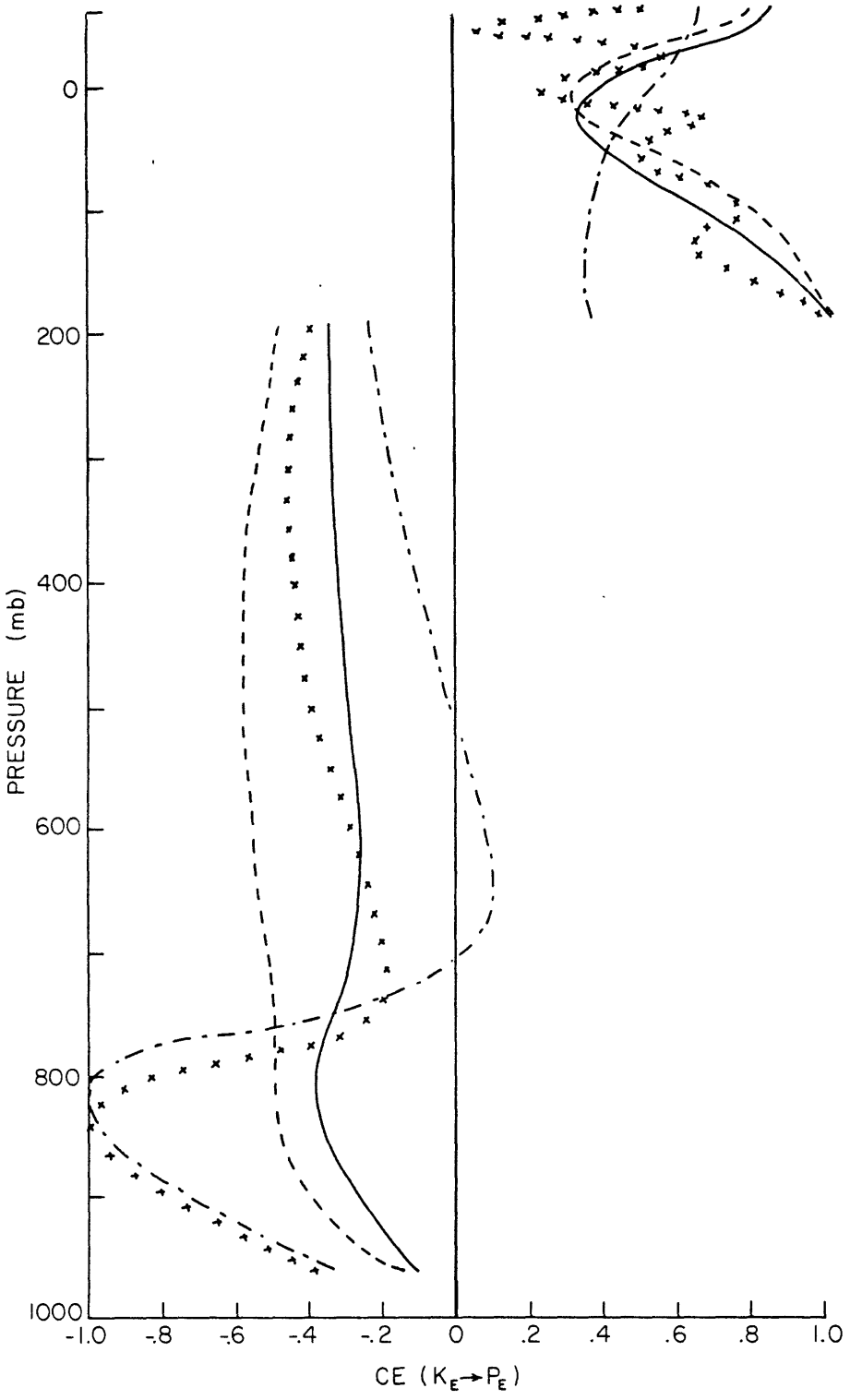

Figure 3.47. As in Figure 3.46, except for the cases γ_T = 2, SR = -1.5, and σ_0 = 10 (dash dot), 40 (solid), 100 (dash), and 1000 (cross).

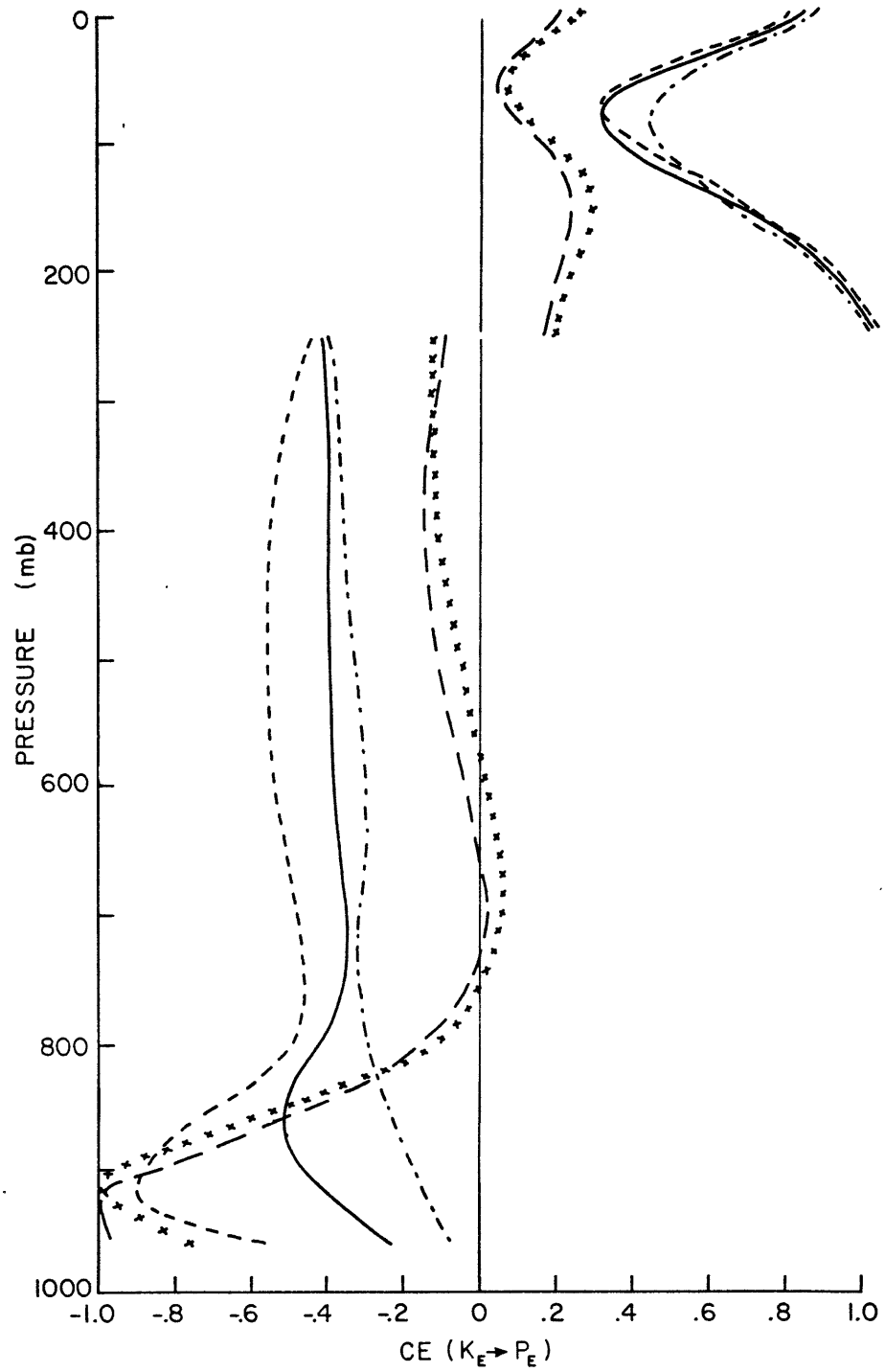

Figure 3.48. As in Figure 3.46, except for the cases SR = -1.5, σ_ρ = 50, and γ_T = 1 (dash dot), 3 (solid), 5 (dash), 7 (cross), and 10 (long dash).

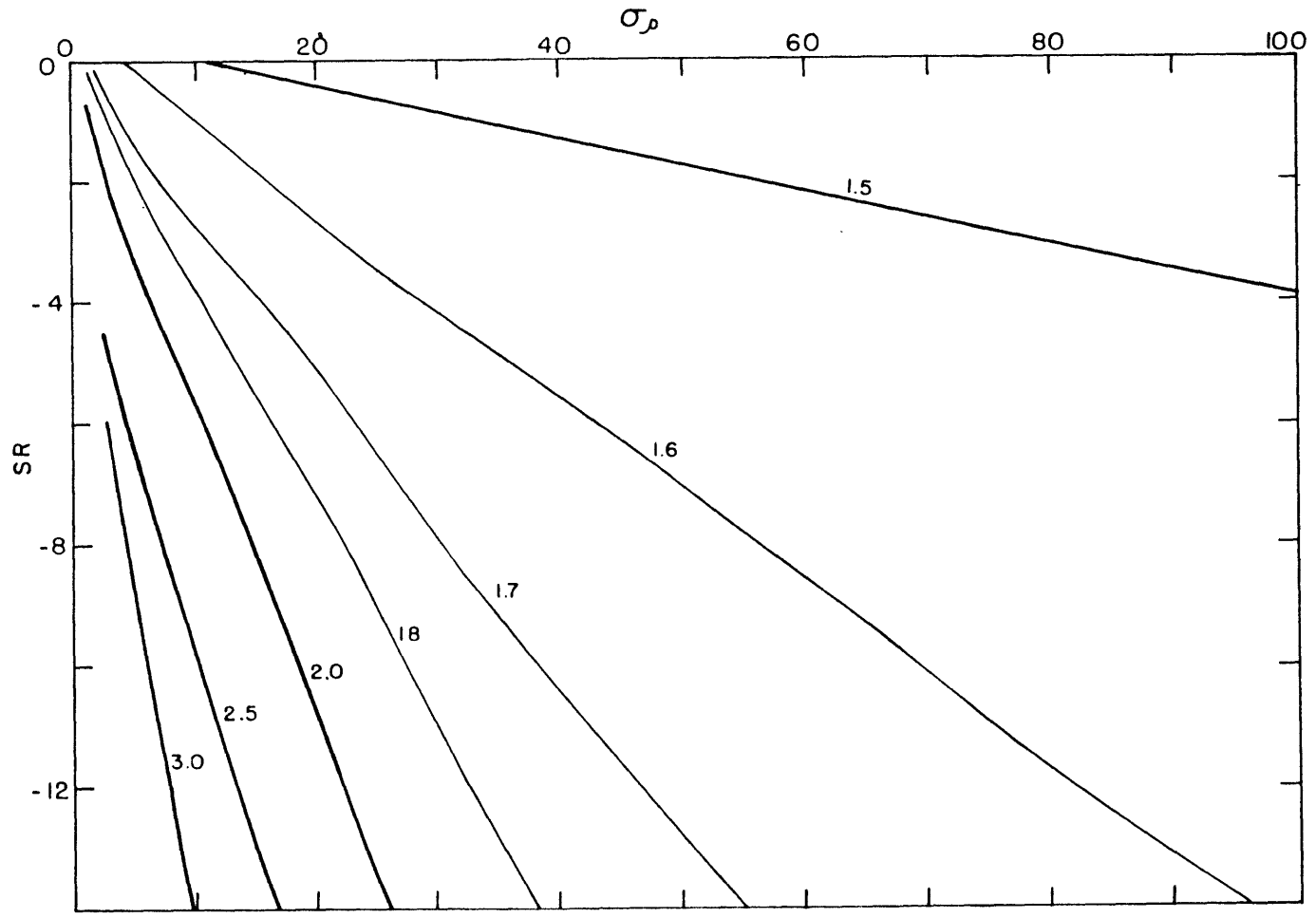

Figure 3.49. Doubling time (days) vs. SR and σ_p for the fastest growing Eady mode for γ_T = .5.

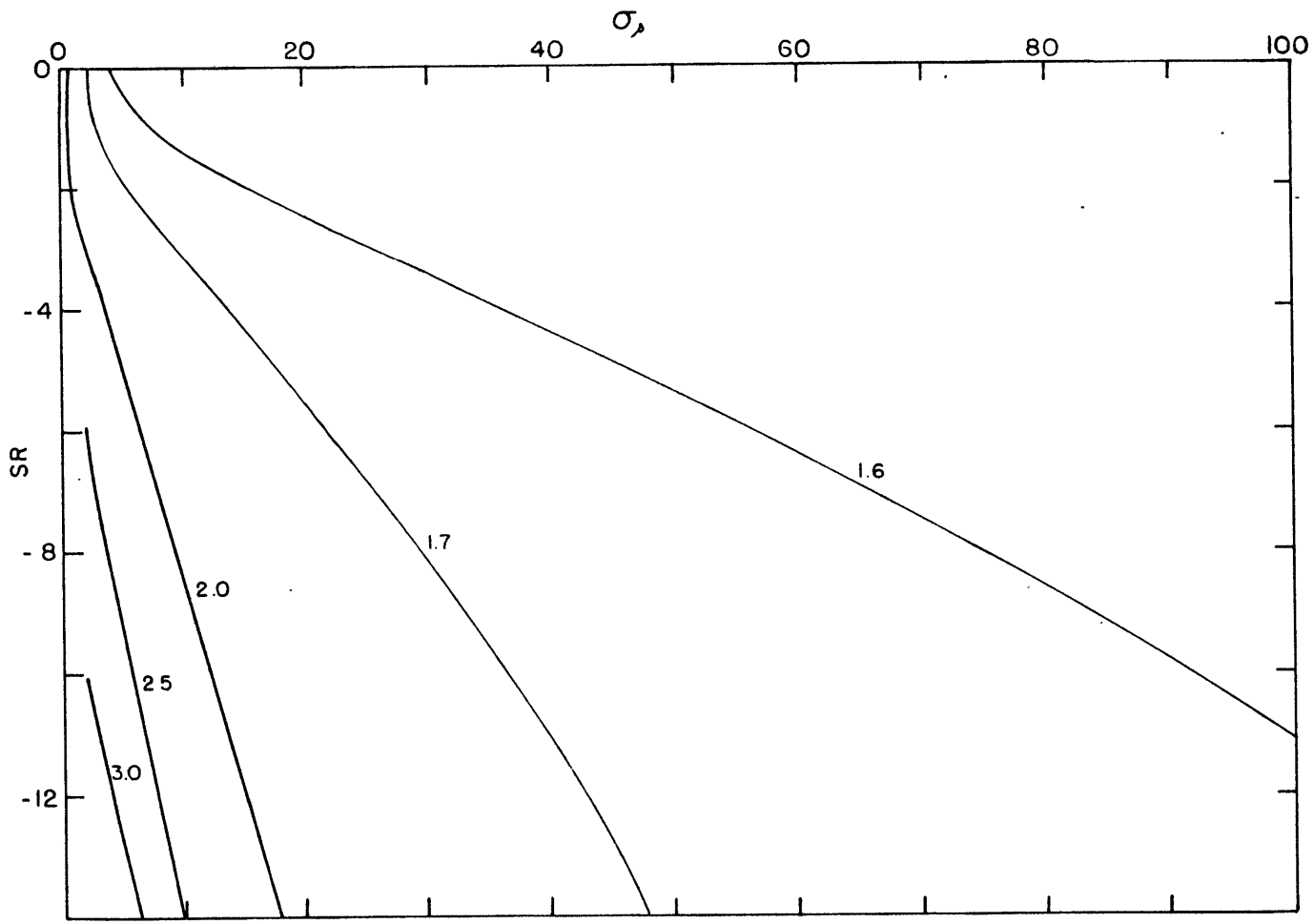

Figure 3.50a. As in Figure 3.49, except for $\gamma_T = 2$.

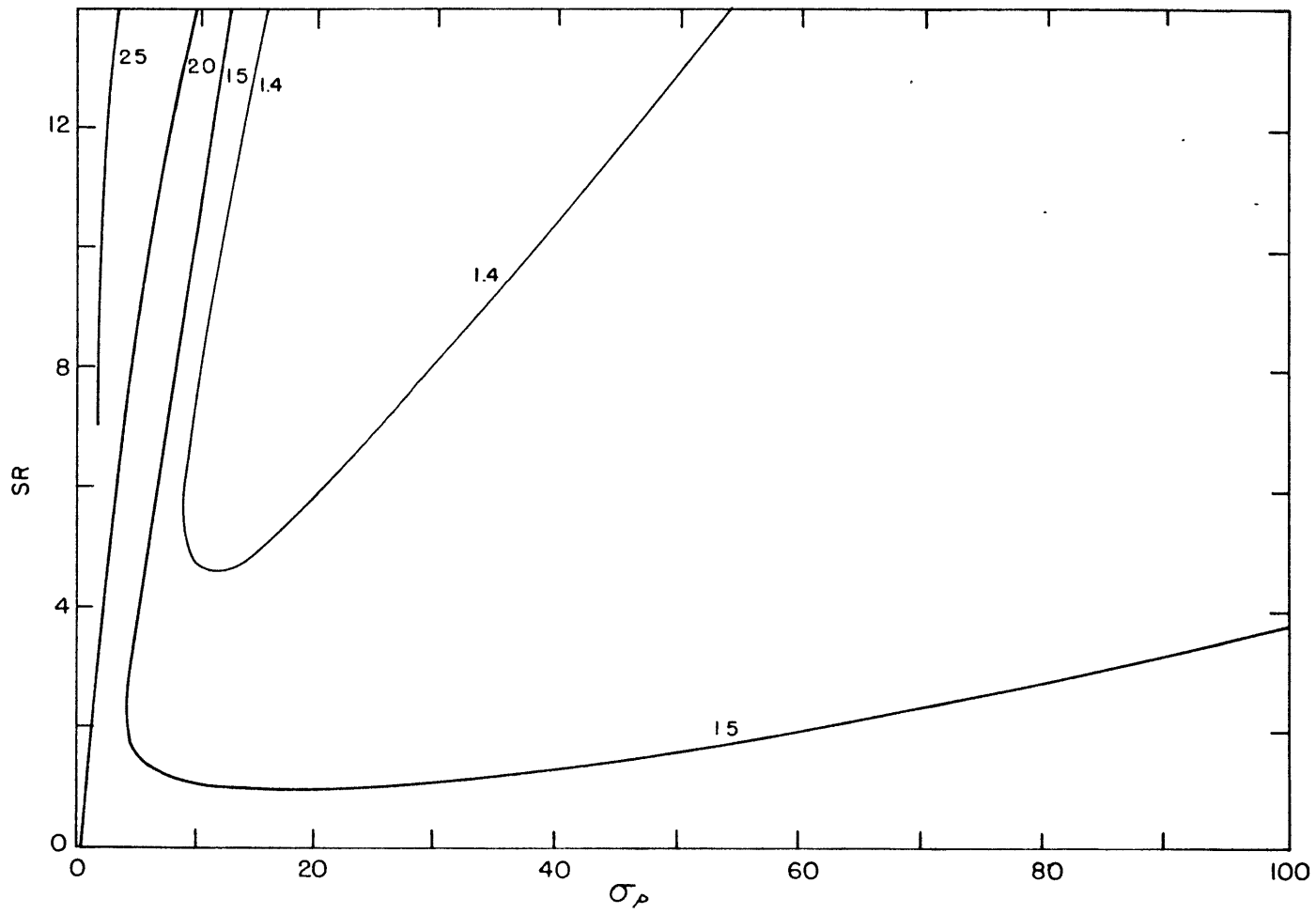

Figure 3.50b. As in Figure 3.49, except for $\gamma_T = 2$ and SR > 0.

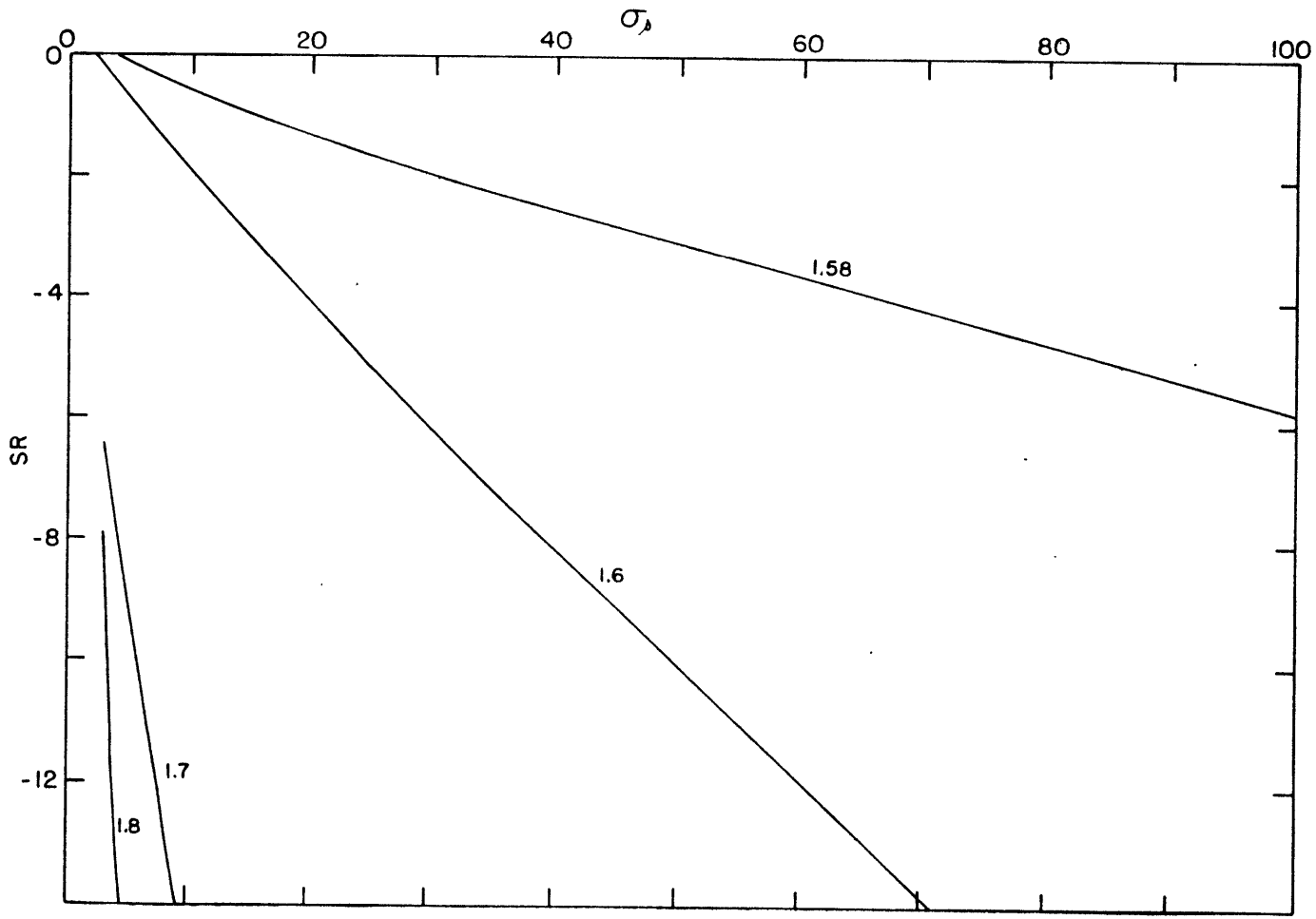

Figure 3.51. As in Figure 3.49, except for $\gamma_T = 6$.

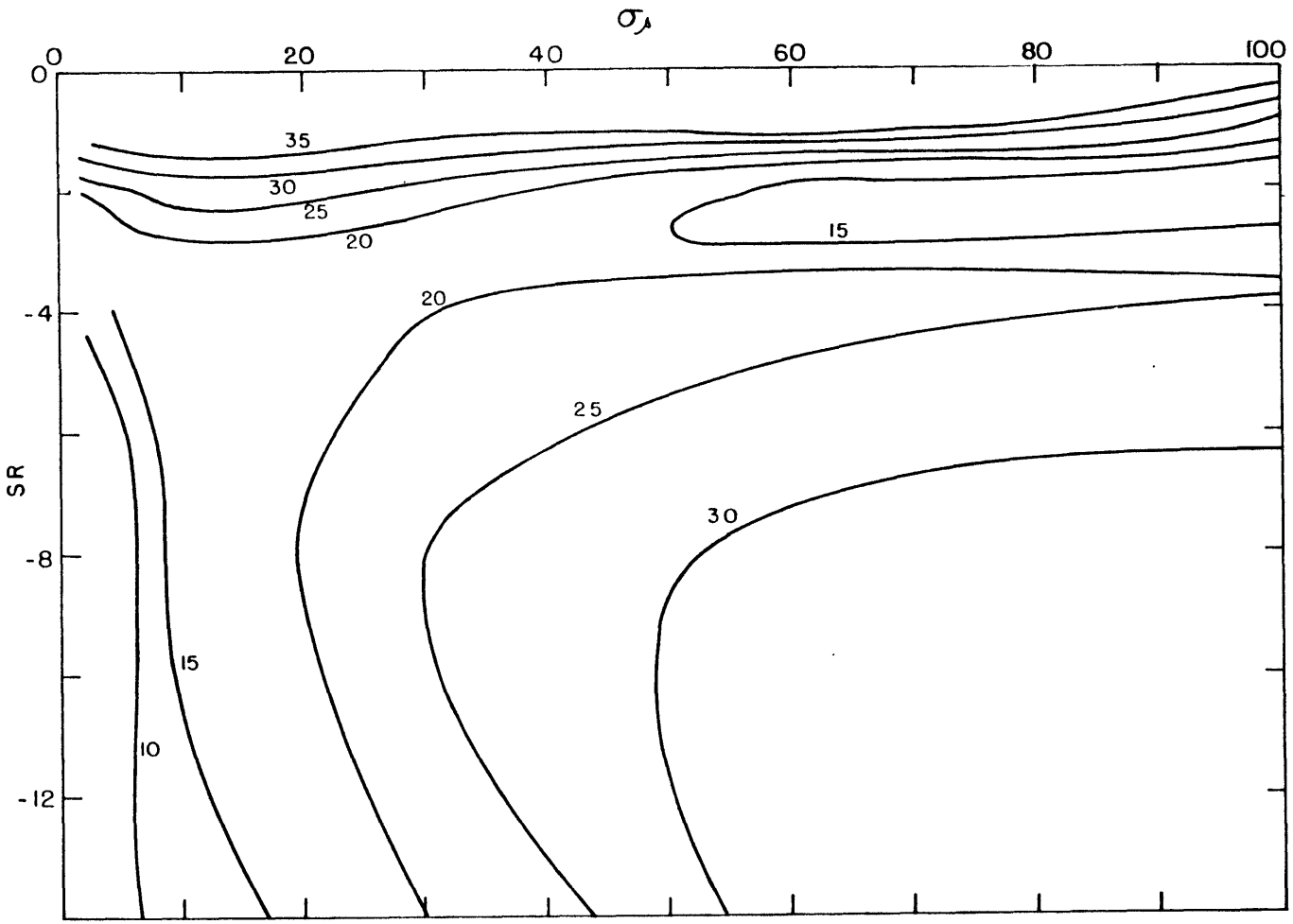

Figure 3.52. Doubling time (days) vs. SR and σ_ρ for the fastest growing Green mode for $\gamma_T = .5$.

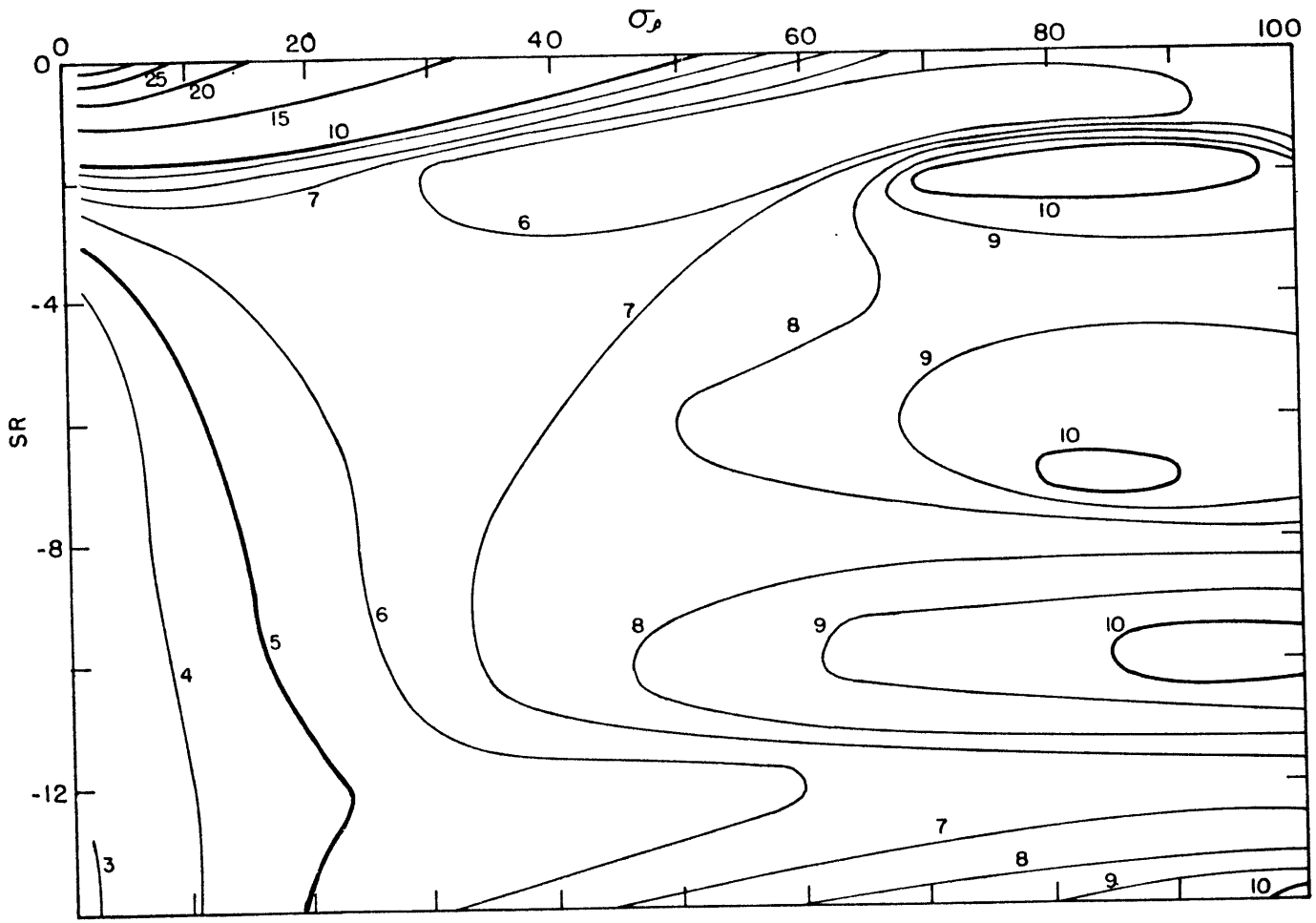

Figure 3.53. As in Figure 3.52, except for $\gamma_T = 2$.

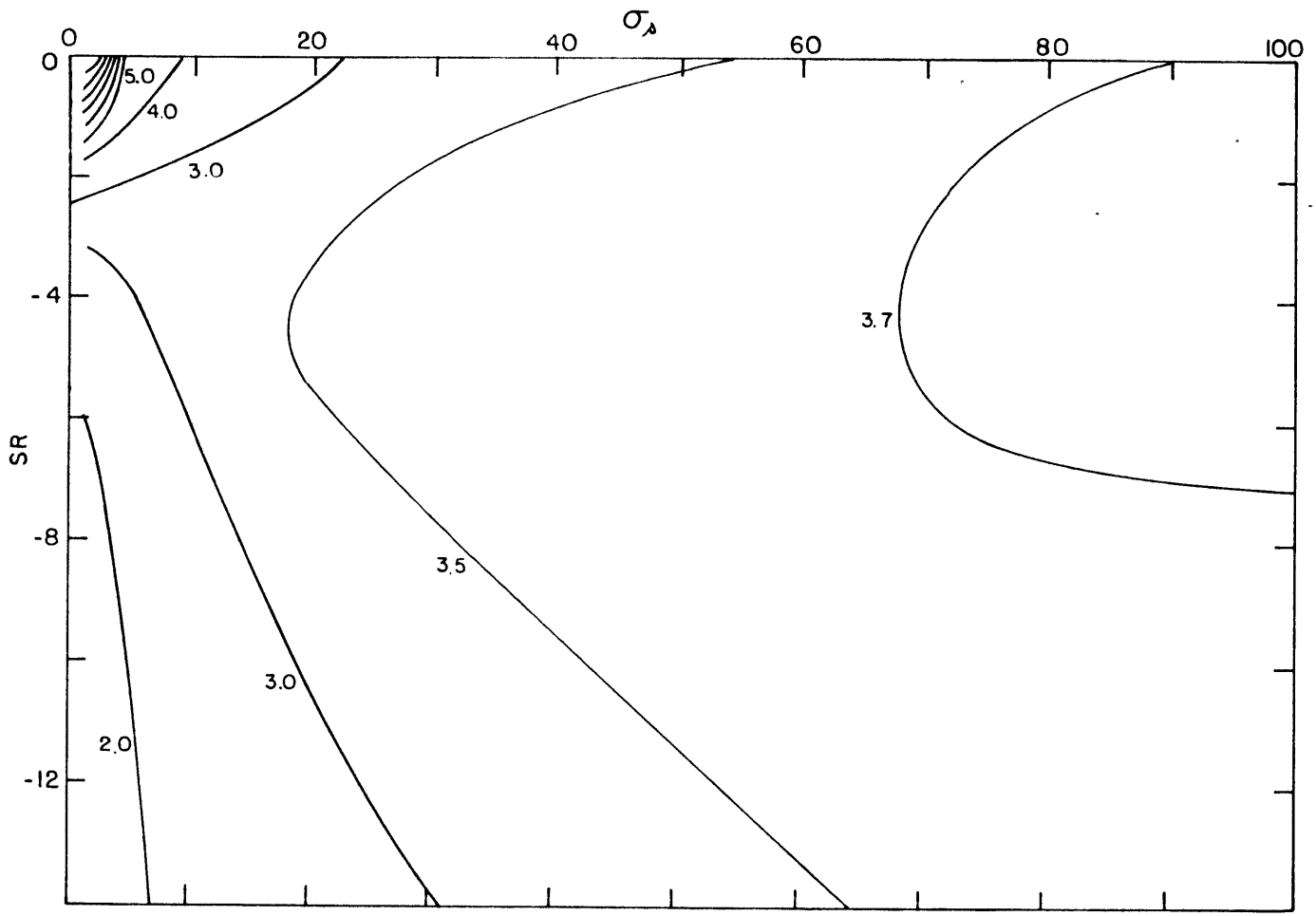

Figure 3.54. As in Figure 3.52, except for $\gamma_T = 6$.

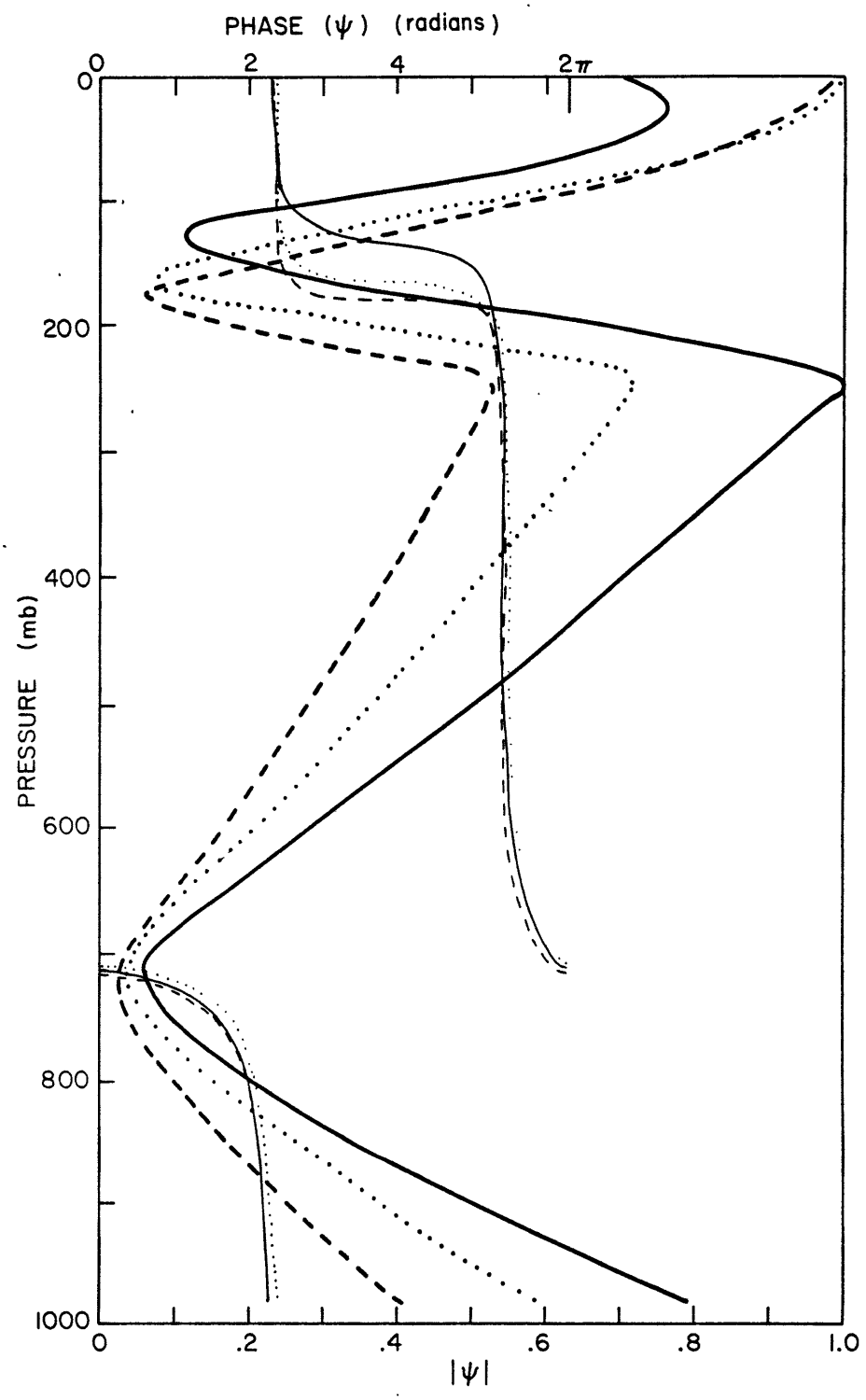

Figure 3.55. Vertical structure of the streamfunction amplitude (thick lines) and phase (thin lines) for the fastest growing Green mode for the same cases as in Figure 3.8. The boundary condition $\omega' = 0$ at $p = 0$ is assumed.

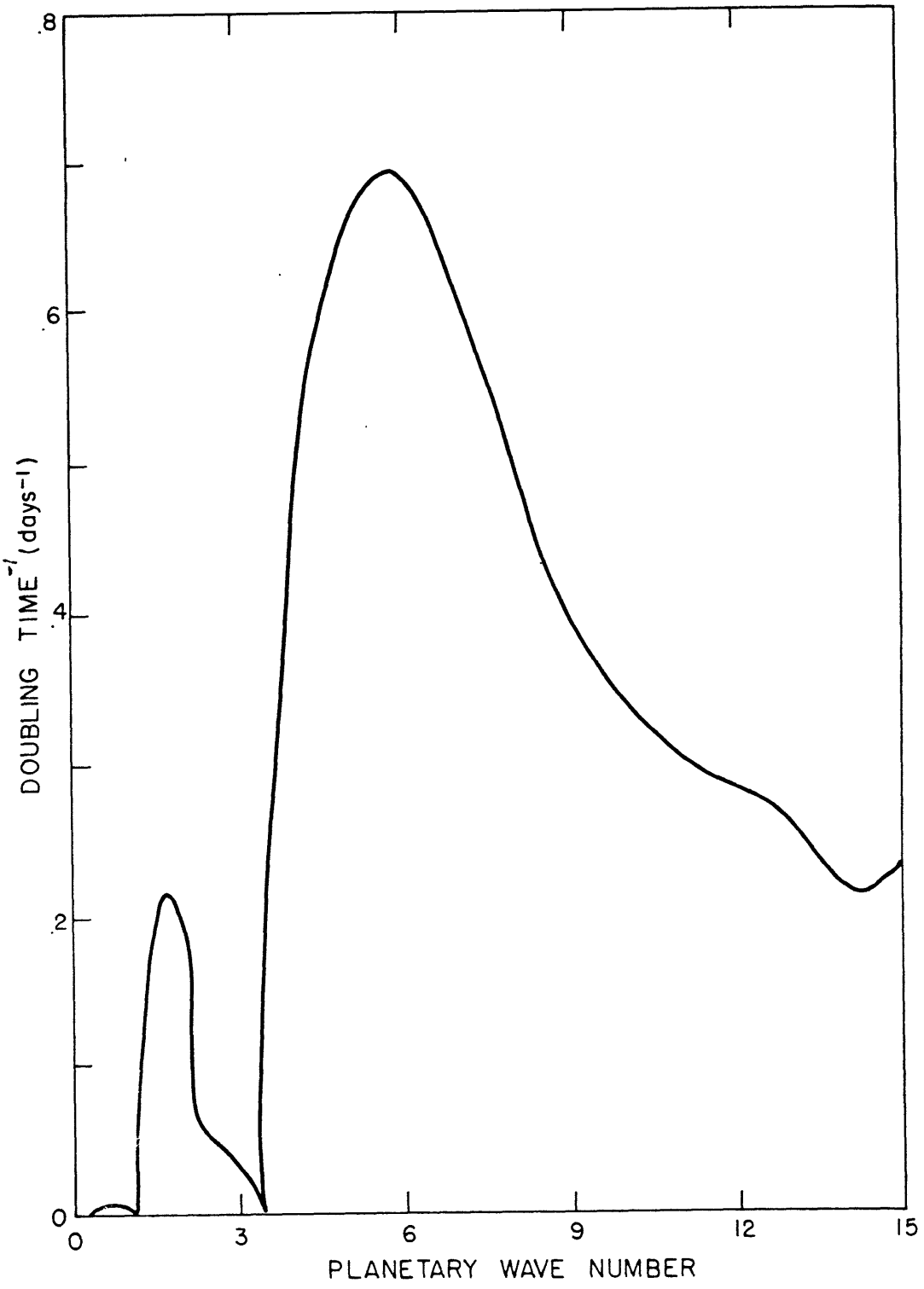

Figure 3.56. Doubling time^{-1} vs. wavenumber for γ_T = 2, SR = 8, σ_ρ = 50, and the upper boundary condition ω' = 0 at p = 0.

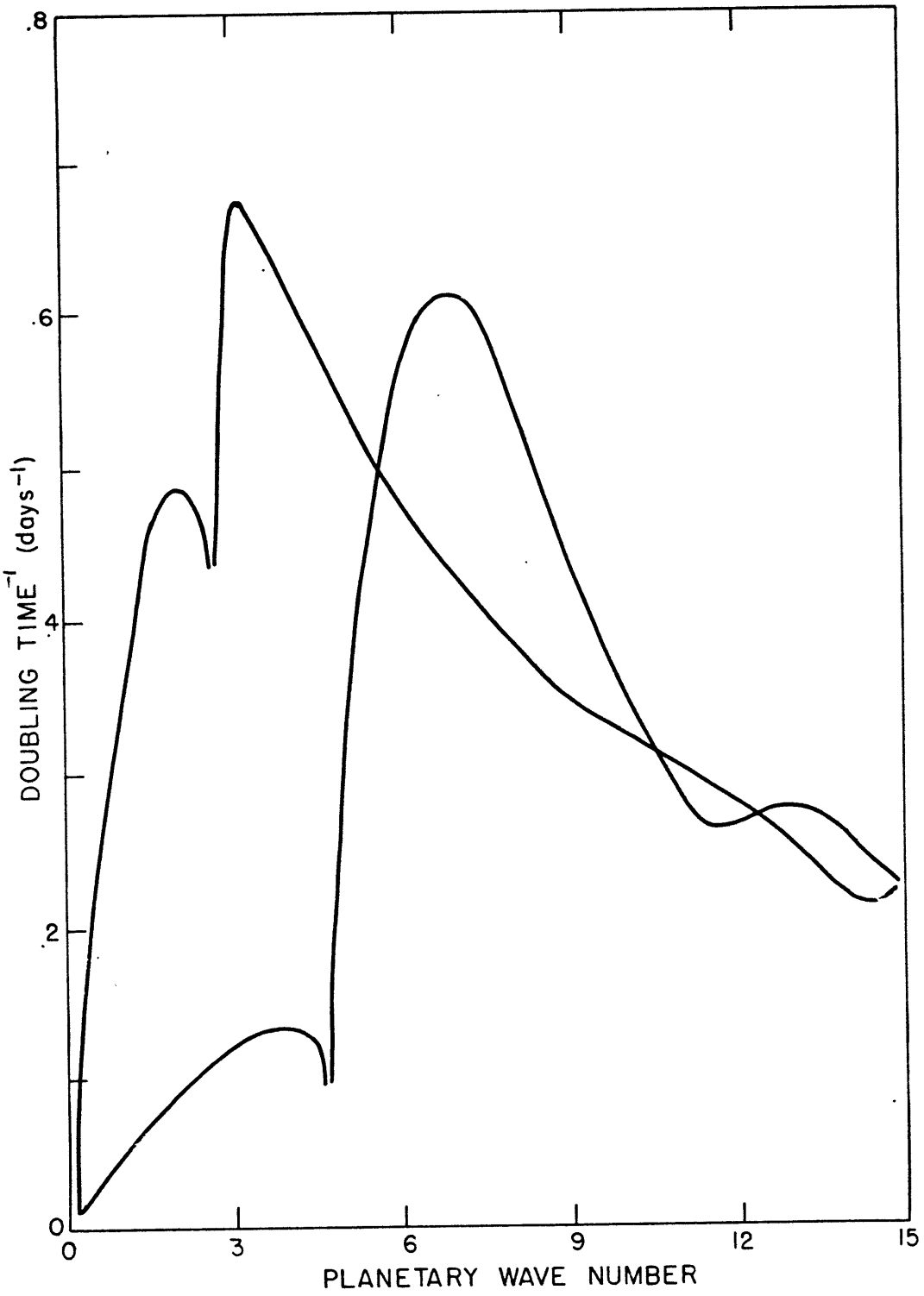

Figure 3.57. As in Figure 3.56, except for SR = -8.

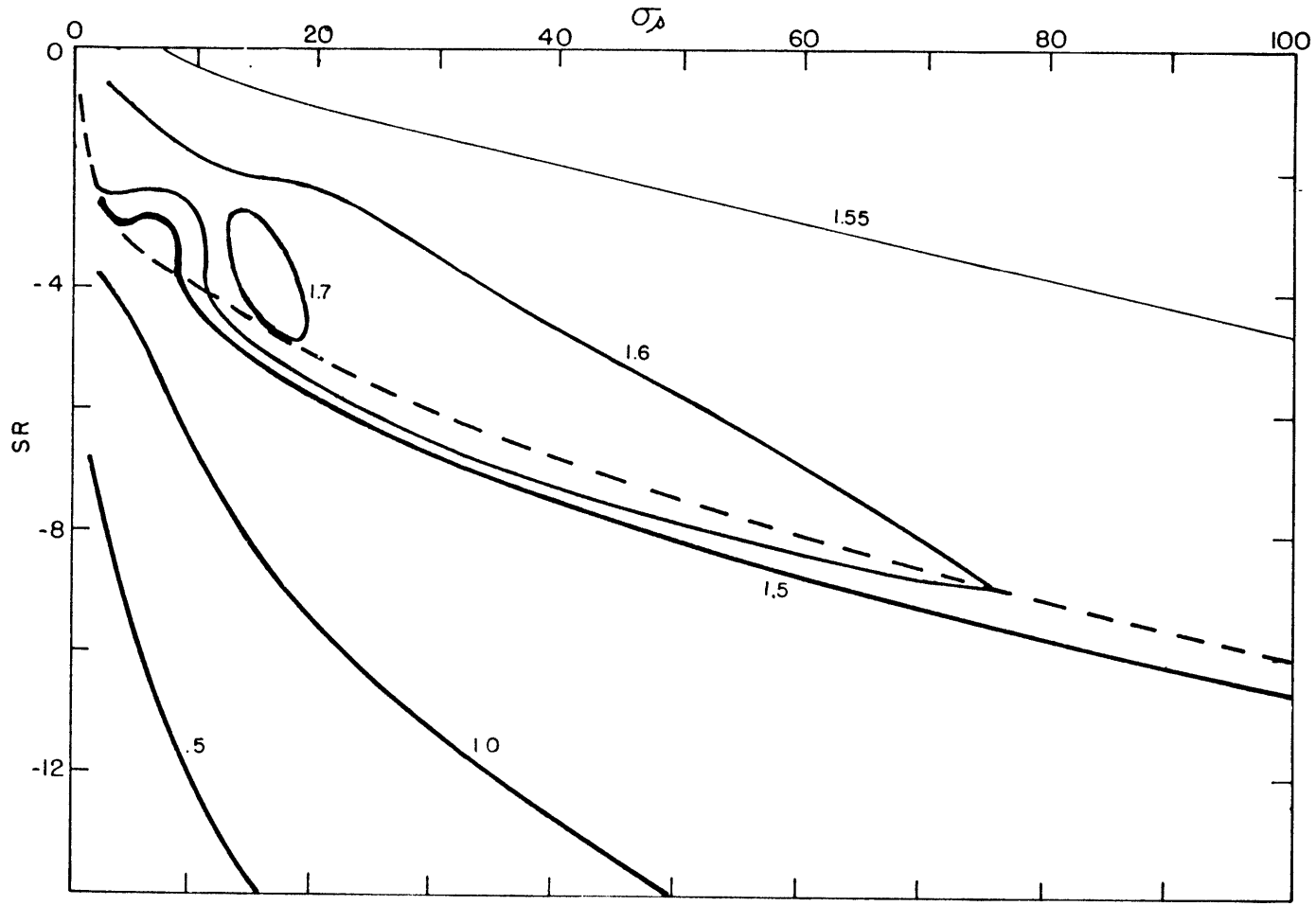

Figure 3.58. Doubling time (days) vs. SR and σ_p for $\gamma_T = 2$, for the fastest growing mode. The upper boundary condition is $\omega' = 0$. Eady modes are to the upper right of the dashed line; new, stratospherically originating modes are to the lower left.

CHAPTER IV

RESULTS FOR THE HIGHLY STRUCTURED BASIC STATES

4.1 Introduction

The simplified temperature and zonal velocity profiles of the previous section do not contain the detail found in true atmospheric profiles. The goal of this chapter is to include such detail. The static stability and unperturbed state of the model atmosphere will be chosen to include seasonal variations. These variations will be represented by monthly averaged $\bar{u}$ and $\bar{T}$ data for the months January, April, July, and October. Latitudes from 20°N to 70°N in 5° intervals will be included.

These months represent seasonal transitions and extremes. The data available allow fine detail to be included in the vertical structure of the unperturbed state. The basic state is kept one-dimensional; longitudinal and meridional variations are excluded.

In calculating the stability characteristics of these detailed basic states, it will be of particular interest to determine how the modes of the simplified profiles are changed; what new modes, if any, appear, whether the modes grow fast enough to reach significant amplitude; and whether these modes could play a significant role in the general circulation of specific regions of the troposphere and stratosphere. These questions are addressed in this chapter by discussing the longitudinal scale, growth rates and phase speeds of the unstable modes, and by examining the vertical structure of their pressure amplitude, their meridional entropy transport, their meridional-vertical velocity correlations, and their conversion of available potential energy to eddy kinetic energy.

4.2 Criteria for Choosing Input Data for the Model

There are 44 pairs of $\bar{u}$ and $\bar{T}$ profiles from the four months and 11 latitudes selected. The pairs used in the calculations will be chosen from these 44 pairs according to two criteria: First, low, middle, and high latitudes should be represented in each seasonal month; the latitudes 25°N, 45°N, and 65°N are selected to meet this criterion. The second criterion is more complicated and requires discussion. The Charney-Stern theorem states that in the absence of boundary temperature gradients a zero in the potential vorticity meridional gradient ($\bar{q}_y$) is a necessary condition for instability. Furthermore, studies of Green (1972), Murray (1960) as corrected by McIntyre (1972), Simmons (1972, 1974), and Dickinson (1973) have shown that a zero in $\bar{q}_y$ has associated unstable disturbances. The studies of Simmons (1974, 1972) also show that pressure amplitudes and meridional heat fluxes of the unstable modes are confined to a region which extends only a few kilometers above or below the height of the zero in $\bar{q}_y$. These results indicate that a zero in the $\bar{q}_y$ profile may result in unstable modes and the location of the zero may be important in determining the vertical structure of those modes. Therefore, when choosing $\bar{u}$ and $\bar{T}$ profiles for the model, this second criterion will be observed: Profiles will be selected which represent all the $\bar{q}_y$ zeros present in the larger data set of 11 latitudes and 4 months.

The second criterion applies, of course, to the one-dimensional calculations of $\bar{q}_y$; because the basic states are one-dimensional; meridional variations in $\bar{u}$ and σ ($\bar{T}$) are ignored. However, calculations of $\bar{q}_y$, including both vertical and meridional variability of $\bar{u}$ and σ ($\bar{T}$) are made for all data

sets and are compared with calculations which exclude meridional variations. Regions where the two methods of $\bar{q}_y$ calculation differ are found to be regions where $\bar{u}_{yy}$ is large. However, the zeros of $\bar{q}_y$ are found to be little affected by the exclusion of meridional variations; thus, the one-dimensional calculation of $\bar{q}_y$ is qualitatively realistic. The second criterion, therefore, allows for an adequate representation of potential source regions for baroclinic instability.

4.3 The Data Sets

The data sets are chosen to cover more than one year where possible, so that the study is climatologically representative. Data from the northern hemisphere is more plentiful and thus better suited for a climatological study. Four data sets are used and are described below. They will be referred to as Data Sources 1 to 4, respectively.

1) Oort and Rasmusson (1971) provide 5-year means (May 1958 to April 1963) for all months, for latitudes 10°S to 75°N in 5° intervals and for levels at 1000, 950, 900, 850, 700, 500, 300, 200, 100, and 50 millibars.

2) R. Newell has provided the tables of $\bar{u}$ and $\bar{T}$ (for the years 1964 to 1968) from which the plots in Newell et al. (1974) were made; this data covered all months and latitudes 20°N, 25°N, 30°N, ... 85°N, and is for levels at 200, 150, 100, 50, 30, and 10 millibars.

3) Tahnk and Newell (1975) supply $\bar{u}$ and $\bar{T}$ values at 5 mb and 2 mb; these data were available only in 10° intervals from 15°N to 75°N, and the data set is only for one year, 1972.

4) Finally, for levels between 1 and .1 mb, data from Newell and Tahnk (in preparation) are used; the data are from Meteorological Rocket Network observations (MRN); the data cover an 11-year period (1961 to 1971), but are only for North America.

Because the last two data sets are very limited as to time and/or spatial coverage, they are used only as guides to extrapolate $\bar{u}$ and $\bar{T}$ profiles above 10 mb. It should be noted that 1) the data sets are from different time periods, 2) they suffer from poor station coverage at levels above 100 mb, and 3) they employ different analysis techniques. These three factors account for the differences among the data sets' values of $\bar{u}$, $\bar{T}$, and hence, values of $\bar{q}_y$ in regions where they overlap. The $\bar{u}$ and $\bar{T}$ values of these data sets are presented in the appendix.

4.4 Calculation of $\bar{q}_y$

The calculation of $\bar{q}_y$ is done for all data sets, with and without meridional variations in $\bar{u}$ and $\sigma(\bar{T})$. First, a cubic spline was applied to the $\bar{u}$ and $\bar{T}$ profiles within each data set to find values at model levels. The cubic spline assures that vertical second derivatives are continuous; this eliminates the possibility of spurious $\bar{q}_y$ values. The splined T profile yields Ψ_p and σ profiles from Equations 6, 8, and 9 in Chapter II, and the definition of σ, and these profiles are used with that of $\bar{u}$ in the exact definitions, Equation 2 of Chapter III, and in the model approximation:

$$\bar{q}_y \approx \beta - f_o^2 \left(\frac{1}{\sigma} \bar{u}_p \right)_p \qquad (1)$$

to obtain the two sets of $\bar{q}_y$ values. The results are in Tables 4.1 to 4.8.

In the $\bar{q}_y$ calculations which include $\bar{u}_{yy}$ and σ_y terms, there is a dominance of positive values which is due to the β effect and vertical shear variation. There is a tendency towards negative values of $\bar{q}_y$ at low levels (below 750 mb) for most latitudes. These negative regions start at levels

ranging from the surface to 900 mb, and in some cases are associated with two zeros. They are caused by large values of the term $f_o^2 \left(\frac{1}{\sigma} \bar{u}_p\right)_p$. This same term results in the high latitude 600-750 mb negative $\bar{q}_y$ regions in January, April, and October, and the July high latitude 375-500 mb negative $\bar{q}_y$ region. There is little seasonal continuity of $\bar{q}_y$ at higher levels for the 5 year data sets; only July has significant negative $\bar{q}_y$ values above 600 mb. The other months have a few weakly negative $\bar{q}_y$ regions in levels covered by both the Oort and Rasmusson (1971) and Newell et al. (1974) data sets, but none of these appears in both sets. In July, the only negative $\bar{q}_y$ region below 5 mb in which the horizontal shear term is comparable to the vertical shear term is that at low latitudes between 125 and 175 mb. $\bar{u}_{yy}$, although relatively small in the regions at 55° and 65°, 90 to 150 mb, and in the region at 65°, 30 to 60 mb, is just enough to tip the balance from positive to negative $\bar{q}_y$ values. These negative $\bar{q}_y$ regions will not be present in the model calculations of $\bar{q}_y$.

The Tahnk and Newell (1975) data set has $\bar{q}_y$ zeros at 30 mb for latitudes 45° and 50°N for all seasons. At 65°N there is a zero at 25 mb for April and a zero at 50 mb for Ocrober. These zeros are due to large values of $f_o^2 \left(\frac{1}{\sigma} u_p\right)_p$. They are not present in the 5-year Newell et al. (1974) data set. Also, the zeros occur in a region where data points are sparse (there is no data in the Tahnk and Newell (1975) data set between 10 and 100 mb). Therefore, their climatological importance is questionable and they will not be included in $\bar{u}$ and $\bar{T}$ profiles used in the model.

The MNR data have zeros at high and low latitudes between 1 mb and 5 mb. These are due to large $\bar{u}_{yy}$ and may result in instabilities which are barotropic in character (Holton (1975), p. 88).

The calculations of Leovy in Charney and Stern (1972) show zeros in $\bar{q}_y$ above 100 mb for 14 October 1957 at 150°W. These zeros are not present in the October monthly averaged data. This is not surprising as one data set is only for a specific day and longitude and the other is averaged over one month and all longitudes. Leovy and Webster (1976) suggest (without presenting calculations) that $\bar{q}_y$ may have zeros in winter on the tropical side of the stratospheric jet (they used hemispheric daily $\bar{u}$ data to calculate $\bar{q}_y$). The MRN data for January have similar zeros but this data is only for North America. The zeros are not in the Tahnk and Newell (1975) data set. Both the Leovy and Webster (1976) and the MRN data $\bar{q}_y$ zeros are due to large horizontal curvature, and instabilities associated with these zeros would be expected to be barotropic in nature (Leovy and Webster, 1976).

The values of $\bar{q}_y$ calculated for the model (Eq. 1 of Ch. IV) when compared with $\bar{q}_y$ values calculated from Eq. 2 of Ch. III) reveal the contribution of meridional shear variation. The term involving meridional variation of σ is a factor of 5 or more smaller than $\bar{u}_{yy}$. The $\bar{u}_{yy}$ term is large and negative between 75 and 450 mb south of 35°N in April and January and October. July values are strongly negative (nearly as large as January values) at the same levels but for latitudes 40°N and 45°N. In all data sets except the MRN, July is the only month with large positive $\bar{u}_{yy}$ values; these are at 25°N and 30°N between 175 and 350 mb; this, of course, reflects the more northerly position of the summer zonal velocity jet. The region where $\left|\bar{u}_{yy}\right|$ is large are those regions where the model values of $\bar{q}_y$ differ most from the observed values. There is a negligible effect on the zeros of $\bar{q}_y$ below 175 mb for all months. In January and October there are some differences above 175 mb, but the zeros here in the observed $\bar{q}_y$ do not appear in

both data sets. In July there is a greater difference, as noted above, and, in addition, in the region 40°N to 50°N, 50 mb to 120 mb. The MRN data set has $\bar{q}_y$ zeros resulting from large $\bar{u}_{yy}$; there are almost no zeros among the corresponding model values.

Overall, however, meridional variations in $\bar{u}_y$ and σ do not have a substantial effect on the number and location of $\bar{q}_y$ zeros calculated from zonally and monthly averaged data. Therefore, one-dimensional $\bar{q}_y$ calculations are qualitatively representative of the full two-dimensional $\bar{q}_y$ field. A one-dimensional basic state thus includes essentially all the potential sources of baroclinic instability that would be included in a two-dimensional basic state. This gives further support to the qualitative realism of studying the baroclinic instability of one-dimensional unperturbed flow.

4.5 Processing the Data for Input to the Model

The profiles of $\bar{u}$ and $\bar{T}$ for the four months, January, April, July and October and latitudes 25°N, 45°N, 65°N have already been chosen to be used in the model. Examination of the $\bar{q}_y$ fields (model values) reveals that January 35°N and October 50°N merit study for associated unstable modes. January 35°N provides $\bar{q}_y$ zeros at high (50, 100 mb) and mid (480, 600 mb) levels. October 50°N provides a close comparison to October 45°N with the major difference being in strength of the negative $\bar{q}_y$ region or closeness of the $\bar{q}_y$ zeros.

None of the data sets includes all model levels. In order to obtain a single $\bar{u}$ or $\bar{T}$ profile for all levels, the data were plotted and smoothed by hand. The Oort and Rasmusson data were followed closely to about 100 mb; the Newell et al. (1974) data from 100 mb to 10 mb. Between 10 and 2 mb,

the Tahnk and Newell (1975) data were used. Above 2 mb, the Newell and Tahnk (in preparation) data were used as a guide. Care was taken so that zeros of $\bar{q}_y$ were affected minimally. The smoothed profiles appear in Figures 4.1 to 4.8.

To minimize error due to interpolation, points at levels for which the data sets have values are then read from the smoothed $\bar{u}$ and $\bar{T}$ profiles*. Next, a cubic spline is applied to each set of $\bar{u}$ or $\bar{T}$ values to yield values at model levels. The cubic spline again assures that vertical second derivatives are continuous, and thereby avoids spurious $\bar{q}_y$ zeros and erroneous small scale variations in model results. The splined $\bar{u}$ and $\bar{T}$ values constitute the input $\bar{u}$ and $\bar{T}$ data for the model.

The $\bar{q}_y$ values associated with the model input profiles are in Tables 4.9 to 4.12. A comparison of these values with those $\bar{q}_y$ values from the model calculations for individual data sets shows that joining the data sets affected $\bar{q}_y$ zeros only within the overlap region of the data sets. Three negative $\bar{q}_y$ regions which appear in only one of the data sets do not appear in the model $\bar{q}_y$ profiles**. One negative $\bar{q}_y$ region (for January 35°N) remains in the model profile, although it is present in only one data set. The final model $\bar{q}_y$ profiles have a weak negative $\bar{q}_y$ region for April 25°N at 400 mb which is not present in observed $\bar{q}_y$ profiles. Two negative $\bar{q}_y$ regions, July 25°N, 125-175 mb and July 65°N, 30-60 mb, are missing from

---

* The levels, 19 in number, are: .1, .2, .5, 1, 2, 5, 10, 30, 50, 100, 200, 300, 400, 500, 700, 850, 900, 950, and 1000 millibars.

** These 3 negative $\bar{q}_y$ regions are for the Newell et al. (1974) data set. They are: April 65°N, levels 37-41; July 25°N, levels 39-41; and October 45°N, levels 27-31.

the final profiles; in the observations the latter region is weak and the former is strong because of large meridional shear variation in $\bar{u}$. Upper level zeros in $\bar{q}_y$ are still present in the input data set of the model: at January 35°N (65-85 mb), July 45°N (85-125 mb), and July 65°N (140-175 mb). Therefore, the $\bar{u}$ and $\bar{T}$ profiles chosen for this instability study on the whole give a reasonably accurate representation of mean atmospheric $\bar{q}_y$ zeros, and thereby also give a good representation of some potential sources of baroclinic instability in the real atmosphere which were not studied before.

In addition to the complete $\bar{u}$ and $\bar{T}$ profiles, the reference values $\sigma_T = .321 \times 10^{-5}$ m^4 sec^{-2} kg^{-2}, $P_{oo} = 10^{+5}$ nt m^{-2}, and $u_o = 10$ m sec^{-1} are used in the numerical calculations. From these γ_T is obtained. The field of $\Sigma_n^{\pm} = \frac{\sigma_T}{\sigma_{n\pm1}}$ is calculated from σ_T and $\sigma = -\frac{R_T}{P}\frac{d}{dP}\left[\ln\left(\left(\frac{P}{P_{oo}}\right)^k \bar{T}\right)\right]$. The parameter γ_T and the fields of $\bar{u}$ and Σ are all now determined and the model set of finite difference equations is ready to be solved for eigenvalues and eigenfunctions for any given wavenumber $\underline{P}$.

4.6 Model Results - Classification of Modes

The doubling times and phase speeds of unstable modes associated with the $\bar{u}$ and $\bar{T}$ profiles are presented in Figures 4.9 to 4.21. All calculations assume $\psi' = 0$ as the upper boundary condition. There is no figure for July at 25°N because no unstable modes were found to exist in that case. This is because there is no temperature gradient at the lower boundary nor any internal zero of $\bar{q}_y$ associated with the July 25°N data; the necessary conditions for instability are thereby not met (the relation of the modes presented in Figures 4.9 to 4.21 to the necessary conditions for instability

will be discussed at the end of this chapter). Modes are presented for planetary wavenumbers .3 to 15 (when vertical resolution permits), except for October at 25°N where the range is 3 to 18 (there are no unstable modes less than wavenumber 3 for this case). Note that the physical wavelength associated with the wavenumbers changes with latitude.

All cases except July 25°N, October 25°N show instability at all zonal wavelengths resolved by the model except isolated wavelengths. Doubling times tend to be longer for 65°N. Modes also tend to peak at shorter physical wavelengths for higher latitudes, which may be due to the increase of β with latitude. Within any given season, there is a large difference between the doubling time and phase velocity curves at different latitudes. As one changes season at the same latitude, there is somewhat less of a difference in these curves only for 65°N.

The modes presented in the 14 cases under discussion are divided into 6 categories:

1) The Eady modes, whose fastest growing mode has the shortest doubling time of all modes and usually occurs between wavenumbers 5 and 8.

2) The Green modes, which are on the long wave side of a cusp which separates them from the Eady modes. Exceptions to this are the cases of April and July at 65°N, where the Green and Eady modes merge. There is still a minimum in the phase velocity curve and the wavenumber of this minimum is defined as the division between Eady and Green modes in these cases. The Eady and Green modes are part of a single conjugate solution to the eigenvalue problem which are separated by a cusp point.

3) The "shortwave Eady modes" which have a local growth rate maximum on the shortwave side of the fastest growing Eady mode. These modes occur only for January, April, and October at 65°N. They are defined to exist for wavenumbers greater than that of the local growthrate minimum in the Eady modes' curve. This minimum is at wavenumbers 6.4, 7.2, and 6.8, respectively, for the 3 cases cited above.

4) The shortwave modes which have their shortest doubling time at the wavenumbers of the local growthrate minimum of the Eady mode curve mentioned immediately above. They have a cutoff on both sides of the peak value, and are always weaker than the Eady modes at the same wavenumbers. These modes form a solution to the eigenvalue problem which is distinct from that containing the Eady and Green modes.

5) Shortwave modes other than those of category 4, whose fastest growing mode has a shorter wavelength than that of the fastest growing Eady mode. These modes are a conjugate solution to the eigenvalue problem which is separate from the solution containing the Green and Eady modes. Their doubling times are generally much longer than that of the fastest growing Eady mode.

6) Longwave modes, other than the Green modes. The fastest growing longwave mode is defined to have a wavelength longer than that of the fastest growing Eady mode. These modes may occur either on the longwave side of a cusp point which separates them from the Green modes (e.g. January, 45°N), or they may form a separate conjugate solution to the eigenvalue problem.

For ease of reference, the modes in the six respective categories are given the symbols E, G, E_s, S_m, S, and L.

Figures 4.9 to 4.21 give several examples of each mode category defined above. Table 4.13 presents properties of the fastest growing mode of all of these examples*. Subsequent discussion of the unstable modes will, like Table 4.13, be organized according to mode category.

4.7 The Eady Modes

The Eady modes are present for all cases except July at 25°N. The fastest growing E modes are usually between 3000 and 5500 km in wavelength (planetary wavenumbers 5 to 8). A notable exception is October 25°N, which has λ = 2000 km and pwn = 18 (see Table 4.13). Doubling times of the fastest growing E modes range between 1.5 and 4.3 days and average about 2 days; they are shortest for 45°N. The case of January 45°N has pwn = 7.7 and doubling time (D.T.) = 1.7 days; this compares well with pwn = 6.6 and D.T. = 1.6 days for the fastest growing Eady mode, when nominal winter parameters are used in constructing the $\bar{u}$ and σ profiles. The fastest growing E mode in Geisler and Garcia's (1977) calculation which used the Lindzen-Hong profile (to simulate winter at 45°N) has a planetary wavenumber greater than 9 and a doubling time of 1.7 days. The doubling time agrees well with this model's value for January 45°N. The wavenumber is difficult to define because the E mode growth rate peak is very flat in the Geisler and Garcia calculation.

With the again notable exception of October 25°N, phase velocities

---

* Modes with doubling times greater than 20 days are not included. The fastest growing Green modes for April and July at 65°N are chosen to be those with their wavenumber just on the longwave side of the point of maximum curvature in the Eady-Green mode growth rate curve.

of all the E modes are positive except when the growth rate goes to zero. The value of the phase velocity is less than 7 m/sec, so there are steering levels for all the E modes in the lower troposphere. $\bar{u} = c_r$ also in the upper stratosphere for some cases (see Table 4.13). The fastest growing E mode has an easterly phase velocity only for October 25°N, but the $\bar{u}$ profile is such that in this case, as in all the others, there is a steering level in the lower troposphere. The phase velocity curve for January 45°N is similar to that for the simple $\bar{u}$ and σ profiles constructed from nominal winter parameters. Geisler and Garcia's (1977) Lindzen-Hong profile phase velocities are higher (around 14 m/sec for the Eady modes), but the Lindzen-Hong profile also has higher $\bar{u}$ values near the ground than does the January 45°N $\bar{u}$ profile, so that the steering levels for both these cases are at nearly the same height (2 km or 800 mb).

Some properties of the vertical structure of the fastest growing Eady modes are presented in Table 4.13 for all the cases for which the mode exists. The complete $|\Psi|$, Phase (Ψ), $\overline{v\theta}$, and eddy energy transfer profiles are presented in Figures 4.22 to 4.29 for 8 of the 13 cases. The cases of January 45°N, April 45°N, and April 65°N are similar in vertical structure to that of January 65°N, and the cases of October 45°N and October 65°N are similar in vertical structure to that of October 50°N.

The streamfunction amplitudes show a peak at the ground and near the tropopause* for all cases except April and October 25°N. There is generally a strong resemblance to the case of simple profiles constructed from

---

* The tropopause is defined to be the pressure level where the temperature stops decreasing as one ascends from the ground. It is between 200 and 100 mb for the profiles of this section and is at lesser pressure for lower latitudes.

nominal winter parameters. The two exceptions decay rapidly in the upper troposphere to extremely small values throughout the stratosphere; they also have the highest planetary wave numbers of all the cases, as one would expect.

The phase profiles show that the pressure wave tilts gradually westward with height except in the upper stratosphere where the westward tilt is very strong. Calculations of the phase difference between v' and ω' show that the meridional circulation associated with this wave is strongly poleward and upward throughout the troposphere and lower stratosphere and changes over to poleward and downward circulation in the upper stratosphere where $|\Psi|$ is small.

The meridional entropy transports are poleward throughout the model atmosphere for nearly all cases. Weak shallow equatorward fluxes at the ground for October 25°N and January 65°N are the only exceptions. The transports are strong only in the lower troposphere and peaks there or at the ground.

Mode kinetic energy release is strongest in the mid and/or lower troposphere (depending on the input $\bar{u}$ and $\overline{T}$ profiles) and goes to zero with ω at the ground. The greatest destruction of mode kinetic energy is in the lower stratosphere, but the amount of destruction is very small compared to the amount of kinetic energy generated in the troposphere.

4.8 The Green Modes

The Green mode spectrum joins that of the Eady mode at a cusp point. The Green modes are present with the Eady modes for all cases except July 25°N. The fastest growing G modes have wavelengths between 5000 and 10000 km (planetary wavenumbers 2.5 to 5, except for a value of 7 for October 25°N).

Doubling times for the fastest growing G modes very from 4.6 to 19 days, and average 8 1/2 days; the longest doubling times are for profiles at 65°N. The case of January 45°N has the fastest growing G mode at pwn = 4.8 with D.T. = 6.9 days. This compares very well with Geisler and Garcia's values of pwn = 5 and D.T. = 7.5 days for the Lindzen-Hong progile. Calculations using simple $\overline{u}$ and $\overline{T}$ profiles constructed from nominal winter parameters give pwn = 3.3 and D.T. = 6 days for the fastest growing G mode.

Phase velocities for the G modes are positive except for April and October at 25°N. The range of phase velocity values is like that of the E modes and steering levels are similar to those for the E modes. The G modes for the case of January 45°N shows the same disagreement with the phase velocity calculations of Geisler and Garcia as did the E modes; the reason for this was discussed above. The phase velocities of the G modes for January 45°N agree well with those for the case using nominal winter parameters.

The vertical structures of the fastest growing G modes for 8 of the 13 cases are presented in Figures 4.30 to 4.37. The cases of April at 25°N, 45°N, 65°N are similar to that of January 25°N and the cases of July 65°N and October 45°N are similar to that of October 25°N, and thus these five cases are not illustrated; all cases, however, are included in Table 4.13.

The streamfunction amplitudes show strong peaks in the stratosphere and secondary peaks near the ground. The January and October 65°N fastest growing G modes have strong amplitudes throughout the stratosphere. Those of January 45°N and, especially, October 50°N have very narrow peaks near the top (p = 0). Stratospheric amplitudes are much stronger than tropospheric amplitudes for the fastest growing G modes; the opposite is true

for the dominant Eady modes. Geisler and Garcia's stratospheric amplitudes for the G mode in some cases are not much stronger than tropospheric values. They attribute this to a very small difference between the minimum zonal wind in the stratosphere and the mode phase speed. The case of January 45°N has a large value for this difference: 6 m/sec. However, for the cases of October 45°N and 50°N the difference is small (< 1 m/sec), yet the fastest growing G modes for these cases have very strong peaks in the stratosphere. Results from this model are inconclusive regarding the dependence of stratospheric G mode amplitudes on the difference between the stratospheric zonal velocity minimum and mode phase speed.

The streamfunction phases indicate a westward tilt with height of the fastest growing G mode pressure wave throughout the atmosphere for all cases except for January 65°N and October 25°N, which have a shallow region of eastward tilt at the ground. The westward tilt is strongest in the stratosphere and mid-troposphere for most cases. Calculations of the v' and ω' phase difference show that the meridional circulation of the fastest growing G modes is poleward and upward in the lower troposphere and poleward and downward in the upper troposphere and stratosphere. January 65°N and October 65°N are exceptions. In these cases, the circulation in the stratosphere is poleward and upward. The stratospheric circulation of the Green modes agrees well with the $\overline{v'\omega'}$ covariance data presented in Newell (1964b). Newell's 18-month data set shows poleward and downward transient eddy motion at 70 and 45 mb in all seasons and latitudes 20°N to 70°N except for the case of winter and spring above 55°N. In this case, the circulation is poleward and upward.*

---

* Molla and Loisel's (1962) v'w' covariance data (for only 2 months) pre-

The meridional entropy transports are poleward with strong peaks in the stratosphere for all cases except January 45°N and 65°N and July 45°N. The pressure wave for the exceptional cases also had a weak westward tilt with height in the stratosphere. January 45°N and October 50°N are the only cases which have peaks of $\overline{v'\theta'}$ near the top, at 20 and 10 mb, respectively. The G modes in general have much stronger stratospheric $\overline{v'\theta'}$ relative to tropospheric values than do the E modes.

The release of mode kinetic energy is strongest in the lower troposphere with some modes also having strong values in the upper troposphere. The destruction of mode kinetic energy is very strong in the stratosphere, and it is much stronger (relative to tropospheric values) for the G modes in comparison with the E modes. Exceptions are the cases of January 65°N, October 65°N, and July 45°N; the first 2 of these exceptions actually have a weak generation of mode kinetic energy in the stratosphere.

4.9 The E_s and S_m Modes

The E_s and S_m modes always occur together. They exist only at 65°N and are present in all seasons except summer. As shown by Table 4.13 and Figures 4.13, 4.16, and 4.21, all the E_s modes are remarkably similar to each other as are all the S_m modes. The most unstable E_s and S_m modes are

---

(cont'd from previous page)

sents a similar picture for the lower stratosphere. However, Wallace (1977) states that: "Calculations of the temporal correlation between vertical velocity and temperature by Molla and Loisel (1962) ... indicates that mean air parcel trajectories in the waves slope upward toward the pole". No vertical velocity-temperature correlations are presented in Molla and Loisel (1962). Their v'w' covariances do show poleward-upward transient eddy motion in a 100-50 mb layer, but only above 55°N for only the 2 months January and April 1958.

planetary wavenumbers 13 and 6 1/2 and have doubling times of 3 and 5 days, respectively. The phase speed and steering level height of the most unstable E_s mode (2 m/sec, 1.5 km) are half of the respective values for the S_m modes.

The vertical structures of the most unstable E_s and S_m modes are presented for January 65°N (Figures 4.38 to 4.41); the structures of the modes for April and October are very similar. The streamfunction amplitude of the S_m mode peaks in the upper troposphere and secondly, near the ground. The much shorter zonal wavelength E_s mode peaks near the ground and is trapped in the lower troposphere. The pressure waves of both modes tilt gradually westward with height except for shallow regions of weak eastward tilt near 750 mb and the ground. The meridional entropy transports in these shallow regions are correspondingly weak and equatorward. The entropy transports are primarily poleward for both modes. They are strong in the mid and lower troposphere for the S_m mode and strong in the lower troposphere for the E_s mode. The meridional circulation for both modes shows a strong poleward and upward correlation of v' and ω' at all levels. The generation of eddy kinetic energy is strongest in the mid troposphere for the S_m mode and in the lower troposphere for the E_s mode. The destruction of eddy kinetic energy is very weak and occurs in shallow regions. The S_m and especially the E_s modes are very short-wave modes and are strongly active only in the lower or mid troposphere. They would be of little importance to the stratospheric general circulation, because of their shallow depth.

4.10 S Modes

The short wave modes have zonal wavelengths less than 3700 km. They

occur at a wide range of mid latitudes and, except for an S_m mode at 65°N, they are not present in October. The doubling times of the most unstable S modes varies from 4 to 15 days. The most unstable S mode for two cases, April and July at 45°N was not resolved by the model; they are both shorter than 1500 km. Modes at pwn = 13 were taken to represent these cases. These two cases also have a cusp point at wavenumber 5.7. At wavenumbers less than 5.7 there are weaker longwave modes which form with the S modes, a distinct unstable solution to the eigenvalue problem at all wavelengths except that of the cusp point.

Phase velocities are high ($\approx$15 m/sec) for the S modes of low latitudes (25°N, 35°N) and are low ($\approx$ 3 m/sec) for the S modes of higher latitudes (45°N, 65°N). The S modes whose fastest growing mode is unresolved and their longwave counterparts have a remarkably constant phase velocity for all wavenumbers except very near the cusp point. The phase velocity is $\approx$ 3 m/sec, and steering levels are at 890 mb. The other S modes have steering levels higher up in the mid troposphere and in the stratosphere.

Figures 4.42 to 4.45 present the vertical structures of 4 of the 6 most unstable S modes. The two S modes for April 25°N are similar in vertical structure, as are the S modes for April and July at 45°N.

The streamfunction amplitudes for all the fastest growing S modes except those which are unresolved are strong only in the upper troposphere and peak just below the tropopause. The April and July 45°N S modes for pwn = 13 are trapped in the lower troposphere and peak at the ground.

The streamfunction phases vary very little with height except near the ground and in the lower stratosphere. In the latter regions, the wave tilts westward except for July 65°N which has a substantial eastward tilt

between 140 and 180 mb. Near the ground the April and July 45°N modes have a westward tilt. For all seasons, the wave has a strong poleward-upward $\overline{v'\omega'}$ correlation in the troposphere which becomes poleward-downward in the stratosphere.

The meridional entropy transports are strongly poleward in the mid- and/or upper troposphere for all cases except April and July at 45°N. The only appreciable transports for these two cases are poleward and near the ground. Only July 65°N has a significant region of equatorward transports and these are near the tropopause.

Eddy kinetic energy is generated only in the upper troposphere for all cases except April and July at 45°N. These two cases have all their kinetic energy generated near the ground; kinetic energy for the S modes of these cases is destroyed between 830 and 900 mb. The S modes for April 25°N lose their kinetic energy in the upper troposphere, just below the tropopause and, to a lesser extent, in the mid-troposphere. January 35°N and July 65°N have shallow regions in the mid and upper troposphere where there is a small loss of mode kinetic energy.

4.11 The L Modes

There are no L modes at 25°N for all four months, nor are there any L modes with doubling times shorter than 25 days for April. The wavelength of the fastest growing L modes varies between 3.5 and 13.5 x 10^3 km. There are only 2 L modes of wavelength less than 8 x 10^3 km, and these have the longest doubling times (13 to 14 days). The doubling times for the most unstable modes of wavelength 8 x 10^3 km or greater varies between 6 and 11 days. The phase velocity of the L modes varies between 2.5 and 7 m/sec

except for the case of January 35°N, whose L modes have much faster phase velocities of 18 to 20 m/sec. The steering levels in the troposphere for the L modes ranges from 920 to 390 mb. January 35°N, July 45°N, and July 65°N also have steering levels in the stratosphere (see Table 4.13).

The vertical structures of 4 of the 7 fastest growing L modes are presented in Figures 4.46 to 4.49. The omitted cases: January 45°N (pwn = 2.3), July 65°N, and October 65°N are similar in vertical structure to those of January 45°N (pwn = 3.6), January 35°N and January 65°N, respectively.

The streamfunction amplitude of all the fastest growing L modes peaks at the tropopause or higher. The fastest growing L modes for January 45°N, January 65°N and October 65°N peak just below the top of the model atmosphere; their structure would be resolved better if there were levels above 1 mb (47 km), the highest level for which streamfunctions are calculated. Only the L modes for July 45°N and January 35°N have appreciable streamfunction amplitudes in the troposphere; these occur in the upper troposphere.

The most unstable L mode's phases show that their pressure waves have a zero or westward tilt with height throughout the model atmosphere for all cases except January 35°N and July 65°N. These cases have a strong eastward tilt between 350 and 75 mb. For all cases, the $v'\omega'$ correlation indicates a poleward upward circulation at lower levels which becomes poleward and downward in the upper troposphere and stratosphere.

The meridional entropy transports for the fastest growing L modes are everywhere zero or poleward except for January 35°N and July 65°N. For these cases, there are strong equatorward transports in the region of the eastward tilt of their pressure wave. The poleward transports of the fastest growing L modes

all peak in the stratosphere, only July 45°N has a secondary peak at the ground. The most unstable L modes whose streamfunction amplitude peaks near the top also have their meridional entropy flux and eddy energy transfer peaks at or near the top.

The fastest growing L modes for July and January at 45°N have most of their kinetic energy generated in the troposphere between 850 and 250 mb. These modes also have a substantial amount of their kinetic energy destroyed in the stratosphere. The remaining four fastest growing L modes have most of their kinetic energy generation in the stratosphere and lose their kinetic energy in the lower stratosphere or upper troposphere. These four modes are examples of in situ baroclinic instability of the stratosphere. Two of these modes (those for January and October at 65°N) have their peak $\overline{v'\theta'}$ and $|\psi|$ values at or near the top. An accurate representation of their structure above 10 mb would require more levels in that region. The other two L modes (January 35°N and July 65°N) are well resolved. Their significance is discussed in the next two sections.

4.12 The Necessary Conditions for Instability and the Existence of Unstable Modes

In the above discussion, it has been shown that there are long and short wave modes (the L, S, and S_m modes) associated with the $\bar{u}$ and $\bar{T}$ profiles obtained from monthly averaged data. Figures 4.9 to 4.21 show that these modes exist at the same wavenumbers as the Green and Eady modes. In one case (April 25°N) 2 S modes exist at the same wavenumbers as an E mode. These long and short wave modes were not present for the parametric $\bar{u}$ and $\bar{T}$ profiles of the previous chapter. For 3 $\bar{u}$ and $\bar{T}$ profile pairs of this chapter,

the Eady modes had a strong shortwave local maximum at approximately wavenumber 13; this also did not occur for the parametric profiles. Why do these new long and shortwave modes exist? Why did the Eady modes' growth-rates in some cases acquire a local maximum near wavenumber 13? The answers to these questions come from an examination of the relevant quasi-geostrophic potential vorticity profiles.

The Eady and Green modes exist for the $\bar{u}$ and $\bar{T}$ profiles of this chapter if 1) there is a temperature gradient at the lower boundary, or 2) there is a zero in the $\bar{q}_y$ profile. The case of January 25°N had a surface temperature gradient and E and G modes, but no $\bar{q}_y$ zeros. The case of April 45°N was altered without affecting the $\bar{q}_y$ zeros so that it had no surface temperature gradient; its E and G modes were only slightly affected. The case of July 25°N shows that indeed no modes exist if the necessary conditions for instability are not met.

Removal of internal $\bar{q}_y$ zeros or changing the surface temperature gradient does substantially alter the gorwth rate spectra of the G and shortwave E modes. Doubling the surface temperature gradient for January 25°N decreased the fastest G mode doubling time from 5.3 to 3.3 days. Removal of the 600-730 mb negative $\bar{q}_y$ region for the cases of January, April, and October 65°N resulted in removing the local maximum of E mode growth rates near wavenumber 13. (By definition, this means removing the E_s modes). The simple parametric $\bar{u}$ and $\bar{T}$ profiles do not have this negative $\bar{q}_y$ region. Removal of the 730-800 mb negative $\bar{q}_y$ region for the cases of April and July at 45°N increased the fastest growing G mode doubling time from about 8 1/2 to 17 days and increased the doubling times of E modes between wavenumbers 11 and 15 from about 2 1/2 to 10 days. The removal of the negative

$\bar{q}_y$ region for the cases at 65°N required increasing u by .3 m/sec at 700 mb and by .1 m/sec at 500 mb; for the cases at 45°N, the removal was accomplished merely by increasing $\bar{u}$ at 850 mb by .3 m/sec. These and other calculations show that a very small change in the $\bar{u}$ profile can result in a drastic change in the zeros of the $\bar{q}_y$ profile. This need not be the case. The curvature of the $\bar{u}$ profile, $\bar{u}_{pp}$, is what has an important role in determining $\bar{q}_y$. Substantial changes in the $\bar{u}$ profile could be made without significantly affecting the zeros of $\bar{q}_y$ if $\bar{u}_{pp}$ is not appreciably affected. The above calculations have shown that small changes in the $\bar{u}$ profile can result in the removal of $\bar{q}_y$ zeros which drastically affects the growth rate spectra. However, the cases of January, April and October at 65°N have widely differing $\bar{u}$ profiles, but very similar $\bar{q}_y$ profiles (all have zeros at 600, 730, and 880 mb). Their growth rate spectra (and even the phase velocities and mode structure) are remarkably similar. Thus, a substantial change in the $\bar{u}$ profile need not have an important effect on the growth rate spectra unless is it accompanied by a substantial change in the zeros of the $\bar{q}_y$ profile. Calculations of Gall and Blakeslee (1977) and Staley and Gall (1977) have also shown that the growth rate spectrum at short wavelengths is very sensitive to low level change in the $\bar{u}$ and static stability profiles. They claimed that this was because the short waves "felt" only the part of the $\bar{u}$ profile below 500 mb. This explanation could not apply to the longwave Green modes of this study, which were affected by low level changes in $\bar{u}$. Gall and Blakeslee (1977) and Staley and Gall (1977) did not discuss the effects of their low level changes in $\bar{u}$ and σ on $\bar{q}_y$.

The S_m modes, like the E_s modes, do not exist if the 600-730 mb negative $\bar{q}_y$ region is removed. This is more than just removing a local maximum

in a growth rate curve. An entire distinct conjugate solution to the eigenvalue problem exists only when a specific negative $\bar{q}_y$ region (with its associated zeros) also exists. The profile of $\bar{q}_y$ requires negative values for it to allow, in conjunction with the surface temperature gradient, the bracketed term in Eq. 1 of Ch. III to be zero so that C_i need not be zero for the S_m modes. The E and G modes in these cases do not need negative values of $\bar{q}_y$ to meet the necessary conditions for instability.

The L modes (except for January 45°N) and S modes exist only when certain negative $\bar{q}_y$ regions are present; these regions are specified in Table 4.13. These modes (with the exclusion of January 45°N) are part of a conjugate solution to the eigenvalue problem which is distinct from that containing the Green and Eady modes. The L modes for January 35°N and July 65°N are the only modes associated with negative $\bar{q}_y$ regions in the stratosphere. These modes are an example of in situ stratospheric baroclinic instability. They have downgradient meridional entropy transports and have their kinetic energy generated at the levels of their associated negative $\bar{q}_y$ regions.

The S_m, S, and L modes were not present when the simple parametric $\bar{u}$ and $\bar{T}$ profiles were used. These modes are seen to exist for the more complicated $\bar{u}$ and $\bar{T}$ profiles of this chapter because these profiles have $\bar{q}_y$ zeros not present in the simple parametric profiles. The S_m, S, L, and E_s modes which exist only when a specific negative $\bar{q}_y$ regions exists always have downgradient meridional entropy fluxes at the levels of that region. In about half the cases, the fluxes peak at one of the $\bar{q}_y$ zeros bounding the negative $\bar{q}_y$ region (See Table 4.13). Modes which are associated with the surface temperature gradient have downgradient fluxes at the surface. Thus all modes have downgradient meridional entropy fluxes in the region of

their source of instability, and their maximum entropy transport is generally above or at the top level of their destabilizing negative $\bar{q}_y$ regions.

Several cases indicate that the amount of negative $\bar{q}_y$ is important in determining the strength of the growth rate of the associated unstable mode or in determining whether it exists at all. October 50°N, July 25°N and January 35°N each have a negative $\bar{q}_y$ value at only one level, and none have an unstable mode associated with this negative $\bar{q}_y$ region (to within model resolution). April 25°N and October 45°N each have negative q_y regions 2 levels deep and do have associated unstable modes which have small growth rates and/or have small extent in wavenumber space. July 45°N, April 45°N, January 35°N, January 65°N, April 65°N, and October 65°N all have much larger negative $\bar{q}_y$ regions and all have associated unstable modes of much larger growthrates.

4.13 Importance of the Unstable Modes to the General Circulation of Specific Regions

For modes of different wavelengths, one cannot conclude that the modes with larger growth rates will dominate the general circulation; their growth may cease sooner than those which have slower growth rates. This was shown by Gall (1976) and Staley and Gall (1977) for the case of long vs. short waves. They found that quasi-geostrophic unstable modes of wavelength < 3000 km were trapped below 500 mb whereas modes of wavelength > 4000 km extended through the depth of the troposphere.* They also showed that modes which were trapped in the lower troposphere (the shortwave modes) stopped growing sooner than modes which extended to upper levels. Therefore, the longwave G and L modes of this model, although having significantly smaller growthrates than the E and E_s modes, may be very important to the general circulation in the upper troposphere and stratosphere.

All the fastest growing G modes (those discussed in this chapter, and those associated with parametric $\bar{u}$ and $\bar{T}$ profiles of Chapter III) have

their strongest streamfunction amplitudes in the stratosphere and/or the upper troposphere just below the tropopause. The peak value of the streamfunction amplitude always occurs near the tropopause. The meridional entropy transports of the fastest growing G modes in all but four cases (see Table 4.13) are strongest in the stratosphere with most cases having their strongest transports in the lower stratosphere. The transports are poleward and may be the cause of the observed secondary maximum of poleward transports in the lower stratosphere (Oort and Rasmusson, 1971; Newell et al., 1974). All but 3 of the fastest growing G modes have most of their kinetic energy depleted in the stratosphere. The Green modes, then, are potentially very important to the general circulation of the lower stratosphere and may also be important for the general circulation of the upper stratosphere and the region just below the tropopause.

The L modes, in addition to the G modes, have strong (> .5 of their peak value) amplitudes, meridional entropy transports, and kinetic energy losses in the stratosphere. Four of the fastest growing L modes may be important to the general circulation above the lower stratosphere. However, these modes have large amplitudes and entropy fluxes very near or at the top of the model atmosphere and may require more levels in this region for an accurate determination of their vertical structure. The fastest growing L mode for July 45°N is the only L mode which has strong poleward entropy fluxes in the lower stratosphere. The L modes for January 35°N and July 65°N are well resolved and are examples of stratospheric in situ baroclinic instability. They both have strong equatorward entropy transport in the lower stratosphere. Observations of Oort and Rasmusson (1971) and Newell et al. (1974) disagree as to the direction of the transport in the lower stratosphere

for January 35°N, but they agree that the transports are weak. For July 65°N, they agree that the transports are weak and poleward. The G modes, which have growth rates comparable to those of the L modes in these cases, show weak poleward fluxes for January 35°N and strong poleward fluxes for July 65°N. Thus, the G modes and L modes arising from in situ baroclinic instability may both be important to the general circulation of the lower stratosphere for January 35°N and July 65°N.

Most S and S_m modes have strong streamfunction amplitudes throughout the troposphere. Three cases, the S modes for April 25°N and July 65°N have strong fluxes in the upper troposphere; all fluxes are poleward except for July 65°N which has a region of equatorward fluxes between 160 and 180 mb. All the other S and S_m modes have poleward $\overline{v'\theta'}$ values which are strongest in the mid or lower troposphere. The S and S_m modes could be important for the general circulation of the upper troposphere. In the mid and lower troposphere they are likely to be dominated by the E and E_s modes which have strong amplitude and entropy transports in these regions and which, in all cases except January 35°N and January 65°N, have much larger growth rates at the same wavenumbers.

The Eady modes, like the S and S_m modes, have strong streamfunction amplitudes throughout the troposphere. In some cases the E modes have strong amplitudes for about 20 mb above the tropopause. The meridional entropy transports of the E modes is strong only in the lower troposphere as is the generation of their kinetic energy (there are no regions where E mode kinetic energy loss is large relative to the amount generated). The above description of the Eady modes associated with the $\bar{u}$ and $\bar{T}$ profiles of this chapter also applies to the Eady modes associated with $\bar{u}$ and $\bar{T}$ profiles generated from the parameter values: γ_T = 2, SR = 0, 1, or -1.5,

and $\sigma_p = 50$. Thus, the general circulation of the troposphere, especially the lower troposphere, is expected to be very strongly affected by the Eady modes.

The E_s modes and E modes of similar wavelength have strong amplitudes, $\overline{v'\theta'}$ values, and eddy energy transfer values only in the lower troposphere. These modes are therefore likely to be important to the general circulation of only the lower troposphere, with E modes being dominant.

The most unstable G modes have been shown to be potentially important to the general circulation of the lower stratosphere, in contrast to the most unstable E modes which have very weak amplitudes and fluxes in the stratosphere (relative to those in the troposphere). The longest E modes have wavelengths comparable to those of the Green modes. The question arises as to whether they share some of the G mode properties and also are potentially important to the stratospheric general circulation. Calculations for 10 of the basic states of this chapter show that the long wave E modes, which are within half a planetary wave number of the cusp point dividing them from the Green modes, do share many of the properties of the Green modes. In particular, they have much stronger stratospheric amplitudes and fluxes than those of the most unstable Eady mode. Amplitudes are at a maximum usually at the tropopause. The $\overline{v'\theta'}$ values are greater than 1/2 the nominal value generally between 90 and 40 mb and sometimes between the tropopause and 40 mb. The circulation of these longwave E modes is poleward and downward. Nearly all of their kinetic energy is generated in the troposphere, and they have a much greater dstruction of kinetic energy in the stratosphere than does the most unstable Eady mode. Thus, in addition to the G (and possibly L) modes, the longest wave E modes may be im-

portant to the general circulation in the stratosphere.

4.14 Calculations for $\omega' = 0$ at $p = 0$

Changing the upper boundary condition in the parametric study of Chapter III resulted in large changes, for some parameter combinations, in the Eady and especially in the Green modes' growth rates, phase velocity, and vertical structure. The changes were drastic when σ_p equaled 1 (no stratosphere). In addition, new modes appeared which were associated with a temperature gradient at the upper boundary when $\omega' = 0$ was the upper boundary condition.

The calculations of this chapter are virtually unaffected by a change in the upper boundary condition from $\psi' = 0$ to $\omega' = 0$. This is because the static stability, σ, becomes very large near $p = 0$ and would damp out the effects of the upper boundary condition. It would also not allow a temperature gradient at the upper boundary to be of any importance in affecting the necessary conditions for instability. From Eq. 1 of Ch. III one sees that large σ at the top allows one to neglect the integral whose integrand is evaluated at the upper boundary. Thus, the necessary conditions for instability for $\omega' = 0$ at $p = 0$ become, for very large σ at $p = 0$, nearly identical to those for $\psi' = 0$ at $p = 0$. Thus, modes which are present for ψ' at $p = 0$ will also be present when $\omega' = 0$ at $p = 0$ and vice versa.

Since σ at $p = 0$ is large but finite, there is a small difference between calculations assuming different upper boundary conditions. When $\omega' = 0$ at $p = 0$ there are for January 65°N and October 65°N additional long-wave modes of planetary wavenumber < 1.5 and doubling time > 2 weeks.

These modes exist only when the temperature gradient at the upper boundary is non-zero and only when $\omega' = 0$ is the upper boundary condition. Their kinetic energy is generated mostly in the stratosphere.

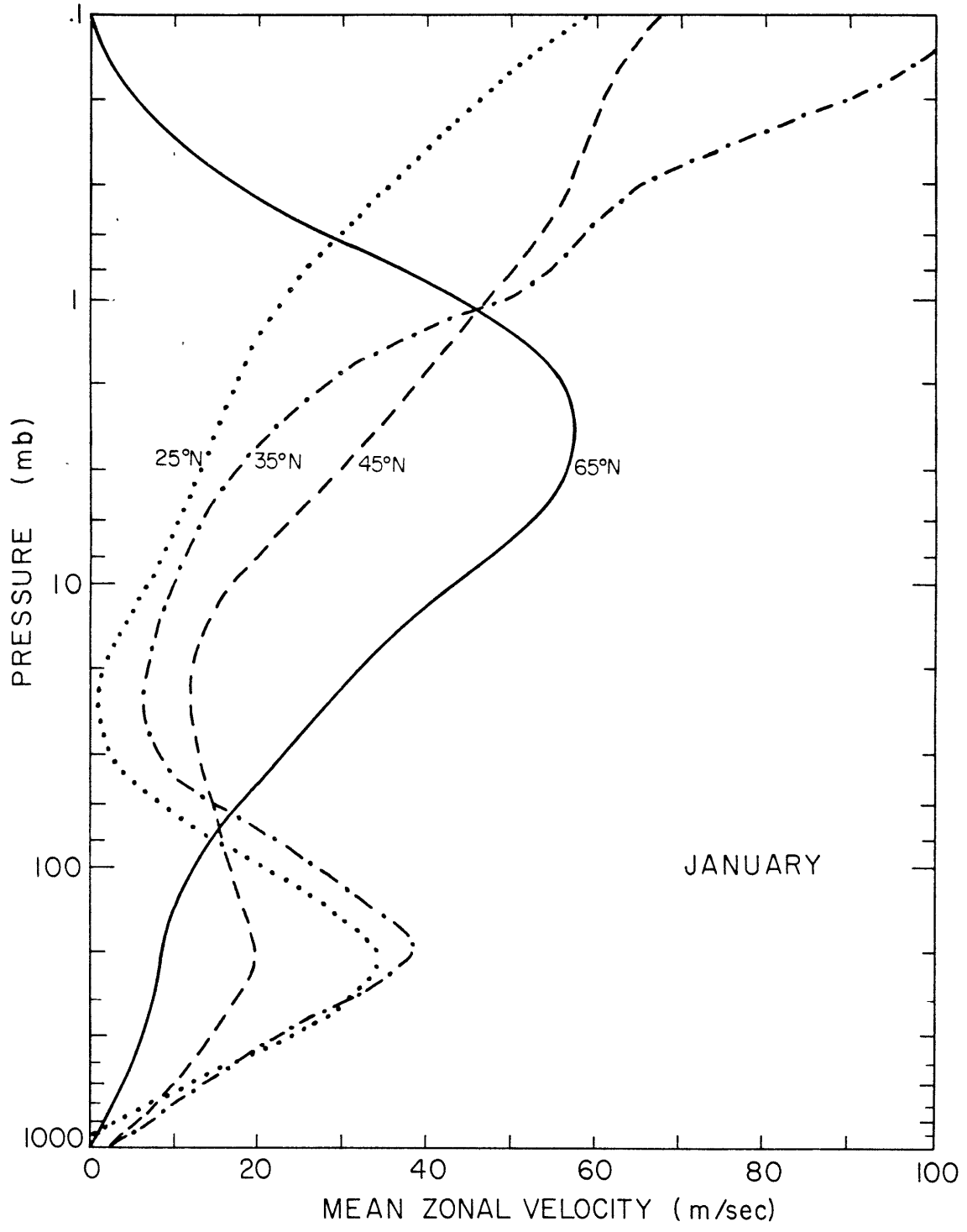

Figure 4.1. Zonal velocity profiles for the basic state for January.

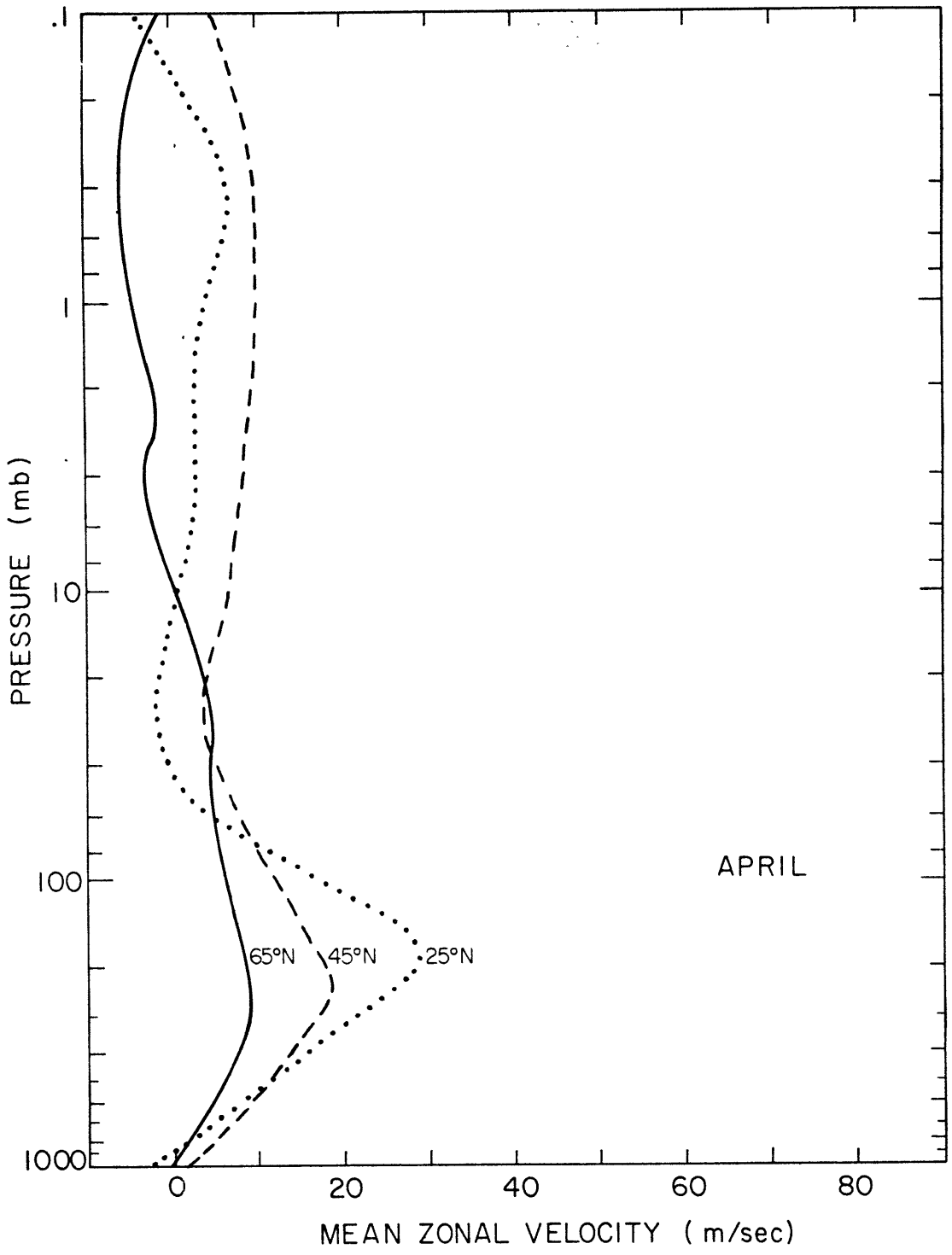

Figure 4.2. As in Figure 4.1, for April.

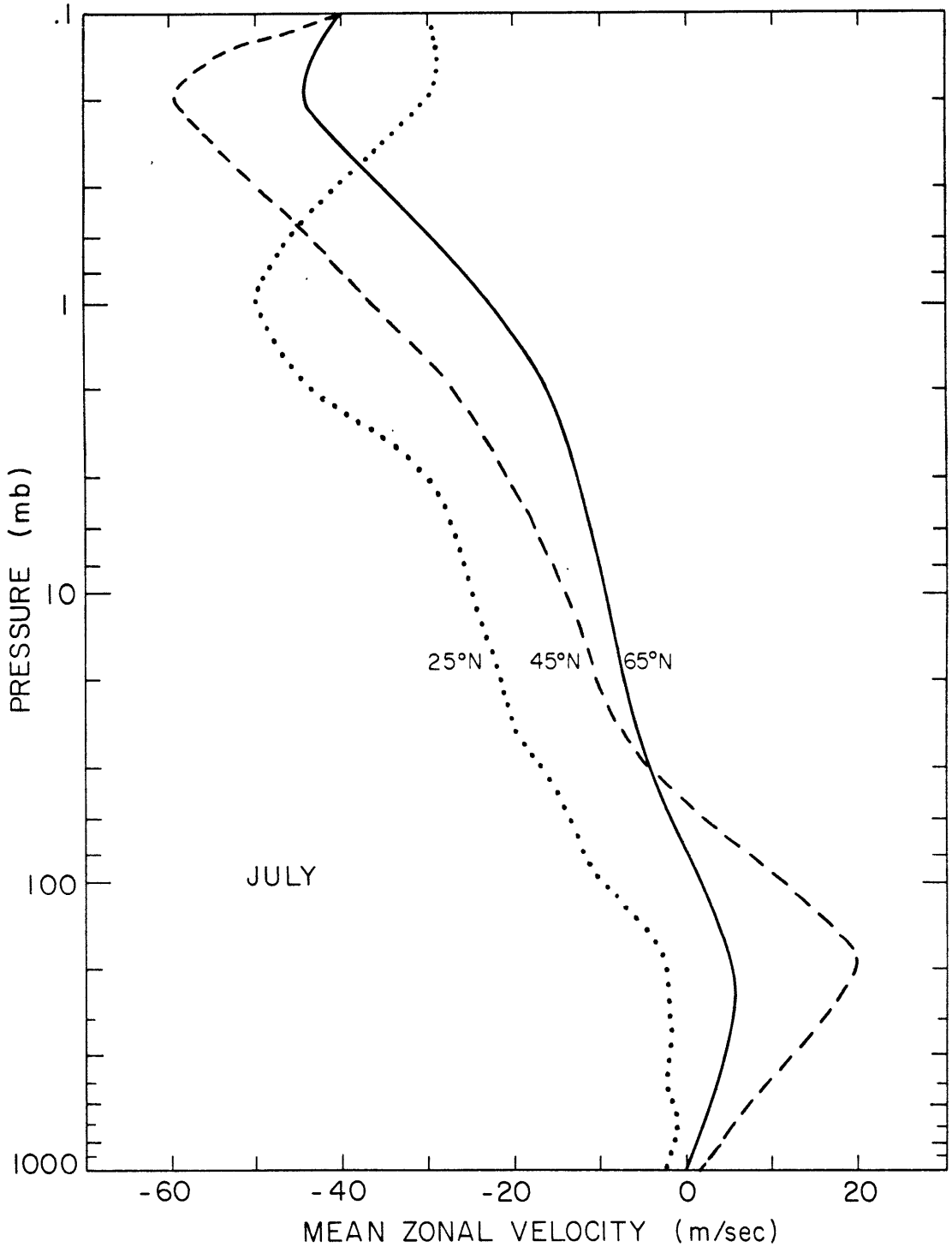

Figure 4.3. As in Figure 4.1, for July .

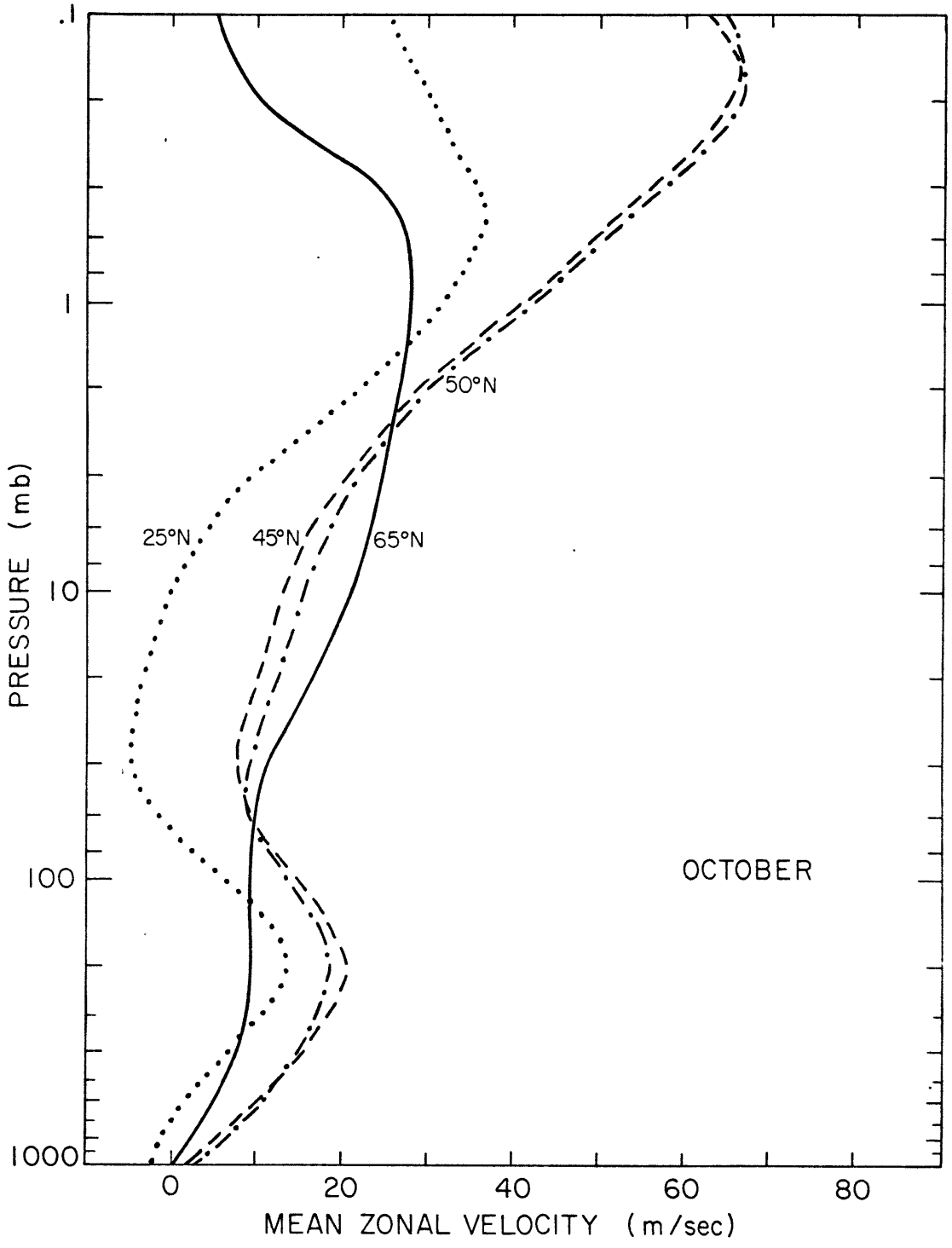

Figure 4.4. As in Figure 4.1, for October.

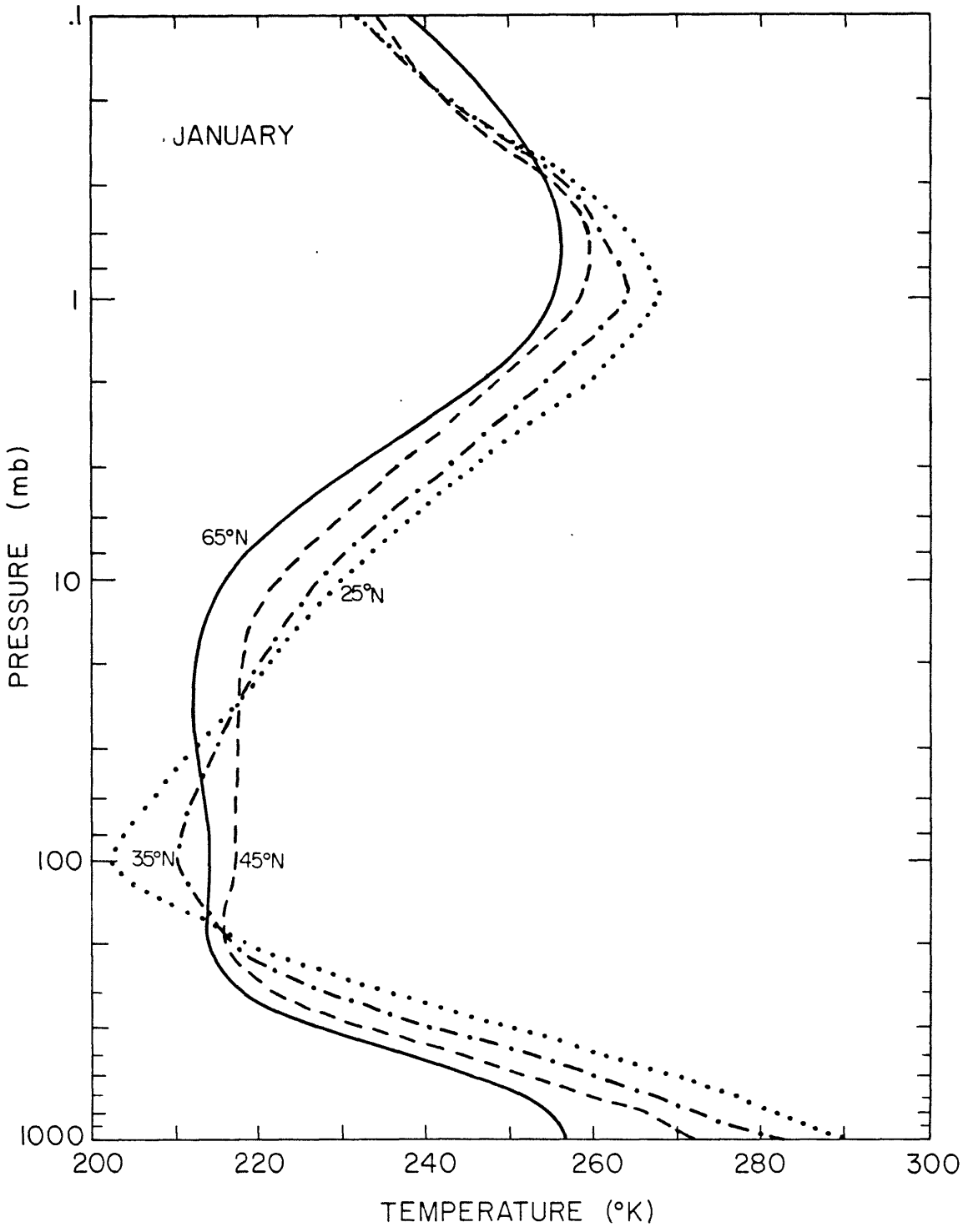

Figure 4.5. Temperature profiles for the basic state, for January.

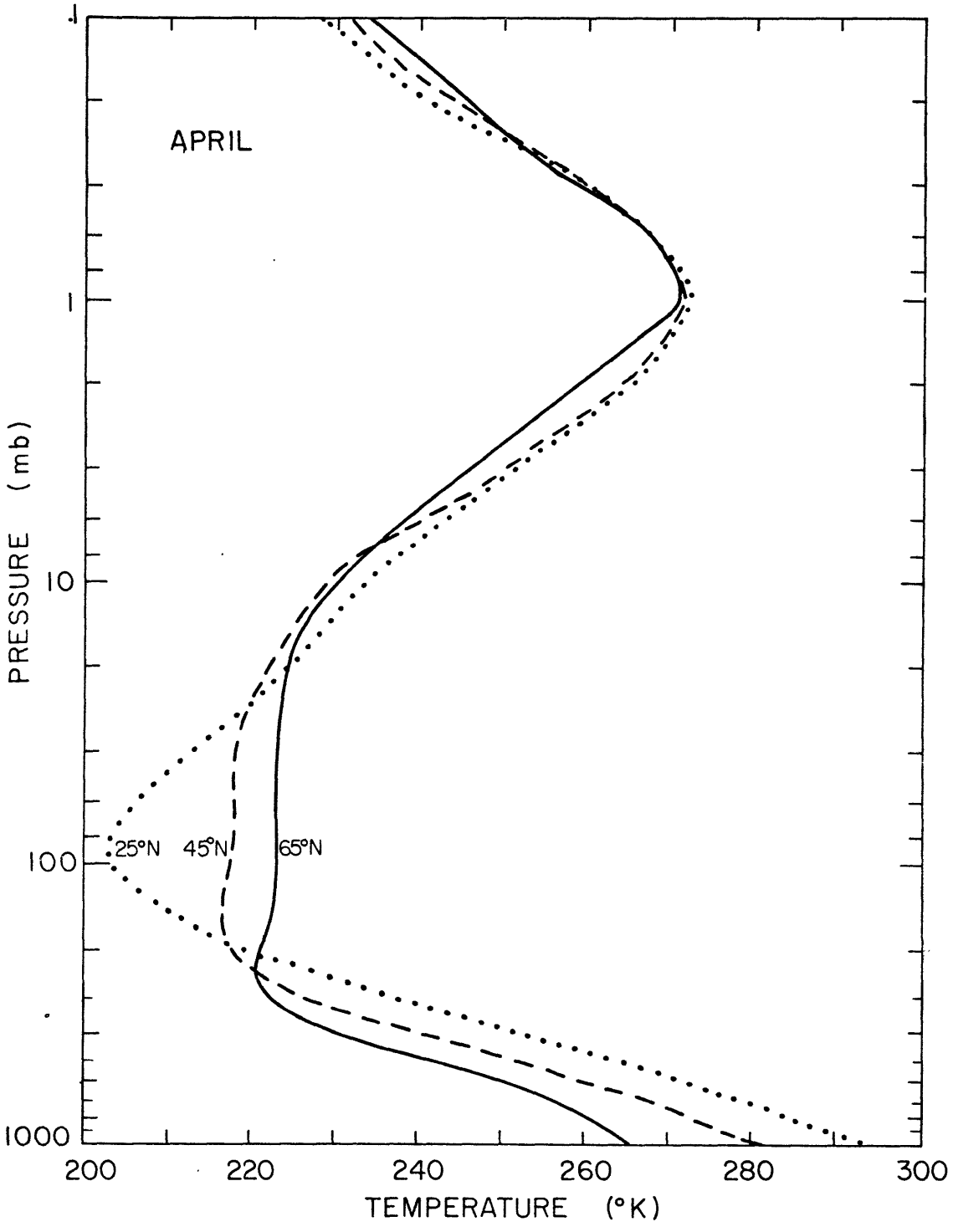

Figure 4.6. As in Figure 4.5, for April.

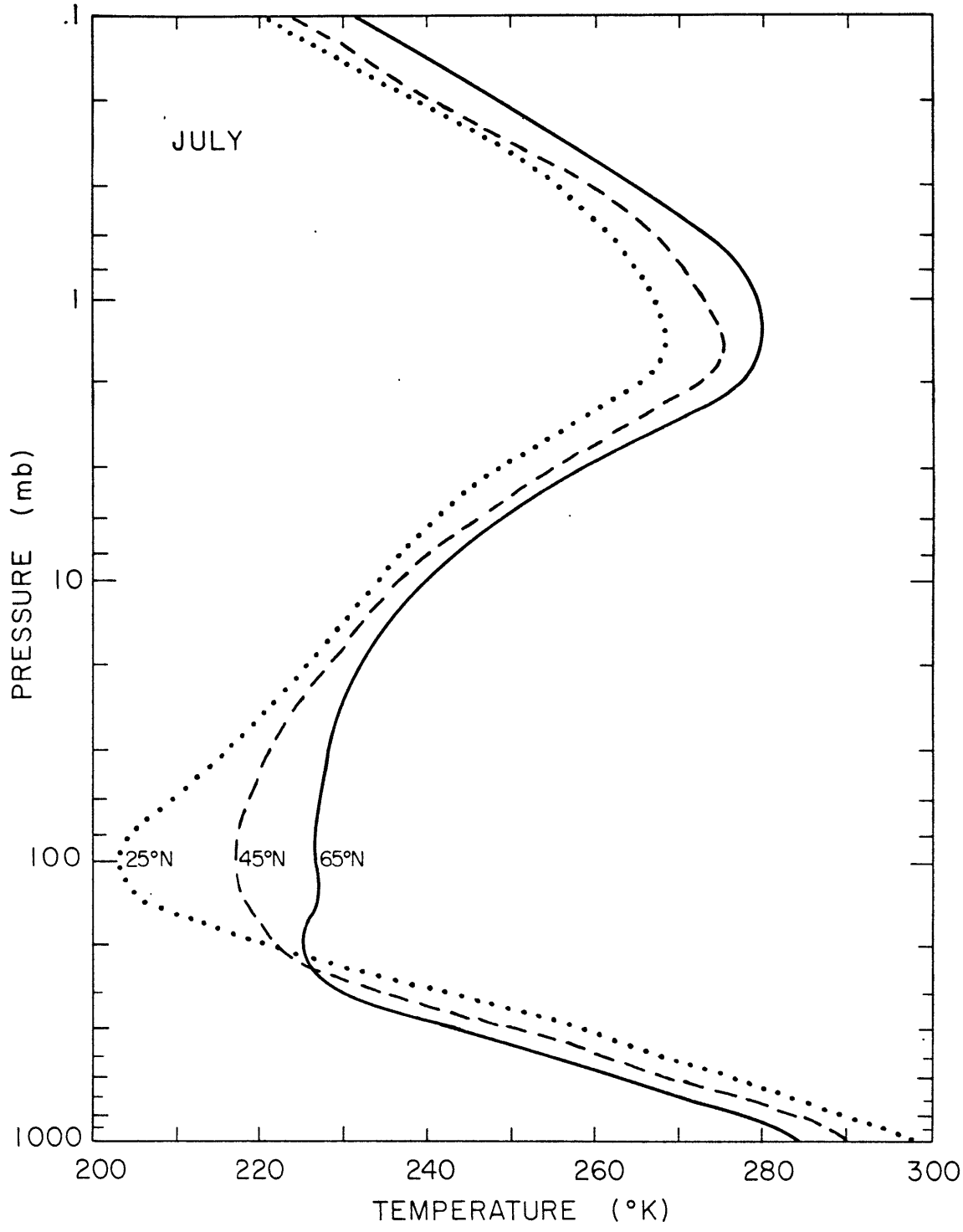

Figure 4.7. As in Figure 4.5, for July.

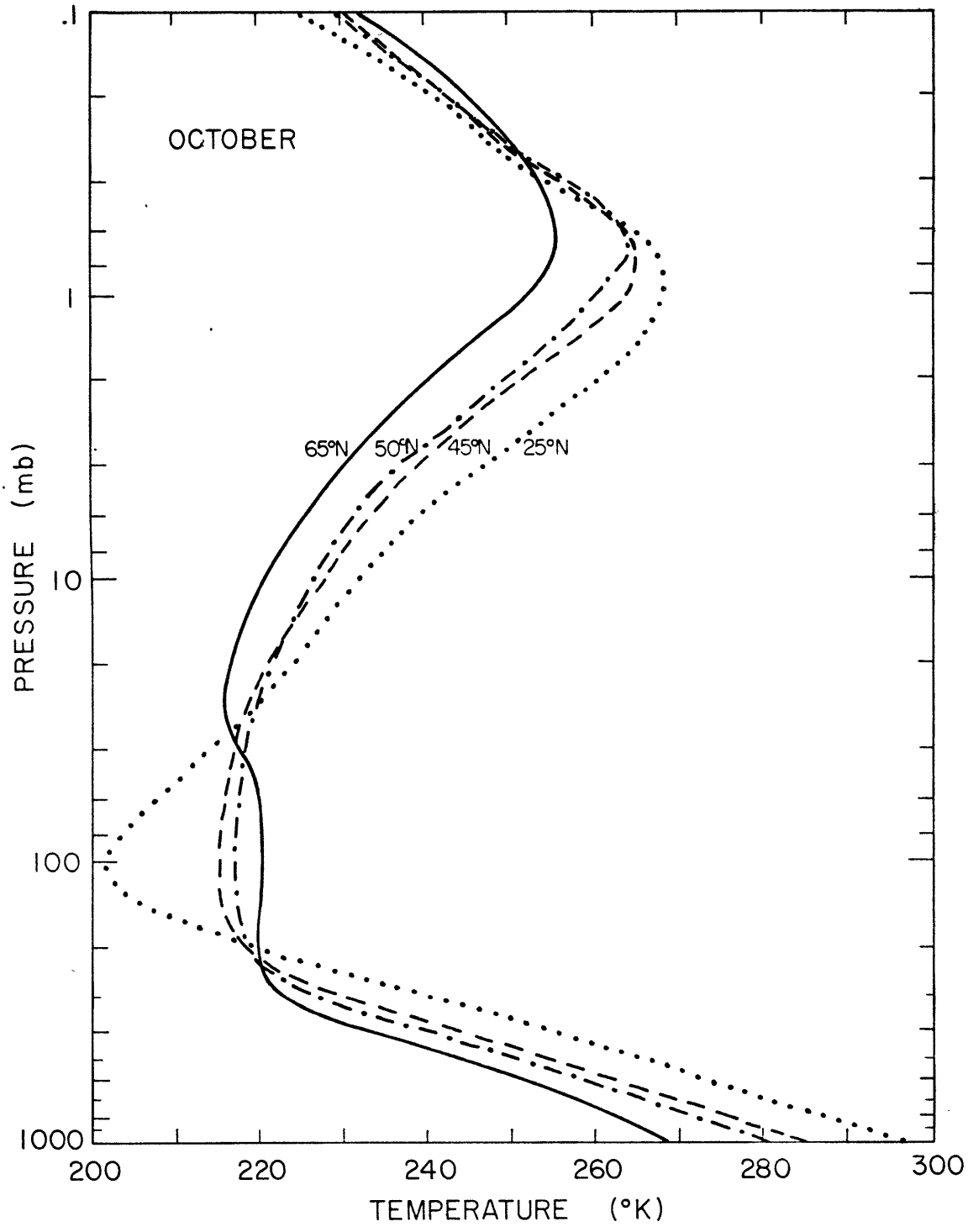

Figure 4.8. As in Figure 4.5, for October.

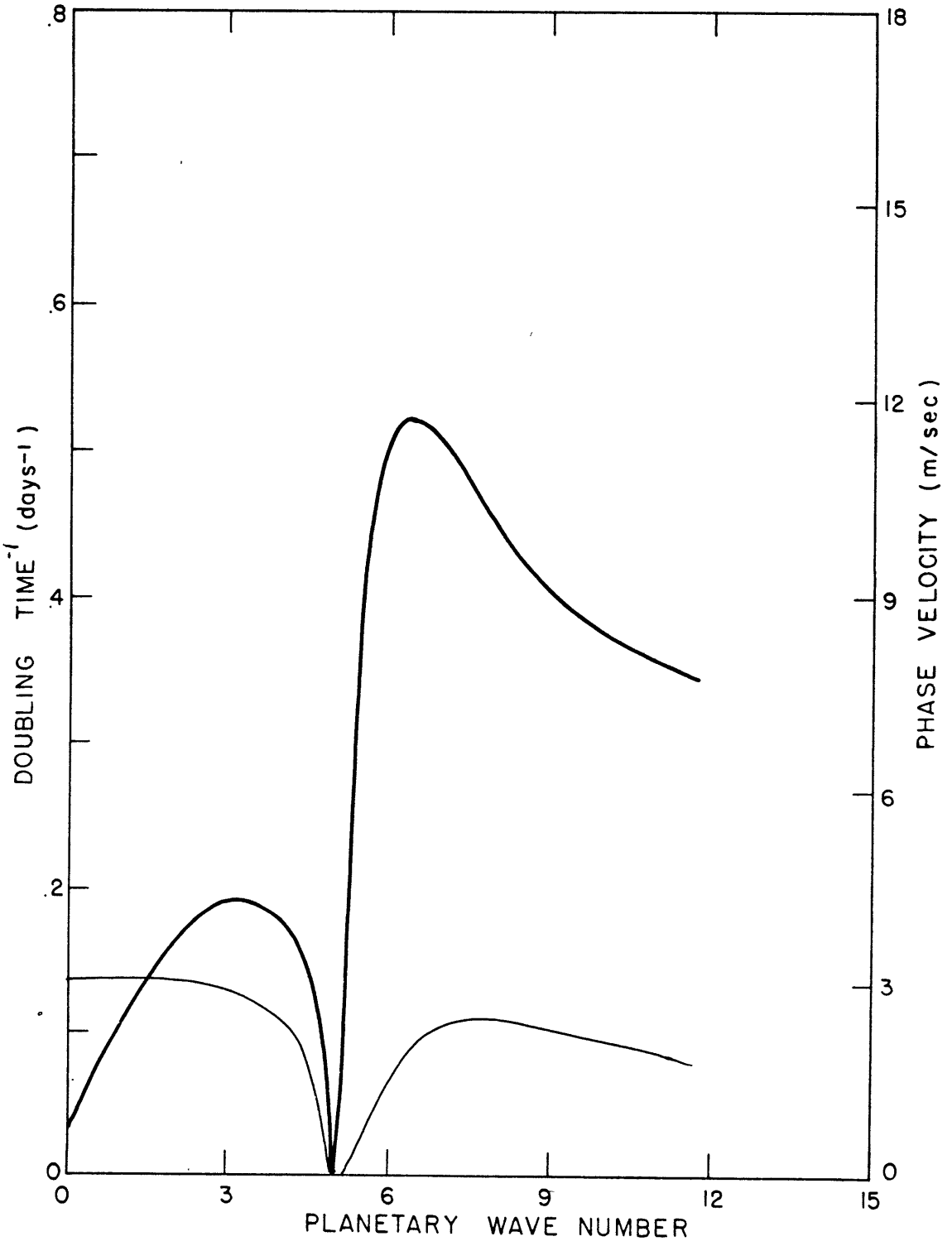

Figure 4.9. Doubling time^{-1} (thick lines) and phase velocity (thin lines) vs. wavenumber of unstable modes for January, 25°N. Solid curves represent the Green and Eady modes.

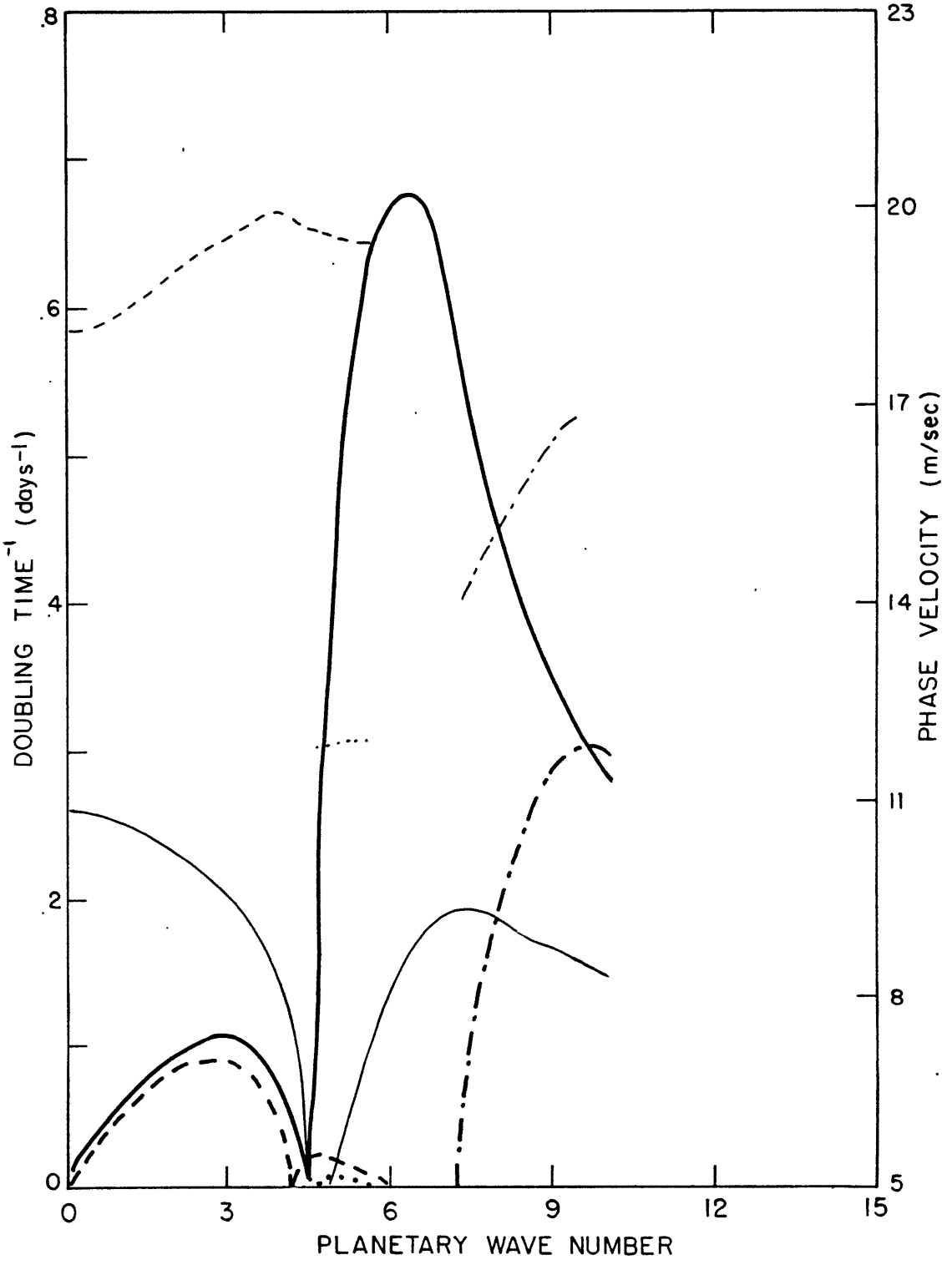

Figure 4.10. As in Figure 4.9, for January, 35°N.

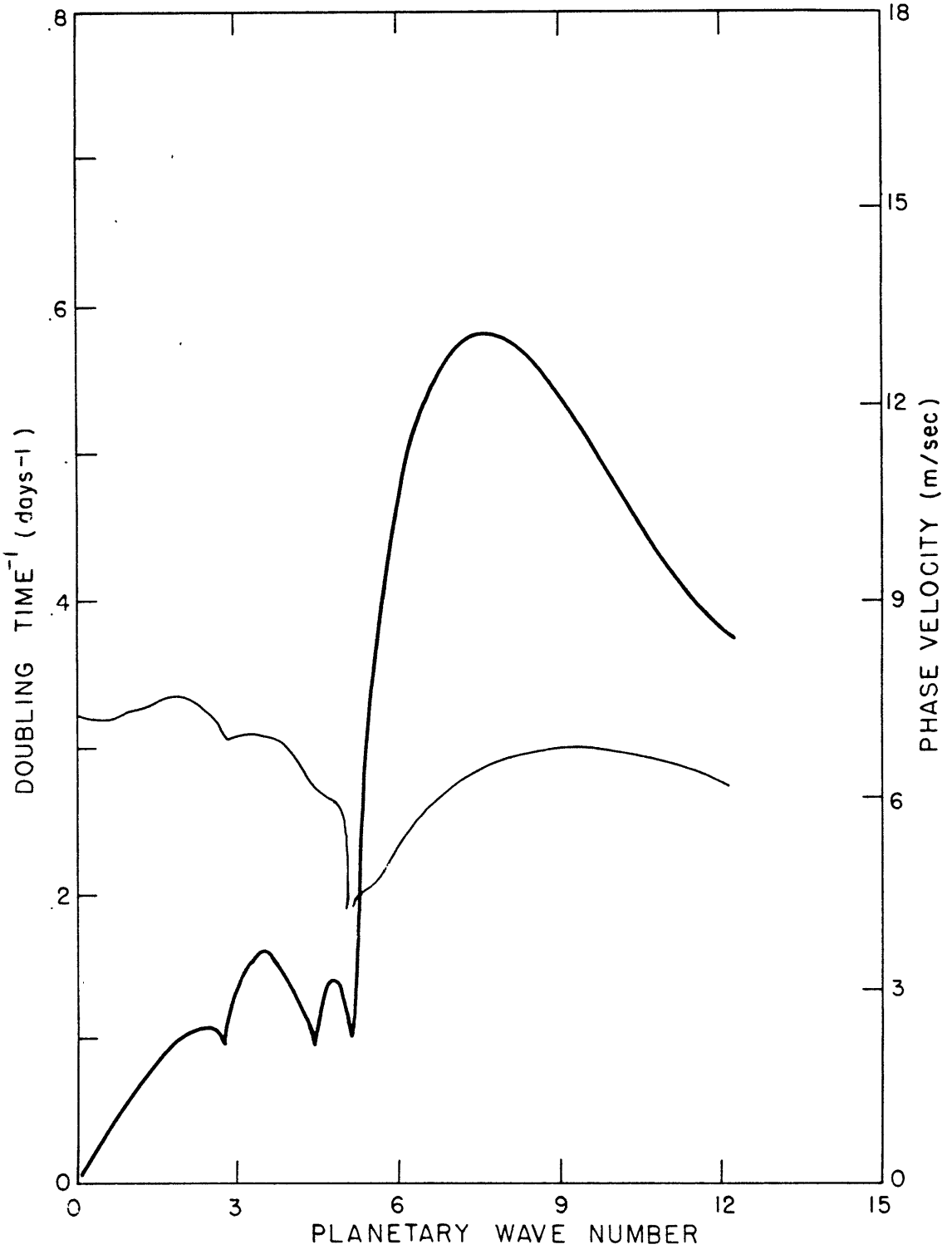

Figure 4.11. As in Figure 4.9, for January, 45°N.

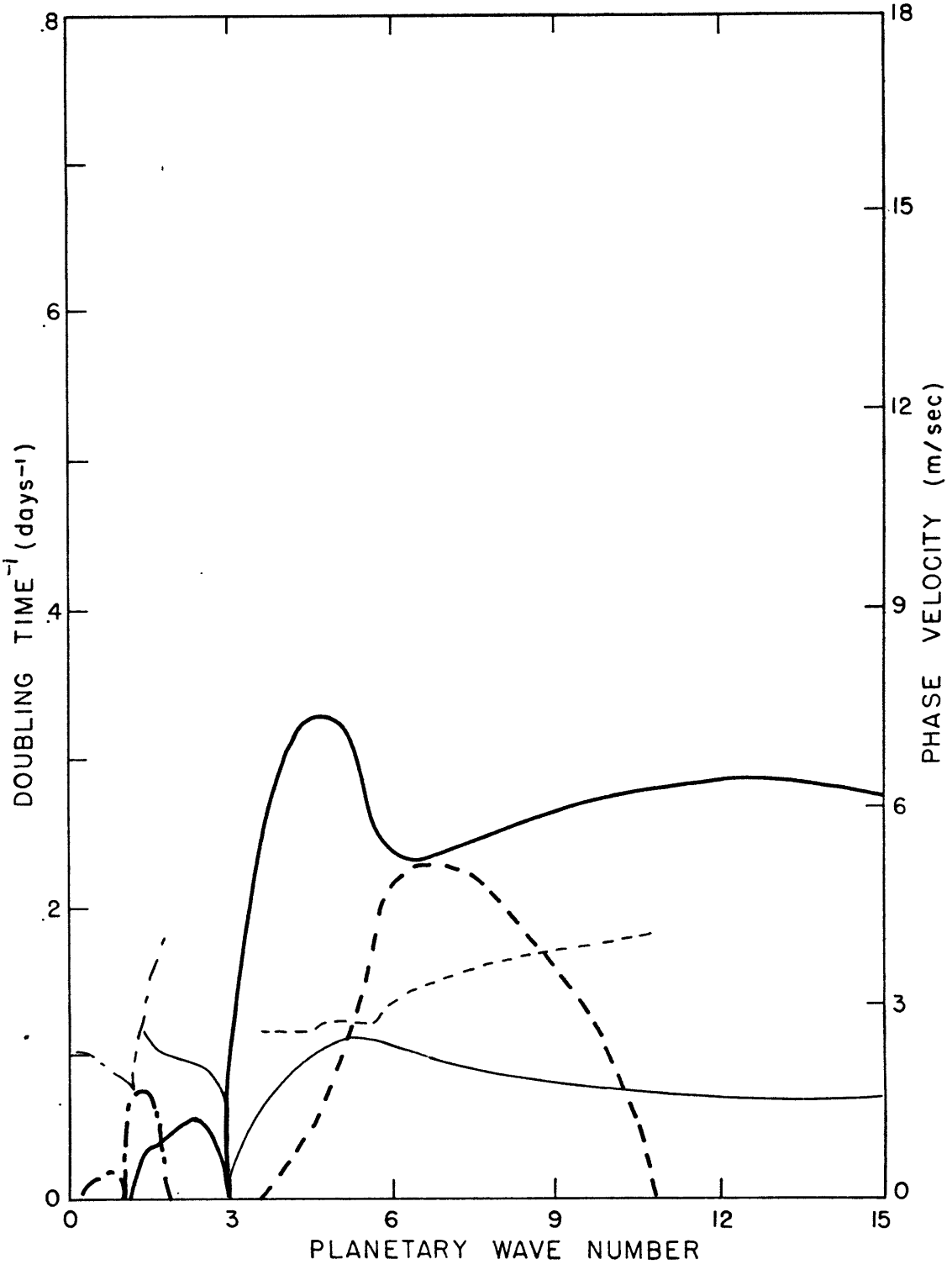

Figure 4.12. As in Figure 4.9, for January, 65°N.

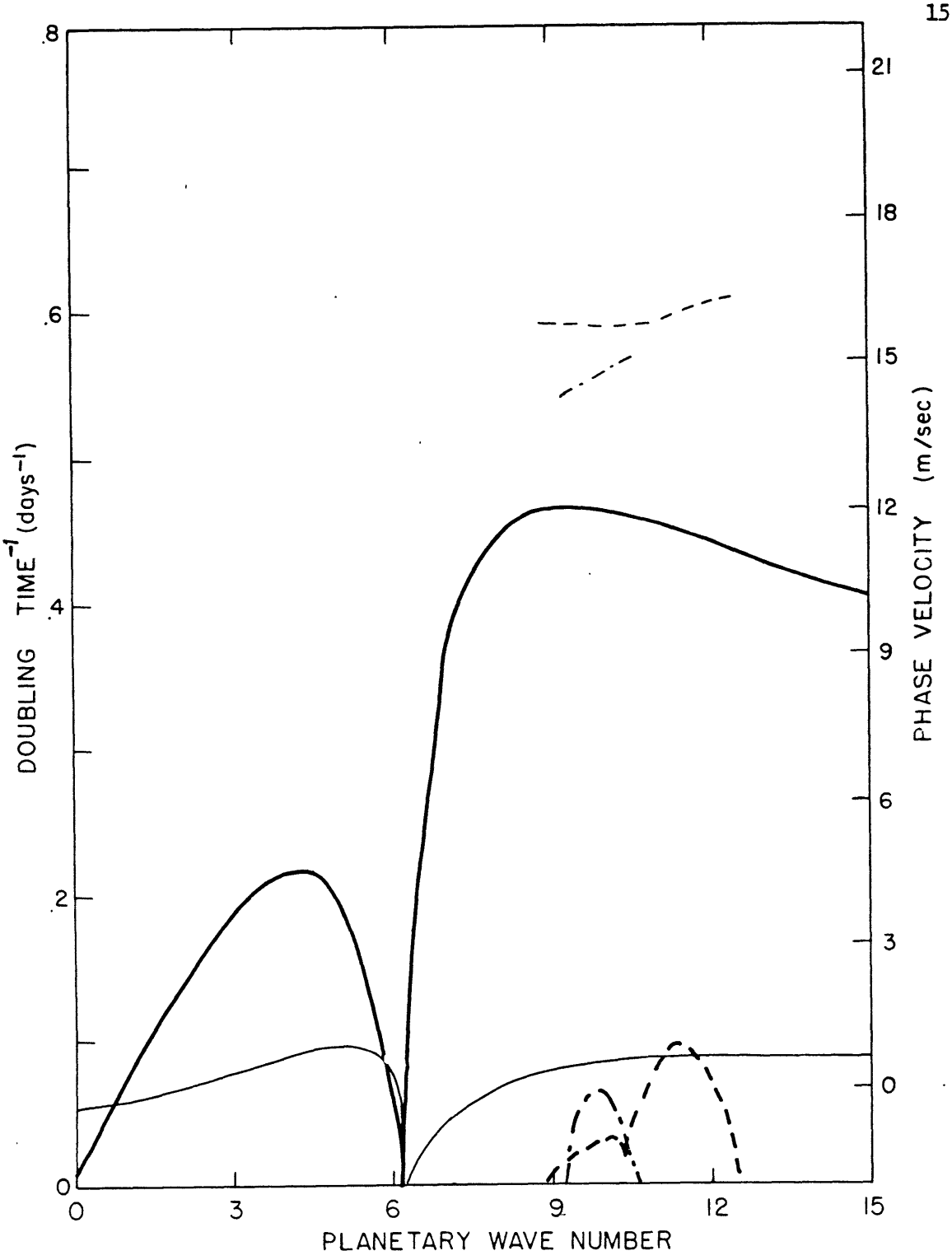

Figure 4.13. As in Figure 4.9, for April, 25°N.

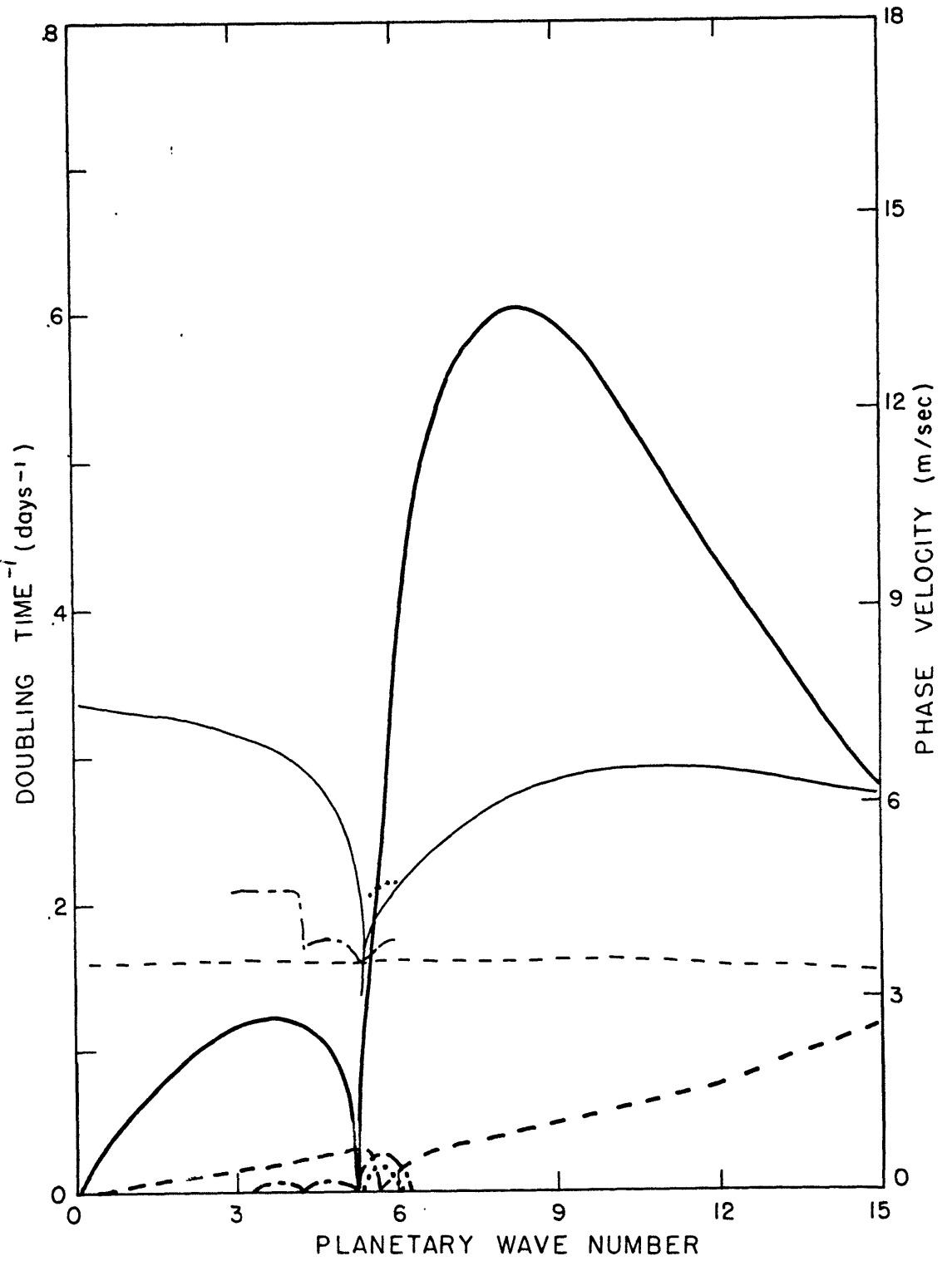

Figure 4.14. As in Figure 4.9, for April 45°N.

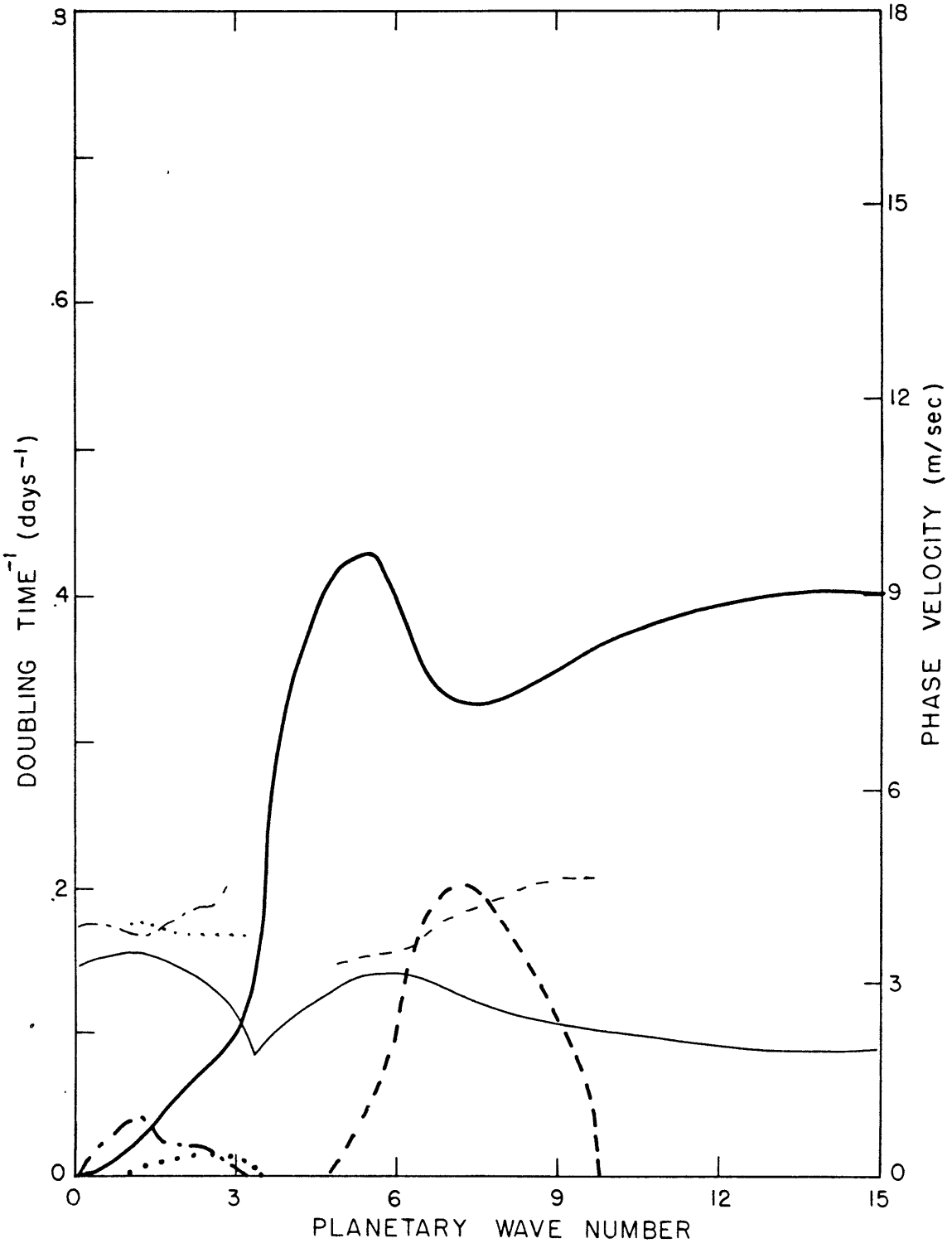

Figure 4.15. As in Figure 4.9, for April 65°N.

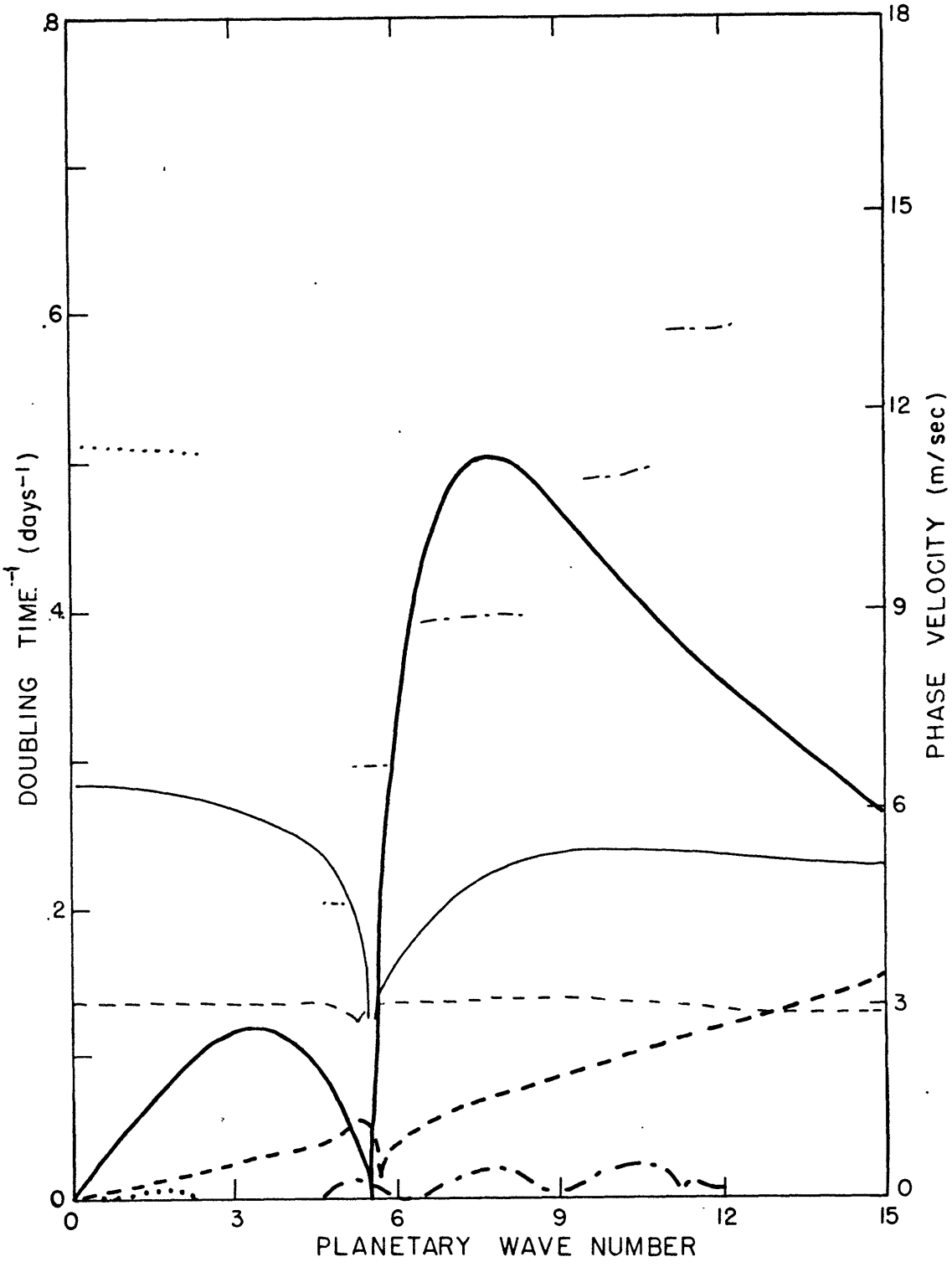

Figure 4.16. As in Figure 4.9, for July, 45°N.

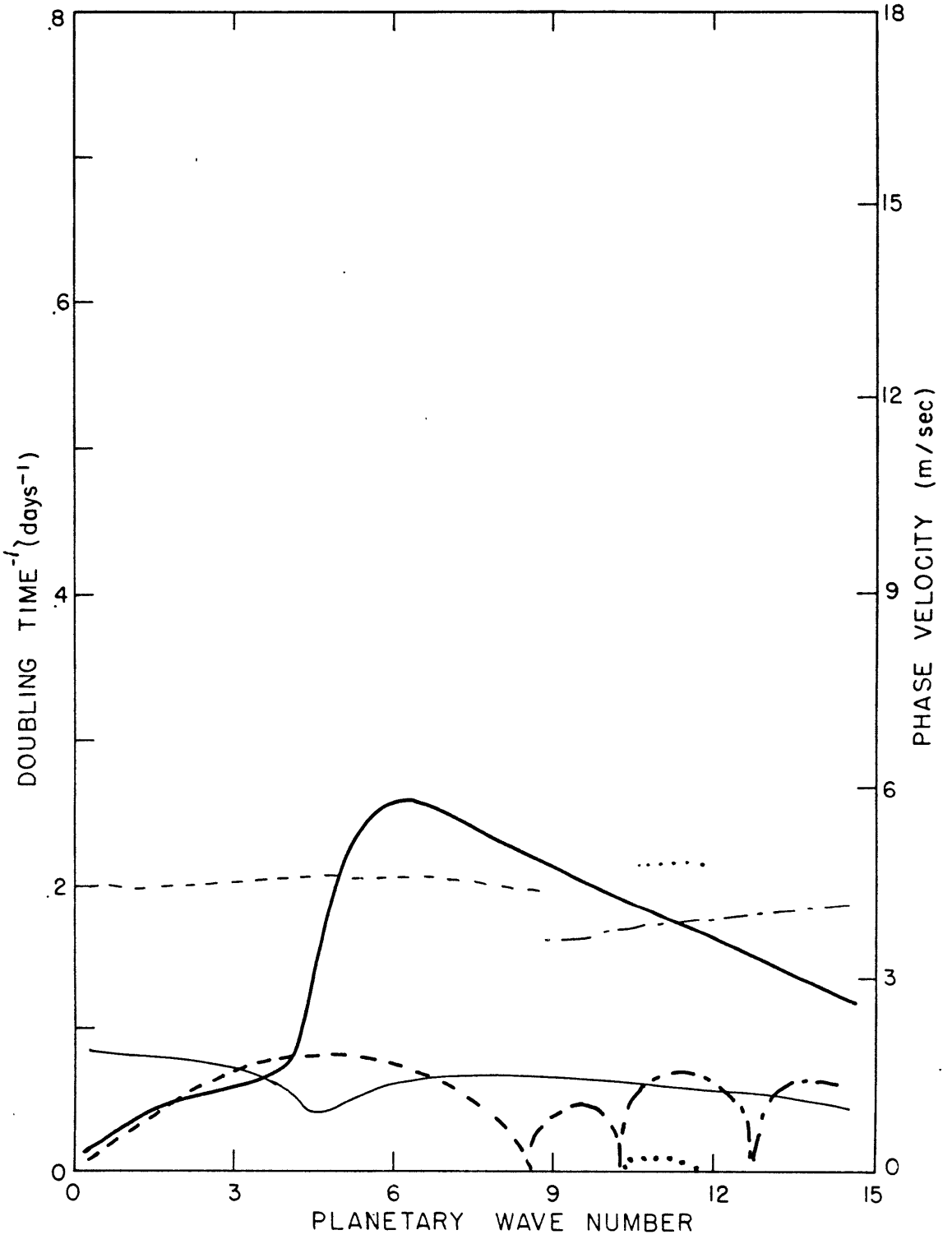

Figure 4.17. As in Figure 4.9, for July 65°N.

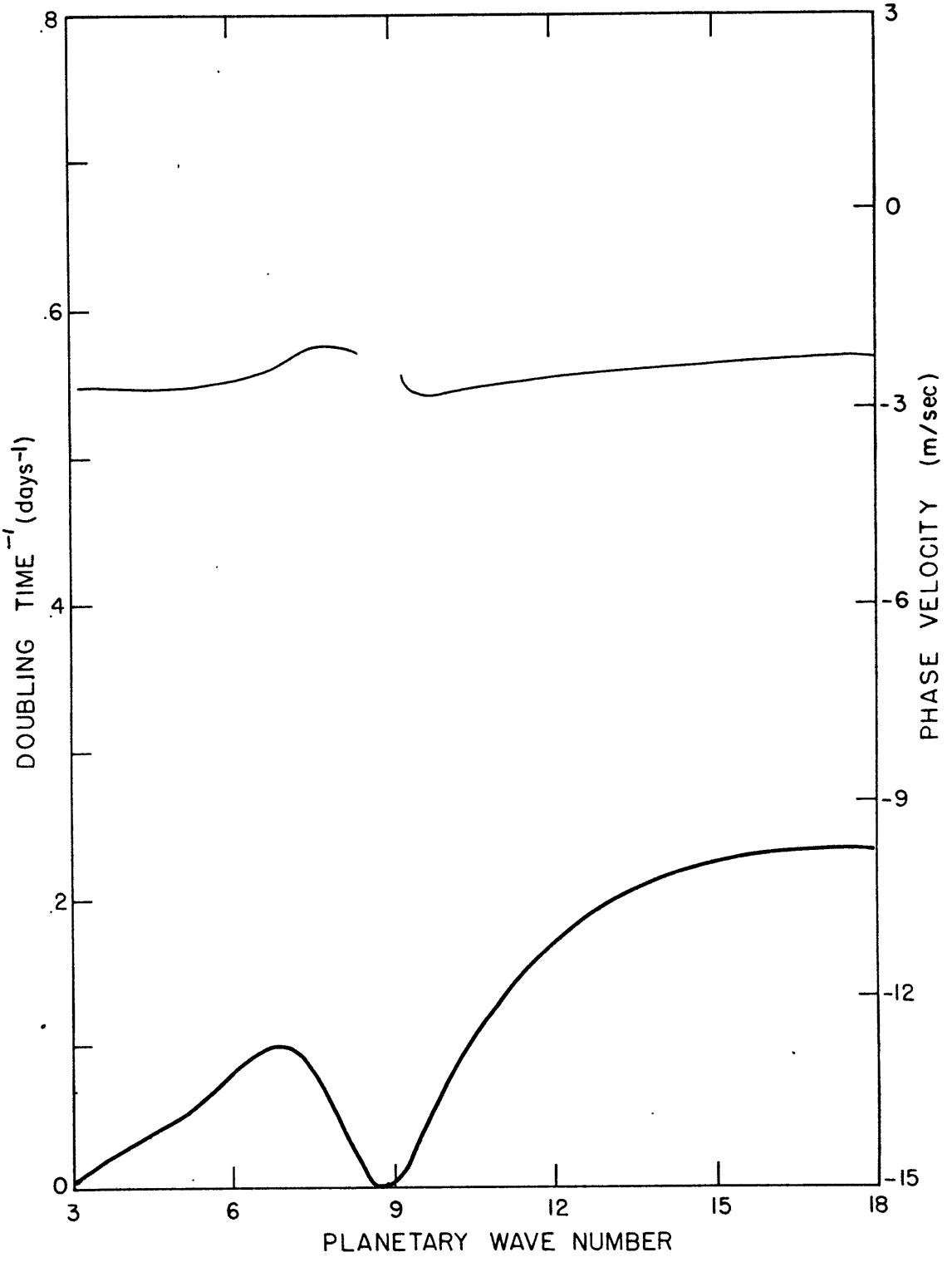

Figure 4.18. As in Figure 4.9, for October 25°N.

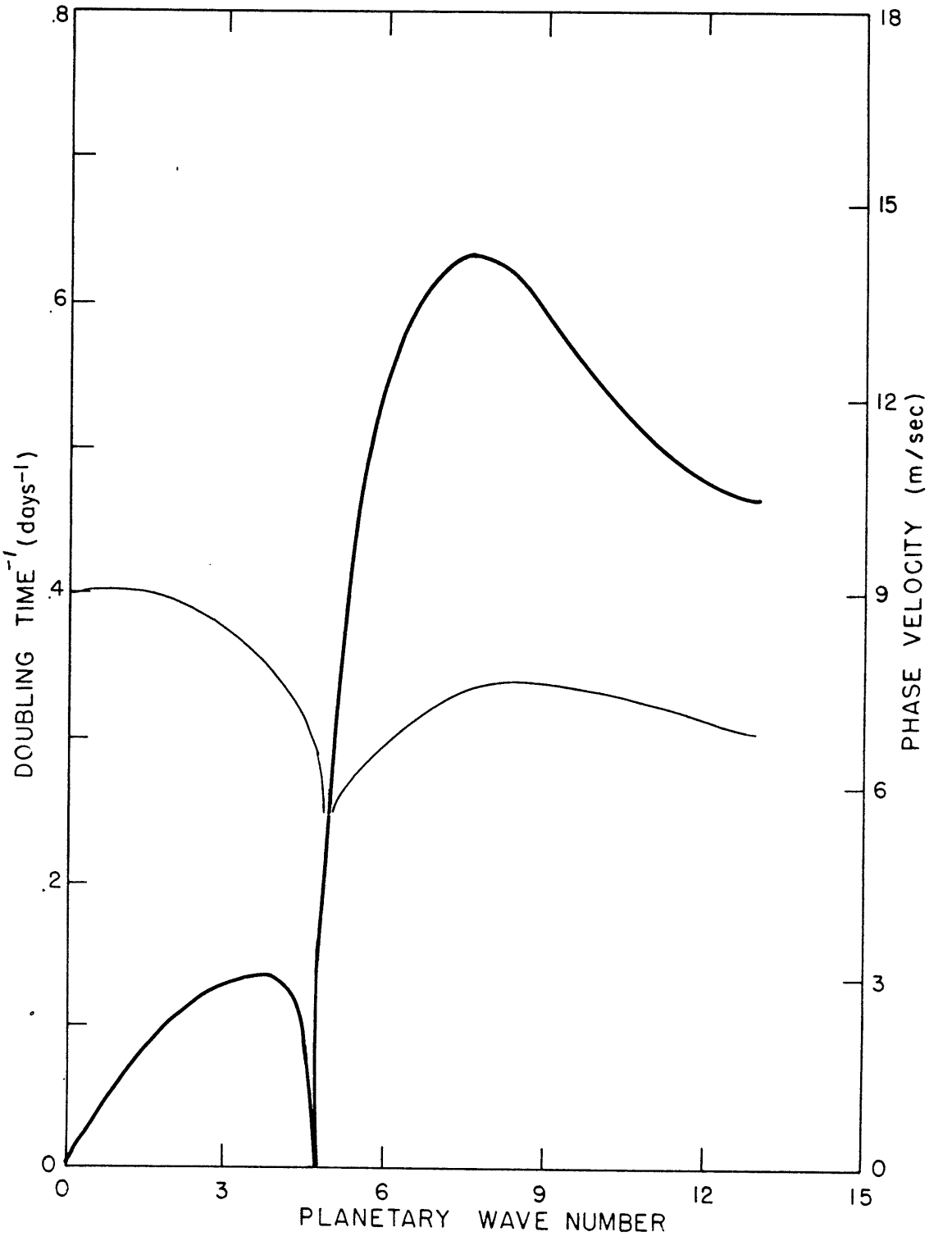

Figure 4.19. As in Figure 4.9, for October 45°N.

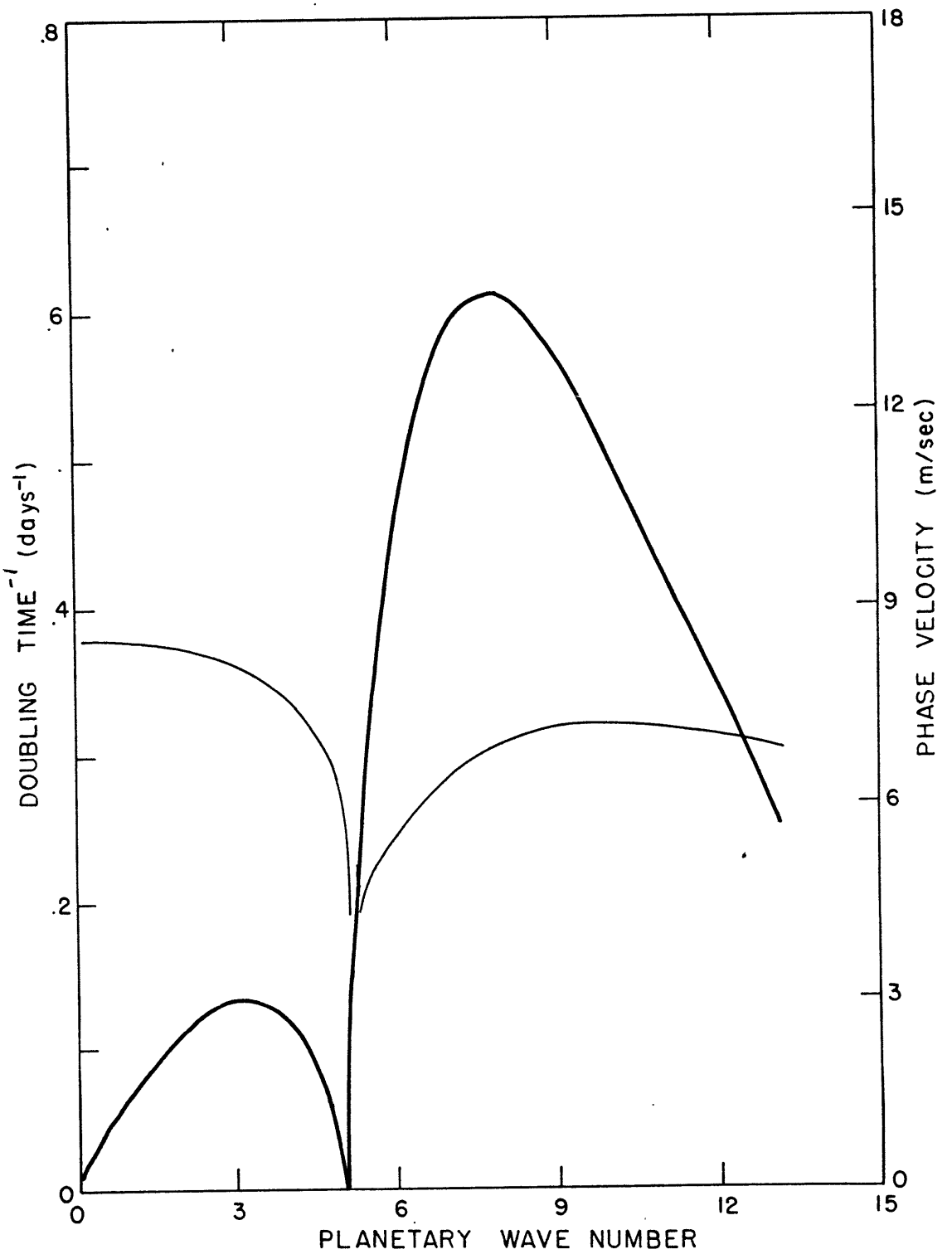

Figure 4.20. As in Figure 4.9, for October 50°N.

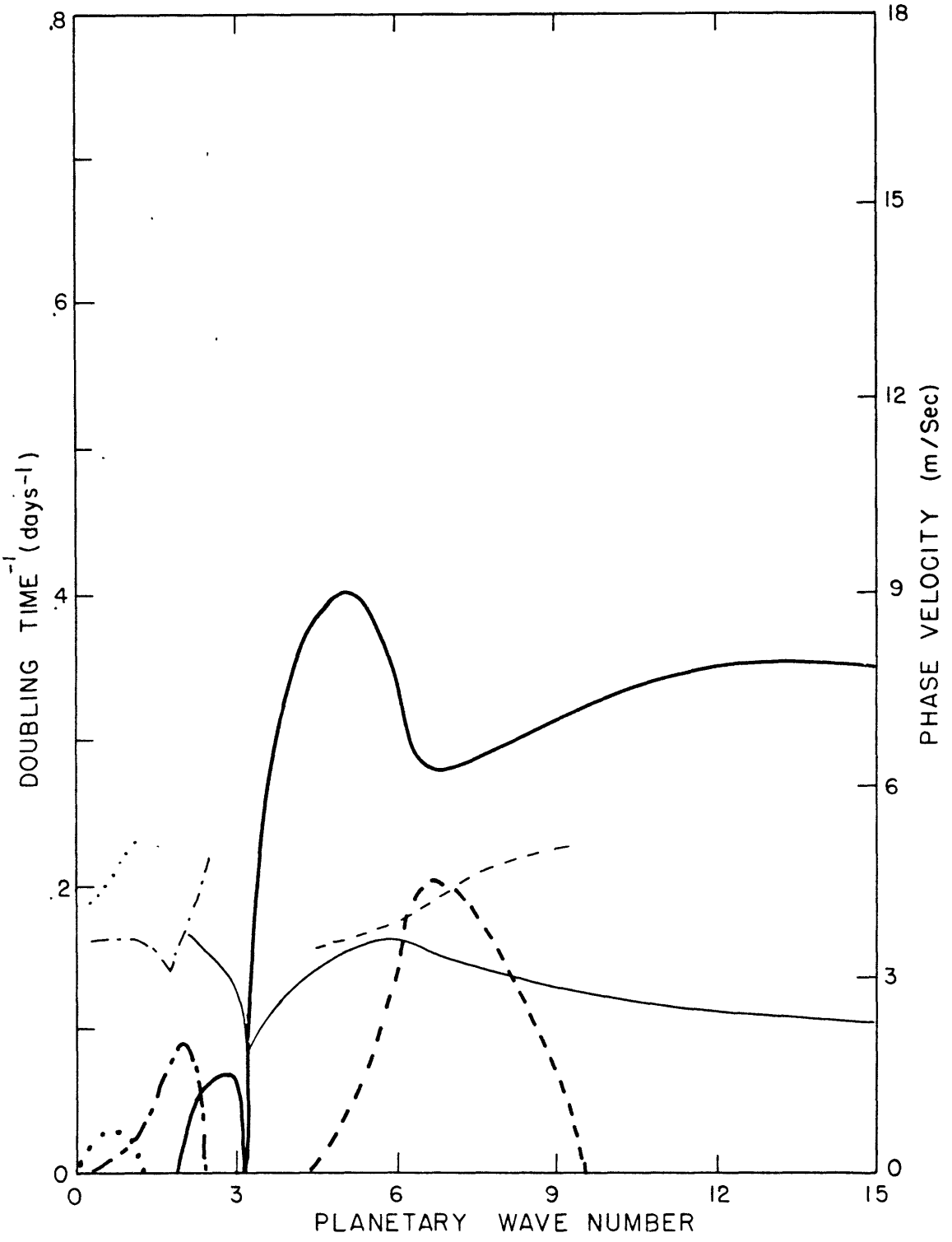

Figure 4.21. As in Figure 4.9, for October 65°N.

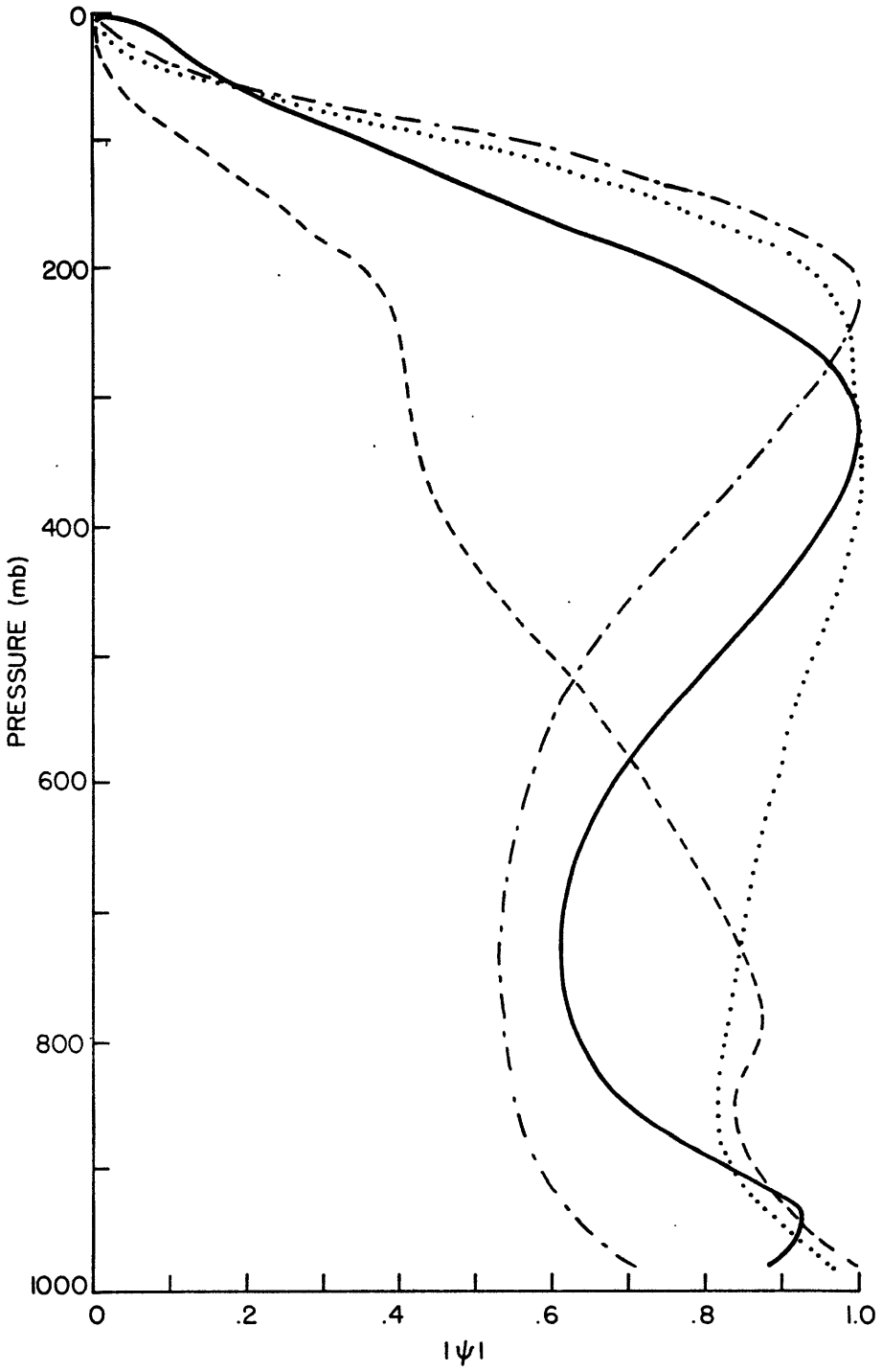

Figure 4.22. Vertical structure of the streamfunction amplitude for the fastest growing Eady mode. Cases: January 25°N (dot), January 35°N (dash dot), January 65°N (solid), and April 25°N (dash).

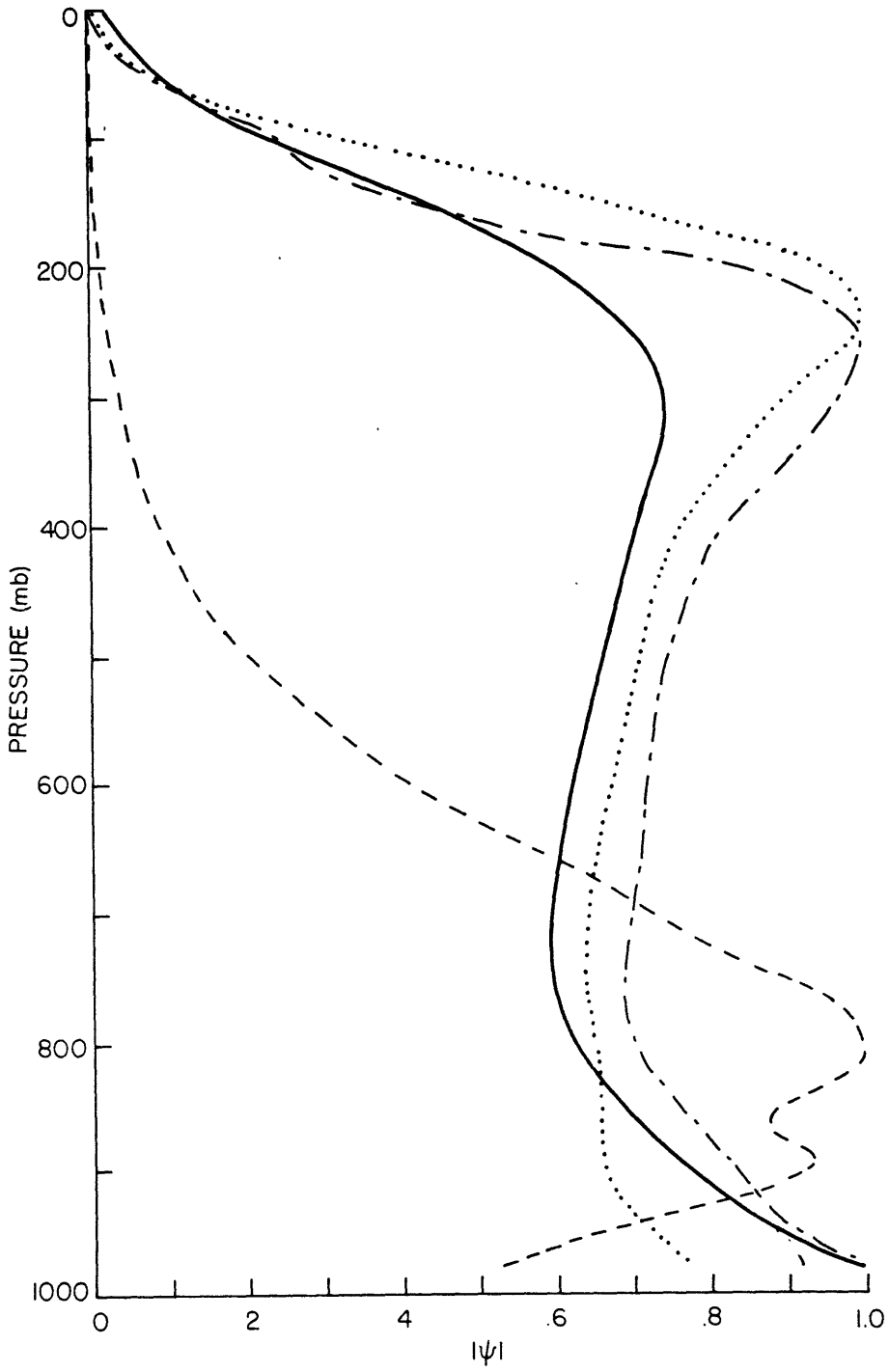

Figure 4.23. As in Figure 4.22, for cases: July 45°N (dot), July 65°N (dash dot), October 25°N (dash), and October 50°N (solid).

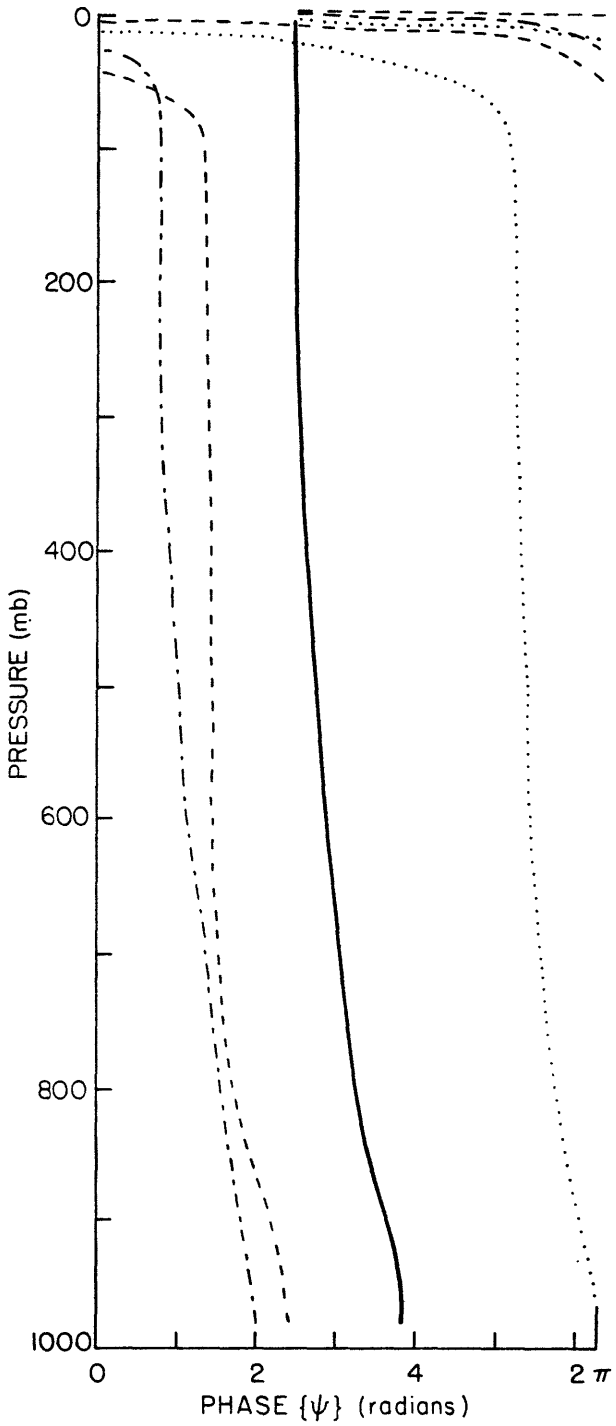

Figure 4.24. Vertical structure of the streamfunction phase for the fastest growing Eady mode. Cases are those in Figure 4.22.

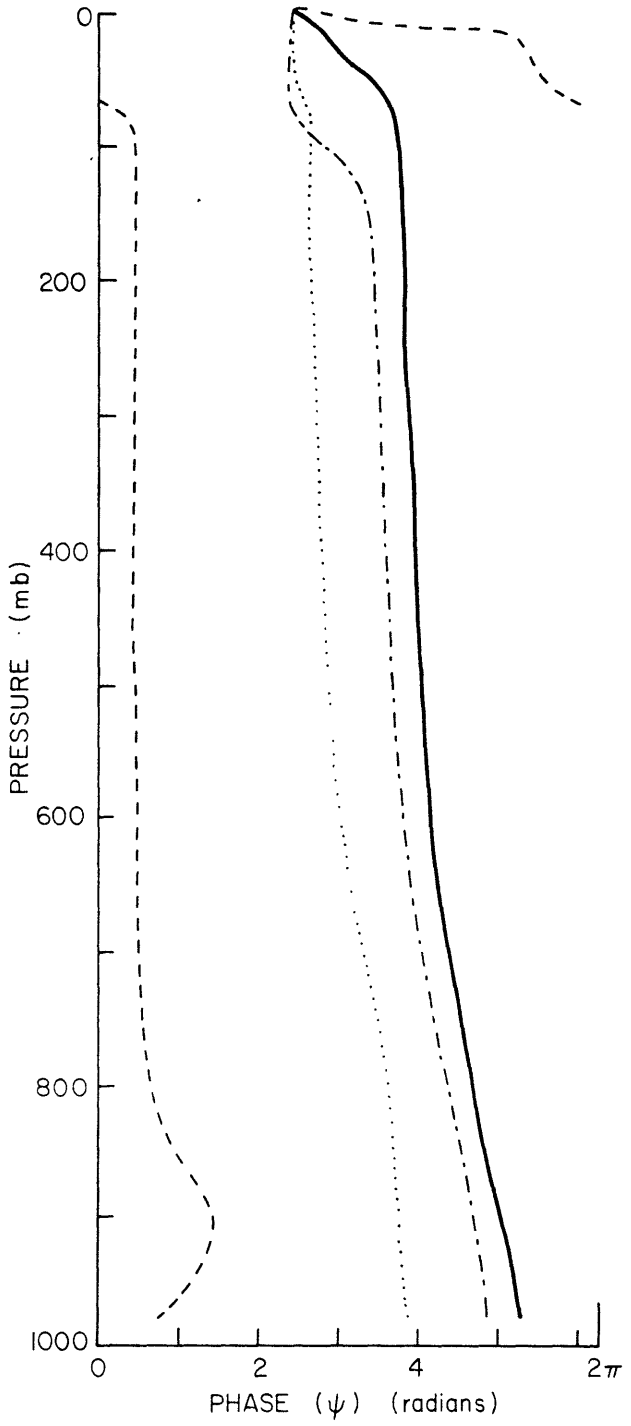

Figure 4.25. As in Figure 4.24, for the cases July 45°N (dot), July 65°N (dash dot), October 25°N (dash), and October 50°N (solid).

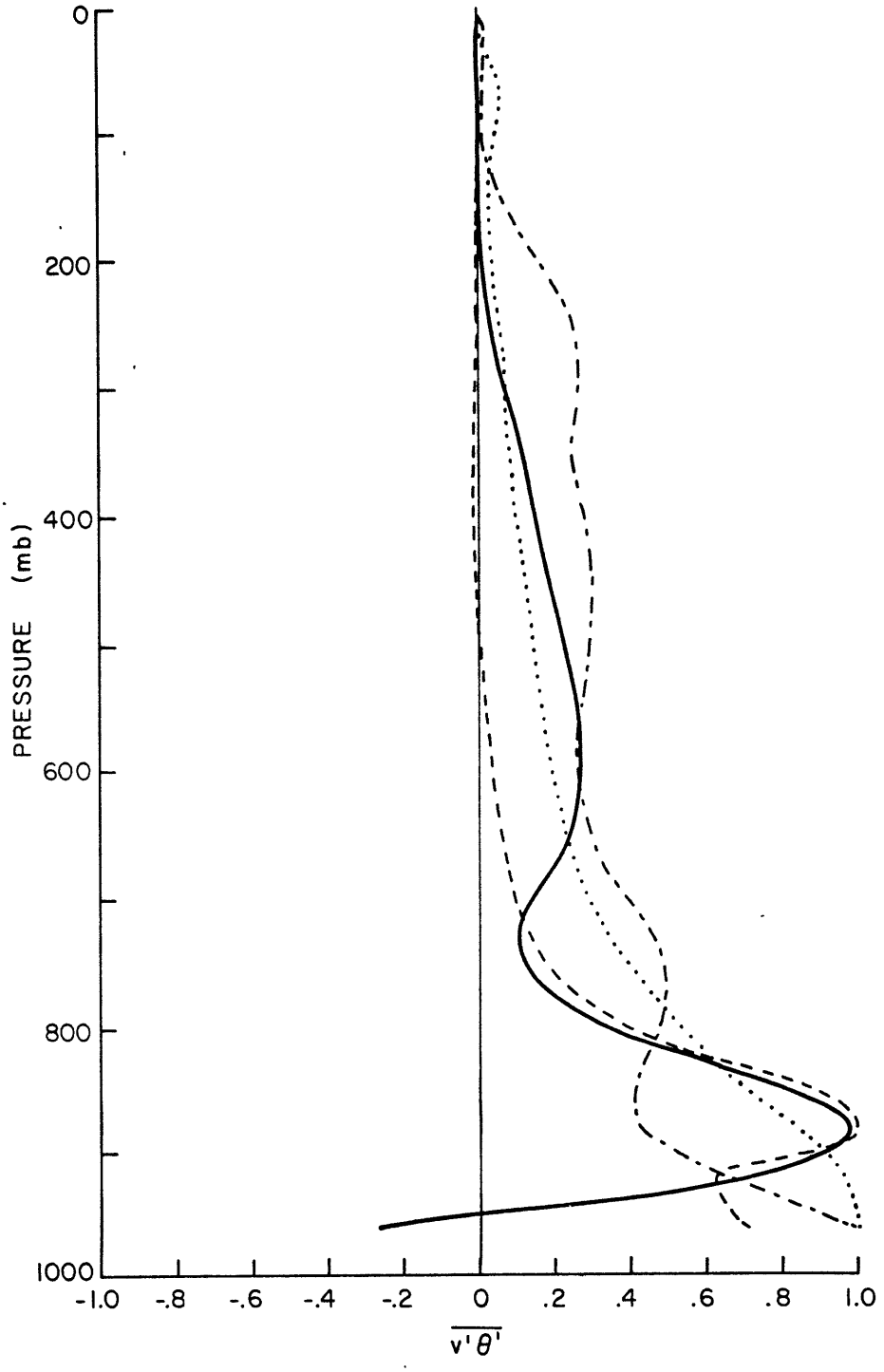

Figure 4.26. Vertical structure of the meridional entropy transport for the fastest growing Eady mode. Cases are those in Figure 4.22.

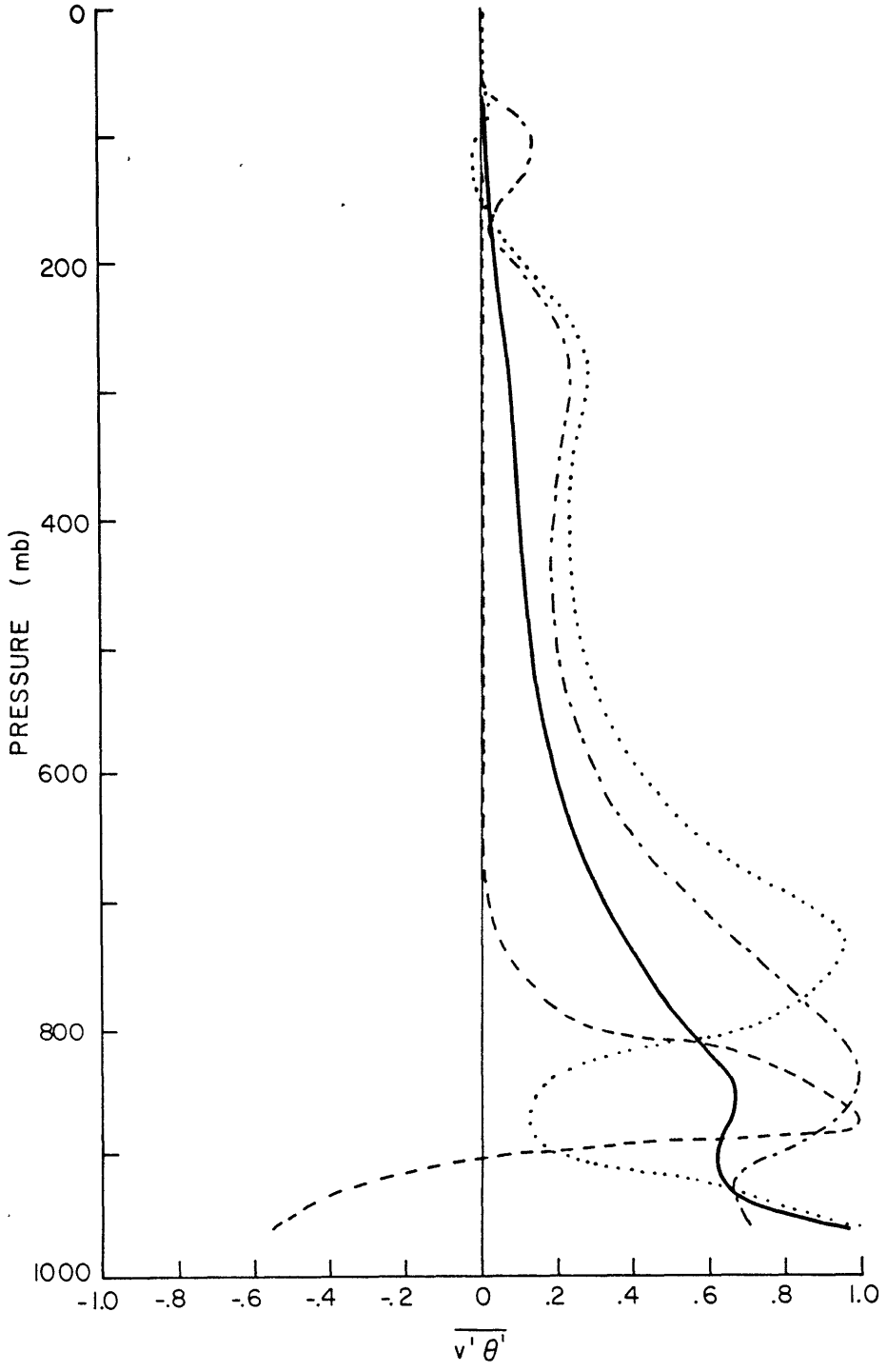

Figure 4.27. As in Figure 4.26, except for the cases July 45°N (dot), July 65°N (dash dot), October 25°N (dash), and October 50°N (solid).

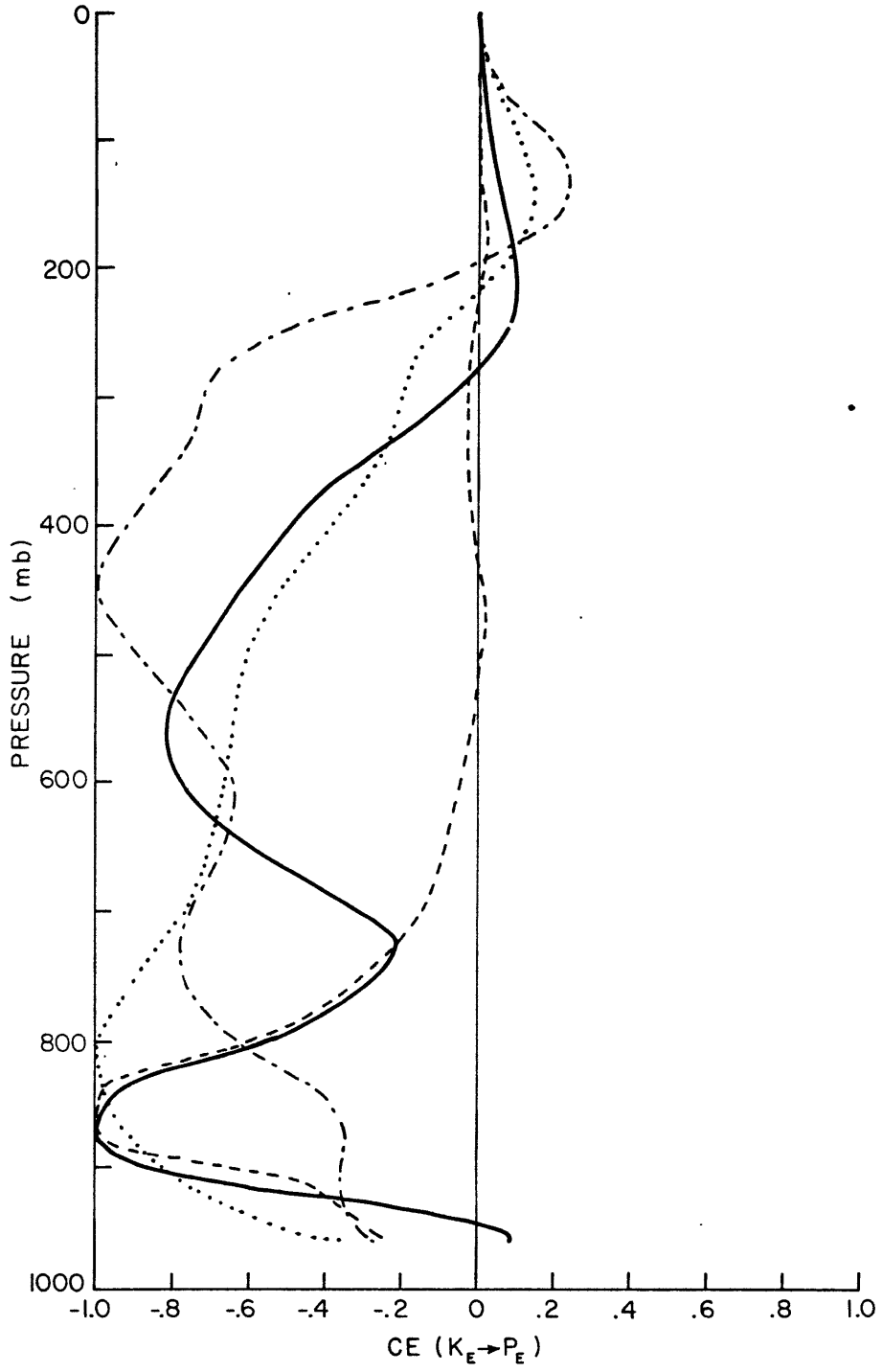

Figure 4.28. Vertical structure of the transfer of eddy kinetic to eddy available potential energy ($K_E \rightarrow P_E$ is positive) for the fastest growing Eady mode. Cases are those in Figure 4.22.

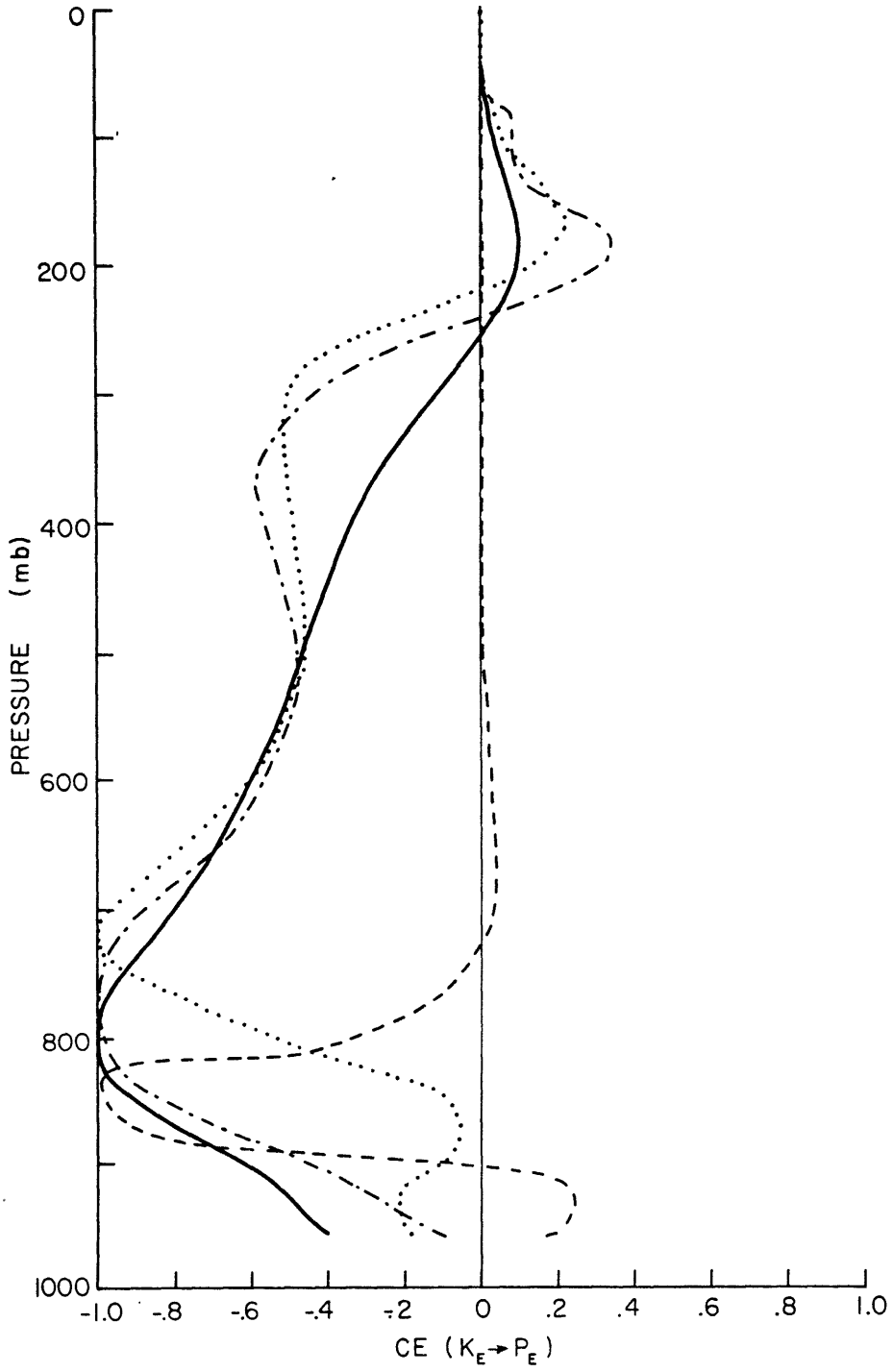

Figure 4.29. As in Figure 4.28, except for the cases July 45°N (dot), July 65°N (dash dot), October 25°N (dash), and October 50°N (solid).

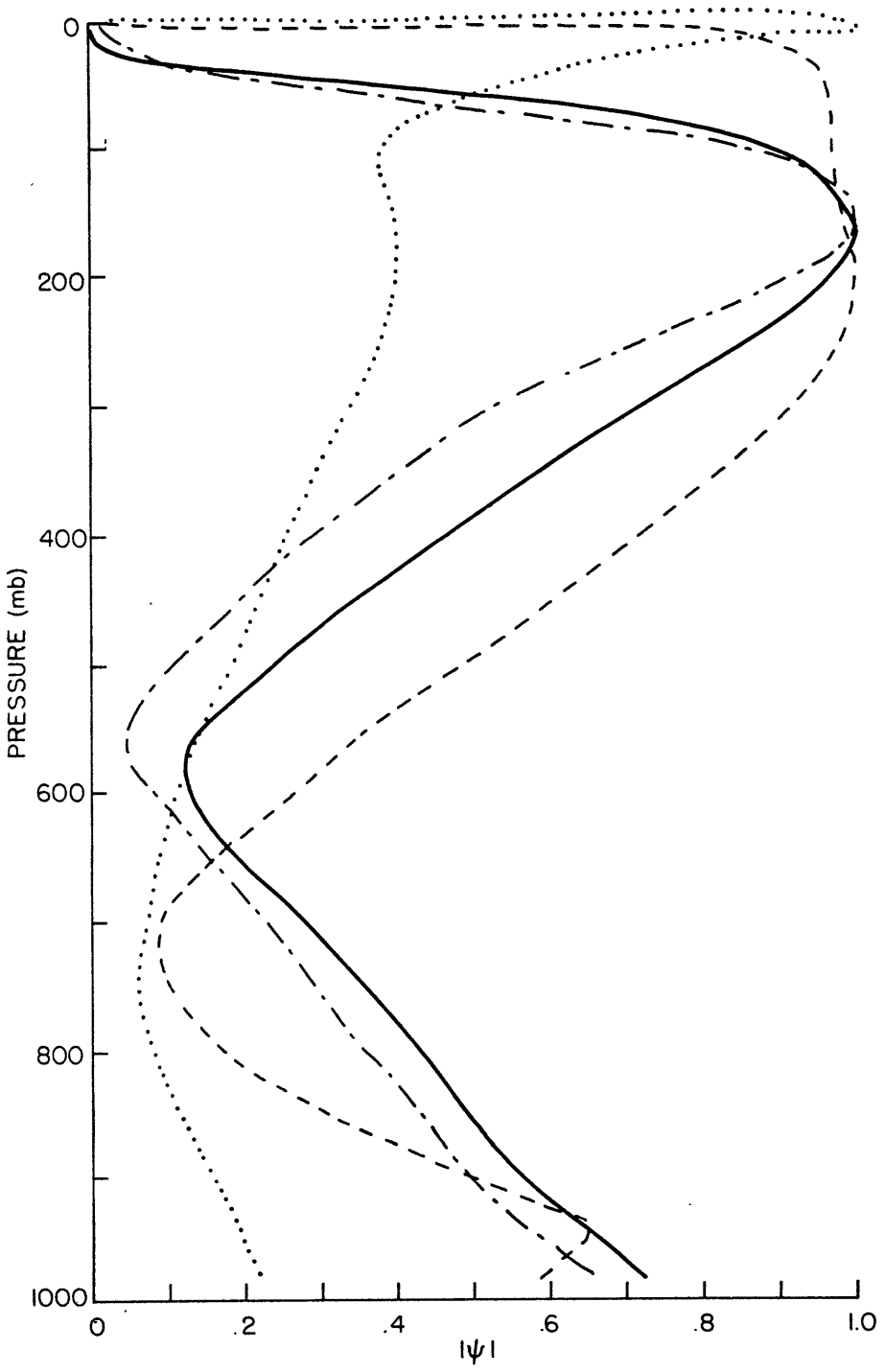

Figure 4.30. Vertical structure of the streamfunction amplitude of the fastest growing Green mode. Cases: January 25°N (solid), January 35°N (dash dot), January 45°N (dot), and January 65°N (dash).

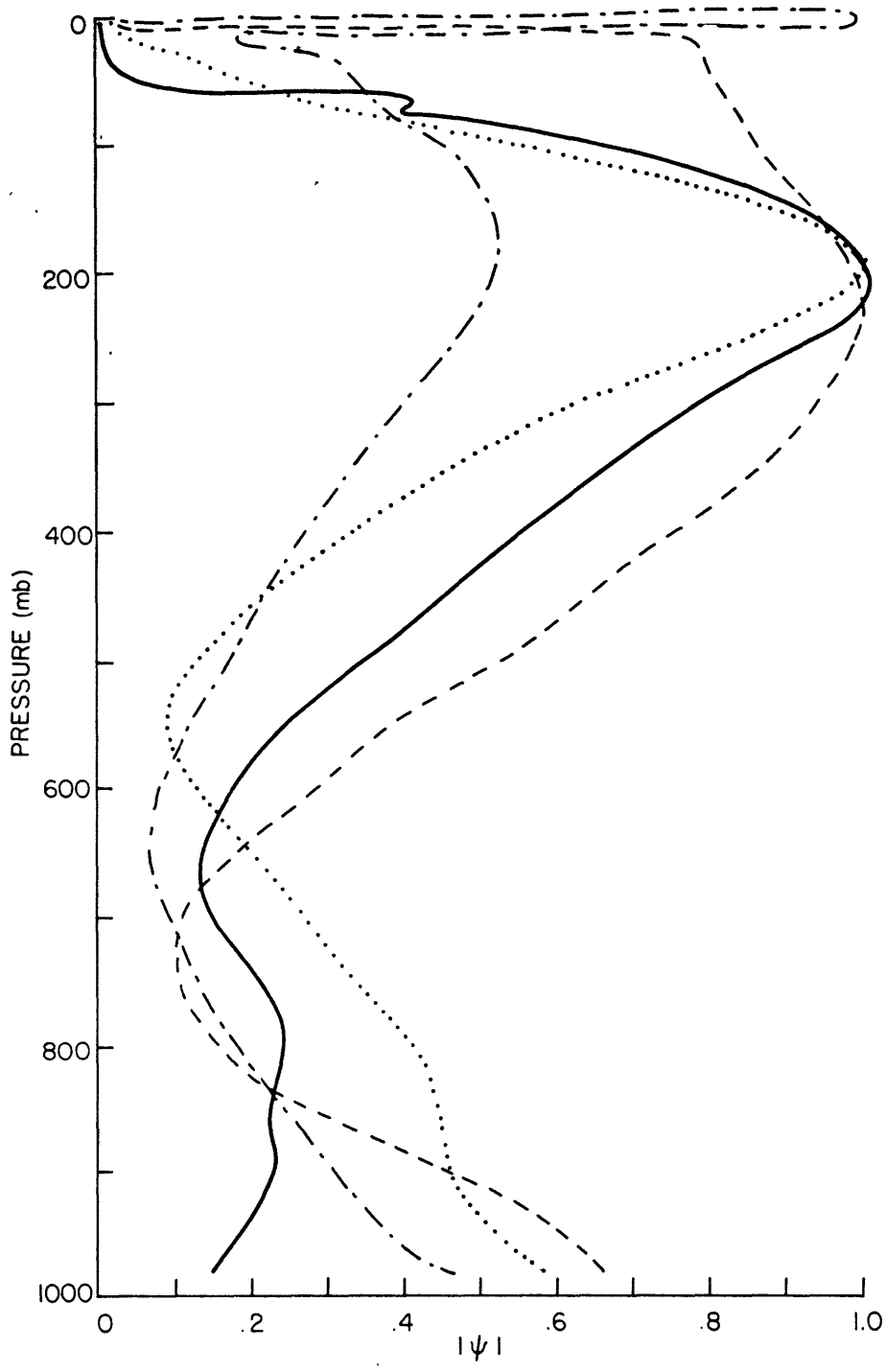

Figure 4.31. As in Figure 4.30, except for the cases: July 45°N (dot), October 25°N (solid), October 50°N (dash dot), and October 65°N (dash).

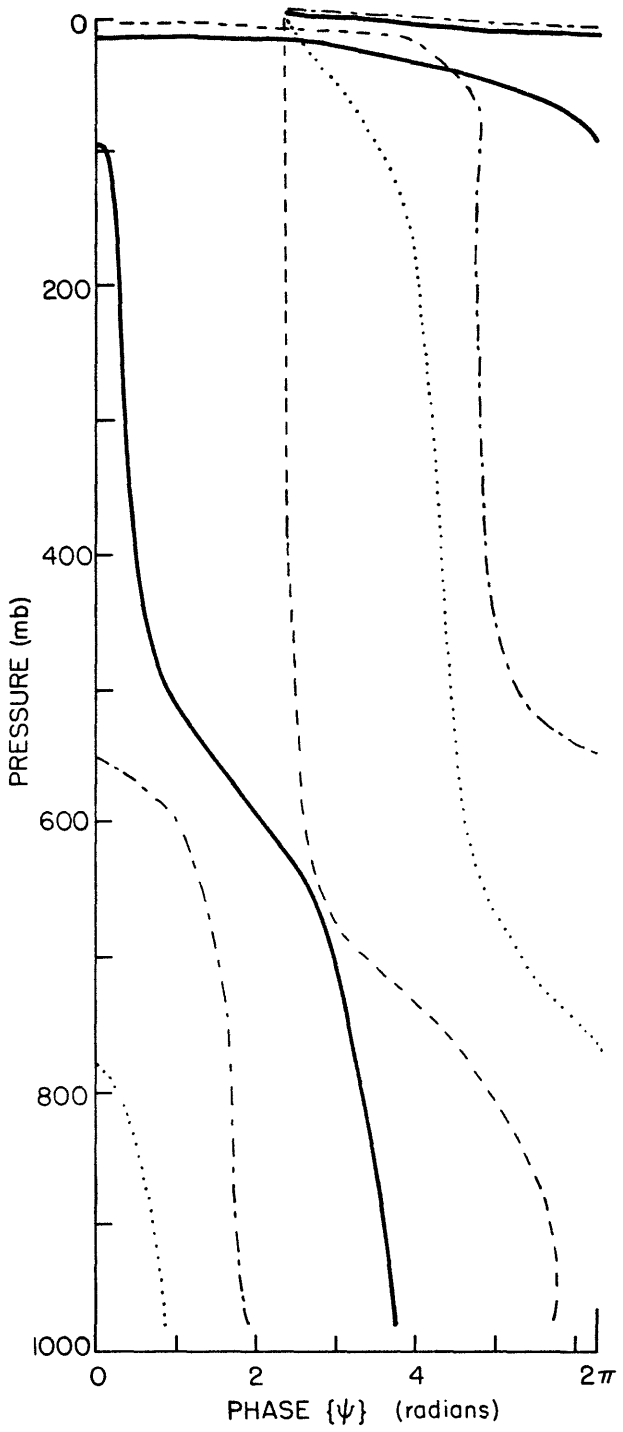

Figure 4.32. Vertical structure of the streamfunction phase of the fastest growing Green mode. Cases are those in Figure 4.30.

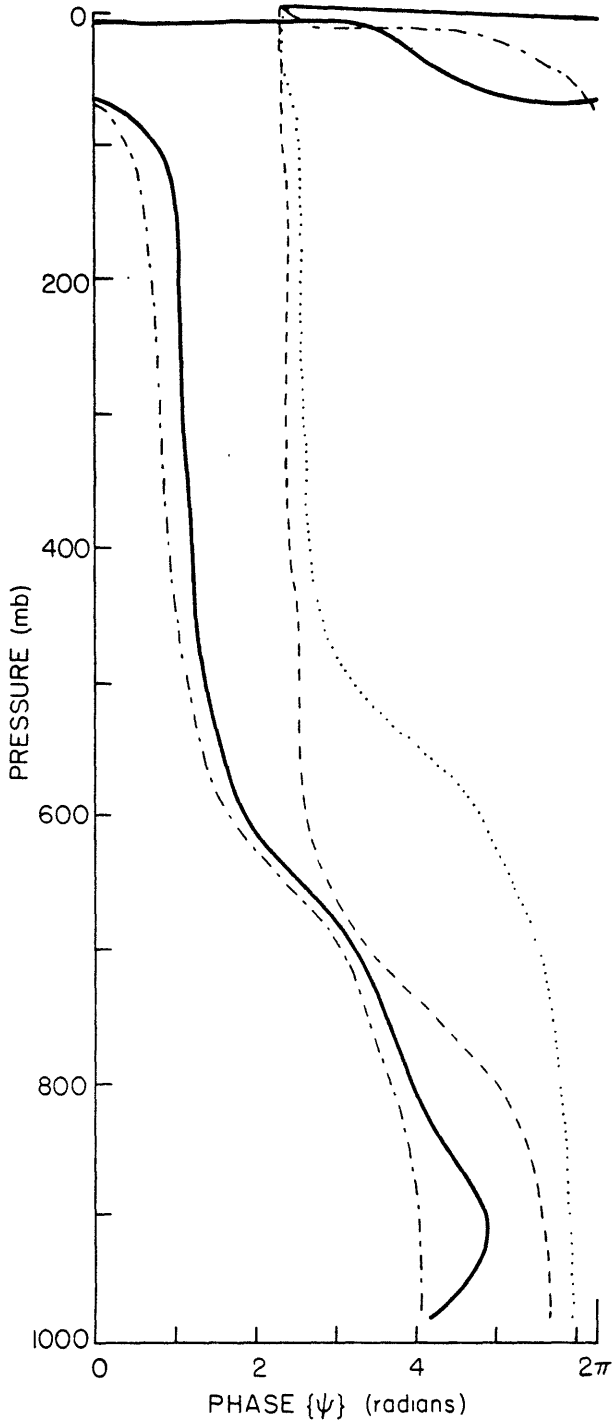

Figure 4.33. As in Figure 4.32, except for the cases July 45°N (dot), October 25°N (solid), October 50°N (dash dot), and October 65°N (dash).

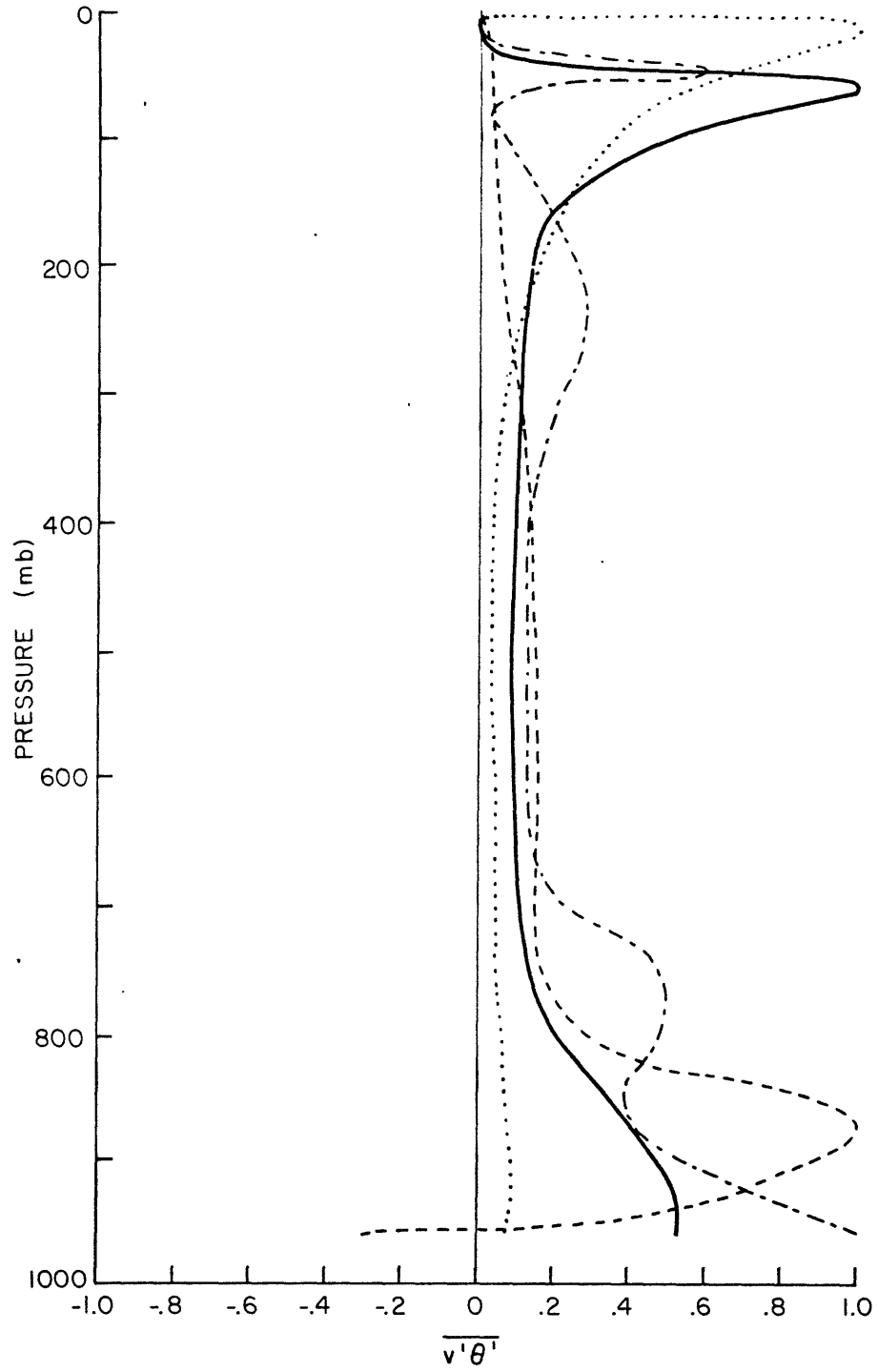

Figure 4.34. Vertical structure of the meridional entropy transport of the fastest growing Green mode. Cases are those in Figure 4.30.

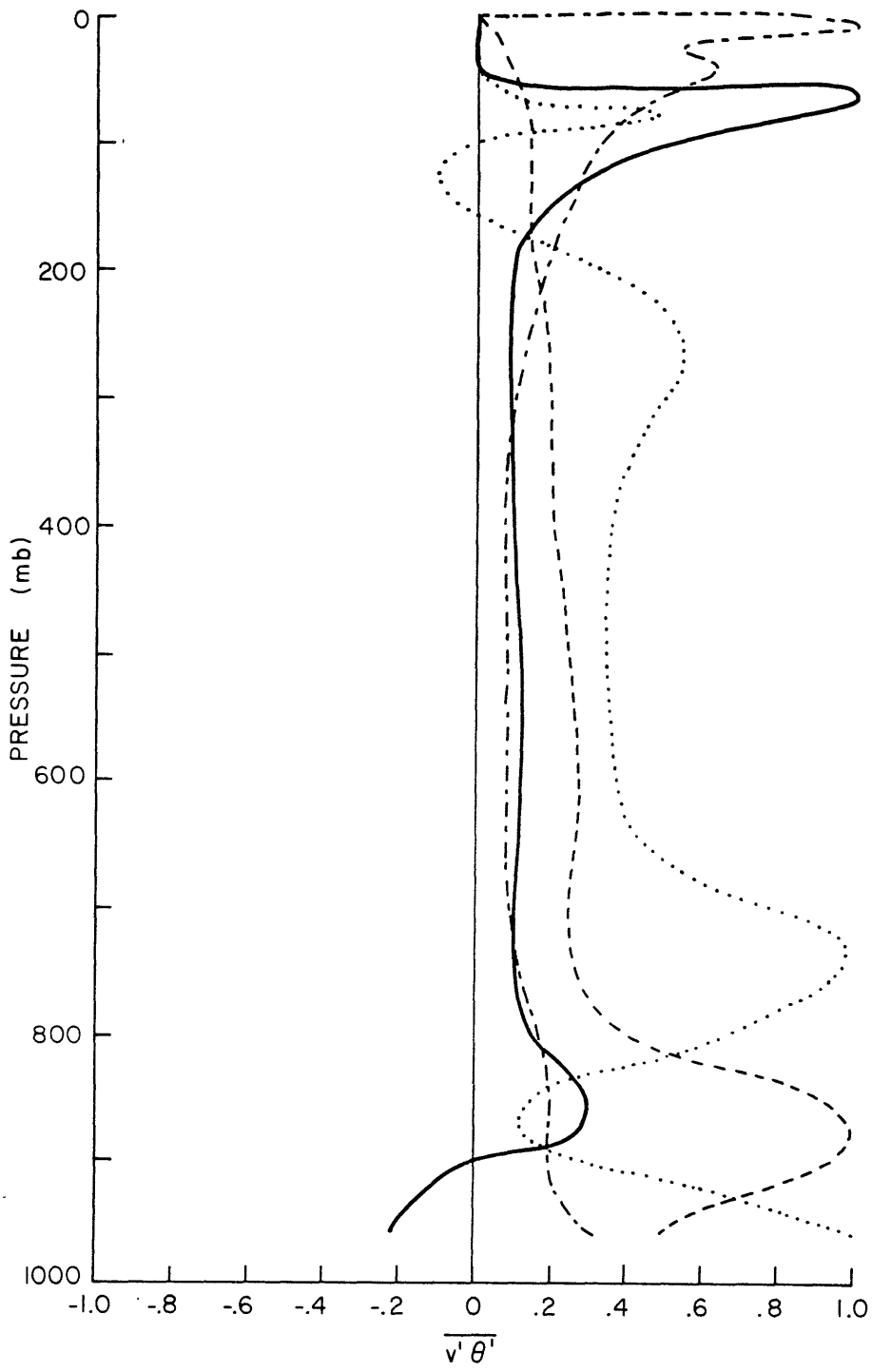

Figure 4.35. As in Figure 4.34, except for the cases July 45°N (dot), October 25°N (solid), October 50°N (dash dot), and October 65°N (dash).

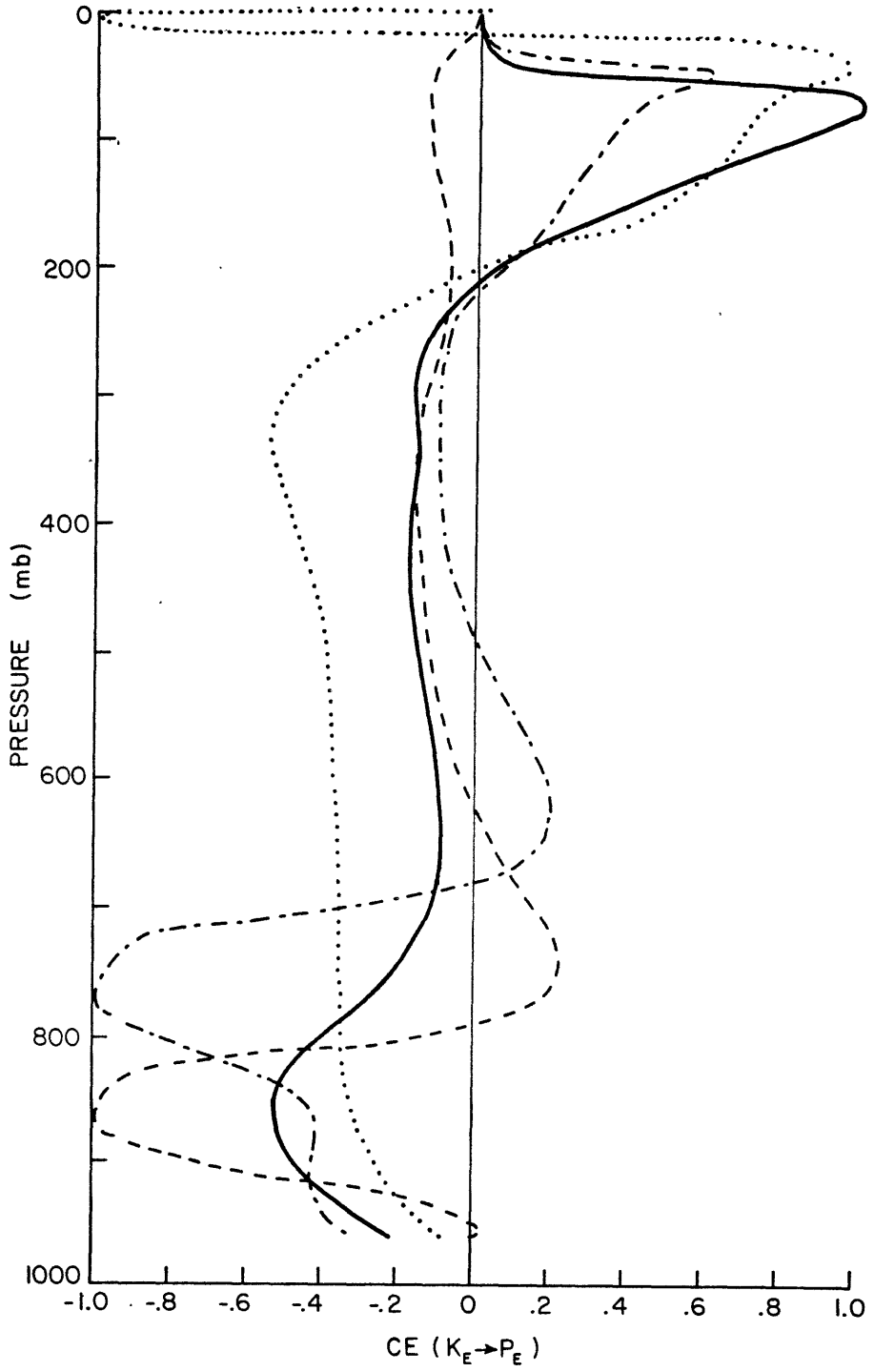

Figure 4.36. Vertical structure of the transfer of eddy kinetic to eddy available potential energy ($K_E \rightarrow P_E$ is positive) for the fastest growing Green mode. Cases are those in Figure 4.30.

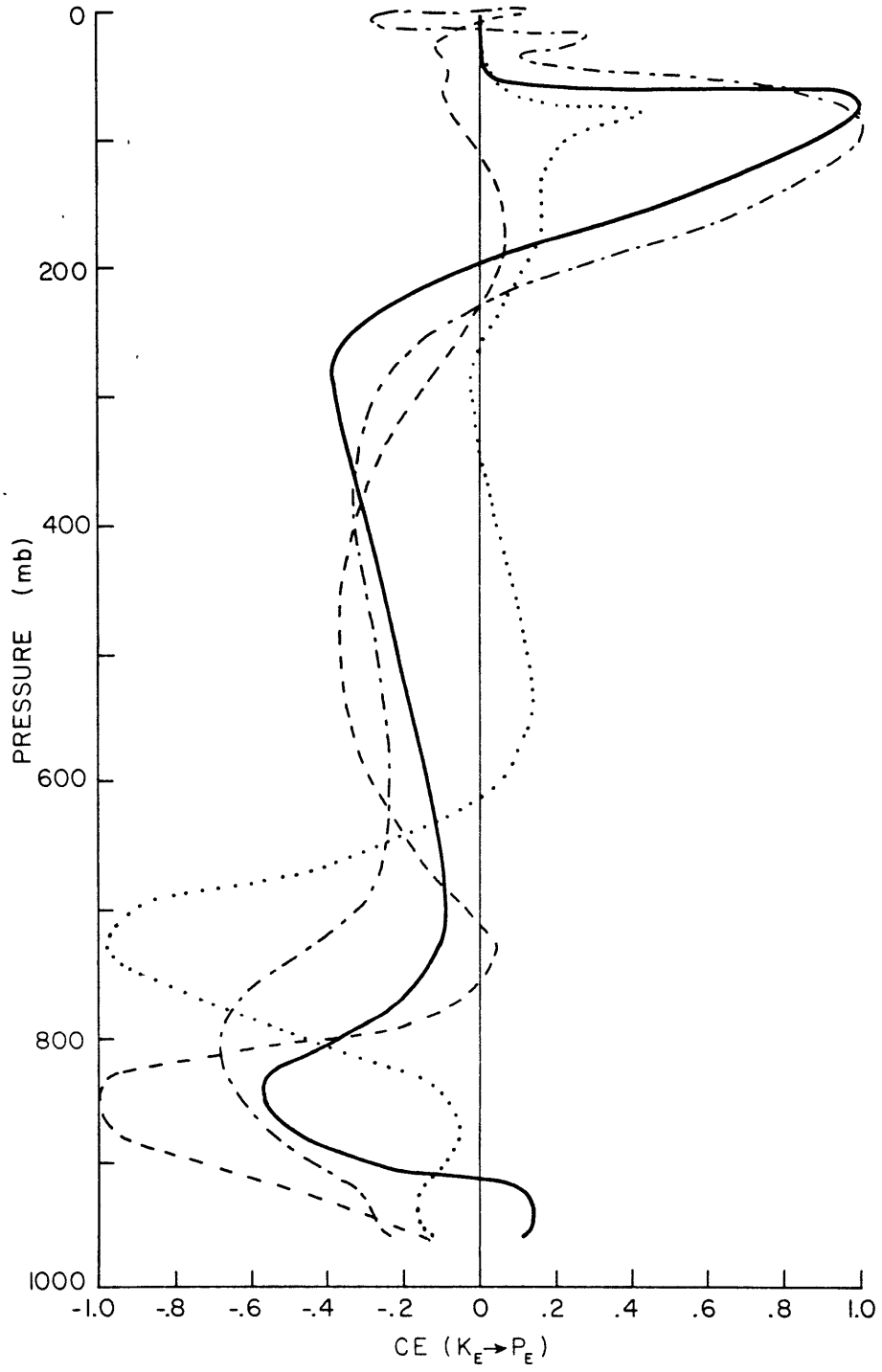

Figure 4.37. As in Figure 4.36, except for the cases July 45°N (dot), October 25°N (solid), October 50°N (dash dot), and October 65°N (dash).

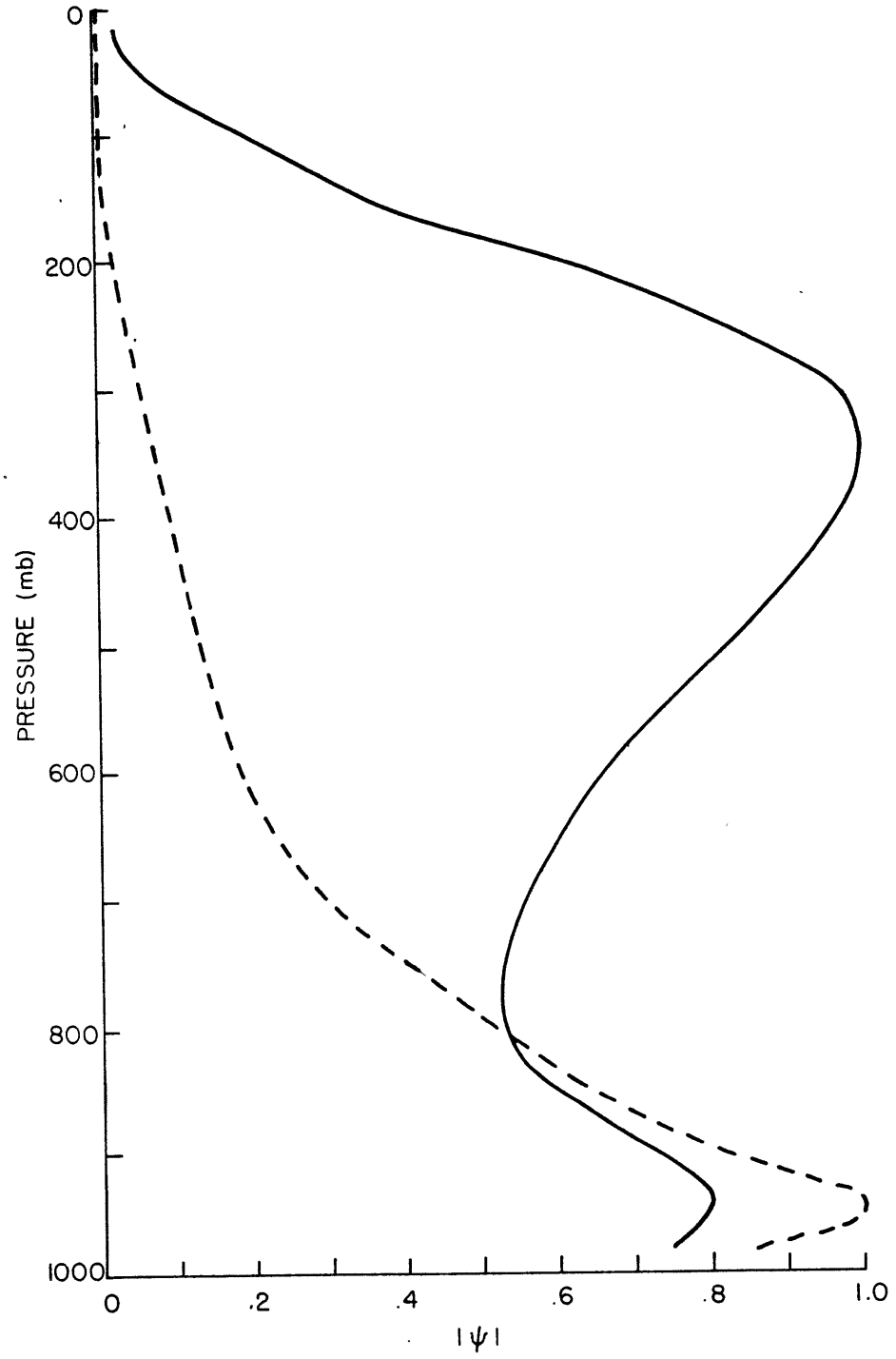

Figure 4.38. Vertical structure of the streamfunction amplitude of the fastest growing E_s and S_m modes. Cases: E_s, January 65°N (dash), and S_m, January 65°N (solid).

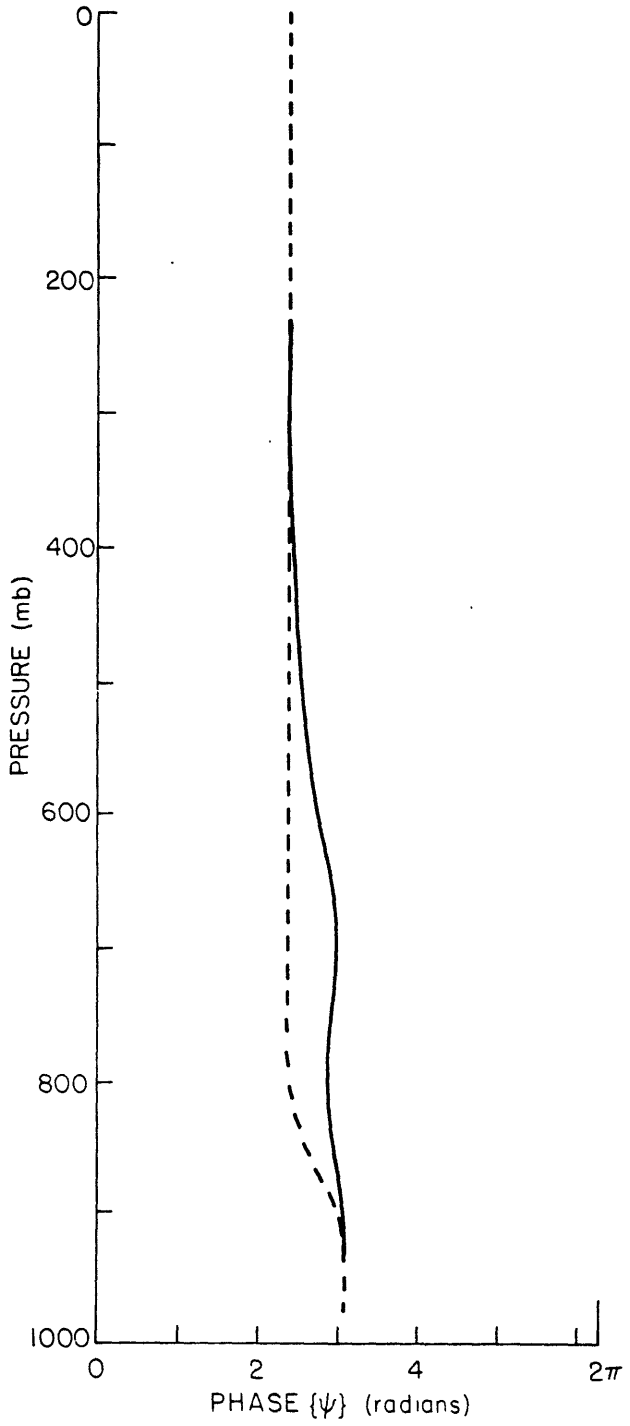

Figure 4.39. Vertical structure of the streamfunction phase of the fastest growing E_s and S_m modes. Cases are those in Figure 4.38.

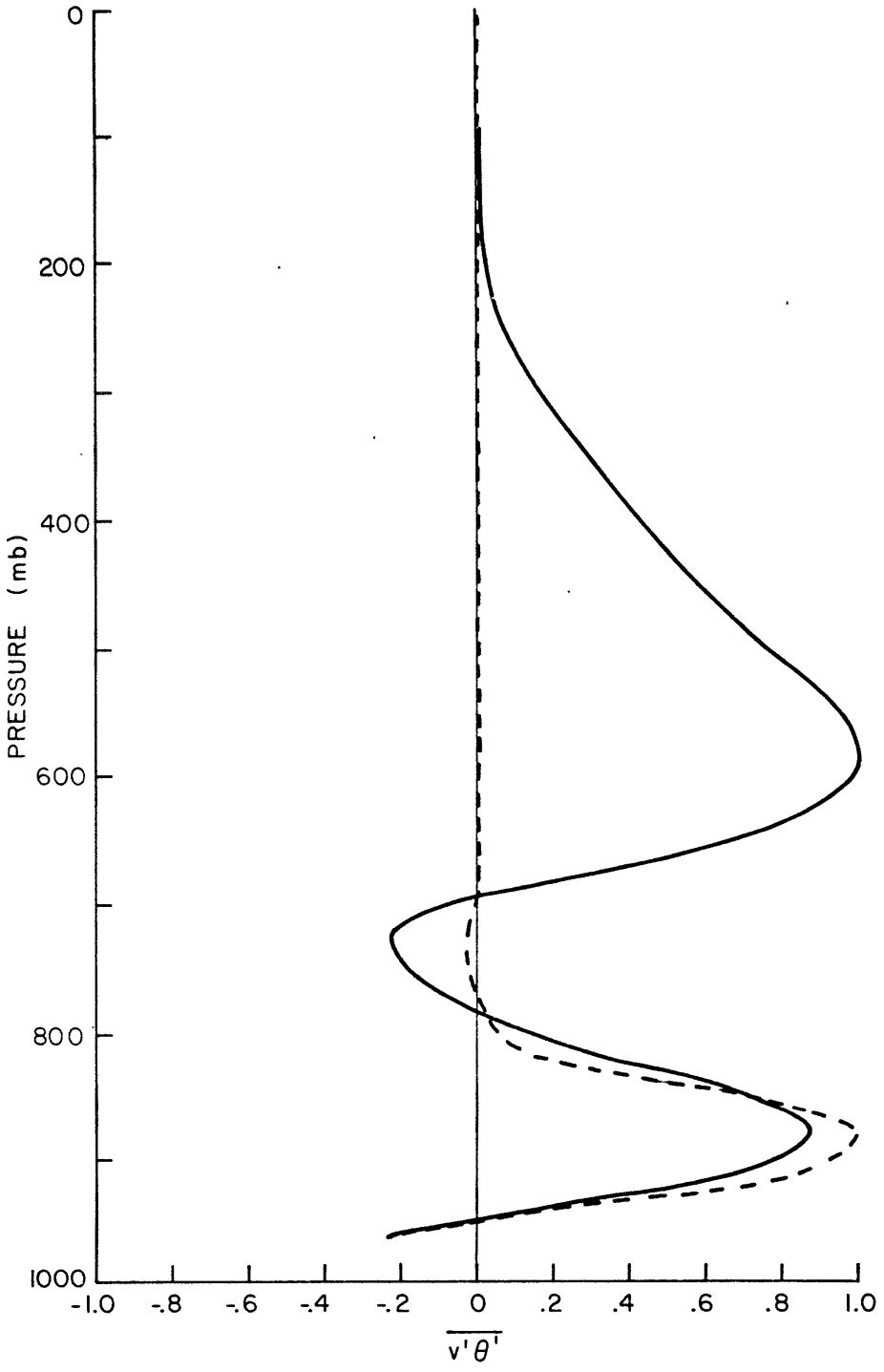

Figure 4.40. Vertical structure of the meridional entropy transport of the fastest growing E_s and S_m modes. Cases are those in Figure 4.38.

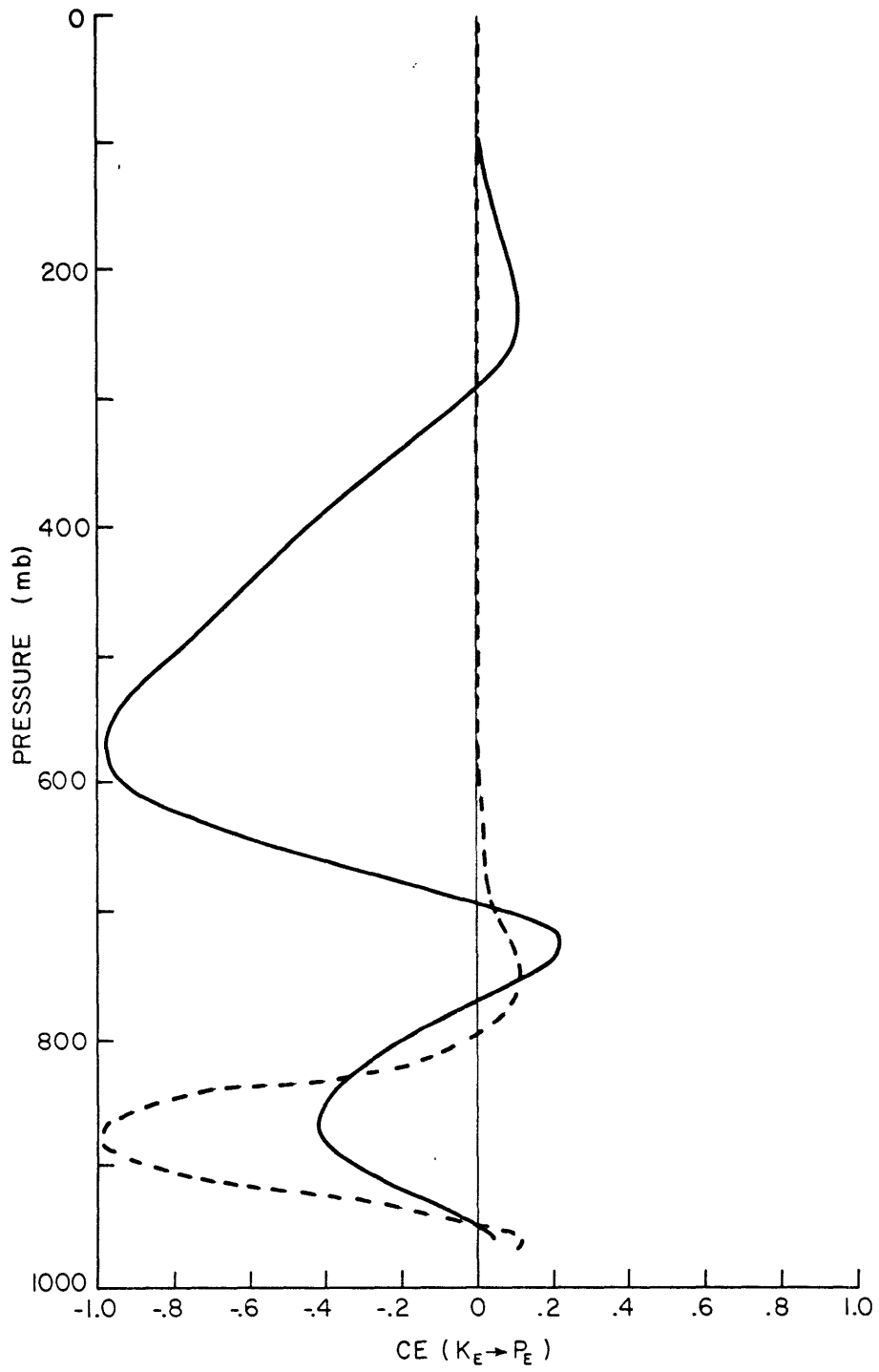

Figure 4.41. Vertical structure of the transfer of eddy kinetic to eddy available potential energy ($K_E \rightarrow P_E$ is positive) for the fastest growing E_S and S_m modes. Cases are those in Figure 4.38.

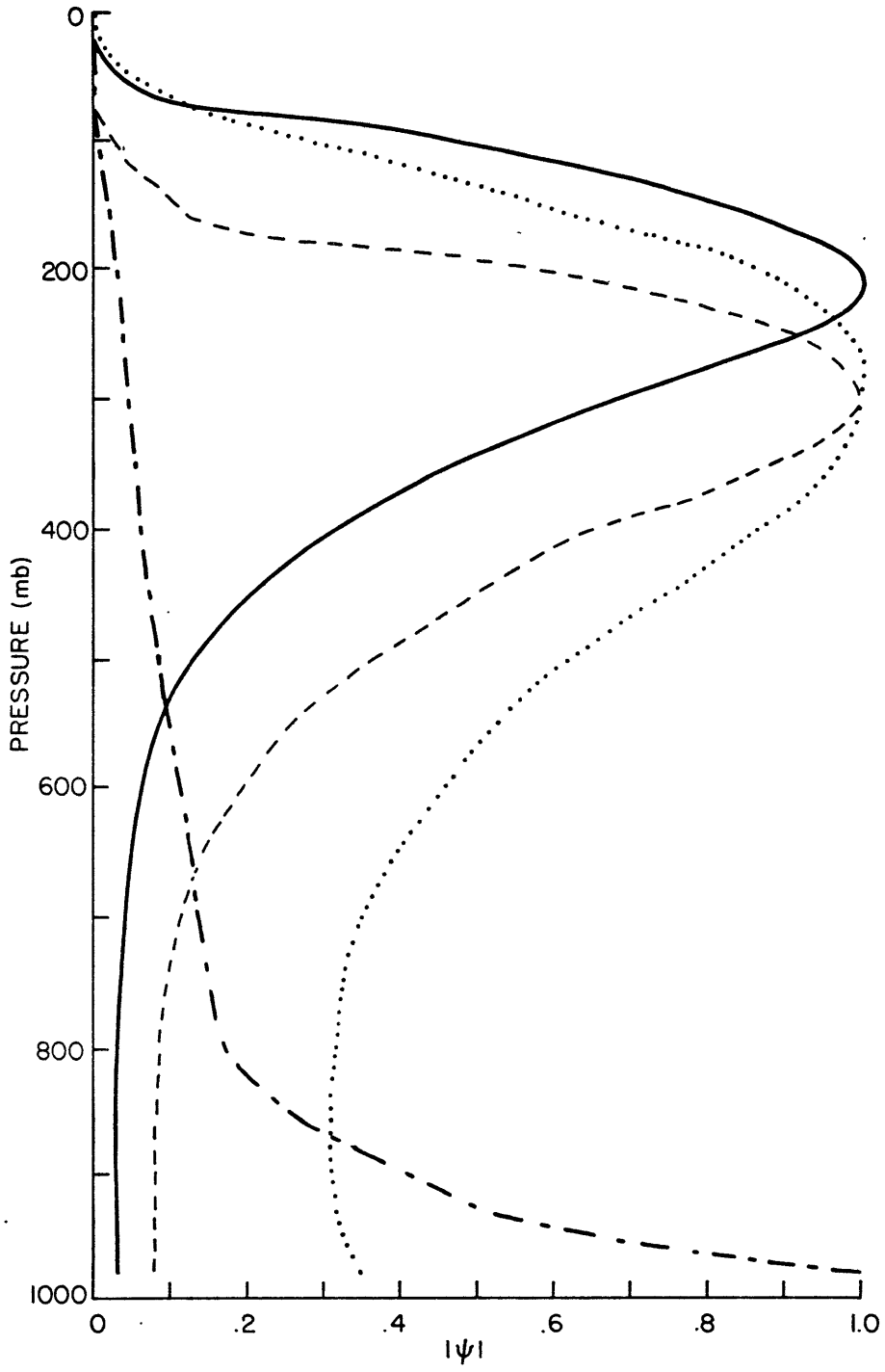

Figure 4.42. Vertical structure of the streamfunction amplitude of the fastest growing S modes. Cases: January 35°N (dot), April 25°N (solid), July 45°N (dash dot), and July 65°N (dash).

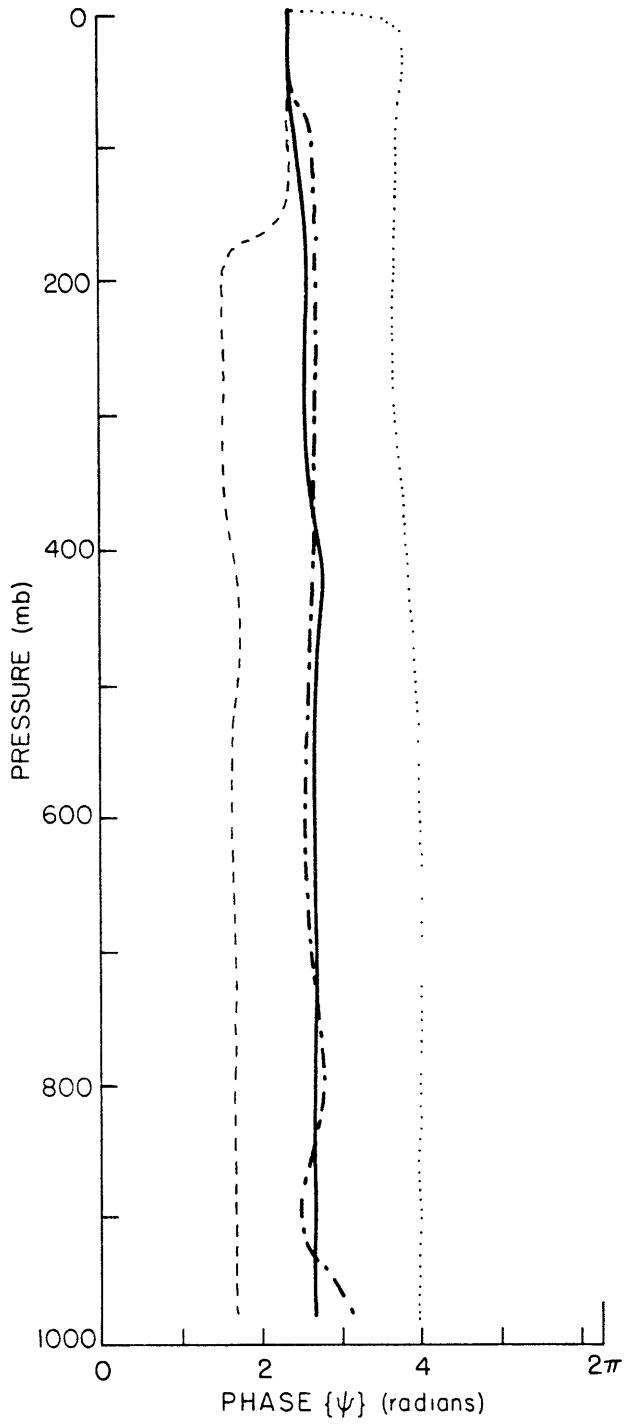

Figure 4.43. Vertical structure of the streamfunction phase of the fastest growing S modes. Cases are those in Figure 4.42.

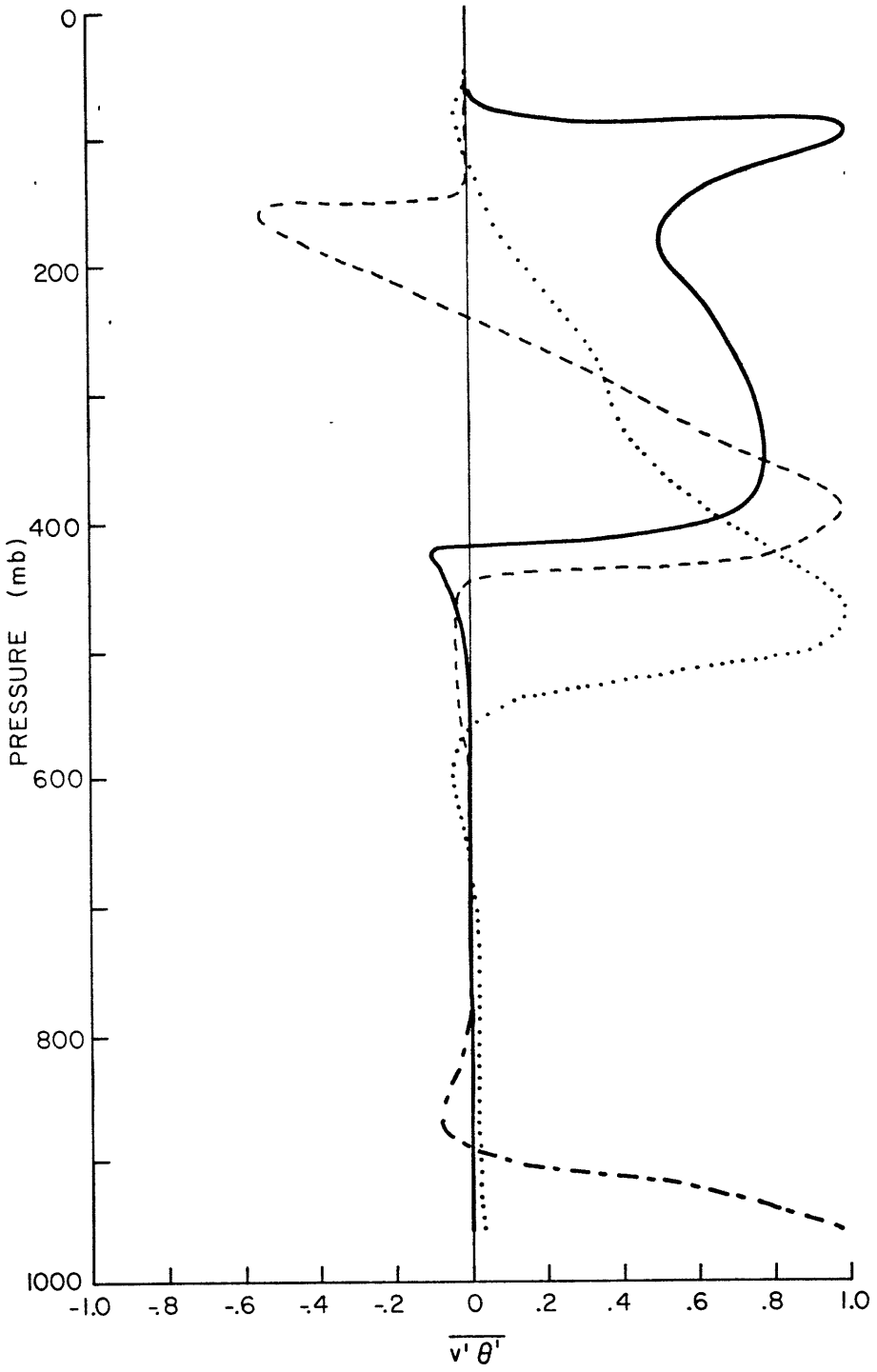

Figure 4.44. Vertical structure of the meridional entropy transport of the fastest growing S modes. Casse are those in Figure 4.42.

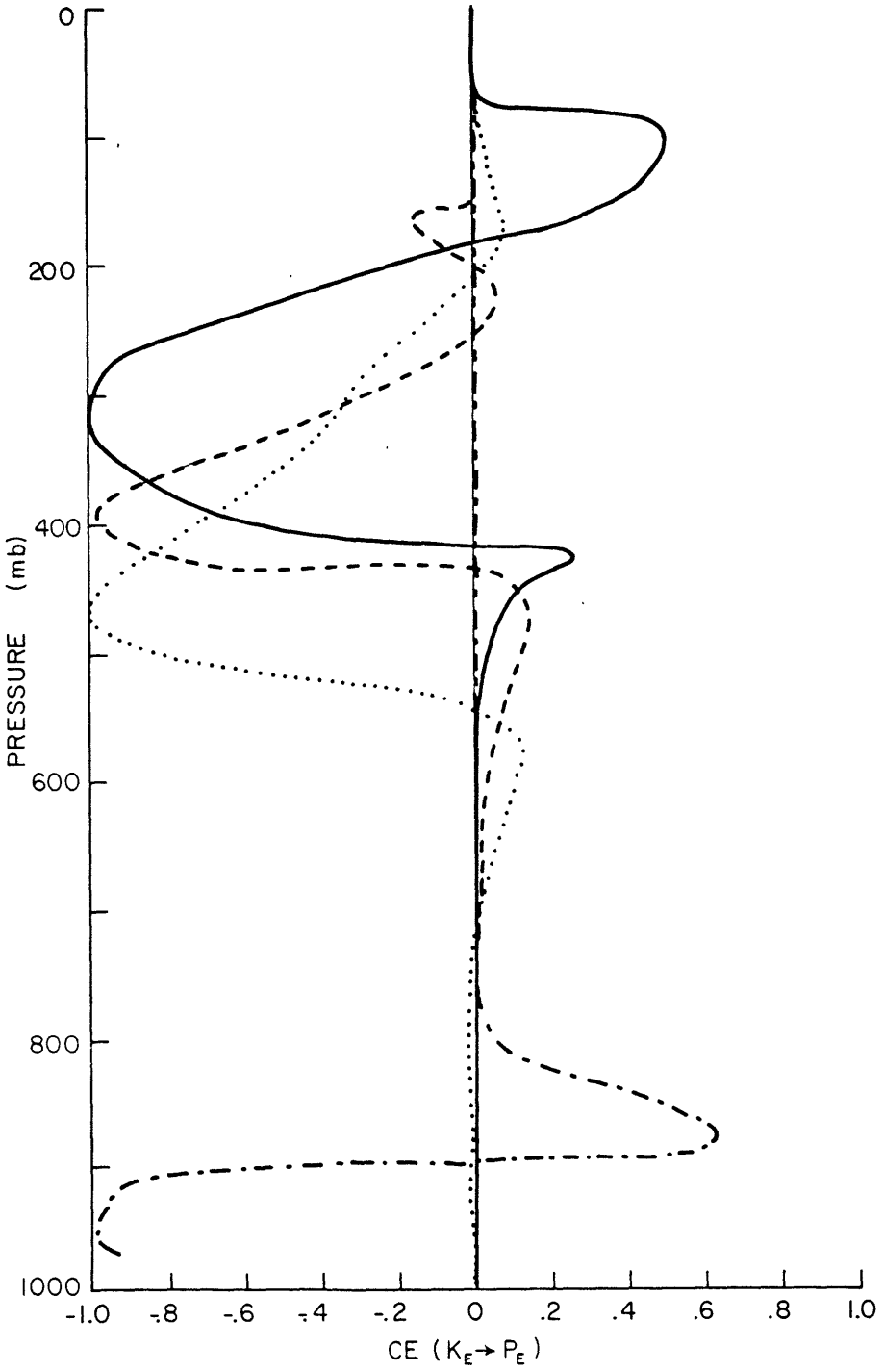

Figure 4.45. Vertical structure of the transfer of eddy kinetic to eddy available potential energy ($K_E \rightarrow P_E$ is positive) for the fastest growing S modes. Cases are those in Figure 4.42.

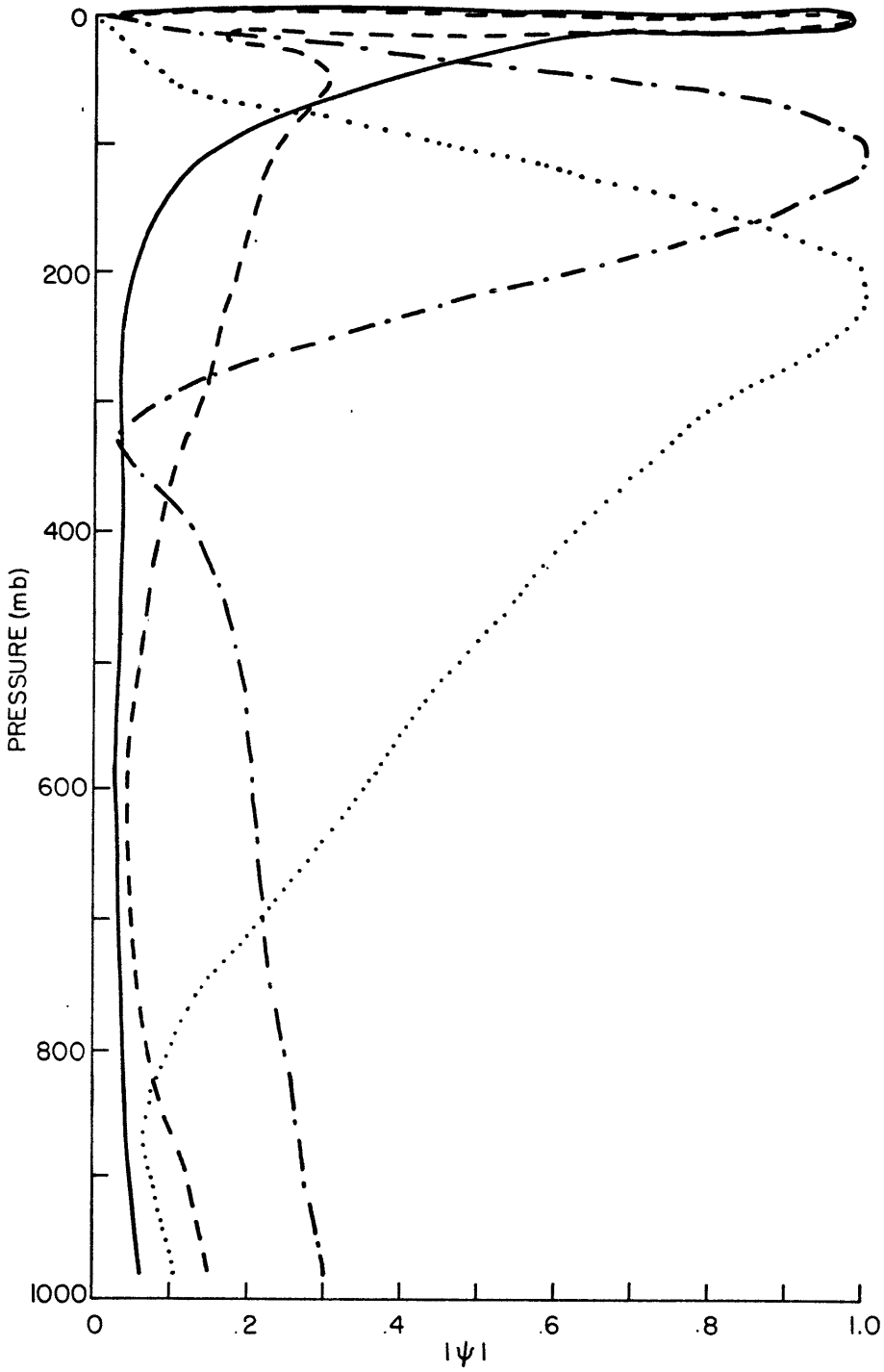

Figure 4.46. Vertical structure of the streamfunction amplitude of the fastest growing L modes. Cases are: January 35°N (dash dot), January 45°N (dash), January 65°N (solid), and July 45°N (dot).

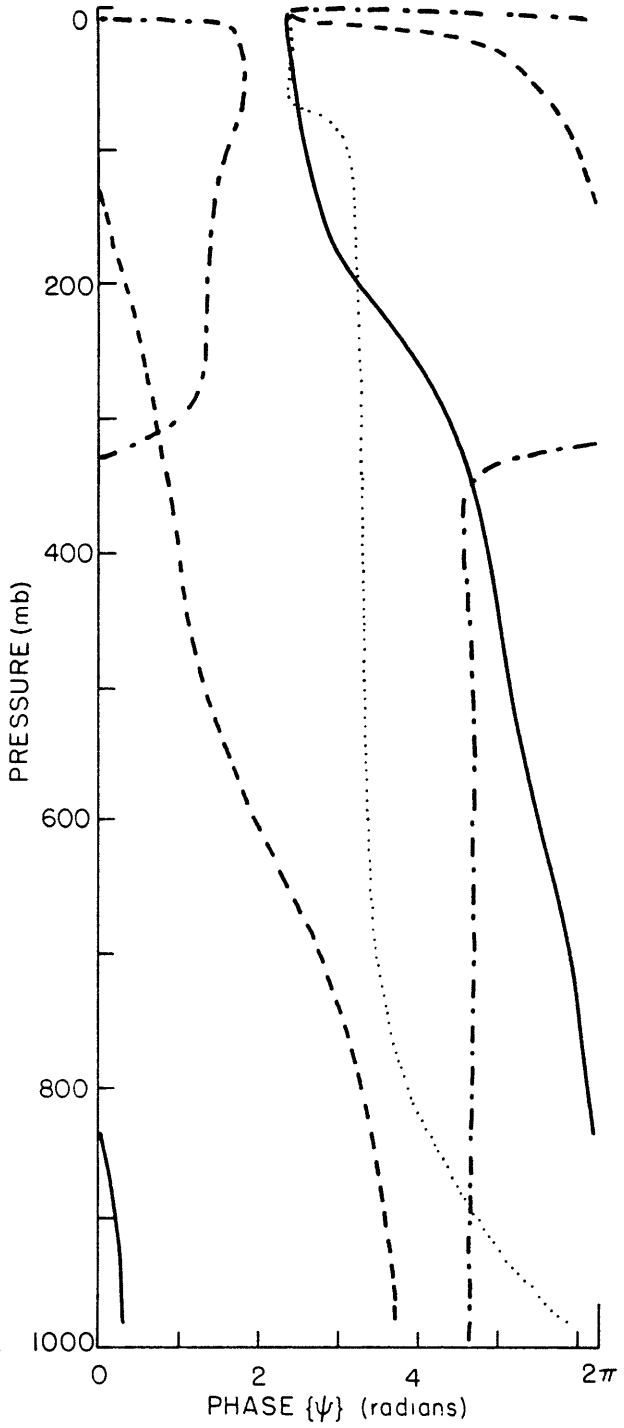

Figure 4.47. Vertical structure of the streamfunction phase of the fastest growing L modes. Cases are those in Figure 4.46.

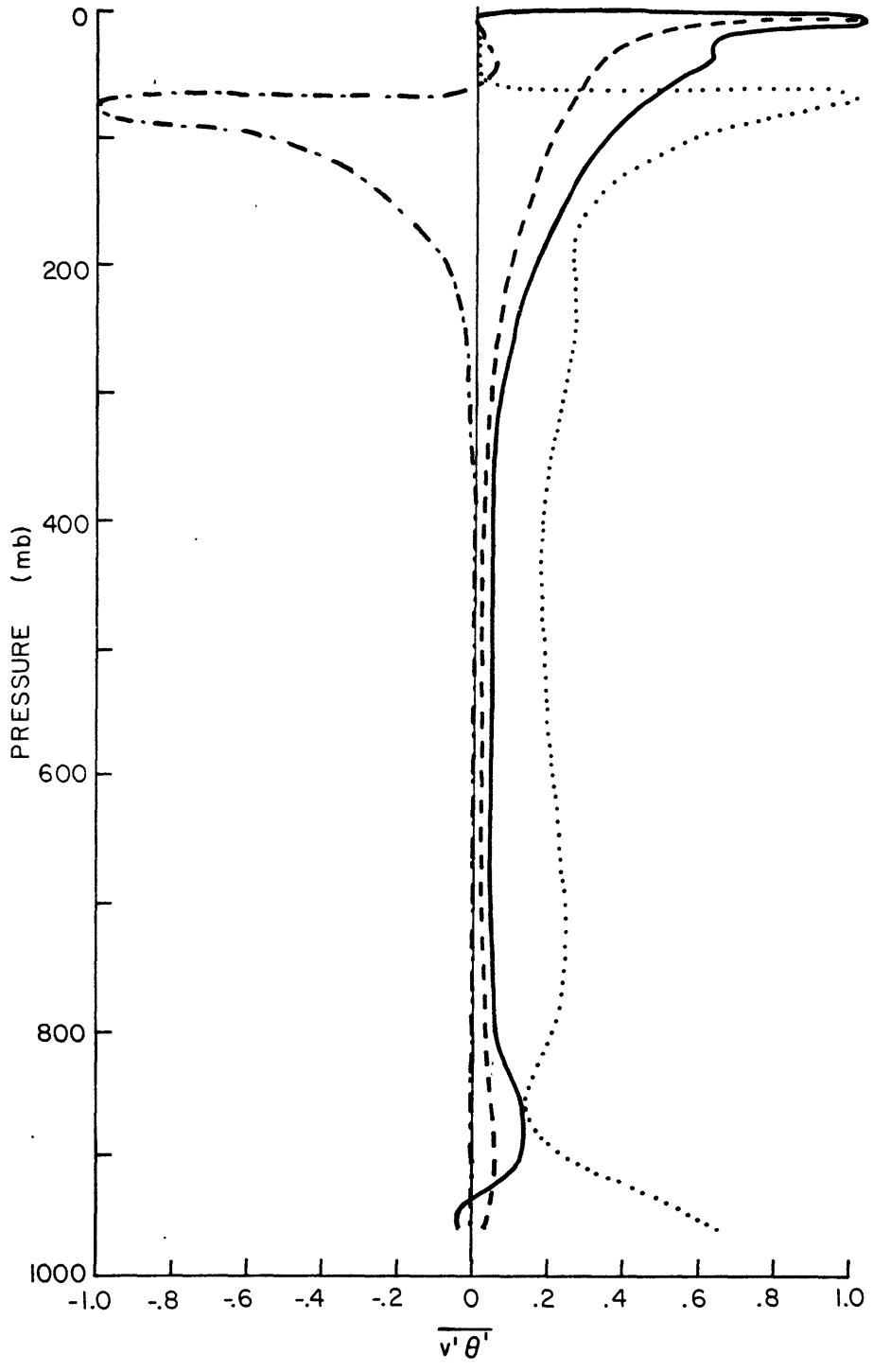

Figure 4.48. Vertical structure of the meridional entropy transport of the fastest growing L modes. Cases are those in Figure 4.46.

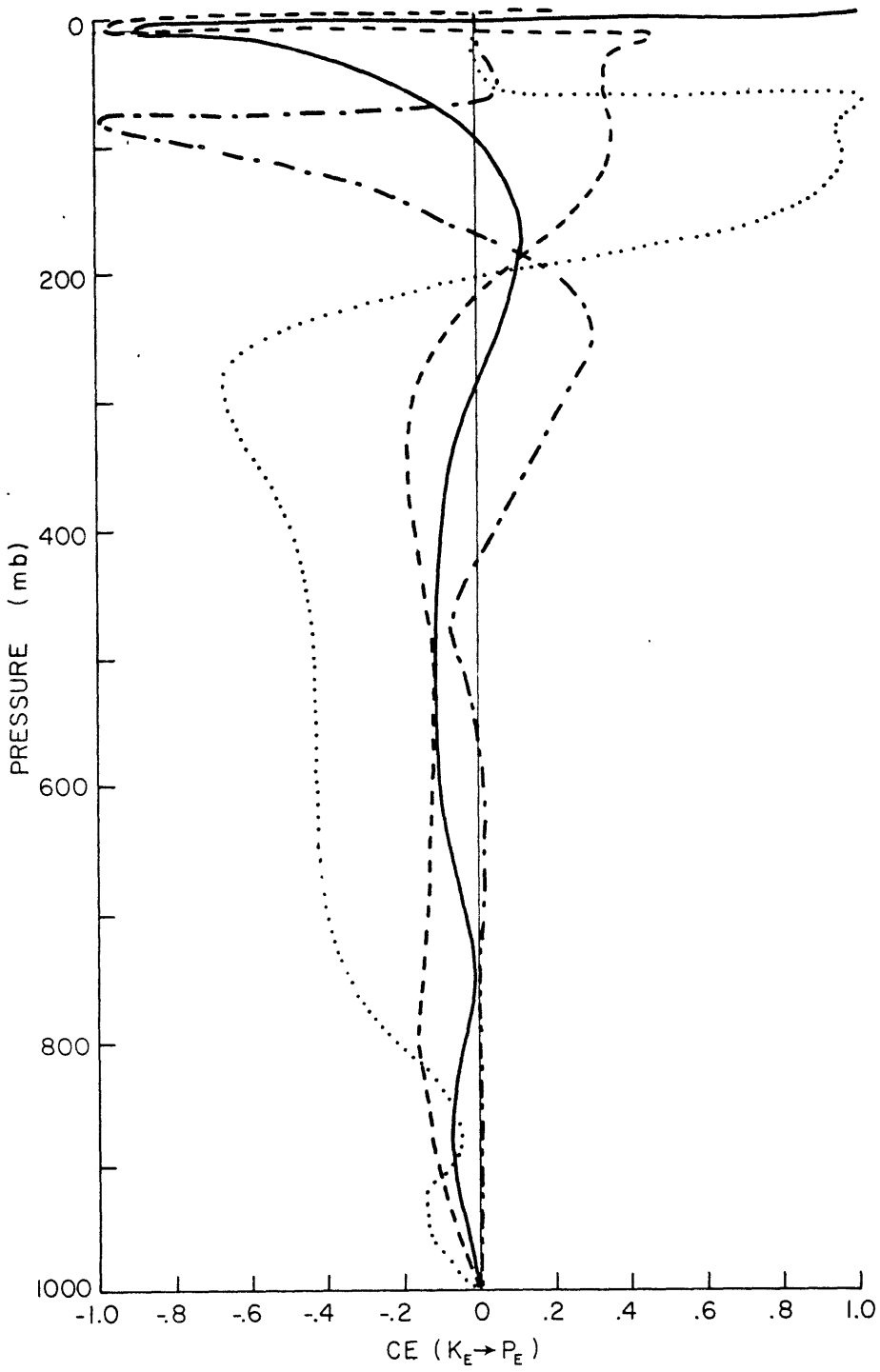

Figure 4.49. Vertical structure of the transfer of eddy kinetic to eddy available potential energy ($K_E \rightarrow P_E$ is positive) for the fastest growing L modes. Cases are those in Figure 4.46.

TABLE 4.1. QUASIGEOSTROPHIC POTENTIAL VORTICITY MERIDIONAL GRADIENT ($\bar{Q}_y$) DATA (10^{14}/(M*SEC)) FOR JANUARY. SOURCES: LEVELS 25-97, #1, LEVELS 13-41, #2, LEVELS 7-29, #3, LEVELS 3-7, #4. SEE SECTION IV-3 FOR A DESCRIPTION OF THE DATA SOURCES.

LATITUDE(N)=	25	30	35	40	45	50	55	60	65
LEVEL*									
3	-531.	10913.	3258.	8944.	4118.	3836.	1064.	14153.	5772.
5	12677.	-1141.	4426.	7507.	4681.	4038.	-5937.	2782.	5447.
7	5818.	4385.	-4111.	9718.	3630.	2030.	-8508.	2740.	14149.
7	1195.		713.		1986.		4387.		5636.
9	1134.		716.		1823.		4264.		5643.
11	1615.		1267.		1589.		3098.		4173.
13	1778.		1324.		1217.		2576.		3784.
15	1935.		1354.		810.		1989.		3382.
17	2084.		1365.		568.		1308.		2957.
19	2224.		1359.		-105.		524.		2508.
21	2349.		1341.		-591.		-355.		2049.
23	2455.		1320.		-1049.		-1272.		1623.
25	2537.		1303.		-1406.		-2088.		1313.
27	2589.		1303.		-1558.		-2550.		1267.
29	2609.		1342.		-1394.		-2369.		1732.
13	2330.	1933.	1318.	933.	1221.	1831.	2449.	2997.	3309.
15	2126.	1678.	1101.	705.	892.	1539.	2155.	2758.	3173.
17	1894.	1369.	729.	254.	317.	992.	1629.	2326.	2909.
19	1611.	1161.	511.	37.	79.	825.	1472.	2165.	2785.
21	1298.	990.	369.	-27.	95.	954.	1593.	2178.	2699.
23	1138.	882.	257.	-25.	208.	1109.	1727.	2212.	2593.
25	1152.	816.	140.	-17.	312.	1128.	1724.	2183.	2448.
27	1149.	706.	30.	80.	542.	1216.	1772.	2210.	2320.
29	981.	445.	-86.	304.	937.	1408.	1894.	2305.	2224.
31	479.	31.	-41.	766.	1507.	1690.	2046.	2407.	2135.
33	323.	915.	1316.	1439.	1568.	1386.	1577.	1873.	1790.
35	2077.	3913.	3925.	2356.	1436.	834.	827.	1053.	1344.
37	5423.	7893.	6898.	3277.	1164.	134.	-94.	52.	874.
39	5688.	8487.	7426.	3326.	945.	-118.	-417.	-181.	807.
41	4306.	6809.	5999.	2658.	847.	138.	-38.	327.	1189.

*Level n is related to pressure level p by: $\frac{n}{N} = \left(p/p_{oo}\right)^{1/2}$ where N=98.

TABLE 4.1 CONTINUED.

LATITUDE(N)=	25	30	35	40	45	50	55	60	65
LEVEL									
25	1871.	1865.	1033.	831.	1361.	1429.	1540.	1857.	1585.
27	1970.	2017.	1130.	767.	1133.	1228.	1520.	1762.	1725.
29	1951.	2095.	1222.	724.	913.	1018.	1485.	1713.	1901.
31	1765.	2105.	1335.	715.	718.	819.	1431.	1649.	2093.
33	1670.	2361.	1692.	867.	690.	781.	1362.	1539.	2055.
35	1702.	2845.	2217.	1113.	746.	814.	1285.	1418.	1931.
37	1997.	3618.	2927.	1472.	893.	909.	1205.	1283.	1729.
39	2873.	4822.	3887.	1987.	1156.	1077.	1127.	1124.	1433.
41	4705.	6600.	5196.	2729.	1577.	1334.	1056.	929.	1021.
43	7488.	9013.	6999.	3815.	2231.	1712.	999.	683.	459.
45	9073.	10668.	8415.	4767.	2849.	2013.	1027.	662.	284.
47	9200.	11305.	9181.	5476.	3376.	2222.	1168.	915.	590.
49	8745.	11466.	9816.	6328.	4043.	2514.	1418.	1332.	1120.
51	7656.	10988.	10241.	7430.	4934.	2968.	1850.	2049.	2030.
53	5989.	9675.	10281.	8955.	6206.	3729.	2607.	3379.	3642.
55	5628.	9156.	10743.	10762.	7546.	4713.	3502.	4750.	4988.
57	6199.	9278.	11168.	11632.	8235.	5434.	4301.	5635.	5637.
59	6852.	9253.	10641.	10153.	7573.	5303.	4629.	5742.	5693.
61	7560.	9048.	8826.	5529.	4854.	3669.	4607.	4359.	4675.
63	7463.	7856.	6286.	2288.	2738.	2463.	3983.	3075.	3829.
65	6397.	5555.	3589.	1996.	2610.	2663.	3452.	2898.	3951.
67	5195.	3044.	842.	1911.	2640.	2932.	2710.	2731.	3987.
69	3924.	809.	-1387.	1879.	2820.	3211.	1965.	2511.	3919.
71	3371.	530.	-1301.	1452.	2683.	3031.	1220.	1749.	2738.
73	3012.	844.	-559.	1021.	2554.	2786.	715.	856.	1344.
75	2695.	1195.	148.	746.	2437.	2549.	310.	26.	-5.
77	2414.	1589.	851.	588.	2331.	2325.	13.	-696.	-1240.
79	2194.	1985.	1542.	557.	2255.	2112.	-180.	-1283.	-2325.
81	2009.	2375.	2185.	641.	2166.	1919.	-283.	-1740.	-3265.
83	2003.	2248.	2162.	1123.	2179.	1955.	1274.	-164.	-1741.
85	2040.	1534.	1419.	1739.	2210.	2239.	4142.	3027.	1831.
87	1991.	704.	474.	2197.	2222.	2508.	6811.	5688.	4599.
89	1851.	-326.	-764.	2514.	2214.	2784.	9408.	7798.	6442.
91	2463.	2280.	2472.	4814.	4016.	6107.	7973.	8531.	4853.
93	4701.	14518.	18667.	12851.	7516.	13062.	-1822.	3479.	-3939.
95	3412.	20392.	23534.	9417.	-8467.	-27569.	-31920.	-43544.	-28276.
97	3375.	12510.	12118.	7993.	-4788.	-28439.	-32460.	-28600.	-15635.

TABLE 4.2. AS IN 4.1, FOR APRIL.

LATITUDE (N)=	25	30	35	40	45	50	55	60	65
LEVEL									
3	569.	3044.	2279.	3159.	2463.	1822.	1343.	5542.	-2395.
5	779.	1395.	5542.	3684.	1590.	2172.	4550.	4626.	-663.
7	1559.	1942.	5701.	4473.	2464.	1157.	1503.	691.	648.
7	2064.		2659.		1907.		1299.		275.
9	2176.		2584.		1829.		909.		26.
11	2334.		2217.		1659.		585.		312.
13	2357.		1927.		1462.		185.		215.
15	2389.		1682.		1209.		-267.		50.
17	2429.		1476.		892.		-792.		-187.
19	2473.		1300.		501.		-1409.		-494.
21	2516.		1150.		37.		-2122.		-863.
23	2551.		1031.		-482.		-2901.		-1269.
25	2568.		955.		-993.		-3650.		-1663.
27	2556.		952.		-1377.		-4173.		-1966.
29	2504.		1067.		-1488.		-4271.		-2122.
13	2495.	2411.	2215.	2174.	1808.	1370.	1041.	824.	639.
15	2282.	2104.	1908.	1786.	1592.	1130.	972.	759.	668.
17	2024.	1718.	1447.	1186.	770.	699.	773.	658.	717.
19	1715.	1335.	1029.	719.	478.	549.	701.	666.	762.
21	1371.	942.	639.	389.	488.	674.	784.	786.	820.
23	1149.	681.	400.	242.	550.	790.	872.	922.	940.
25	1084.	590.	324.	220.	474.	712.	876.	1039.	1173.
27	1048.	562.	346.	327.	431.	630.	906.	1207.	1502.
29	967.	577.	495.	598.	460.	568.	975.	1448.	1949.
31	813.	723.	892.	1103.	641.	579.	1100.	1756.	2447.
33	1083.	1407.	1372.	1307.	933.	747.	1057.	1552.	1908.
35	2434.	2955.	2171.	1504.	1380.	1041.	932.	1068.	861.
37	4918.	5073.	3084.	1657.	1849.	1361.	724.	361.	-628.
39	5879.	5746.	3242.	1562.	1909.	1394.	567.	28.	-1325.
41	4990.	4846.	2697.	1321.	1570.	1154.	479.	163.	-832.

TABLE 4.2 CONTINUED.

LATITUDE (N)= LEVEL	25	30	35	40	45	50	55	60	65
25	1792.	1689.	1284.	867.	1242.	774.	877.	600.	728.
27	1811.	1773.	1314.	847.	979.	668.	739.	635.	791.
29	1722.	1802.	1348.	844.	730.	553.	597.	679.	877.
31	1484.	1788.	1403.	856.	510.	441.	462.	725.	978.
33	1426.	2041.	1641.	951.	458.	478.	449.	754.	990.
35	1556.	2501.	2000.	1094.	488.	577.	493.	782.	974.
37	2010.	3226.	2515.	1323.	610.	740.	592.	817.	940.
39	3097.	4377.	3269.	1697.	846.	983.	752.	862.	888.
41	5204.	6218.	4520.	2315.	1241.	1330.	985.	920.	820.
43	8472.	9186.	6636.	3395.	1886.	1825.	1309.	993.	736.
45	10664.	11888.	8920.	4677.	2661.	2302.	1590.	1136.	851.
47	11229.	13293.	10612.	5919.	3534.	2776.	1852.	1387.	1186.
49	10961.	13618.	11813.	7312.	4723.	3469.	2258.	1795.	1673.
51	9546.	11762.	11427.	8635.	6397.	4600.	2955.	2513.	2453.
53	6789.	6782.	8026.	9409.	8855.	6701.	4288.	3975.	3880.
55	4652.	3596.	5764.	9889.	11123.	9344.	6061.	5925.	5546.
57	3080.	2522.	5205.	9638.	11852.	11087.	7600.	7717.	7090.
59	1522.	1648.	4414.	7728.	9901.	9965.	7978.	8433.	8331.
61	218.	1147.	3572.	4233.	4580.	4278.	5673.	6117.	8214.
63	306.	1177.	2703.	2089.	1202.	851.	3519.	3718.	7317.
65	1413.	1470.	1809.	2005.	1449.	1679.	3462.	3619.	6622.
67	2487.	1811.	1060.	2114.	1951.	2642.	3432.	3547.	5173.
69	3510.	2166.	565.	2366.	2595.	3589.	3423.	3465.	3385.
71	3542.	2426.	1182.	2415.	2834.	3655.	3038.	2816.	2115.
73	3298.	2662.	1995.	2458.	3035.	3532.	2656.	2096.	1165.
75	3053.	2884.	2780.	2459.	3238.	3401.	2285.	1397.	241.
77	2798.	3103.	3491.	2489.	3414.	3301.	1922.	731.	-654.
79	2560.	3303.	4228.	2492.	3574.	3172.	1580.	97.	-1513.
81	2530.	3491.	4893.	2549.	3744.	3082.	1250.	-475.	-2351.
83	2592.	2884.	3411.	1241.	2136.	2762.	2048.	1091.	-687.
85	3324.	1624.	-110.	-1287.	-1191.	2204.	4002.	4694.	3329.
87	4034.	613.	-3188.	-3756.	-4510.	1561.	5140.	8506.	6954.
89	4758.	-22.	-5530.	-6117.	-7824.	770.	8698.	12805.	9970.
91	2823.	1061.	-2674.	-3363.	-4223.	-859.	6865.	9360.	6201.
93	-4344.	2498.	8106.	9265.	11822.	-3019.	-5107.	-11389.	-10305.
95	1279.	1937.	10822.	15857.	9101.	8075.	-15537.	-29604.	-16781.
97	2844.	2291.	7339.	9896.	5167.	6024.	-4945.	-12071.	-7206.

TABLE 4.3. AS IN 4.1, FOR JULY.

LATITUDE(N)=	25	30	35	40	45	50	55	60	65
LEVEL									
3	-657.	-220.	-17.	1480.	2507.	2255.	306.	2211.	-207.
5	2593.	1902.	2061.	1587.	582.	93.	1102.	3096.	2374.
7	3428.	2078.	1940.	2019.	1427.	1786.	523.	-148.	275.
7	1298.		1409.		1758.		1086.		-182.
9	1791.		1674.		1673.		890.		-328.
11	1630.		2107.		1143.		545.		176.
13	1575.		2405.		841.		277.		282.
15	1521.		2620.		586.		39.		473.
17	1470.		2763.		370.		-176.		746.
19	1420.		2837.		189.		-375.		1091.
21	1371.		2846.		41.		-560.		1482.
23	1321.		2791.		-67.		-730.		1877.
25	1271.		2676.		-120.		-872.		2202.
27	1218.		2496.		-92.		-962.		2356.
29	1170.		2271.		61.		-968.		2231.
13	2594.	2362.	2011.	1690.	1437.	1168.	924.	692.	473.
15	2454.	2288.	1999.	1670.	1399.	1071.	771.	488.	348.
17	2359.	2220.	1954.	1618.	1309.	913.	538.	209.	143.
19	2249.	2107.	1753.	1376.	1015.	669.	332.	42.	-31.
21	2096.	1945.	1454.	1006.	588.	388.	194.	22.	-106.
23	1946.	1798.	1226.	709.	259.	187.	149.	104.	-42.
25	1804.	1669.	1102.	530.	82.	72.	163.	222.	135.
27	1623.	1503.	960.	321.	-94.	-29.	236.	424.	427.
29	1442.	1305.	750.	14.	-310.	-110.	400.	758.	877.
31	1328.	1106.	452.	-389.	-500.	-73.	719.	1251.	1484.
33	935.	826.	485.	110.	226.	475.	790.	1043.	1057.
35	296.	582.	1029.	1632.	1866.	1508.	792.	483.	99.
37	-888.	425.	2449.	4445.	4320.	2773.	688.	-326.	-1182.
39	-2514.	221.	3755.	6367.	5489.	3061.	471.	-716.	-1656.
41	-3737.	-172.	3577.	5769.	4674.	2328.	182.	-663.	-1306.

TABLE 4.3 CONTINUED.

LATITUDE(N)= LEVEL	25	30	35	40	45	50	55	60	65
25	1339.	1409.	1395.	1123.	1341.	497.	757.	298.	313.
27	1159.	1278.	1379.	1177.	965.	402.	449.	254.	191.
29	902.	1053.	1250.	1111.	535.	258.	127.	196.	66.
31	511.	687.	971.	919.	92.	95.	-188.	120.	-55.
33	160.	323.	603.	1091.	231.	340.	-223.	92.	-71.
35	-196.	-40.	743.	1517.	672.	761.	-140.	79.	-41.
37	-529.	-346.	879.	2265.	1431.	1379.	73.	100.	35.
39	-656.	-416.	1440.	3540.	2632.	2287.	465.	160.	162.
41	-119.	104.	2797.	5662.	4518.	3655.	1120.	355.	356.
43	1785.	1710.	5405.	9130.	7583.	5814.	2207.	677.	637.
45	3537.	3400.	7935.	12263.	10433.	7584.	3190.	1056.	973.
47	3938.	4285.	9289.	13829.	12072.	8365.	3848.	1507.	1407.
49	3379.	4346.	9377.	14072.	13002.	8796.	4568.	2213.	2090.
51	1934.	3272.	7562.	12023.	12348.	8511.	5345.	3407.	3285.
53	330.	1592.	4338.	7357.	9019.	6750.	6149.	5718.	5701.
55	263.	976.	2857.	4827.	6775.	6019.	7289.	8731.	8780.
57	778.	945.	2563.	4229.	5813.	6275.	7705.	10523.	10914.
59	1232.	897.	2246.	3651.	4398.	5680.	5706.	7924.	9529.
61	1676.	824.	1857.	3082.	2812.	4278.	1177.	-567.	1814.
63	1696.	878.	1701.	2767.	1899.	2590.	-1285.	-4307.	-3037.
65	1287.	1081.	1871.	2808.	1688.	996.	-1061.	-2653.	-2204.
67	829.	1304.	2130.	2953.	1679.	-297.	-640.	-1160.	-1077.
69	306.	1533.	2445.	3209.	1837.	-1190.	-75.	145.	100.
71	495.	1768.	2558.	3116.	2267.	-166.	740.	757.	590.
73	930.	2004.	2635.	2970.	2740.	1095.	1521.	1204.	906.
75	1424.	2243.	2722.	2835.	3171.	2228.	2217.	1609.	1145.
77	1956.	2489.	2823.	2678.	3570.	3332.	2915.	2020.	1340.
79	2505.	2751.	2934.	2545.	3977.	4515.	3706.	2487.	1538.
81	3047.	3027.	3050.	2396.	4414.	5854.	4634.	3013.	1722.
83	3262.	2980.	2414.	877.	2756.	5234.	3886.	2441.	1704.
85	3207.	2557.	1089.	-1720.	-1057.	2170.	955.	428.	1426.
87	3191.	2123.	0.	-3703.	-4475.	-1163.	-2121.	-1634.	1153.
89	3182.	1757.	-732.	-4911.	-7102.	-4494.	-4908.	-3408.	941.
91	1245.	877.	-1043.	-2055.	-2723.	-2911.	-225.	-2668.	-907.
93	-2026.	-473.	-361.	6620.	10534.	6563.	12309.	1367.	-5406.
95	698.	-700.	8350.	10788.	7214.	6091.	-7752.	220.	-102.
97	1647.	-397.	7733.	6202.	4551.	4255.	-3498.	926.	1428.

TABLE 4.4. AS IN 4.1, FOR OCTOPER.

LATITUDE(N)=	25	30	35	40	45	50	55	60	65
LEVEL									
3	5367.	2389.	-145.	6465.	5443.	3540.	3774.	9245.	-3048.
5	4859.	2440.	2826.	4096.	1596.	1406.	2101.	6400.	2533.
7	4962.	2087.	2524.	3765.	3141.	1443.	-1250.	5022.	2096.
7	2023.		1665.		2447.		2011.		2072.
9	2094.		1595.		2156.		1966.		2240.
11	2592.		1952.		1780.		1926.		2094.
13	2867.		2025.		1337.		1686.		1863.
15	3015.		2041.		902.		1375.		1558.
17	3047.		2006.		484.		1006.		1191.
19	2980.		1931.		94.		602.		777.
21	2831.		1830.		-247.		190.		343.
23	2620.		1718.		-513.		-190.		-71.
25	2368.		1612.		-666.		-487.		-405.
27	2100.		1532.		-666.		-645.		-583.
29	1846.		1509.		-460.		-603.		-532.
13	2448.	2424.	2218.	1983.	1929.	1870.	1837.	2020.	2150.
15	2259.	2234.	2048.	1796.	1726.	1601.	1485.	1651.	1831.
17	2064.	1988.	1764.	1459.	1318.	1096.	867.	997.	1236.
19	1883.	1750.	1469.	1156.	994.	821.	572.	684.	958.
21	1704.	1517.	1162.	878.	741.	730.	558.	677.	958.
23	1587.	1365.	942.	689.	559.	660.	596.	753.	1012.
25	1518.	1286.	814.	574.	406.	485.	512.	733.	946.
27	1434.	1198.	706.	496.	307.	339.	478.	789.	935.
29	1304.	1052.	587.	451.	270.	247.	512.	931.	990.
31	1112.	828.	491.	502.	358.	265.	623.	1132.	1091.
33	880.	770.	894.	1038.	866.	615.	656.	930.	850.
35	880.	1266.	2000.	2121.	1781.	1232.	722.	594.	494.
37	1479.	2663.	3944.	3777.	3065.	2064.	829.	187.	74.
39	2102.	3694.	5145.	4670.	3648.	2369.	842.	6.	-92.
41	1912.	3369.	4574.	4111.	3162.	1952.	716.	92.	42.

TABLE 4.4 CONTINUED.

LATITUDE(N)=	25	30	35	40	45	50	55	60	65
LEVEL									
25	1511.	1654.	1587.	1282.	1310.	719.	1044.	1080.	1199.
27	1470.	1594.	1515.	1249.	1089.	735.	873.	877.	1059.
29	1337.	1433.	1366.	1176.	862.	731.	676.	632.	869.
31	1050.	1125.	1138.	1078.	652.	715.	473.	369.	644.
33	812.	997.	1162.	1216.	694.	871.	500.	345.	562.
35	614.	1035.	1389.	1502.	867.	1100.	617.	410.	519.
37	555.	1359.	1884.	1967.	1181.	1413.	823.	551.	509.
39	973.	2265.	2808.	2703.	1692.	1849.	1140.	780.	538.
41	2508.	4181.	4384.	3858.	2495.	2470.	1606.	1110.	618.
43	5599.	7377.	6883.	5686.	3785.	3386.	2284.	1565.	760.
45	7583.	9628.	8938.	7296.	5048.	4169.	2857.	1887.	933.
47	7713.	10095.	9849.	8187.	5996.	4692.	3279.	2099.	1162.
49	6928.	9440.	10016.	8743.	6932.	5283.	3825.	2440.	1537.
51	5235.	7392.	8914.	8580.	7697.	5976.	4601.	3051.	2195.
53	2967.	4136.	6137.	7141.	8007.	6833.	5825.	4274.	3474.
55	2148.	2908.	4746.	6389.	8381.	8018.	7259.	6161.	5244.
57	2220.	3148.	4692.	6277.	8439.	8958.	8107.	8009.	7059.
59	2319.	3489.	4652.	5649.	7402.	8491.	7517.	8456.	8219.
61	2435.	3907.	4635.	4571.	5138.	6114.	4697.	5659.	7090.
63	2410.	3666.	3953.	3434.	3472.	4237.	2751.	3052.	5197.
65	2236.	2725.	2564.	2475.	3052.	3869.	3046.	2717.	4407.
67	2083.	1826.	1238.	1638.	2764.	3605.	3462.	2473.	3490.
69	1945.	1097.	179.	1086.	2662.	3385.	3093.	2202.	2566.
71	1914.	1251.	419.	1285.	2755.	3245.	3500.	1714.	1614.
73	1897.	1598.	975.	1667.	2922.	3196.	3000.	1187.	755.
75	1868.	1906.	1500.	1992.	3052.	3138.	2526.	711.	-61.
77	1832.	2192.	1988.	2283.	3184.	3085.	2082.	319.	-842.
79	1802.	2480.	2465.	2545.	3279.	3053.	1653.	-15.	-1572.
81	1773.	2759.	2938.	2806.	3374.	3034.	1265.	-276.	-2276.
83	2181.	2849.	2656.	1944.	2568.	3409.	2191.	1033.	-947.
85	3054.	2733.	1691.	49.	874.	4111.	4393.	3726.	2239.
87	3932.	2607.	726.	-1698.	-932.	4871.	6782.	6479.	5185.
89	4734.	2511.	-146.	-3200.	-2948.	5751.	9715.	9539.	7840.
91	1594.	675.	-369.	196.	261.	4393.	9230.	9443.	6313.
93	-10969.	-9417.	-3180.	12724.	14434.	-846.	838.	1043.	-3504.
95	-5084.	-10508.	-3884.	5364.	13579.	31578.	21112.	5199.	-9289.
97	-235.	-3087.	204.	2124.	8243.	21929.	17073.	5480.	-4380.

TABLE 4.5. QUASIGEOSTROPHIC POTENTIAL VORTICITY MERIDIONAL GRADIENT ($\bar{q}_y$), (10^{M}/(M·SEC)). THE MODEL APPROXIMATION, FOR JANUARY. SOURCES: LEVELS 25-97, #1, LEVELS 13-41, #2, LEVELS 7-29, #3, LEVELS 3-7, #4. SEE SECTION IV-3 FOR A DESCRIPTION OF THE DATA SOURCES.

LATITUDE(N)=	25	30	35	40	45	50	55	60	65
LEVEL									
3	948.	2313.	1845.	2312.	2446.	2891.	3619.	4118.	1790.
5	2995.	1806.	2970.	2328.	2586.	2704.	1856.	802.	-295.
7	1995.	2418.	1731.	2503.	2327.	1998.	1184.	2231.	1875.
7	1700.		1598.		2274.		3310.		3337.
9	1594.		1432.		2183.		3406.		3787.
11	1886.		1735.		2023.		2567.		2841.
13	1918.		1667.		1763.		2273.		2775.
15	1961.		1588.		1416.		1835.		2630.
17	2009.		1501.		987.		1242.		2404.
19	2059.		1407.		485.		492.		2104.
21	2106.		1311.		-63.		-398.		1752.
23	2142.		1219.		-609.		-1363.		1397.
25	2162.		1140.		-1072.		-2254.		1133.
27	2157.		1085.		-1337.		-2803.		1119.
29	2121.		1069.		-1297.		-2720.		1602.
13	2134.	2030.	1894.	1790.	1789.	1882.	2063.	2244.	2339.
15	2051.	1826.	1592.	1426.	1409.	1547.	1811.	2099.	2311.
17	1903.	1493.	1102.	831.	776.	966.	1328.	1754.	2135.
19	1649.	1168.	737.	476.	488.	797.	1220.	1665.	2067.
21	1304.	820.	431.	280.	461.	957.	1402.	1740.	2025.
23	1063.	541.	180.	173.	533.	1168.	1613.	1844.	1986.
25	945.	314.	-56.	104.	606.	1271.	1702.	1892.	1931.
27	785.	30.	-286.	157.	834.	1467.	1855.	1998.	1896.
29	513.	-396.	-524.	382.	1260.	1780.	2088.	2176.	1888.
31	94.	-929.	-621.	883.	1899.	2178.	2348.	2369.	1874.
33	164.	-278.	436.	1565.	2039.	1959.	1975.	1933.	1577.
35	1862.	2232.	2615.	2461.	1985.	1461.	1307.	1210.	1166.
37	4544.	5553.	5161.	3345.	1769.	786.	454.	331.	729.
39	4628.	5892.	5516.	3388.	1574.	534.	184.	109.	703.
41	3438.	4316.	4146.	2702.	1459.	766.	603.	638.	1135.

TABLE 4.5 CONTINUED.

LATITUDE(N)=	25	30	35	40	45	50	55	60	65
LEVEL									
25	1392.	966.	777.	934.	1258.	1492.	1606.	1647.	1455.
27	1270.	848.	721.	921.	1209.	1426.	1614.	1679.	1595.
29	1074.	684.	672.	928.	1154.	1338.	1615.	1706.	1773.
31	779.	488.	650.	964.	1103.	1242.	1612.	1725.	1971.
33	622.	529.	843.	1138.	1193.	1284.	1614.	1688.	1950.
35	645.	811.	1210.	1401.	1343.	1375.	1618.	1623.	1846.
37	979.	1405.	1781.	1775.	1560.	1513.	1623.	1528.	1665.
39	1883.	2443.	2628.	2299.	1870.	1709.	1629.	1398.	1390.
41	3603.	4051.	3854.	3042.	2312.	1987.	1637.	1221.	998.
43	6018.	6280.	5606.	4116.	2961.	2382.	1646.	986.	454.
45	7311.	7853.	7026.	5046.	3543.	2694.	1718.	965.	295.
47	7330.	8468.	7846.	5723.	4005.	2909.	1878.	1213.	615.
49	6775.	8657.	8553.	6535.	4592.	3202.	2132.	1624.	1162.
51	5593.	8228.	9041.	7590.	5396.	3647.	2552.	2339.	2096.
53	3849.	6981.	9109.	9058.	6579.	4387.	3286.	3676.	3749.
55	3444.	6599.	9611.	10800.	7839.	5330.	4150.	5062.	5136.
57	3983.	6928.	10136.	11611.	8457.	5988.	4915.	5960.	5795.
59	4617.	7148.	9784.	10102.	7730.	5770.	5406.	6057.	5812.
61	5343.	7218.	8234.	5512.	4959.	4038.	5142.	4624.	4690.
63	5329.	6295.	5885.	2288.	2804.	2745.	4468.	3307.	3786.
65	4416.	4235.	3249.	1956.	2635.	2870.	3889.	3134.	3937.
67	3405.	1948.	537.	1829.	2625.	3077.	3105.	2970.	4016.
69	2333.	-111.	-1670.	1765.	2764.	3308.	2229.	2750.	3986.
71	1944.	-282.	-1563.	1324.	2571.	3101.	1576.	1978.	2799.
73	1738.	99.	-815.	894.	2395.	2837.	1061.	1072.	1387.
75	1579.	501.	-122.	624.	2248.	2586.	634.	227.	23.
77	1453.	933.	559.	473.	2125.	2352.	305.	-509.	-1222.
79	1385.	1361.	1224.	445.	2046.	2134.	69.	-1112.	-2314.
81	1342.	1785.	1842.	523.	1966.	1939.	-81.	-1585.	-3255.
83	1480.	1702.	1788.	992.	2035.	1977.	1424.	3.	-1690.
85	1655.	1042.	1013.	1585.	2150.	2263.	4243.	3210.	1929.
87	1728.	261.	39.	2016.	2242.	2531.	6878.	5864.	4702.
89	1701.	-733.	-1242.	2314.	2312.	2800.	9468.	7950.	6521.
91	2304.	1831.	2050.	4636.	4085.	6138.	8090.	8635.	4869.
93	4363.	13899.	18605.	12670.	7378.	13154.	-1607.	3591.	-3975.
95	3338.	20149.	23115.	9127.	-8707.	-27669.	-31545.	-43234.	-28243.
97	3492.	12451.	11581.	7744.	-4960.	-28675.	-32996.	-28399.	-15603.

TABLE 4.6. AS IN 4.5. FOR APRIL.

LATITUDE (N)=	25	30	35	40	45	50	55	60	65
LEVEL									
3	2248.	2169.	1820.	1817.	1866.	1737.	1437.	1523.	1082.
5	1924.	1876.	2098.	1983.	1922.	2277.	2770.	2488.	1226.
7	2131.	2210.	2496.	2399.	2199.	1748.	1363.	865.	1047.
7	1869.		1997.		1801.		1495.		609.
9	1846.		1975.		1730.		1346.		392.
11	1960.		1838.		1575.		1218.		612.
13	1992.		1752.		1399.		930.		428.
15	2034.		1641.		1161.		542.		197.
17	2085.		1503.		852.		39.		-85.
19	2141.		1339.		463.		-593.		-420.
21	2198.		1155.		-5.		-1352.		-803.
23	2250.		963.		-529.		-2205.		-1212.
25	2287.		789.		-1048.		-3050.		-1604.
27	2298.		673.		-1435.		-3691.		-1906.
29	2271.		663.		-1548.		-3926.		-2062.
13	2104.	2065.	1990.	1877.	1680.	1400.	1099.	830.	582.
15	2016.	1896.	1742.	1569.	1336.	1121.	935.	737.	568.
17	1864.	1605.	1312.	1031.	742.	656.	680.	613.	587.
19	1628.	1272.	920.	633.	448.	488.	601.	592.	598.
21	1317.	881.	540.	361.	448.	618.	709.	688.	625.
23	1092.	588.	288.	233.	517.	765.	840.	824.	734.
25	975.	431.	185.	205.	476.	744.	895.	962.	973.
27	841.	304.	188.	313.	488.	735.	980.	1159.	1312.
29	651.	208.	343.	612.	571.	743.	1106.	1433.	1774.
31	431.	254.	782.	1188.	784.	801.	1285.	1766.	2292.
33	635.	780.	1291.	1487.	1056.	970.	1277.	1547.	1771.
35	1832.	2093.	2075.	1770.	1447.	1234.	1178.	1038.	740.
37	3942.	3918.	2922.	1964.	1848.	1518.	998.	317.	-738.
39	4645.	4426.	3012.	1872.	1858.	1536.	688.	20.	-1432.
41	3811.	3554.	2410.	1536.	1495.	1282.	858.	228.	-942.

TABLE 4.6 CONTINUED.

LATITUDE(N)=	25	30	35	40	45	50	55	60	65
LEVEL									
25	1441.	1088.	914.	913.	1007.	942.	899.	744.	632.
27	1314.	990.	884.	912.	936.	858.	832.	750.	675.
29	1111.	860.	870.	937.	860.	762.	755.	771.	745.
31	808.	713.	884.	987.	785.	664.	677.	807.	837.
33	695.	814.	1062.	1117.	848.	716.	718.	845.	850.
35	795.	1137.	1371.	1306.	961.	825.	807.	894.	840.
37	1241.	1754.	1857.	1584.	1135.	993.	942.	955.	812.
39	2294.	2828.	2623.	2002.	1396.	1237.	1134.	1028.	764.
41	4244.	4614.	3868.	2658.	1795.	1584.	1397.	1116.	695.
43	7140.	7529.	6021.	3766.	2431.	2080.	1752.	1217.	600.
45	9054.	10247.	8371.	5045.	3157.	2542.	2054.	1375.	692.
47	9552.	11762.	10139.	6239.	3935.	2985.	2328.	1635.	998.
49	9264.	12211.	11389.	7545.	5009.	3649.	2746.	2051.	1459.
51	7890.	10499.	10984.	8726.	6542.	4752.	3450.	2788.	2226.
53	5251.	5701.	7476.	9267.	8805.	6819.	4781.	4285.	3673.
55	3272.	2653.	5105.	9548.	10899.	9414.	6532.	6281.	5384.
57	1899.	1659.	4479.	9198.	11545.	11077.	8009.	8094.	6966.
59	537.	871.	3683.	7271.	9625.	9851.	8273.	8748.	8200.
61	-589.	461.	2912.	3859.	4482.	4125.	5838.	6252.	7983.
63	-412.	579.	2145.	1796.	1199.	722.	3632.	3761.	7002.
65	723.	950.	1347.	1744.	1404.	1558.	3579.	3689.	6319.
67	1805.	1357.	686.	1881.	1863.	2522.	3567.	3653.	4919.
69	2836.	1757.	251.	2161.	2479.	3466.	3572.	3597.	3195.
71	2869.	2020.	882.	2238.	2720.	3526.	3183.	2945.	1967.
73	2632.	2251.	1685.	2313.	2930.	3395.	2790.	2212.	1048.
75	2402.	2475.	2455.	2349.	3139.	3258.	2408.	1500.	149.
77	2169.	2705.	3152.	2410.	3324.	3152.	2033.	822.	-726.
79	1959.	2921.	3887.	2437.	3499.	3019.	1678.	178.	-1572.
81	1759.	3135.	4569.	2497.	3690.	2927.	1333.	-403.	-2405.
83	2083.	2560.	3116.	1159.	2104.	2595.	2114.	1173.	-722.
85	2901.	1393.	-368.	-1429.	-1211.	2021.	4051.	4805.	3317.
87	3699.	446.	-3408.	-3965.	-4527.	1373.	6178.	8652.	6944.
89	4527.	-127.	-5744.	-6391.	-7866.	585.	8735.	12999.	9958.
91	2563.	990.	-2888.	-3639.	-4303.	-981.	6934.	9557.	6169.
93	-4733.	2393.	7926.	9059.	11753.	-3035.	-6001.	-11275.	-10381.
95	1221.	1869.	10499.	15641.	9106.	8029.	-15493.	-29478.	-16925.
97	3013.	2306.	6956.	9649.	5064.	6004.	-4888.	-11965.	-6307.

TABLE 4.7. AS IN 4.5, FOR JULY.

LATITUDE(N)=	25	30	35	40	45	50	55	60	65
LEVEL									
3	1529.	1706.	1828.	1692.	1563.	1557.	1356.	1012.	798.
5	1900.	1719.	1627.	1675.	1552.	997.	1290.	1845.	1671.
7	2170.	2114.	1943.	1782.	1613.	1726.	1226.	566.	283.
7	2069.		1554.		1625.		1139.		-186.
9	2122.		1530.		1608.		1079.		-327.
11	1947.		1518.		1257.		908.		222.
13	1935.		1533.		1109.		799.		388.
15	1924.		1558.		934.		669.		625.
17	1913.		1590.		731.		516.		928.
19	1901.		1626.		503.		339.		1290.
21	1889.		1657.		260.		141.		1687.
23	1876.		1677.		16.		-69.		2079.
25	1860.		1677.		-204.		-271.		2395.
27	1843.		1649.		-365.		-437.		2536.
29	1829.		1590.		-416.		-528.		2394.
13	1972.	1831.	1656.	1457.	1248.	1045.	869.	712.	554.
15	1951.	1791.	1613.	1394.	1156.	905.	698.	528.	408.
17	1923.	1735.	1553.	1305.	1024.	700.	444.	253.	195.
19	1828.	1621.	1368.	1044.	717.	427.	231.	88.	44.
21	1687.	1468.	1096.	657.	282.	131.	101.	78.	4.
23	1607.	1370.	887.	330.	-81.	-83.	72.	169.	85.
25	1613.	1341.	763.	87.	-330.	-211.	116.	311.	266.
27	1646.	1317.	605.	-226.	-610.	-314.	244.	559.	565.
29	1725.	1297.	373.	-675.	-954.	-389.	492.	957.	1037.
31	1905.	1307.	60.	-1256.	-1283.	-337.	923.	1528.	1685.
33	1833.	1252.	83.	-971.	-705.	232.	1120.	1400.	1321.
35	1538.	1254.	662.	350.	782.	1275.	1244.	916.	430.
37	766.	1375.	2203.	3016.	3076.	2525.	1240.	177.	-797.
39	-354.	1475.	3698.	4825.	4058.	2770.	1093.	-148.	-1243.
41	-1150.	1320.	3632.	4106.	3054.	1994.	844.	-40.	-900.

TABLE 4.7 CONTINUED.

LATITUDE(N)= LEVEL	25	30	35	40	45	50	55	60	65
25	1850.	1566.	1108.	621.	481.	416.	616.	579.	464.
27	1750.	1475.	971.	409.	224.	233.	485.	540.	394.
29	1574.	1325.	757.	99.	-121.	9.	327.	505.	314.
31	1269.	1087.	446.	-310.	-529.	-231.	162.	476.	230.
33	1005.	898.	280.	-364.	-443.	-65.	255.	527.	247.
35	740.	753.	262.	-146.	-104.	289.	447.	615.	302.
37	515.	698.	477.	429.	529.	861.	748.	744.	393.
39	510.	891.	1138.	1568.	1599.	1746.	1207.	932.	531.
41	1141.	1624.	2570.	3589.	3368.	3120.	1910.	1202.	732.
43	2985.	3261.	5152.	6976.	6350.	5320.	3023.	1600.	1020.
45	4594.	4822.	7567.	10075.	9157.	7157.	3998.	2009.	1352.
47	4889.	5492.	8733.	11635.	10772.	8015.	4613.	2445.	1775.
49	4239.	5249.	8530.	11842.	11664.	8512.	5265.	3114.	2453.
51	2780.	3941.	6456.	9733.	10913.	8246.	5947.	4256.	3652.
53	1217.	2188.	3171.	5068.	7419.	6395.	6603.	6498.	6085.
55	1174.	1603.	1862.	2744.	5139.	5497.	7565.	9411.	9180.
57	1665.	1581.	1751.	2429.	4332.	5629.	7847.	11051.	11274.
59	2068.	1509.	1568.	2120.	3195.	5083.	5863.	8320.	9737.
61	2447.	1389.	1286.	1804.	1942.	3924.	1551.	-81.	1875.
63	2410.	1391.	1220.	1680.	1207.	2356.	-829.	-3714.	-2926.
65	1956.	1541.	1465.	1853.	1022.	752.	-688.	-2070.	-1997.
67	1454.	1701.	1791.	2120.	1016.	-542.	-348.	-599.	-814.
69	893.	1873.	2159.	2485.	1172.	-1441.	148.	680.	387.
71	1033.	2042.	2301.	2476.	1595.	-446.	913.	1263.	865.
73	1419.	2226.	2397.	2412.	2080.	777.	1657.	1663.	1170.
75	1873.	2429.	2501.	2362.	2539.	1870.	2327.	2064.	1405.
77	2368.	2654.	2618.	2289.	2978.	2931.	3004.	2455.	1600.
79	2883.	2900.	2744.	2234.	3431.	4072.	3776.	2902.	1800.
81	3390.	3164.	2874.	2153.	3915.	5377.	4689.	3410.	1988.
83	3590.	3140.	2252.	690.	2302.	4738.	3934.	2823.	1959.
85	3536.	2761.	939.	-1864.	-1463.	1678.	1008.	798.	1648.
87	3529.	2348.	-141.	-3823.	-4834.	-1631.	-2069.	-1281.	1339.
89	3556.	1981.	-864.	-5032.	-7419.	-4918.	-4866.	-3082.	1093.
91	1643.	1015.	-1206.	-2196.	-2918.	-3251.	-270.	-2409.	-794.
93	-1666.	-379.	-529.	6485.	10452.	6316.	12214.	1541.	-5310.
95	1011.	-317.	8460.	10720.	7056.	5885.	-7670.	379.	49.
97	1834.	51.	7864.	6116.	4366.	4107.	-3473.	1041.	1513.

TABLE 4.8. AS IN 4.5, FOR OCTOBER.

LATITUDE(N)=	25	30	35	40	45	50	55	60	65
LEVEL									
3	2439.	2309.	2095.	2207.	1950.	1847.	2008.	2228.	2132.
5	2256.	2181.	2115.	1943.	1720.	1992.	2529.	2121.	1502.
7	2423.	2460.	2670.	2822.	2680.	1677.	646.	1700.	1328.
7	1974.		1791.		2133.		1965.		1829.
9	1894.		1635.		2004.		1864.		1815.
11	2052.		1843.		1871.		1763.		1606.
13	2009.		1751.		1611.		1521.		1403.
15	1957.		1641.		1295.		1217.		1130.
17	1897.		1519.		936.		862.		796.
19	1831.		1389.		554.		477.		417.
21	1763.		1261.		177.		91.		20.
23	1699.		1144.		-160.		-257.		-355.
25	1647.		1052.		-414.		-520.		-645.
27	1615.		1000.		-537.		-637.		-775.
29	1622.		1011.		-471.		-556.		-678.
13	2103.	2050.	1973.	1880.	1798.	1750.	1747.	1747.	1697.
15	2039.	1936.	1810.	1661.	1538.	1442.	1412.	1424.	1418.
17	1929.	1740.	1528.	1280.	1081.	895.	800.	808.	859.
19	1778.	1515.	1230.	932.	730.	591.	518.	539.	629.
21	1604.	1275.	915.	604.	461.	491.	524.	577.	684.
23	1506.	1128.	694.	368.	268.	436.	583.	685.	791.
25	1473.	1053.	556.	205.	102.	299.	526.	668.	777.
27	1433.	964.	418.	74.	-15.	206.	532.	773.	823.
29	1371.	835.	261.	-21.	-72.	167.	615.	957.	939.
31	1302.	683.	134.	-14.	-6.	226.	784.	1217.	1102.
33	1244.	714.	448.	448.	454.	581.	876.	1090.	921.
35	1460.	1283.	1432.	1444.	1304.	1182.	992.	833.	621.
37	2207.	2638.	3236.	3013.	2510.	1990.	1134.	493.	249.
39	2859.	3564.	4362.	3829.	3000.	2271.	1156.	354.	129.
41	2730.	3212.	3830.	3211.	2412.	1837.	1015.	454.	293.

TABLE 4.8 CONTINUED.

LATITUDE(N)= LEVEL	25	30	35	40	45	50	55	60	65
25	1725.	1428.	1163.	977.	928.	814.	930.	1051.	1104.
27	1623.	1291.	1039.	889.	832.	733.	809.	910.	991.
29	1446.	1067.	857.	778.	717.	643.	656.	720.	832.
31	1147.	720.	616.	659.	597.	553.	490.	505.	645.
33	922.	550.	613.	765.	688.	649.	544.	521.	612.
35	777.	561.	816.	1030.	884.	831.	680.	618.	624.
37	828.	881.	1296.	1490.	1204.	1112.	898.	785.	669.
39	1393.	1787.	2206.	2237.	1705.	1529.	1221.	1036.	753.
41	2969.	3634.	3754.	3412.	2485.	2140.	1690.	1388.	882.
43	5719.	6593.	6185.	5266.	3743.	3057.	2370.	1865.	1066.
45	7325.	8633.	8190.	6521.	4961.	3833.	2927.	2202.	1262.
47	7298.	9020.	9062.	7873.	5842.	4335.	3317.	2426.	1502.
49	6386.	8301.	9205.	8474.	6696.	4896.	3826.	2780.	1881.
51	4628.	6226.	8032.	8323.	7356.	5544.	4559.	3401.	2538.
53	2369.	3010.	5188.	6847.	7527.	6319.	5718.	4619.	3821.
55	1611.	1893.	3830.	6051.	7800.	7444.	7085.	6479.	5592.
57	1749.	2252.	3897.	5925.	7833.	8251.	7894.	8274.	7382.
59	1907.	2698.	4020.	5331.	6833.	7725.	7311.	8671.	8466.
61	2075.	3214.	4167.	4340.	4663.	5369.	4580.	5891.	7216.
63	2119.	3078.	3638.	3273.	3044.	3520.	2668.	3323.	5290.
65	2020.	2246.	2327.	2340.	2599.	3174.	2699.	2995.	4549.
67	1929.	1445.	1068.	1524.	2286.	2902.	3246.	2756.	3684.
69	1843.	792.	58.	990.	2173.	2700.	3626.	2484.	2793.
71	1843.	969.	326.	1195.	2278.	2582.	3223.	1985.	1822.
73	1856.	1364.	897.	1548.	2467.	2550.	2729.	1435.	934.
75	1860.	1700.	1427.	1929.	2625.	2503.	2253.	929.	95.
77	1854.	2015.	1914.	2235.	2791.	2468.	1827.	503.	-700.
79	1843.	2335.	2393.	2512.	2927.	2433.	1406.	132.	-1439.
81	1815.	2650.	2870.	2786.	3071.	2421.	1024.	-160.	-2140.
83	2197.	2779.	2595.	1915.	2302.	2798.	1949.	1137.	-767.
85	3026.	2700.	1640.	-0.	635.	3505.	4146.	3836.	2483.
87	3883.	2617.	686.	-1779.	-1158.	4288.	6534.	6597.	5465.
89	4718.	2567.	-182.	-3322.	-3190.	5211.	9474.	9671.	8121.
91	1678.	752.	-423.	68.	47.	3942.	9004.	9572.	6522.
93	-10812.	-9392.	-5259.	12722.	14332.	-1211.	628.	1125.	-3402.
95	-4927.	-10265.	-3804.	5174.	13282.	31168.	20929.	5160.	-9226.
97	-44.	-2900.	134.	2011.	7964.	21640.	16893.	5526.	-4368.

TABLE 4.9. QUASIGEOSTROPHIC POTENTIAL VORTICITY MERIDIONAL GRADIENT ($\bar{q}_y$), (10^{14}/(M•SEC)), MODEL APPROXIMATION AND COMPOSITE FOR ALL DATA SOURCES, FOR JANUARY.

LATITUDE(N) =	25	35	45	65
LEVEL				
3	2097.	2736.	2213.	500.
5	2148.	1473.	2472.	2102.
7	2228.	2101.	2422.	3265.
9	2229.	2154.	2004.	3310.
11	2161.	1871.	1421.	2357.
13	2065.	1672.	1024.	2159.
15	1919.	1520.	903.	2188.
17	1742.	1478.	1212.	2639.
19	1549.	1063.	1256.	2450.
21	1303.	332.	1317.	2037.
23	1086.	-304.	1357.	1629.
25	959.	-478.	1315.	1368.
27	867.	-391.	1253.	1140.
29	825.	63.	1170.	970.
31	876.	925.	1083.	881.
33	862.	1425.	1171.	779.
35	996.	2026.	1322.	711.
37	1411.	2841.	1541.	679.
39	2289.	3926.	1853.	689.
41	3780.	5346.	2302.	749.
43	5761.	7185.	2965.	876.
45	6903.	8431.	3562.	1052.
47	7040.	8848.	4028.	1306.
49	6613.	8944.	4617.	1717.
51	5553.	8532.	5416.	2396.
53	3934.	7244.	6575.	3562.
55	3595.	7066.	7812.	4642.
57	4057.	7865.	8423.	5292.
59	4648.	8491.	7705.	5476.
61	5324.	8698.	4966.	4777.
63	5293.	7278.	2833.	4140.
65	4396.	4205.	2654.	4199.
67	3396.	904.	2632.	4127.
69	2344.	-1943.	2759.	3915.
71	1948.	-1874.	2965.	2706.
73	1744.	-1052.	2391.	1316.
75	1592.	-271.	2246.	-22.
77	1460.	490.	2127.	-1243.
79	1379.	1226.	2041.	-2311.
81	1342.	1934.	1972.	-3230.
83	1481.	1874.	2032.	-1664.
85	1649.	1069.	2158.	1943.
87	1781.	60.	2238.	4706.
89	1700.	-1262.	2312.	6518.
91	2306.	2019.	4085.	4863.
93	4362.	10619.	7574.	-3975.
95	5338.	23115.	-8707.	-28243.
97	3492.	11579.	-4960.	-15604.

TABLE 4.10. AS IN 4.9, FOR APRIL.

LEVEL	LATITUDE(N)= 25	45	65
3	2112.	1654.	500.
5	2114.	1785.	1336.
7	2121.	1629.	715.
9	2150.	1762.	462.
11	2167.	2003.	429.
13	2124.	1878.	442.
15	2004.	1267.	783.
17	1918.	259.	1406.
19	1641.	326.	1271.
21	1390.	937.	705.
23	1135.	1418.	265.
25	975.	1373.	264.
27	861.	1231.	375.
29	825.	978.	618.
31	916.	650.	966.
33	974.	692.	1017.
35	1193.	813.	1001.
37	1709.	1002.	950.
39	2697.	1292.	858.
41	4359.	1740.	722.
43	6796.	2470.	537.
45	8655.	3268.	592.
47	9395.	4068.	912.
49	9304.	5148.	1393.
51	7972.	6647.	2192.
53	5235.	8781.	3696.
55	3201.	10753.	5441.
57	1866.	11359.	7022.
59	549.	9494.	8256.
61	-569.	4529.	7972.
63	-420.	1332.	6965.
65	712.	1485.	6293.
67	1794.	1850.	4909.
69	2845.	2457.	3202.
71	2870.	2690.	1976.
73	2643.	2924.	1054.
75	2402.	3119.	153.
77	2173.	3321.	-723.
79	1959.	3499.	-1573.
81	1796.	3700.	-2407.
83	2092.	2107.	-725.
85	2898.	-1197.	3315.
87	3700.	-4531.	6944.
89	4526.	-7867.	9959.
91	2564.	-4304.	6170.
93	-4754.	11754.	-10382.
95	1221.	9106.	-16925.
97	3013.	5064.	-6207.

TABLE 4.11. AS IN 4.9, FOR JULY.

LATITUDE(N) =	2[illegible]	45	65
LEVEL			
3	15[illegible].	1541.	266.
5	1760.	2030.	1197.
7	2250.	1153.	923.
9	2284.	1048.	557.
11	1992.	1483.	498.
13	1821.	1454.	439.
15	1789.	1157.	428.
17	1809.	536.	450.
19	1672.	453.	331.
21	2008.	716.	103.
23	20[illegible].	885.	49.
25	2037.	700.	273.
27	1918.	398.	672.
29	1675.	-45.	1313.
31	1247.	-609.	2009.
33	909.	-532.	1491.
35	600.	-192.	76.
37	342.	443.	-1639.
39	305.	1518.	-1677.
41	979.	3303.	-21.
43	3018.	6346.	2248.
45	4622.	9242.	3819.
47	5161.	10824.	4484.
49	4448.	11852.	4957.
51	2824.	11047.	5311.
53	1030.	7347.	5475.
55	1061.	4956.	6185.
57	1598.	4121.	6958.
59	2044.	5121.	5900.
61	2463.	1980.	2017.
63	2440.	1287.	-632.
65	1974.	1074.	-667.
67	1461.	1021.	-355.
69	866.	1168.	101.
71	1027.	1580.	627.
73	1414.	2068.	1024.
75	1870.	2535.	1340.
77	2367.	2971.	1617.
79	2962.	3430.	1902.
81	3392.	3922.	2209.
83	3[illegible]3.	3300.	2204.
85	3547.	-1453.	1810.
87	3560.	-4[illegible]57.	1395.
89	3[illegible]5.	-7420.	993.
91	1640.	-9920.	-1152.
93	-1[illegible]69.	10452.	-4213.
95	1011.	7056.	-482.
97	1[illegible]74.	4[illegible]66.	1913.

TABLE 4.12. AS IN 4.9, FOR OCTOBER

LATITUDE(N)=	25	45	50	65
LEVEL				
3	2421.	2197.	2254.	1814.
5	2452.	1602.	1260.	1969.
7	2072.	1988.	1773.	951.
9	2004.	1939.	1892.	1200.
11	2136.	1645.	1713.	2126.
13	2090.	1511.	1608.	2315.
15	2029.	1506.	1520.	2066.
17	1965.	1664.	1449.	1138.
19	1850.	1362.	1184.	825.
21	1689.	763.	785.	942.
23	1555.	296.	451.	1070.
25	1479.	186.	303.	950.
27	1401.	224.	262.	817.
29	1307.	448.	357.	656.
31	1196.	848.	583.	463.
33	1049.	1026.	721.	401.
35	978.	1231.	904.	403.
37	1105.	1529.	1177.	469.
39	1706.	1962.	1575.	610.
41	3185.	2610.	2156.	836.
43	5594.	3629.	3027.	1159.
45	6989.	4683.	3781.	1414.
47	6994.	5549.	4294.	1631.
49	6177.	6435.	4866.	1978.
51	4566.	7214.	5533.	2585.
53	2483.	7628.	6333.	3782.
55	1755.	8030.	7465.	5510.
57	1840.	8038.	8263.	7321.
59	1942.	6945.	7722.	8454.
61	2055.	4615.	5366.	7238.
63	2077.	2922.	3518.	5303.
65	1994.	2518.	3172.	4552.
67	1920.	2258.	2901.	3683.
69	1851.	2201.	2700.	2791.
71	1850.	2297.	2582.	1823.
73	1861.	2480.	2558.	934.
75	1867.	2649.	2494.	94.
77	1855.	2791.	2469.	-704.
79	1842.	2922.	2438.	-1437.
81	1814.	3070.	2419.	-2137.
83	2194.	2295.	2797.	-768.
85	3024.	631.	3505.	2483.
87	3882.	-1159.	4288.	5468.
89	4719.	-3189.	5211.	8120.
91	1679.	50.	3942.	6521.
93	-10812.	14331.	-1211.	-3402.
95	-4927.	13282.	31168.	-9226.
97	-44.	7964.	21640.	-4369.

Table 4.13. Summary of unstable mode properties. Explanation of columns: 1) MODE - mode types as defined in sections IV-6. 2) MO - month of profile. 3) LAT - latitude of profile (°N). 4) WL - wavelength. 5) PWN - planetary wavenumber. 6) DT - doubling time. 7) CR - real part of the phase speed. 8) CI - imaginary part of the phase speed. 9) S.L. - steering level(s). 10) $|\psi|_{PK}$ - pressure level of the maximum value of the streamfunction amplitude 11) $|\overline{v\theta}|_{PK}$ - pressure level of the maximum absolute value of the meridional entropy flux. The $\overline{v'\theta'}$ peaks are positive unless a "-" preceeds the entry. 12) $|\psi| > .5$ - the region where the streamfunction amplitude is greater than 1/2 the maximum absolute value. 13) $|\overline{v'\theta'}| > .5$ - the region(s) where the absolute value of the meridional entropy flux is greater than 1/2 the maximum absolute value. The regions contain positive $\overline{v'\theta'}$ values unless otherwise indicated by (*). 14) $|CE| > .5$ - the regions where the absolute value of the eddy kinetic to eddy available potential energy transfer is greater than half the maximum absolute value. The regions are for kinetic energy generation unless otherwise indicated by (*). 15) $Q_y < 0$ - regions (1) where the quasi-geostrophic potential energy vorticity meridional gradient is less than zero and (2) which are associated with the given unstable mode. See section IV-12. Each mode described is the fastest growing mode for the mode type given.

TABLE 4.13

MODE	MO	LAT (°N)	WL (KM)	PWN	DT (DAYS)	CR (M/SEC)	CI (M/SEC)	S.L. (MB)	$\lvert\Psi\rvert$ (MB)	$\lvert\overline{v\theta}\rvert$ (MB)	$\lvert\Psi\rvert>.5$ (MB)	$\lvert\overline{v\theta}\rvert>.5$ (MB)	$\lvert C_E\rvert>.5$ (MB)
E	1	25	5400	6.8	1.9	1.72	3.59	843	362	1000	115-1000	800-1000	440- 940
E	1	35	5500	6.6	1.5	8.17	4.53	755	230	1000	110-1000	900-1000	250- 830
E	1	45	3700	7.7	1.7	6.40	2.71	770	1000	920	150-1000	720-1000	500- 940
E	1	65	3500	4.8	3.0	2.20	1.49	780	338	880	140-1000	820- 940	400- 670 800- 920
E	4	25	3900	9.4	2.2	0.39	2.32	843, 60,15,1	1000	880	430-1000	820-1000	800- 920
E	4	45	3500	8.2	1.7	6.12	2.62	730, 50,15	315	735	150-1000	600- 830 920-1000	530- 810
E	4	65	3100	5.4	2.3	3.00	1.71	752, 20	1000	880	180-1000	810- 950	430- 690 770- 920
E	7	45	3700	7.7	2.0	4.92	2.33	735, 76	230	1000	130-1000	620- 820 910-1000	300- 810
E	7	65	2700	6.2	4.0	1.32	0.89	770, 88	270	840	170-1000	690-1000	330- 900
E	10	25	2000	18.2	4.3	-2.21	0.60	870, 50,30	820	880	630- 980	810- 900	820- 900
E	10	45	3700	7.7	1.6	6.89	2.84	750	1000	1000	130-1000	680-1000	500- 840
E	10	50	3200	8.1	1.6	7.45	2.70	770	1000	1000	170-1000	790-1000	540- 920
E	10	65	3200	5.2	2.5	3.44	1.66	752	1000	880	160-1000	810- 960	400- 700 770- 920
G	1	25	10000	3.6	5.3	2.84	2.46	806	175	60	60- 400 860-1000	50- 100	50- 140* 830- 880
G	1	35	10000	3.3	9.6	9.31	1.37	735	160	1000	70- 310 900-1000	45- 55 900-1000	45- 65* 720- 840
G	1	45	5900	4.8	6.9	5.95	1.06	806	8	20	10- 60	10- 70	20- 150* 300- 390
G	1	65	6500	2.6	19.0	1.96	0.43	820	211	880	10- 500 900-1000	830- 950	820- 920
G	4	25	8300	4.4	4.6	0.72	2.31	862, 50,10,2	175	70	60- 350 970-1000	55- 110	55- 140* 810- 900
G	4	45	8000	3.6	8.1	6.83	1.19	700, 50,10	193	70	60- 400 820-1000	55- 170	55- 180* 700- 750
G	4	65	7400	2.6	13.0	2.96	0.64	752, 20	130	42	30- 440 850-1000	25- 90	25- 120* 800- 910
G	7	45	8000	3.6	8.6	5.75	1.16	700, 80	193	1000	90- 350 940-1000	240- 300 660-820,910-1000	680- 800
G	7	65	5000	3.4	17.1	1.36	0.39	770, 88	230	107	150- 430	85- 200	85- 200*
G	10	25	5200	7.0	10.7	-2.32	0.63	880, 60,15	211	70	80- 450	60- 100	60- 150* 830- 880
G	10	45	9300	3.1	7.7	8.10	1.50	700	143	60	60- 320 820-1000	35- 200	45- 180* 680- 810
G	10	50	6300	4.1	7.4	7.84	1.16	750	5	10	5- 20 130- 200	10- 60	50- 180* 750- 900
G	10	65	5600	3.0	15.0	2.95	0.48	790	230	880	10- 510 920-1000	810- 960	820- 920

TABLE 4.13 CONTINUED

MODE	MO	LAT (°N)	WL (KM)	PWN	DT (DAYS)	CR (M/SEC)	CI (M/SEC)	S.L. (MB)	|Ψ| (MB)	$\overline{\|v'\theta'\|}$ (MB)	|Ψ|>.5 (MB)	$\overline{\|v'\theta'\|}$>.5 (MB)	|Cε|>.5 (MB)	$\bar{\omega}_y$<0 (MB)
ES	1	65	1400	12.4	3.5	1.56	0.50	843	940	880	800-1000	840- 930	840- 920	600- 730
ES	4	65	1200	14.2	2.5	1.95	0.61	840 18	1000	880	790-1000	830- 930	840- 920	600- 730
ES	10	65	1200	13.8	2.8	2.38	0.56	840	1000	880	800-1000	840- 950	830- 920	600- 730
SM	1	65	2600	6.4	4.3	3.17	0.77	650	360	600	190-1000	430- 670 830- 930	430- 660	600- 730
SM	4	65	2300	7.2	5.0	3.98	0.60	650 30	360	600	210-1000	400- 670 820- 920	430- 660	600- 730
SM	10	65	2500	6.8	4.9	4.32	0.65	650	340	600	190-1000	400- 670 820- 960	430- 660	600- 730
S	1	35	3100	10.0	3.6	16.90	1.30	510 75.4	290	480	140- 590	360- 530	350- 520	480- 600
S	4	25	3200	11.6	10.0	16.00	0.40	380 96	230	110	140- 380	95- 150	95- 150 * 240- 410	380- 430
S	4	25	3700	10.0	15.4	14.60	0.31	413 94	210	110	110- 350	100- 420	240- 410	380- 430
S	4	45	2200	13.0	11.0	3.52	0.24	880	1000	1000	930-1000	920-1000	860- 890 * 910-1000	730- 880
S	7	45	2200	13.0	8.0	2.90	0.36	900 67	1000	1000	930-1000	920-1000	860- 890 * 910-1000	730- 880
S	7	65	1500	11.4	15.6	3.90	0.12	435 155	290	400	190- 460	160- 180 * 310- 440	330- 440	400- 480
L	1	35	13500	2.2	11.3	19.10	1.52	491 89.3	110	-80	40- 220	65- 110 *	75- 120	50- 80
L	1	45	8000	3.6	6.3	6.94	1.56	752	3	10	2- 15	5- 20	2- 10	
L	1	45	12400	2.3	8.9	7.40	1.75	735	1	0	2- 15	0- 20	0- 10	
L	1	65	12000	1.4	11.0	2.69	1.33	717	5	10	3- 35	5- 60	5- 25	600- 730
L	7	45	5000	5.4	14.0	2.65	0.48	920 65	210	70	100- 470	65- 110 940-1000	65- 180 * 250- 400	730- 880
L	7	65	3500	5.0	13.1	4.45	0.34	386 165	160	-170	110- 240	160- 200 *	160- 200	140- 180
L	10	65	8400	2.0	11.0	3.54	1.02	740	3	20	3- 35	5- 60	10- 30	600- 730

CHAPTER V

SUMMARY OF IMPORTANT RESULTS

The climatological profiles are shown to be unstable to several long and short wave modes. This may due in part to the absence of thermal and frictional dissipation. Newtonian cooling would lessen the growth rate of long wave modes (Geisler and Garcia, 1977), and surface frictional dissipation would tend to stabilize the short wave modes which are confined to the ground. In the more realistic case, which includes thermal driving and dissipation, the unstable mean flow supplies potential energy to the perturbations to balance the loss of perturbation potential energy through thermal dissipation, and the loss of perturbation kinetic energy through frictional dissipation (Charney, 1959; Pedlosky, 1970, 1971; Stone, 1972).

The long wave modes discovered by Green (1960) are shown to have several interesting properties. To exist, they require a non-zero value of $\bar{q}_y$ and are made much more unstable by a stratosphere or rigid lid. Their wavelength becomes ∞ as γ_T (or β) goes to zero, and the Green modes become shortwave modes as γ_T becomes large. Doubling times of the fastest growing Green modes are moderately short: about 6 days in the case of a nominal winter stratosphere with linear $\bar{u}$ and $\bar{T}$ profiles, and less than 10 days for most of the climatological profiles. In the parameter study, the Green mode amplitudes are particularly strong in the lower stratosphere (relative to other levels) when nominal winter conditions are assumed. Amplitudes are also strong in the lower stratosphere for the cases in the climatological study. For both the parametric and climatological studies, the streamfunction phase of the Green modes varied much more than that of the Eady modes, and the variation was usually confined to small regions in the lower stratosphere and mid troposphere. The phase difference between the meri-

dional and vertical velocities indicates that the Green modes have a meridional circulation in the lower stratosphere like that observed. The meridional entropy transport for the Green modes in the parameter study is countergradient and particularly strong in the lower stratosphere when nominal winter conditions are assumed. In the climatological study, transports are strong and polewards in the stratosphere in nearly all cases; they are countergradient for the cases with reversed shear. The Green modes' amplitude, meridional heat flux, and kinetic energy destruction are much larger in the stratosphere than are the same quantities for the Eady mode; this is true for both the parametric and climatological studies. The Green modes are thereby more sensitive to changes in the unperturbed state of the upper layer.

Quasi-geostrophic potential vorticity meridional gradient profiles calculated from monthly averaged $\bar{u}$ and $\bar{T}$ values possess a considerable number of zeros. The zeros and their associated negative regions of $\bar{q}_y$ have a substantial effect on the spectra of the unstable modes. Some modes had their growth rate drastically reduced when a negative $\bar{q}_y$ region was removed. New modes, distinct from the Eady and Green modes, were shown to exist because certain negative $\bar{q}_y$ regions are present, and these modes tend to have a larger growth rate when their associated $\bar{q}_y$ regions extend over greater depths. Their fluxes at the levels of those regions are always downgradient. Certain of the new modes are potentially important for the general circulation of specific regions of the atmosphere. Some S and S_m modes could be important for the circulation of the upper troposphere. The E_s and some S modes could influence middle and lower tropospheric circulation. In addition to the G modes, some L modes could be important for the stratospheric circulation. Two of these L modes are destabilized by negative $\bar{q}_y$ regions in the stratosphere

and are examples of in situ stratospheric baroclinic instability.

A very small change in the $\bar{u}$ profile (.3 m/sec or less) can have a drastic effect on the unstable mode spectra by reducing growthrates or by entirely eliminating certain modes. Both long and short wave modes are affected. Staley and Gall (1977) and Gall and Blakeslee (1977) reported extreme sensitivity of short wave mode growth rates to small low level changes in $\bar{u}$ and the static stability. They attributed this to the short-wave vertical structure which they claim causes the mode to "feel" only low level parts of the basic state profiles. This explanation cannot hold for the long wave modes of this study, which were affected by low level changes in $\bar{u}$. Rather, it was shown that only the small changes in $\bar{u}$ which drastically alter the stability properties of the $\bar{q}_y$ profiles (by removing negative $\bar{q}_y$ regions and their associated zeros) result in a substantial change in the unstable mode spectra.

In the stratosphere, long wave modes have been shown to be potentially important in transporting most of the heat, even when the flux is countergradient (see Section III-4 and -5, and IV-8, -11, and -13). Most parameterizations of the eddy heat flux (e.g. Green, 1970; Stone, 1972; and Held, 1978) have assumed that the most unstable Eady mode is responsible for the eddy heat flux. These parameterizations are therefore not likely to be capable of representing the stratospheric heat flux. Most of the long wave modes which are potentially important for stratospheric heat transport have their kinetic energy generated in the troposphere. Therefore, a successful parameterization of the stratospheric heat fluxes is likely to have to consider these long wave modes and to treat the stratosphere and troposphere together.

APPENDIX

Zonal Velocity and Temperature Data

TABLE A1. ZONAL VELOCITY DATA (M/SEC) FOR JANUARY. SOURCES: 50-1000MB, #1, 10-200MB, #2, 2-10MB, #3, .10-10MB, #4. SEE SECTION IV-3 FOR A DESCRIPTION OF THE DATA SOURCES.

LATITUDE(N)=	20	25	30	35	40	45	50	55	60	65	70
PRESSURE (MB)											
0.10	45.0	59.0	66.0	105.0	86.0	68.0	61.0	50.0	25.0	0.0	-5.0
0.20	30.0	46.0	62.0	90.0	80.0	60.0	45.0	39.0	26.0	5.0	-9.0
0.50	-2.0	23.0	50.0	69.0	72.0	56.0	44.0	37.0	42.0	22.0	-2.0
1.00	-22.0	5.0	39.0	49.0	56.0	47.0	37.0	30.0	38.0	23.0	3.0
2.00	-12.0	20.0	28.0	39.0	44.0	37.0	26.0	14.0	24.0	23.0	7.0
5.00	5.0	20.0	22.0	18.0	31.0	22.0	10.0	-2.0	15.0	30.0	8.0
10.00	10.0	16.0	14.0	9.0	18.0	10.0	0.0	-7.0	8.0	30.0	12.0
2.		14.3		27.8		42.4		52.3		57.8	
5.		2.2		13.0		31.6		50.9		59.0	
10.		4.0		10.0		22.5		39.9		49.2	
100.		21.8		24.0		22.4		21.1		15.1	
10.	9.4	10.6	10.5	10.2	12.0	17.1	24.2	31.7	37.8	41.1	40.8
30.	6.4	6.3	6.3	6.8	8.6	12.3	17.5	22.7	27.0	29.5	29.6
50.	6.4	6.0	9.7	10.8	12.0	14.0	17.0	20.0	22.5	23.8	23.2
100.	19.0	24.5	27.8	27.1	23.8	20.4	18.0	17.0	16.9	16.7	15.7
150.	26.1	33.8	39.2	37.3	29.9	22.8	17.7	14.7	13.5	13.1	12.3
200.	27.4	35.4	40.7	38.7	31.4	24.0	18.2	14.1	12.1	11.1	10.2
50.	1.2	4.8	8.1	10.0	11.9	13.9	14.7	15.0	15.4	14.6	13.4
100.	13.6	21.4	25.6	24.2	20.2	16.7	14.3	13.2	12.7	12.5	12.0
200.	24.9	34.9	39.8	35.9	27.5	19.9	14.4	10.9	9.4	8.8	8.2
300.	21.2	30.6	34.3	30.7	24.2	18.0	12.8	9.5	8.2	7.7	7.3
400.	16.1	24.5	26.5	23.6	19.2	14.9	11.0	8.2	6.9	6.4	6.1
500.	11.6	18.0	19.4	17.8	15.3	12.5	9.5	6.9	5.6	5.1	4.8
700.	3.5	7.5	9.7	10.1	9.3	8.1	6.4	4.7	3.5	2.8	2.2
850.	-1.3	1.9	4.5	5.8	5.8	4.9	3.9	2.9	2.1	1.5	0.9
900.	-2.5	0.6	3.4	4.9	4.9	3.9	2.9	1.9	1.2	0.7	0.1
950.	-3.0	-0.5	2.2	3.8	3.8	3.0	2.0	1.2	0.5	0.2	-0.2
1000.	-3.1	-1.4	0.7	2.3	2.7	2.5	2.0	1.4	1.0	0.6	0.2

TABLE A2. AS IN A1, FOR APRIL.

LATITUDE (N)=	20	25	30	35	40	45	50	55	60	65	70
PRESSURE (MB)											
0.10	-5.0	-5.0	1.0	3.0	4.0	5.0	6.0	7.0	9.0	0.0	-9.0
0.20	-6.0	1.0	6.0	7.0	8.0	8.0	9.0	10.0	10.0	-5.0	-9.0
0.50	6.0	7.0	12.0	15.0	16.0	15.0	16.0	17.0	15.0	-5.0	-9.0
1.00	2.0	4.0	12.0	17.0	19.0	17.0	15.0	13.0	10.0	-5.0	-9.0
2.00	-6.0	0.0	10.0	20.0	21.0	17.0	14.0	12.0	7.0	-5.0	-9.0
5.00	-6.0	1.0	10.0	20.0	20.0	14.0	8.0	4.0	-1.0	-6.0	-10.0
10.00	-3.0	1.0	7.0	12.0	13.0	8.0	3.0	-1.0	-4.0	-7.0	-11.0
2.		5.3		7.0		5.5		1.9		-1.0	
5.		3.9		9.1		3.0		-3.7		-7.2	
10.		7.7		7.2		0.6		-7.0		-8.1	
100.		15.7		17.4		13.0		8.4		6.1	
10.	-4.3	1.3	5.0	6.8	7.5	6.8	5.2	3.9	3.4	3.1	2.9
30.	-3.9	-1.8	-0.1	1.4	2.7	3.7	4.7	5.6	6.2	6.6	6.5
50.	-0.9	0.7	2.3	3.8	5.0	6.1	7.0	7.7	8.2	8.4	8.0
100.	14.8	17.7	18.7	17.6	15.7	13.8	12.2	11.2	10.7	10.1	9.0
150.	22.9	27.6	28.5	25.3	21.4	18.4	15.3	12.7	11.1	9.6	7.8
200.	23.8	28.9	30.4	28.1	24.5	21.0	17.2	13.9	12.0	10.6	8.8
50.	-1.9	0.9	3.4	5.0	5.8	6.7	5.9	5.5	4.8	4.7	4.4
100.	10.9	16.3	19.0	17.9	14.6	11.6	9.4	7.9	7.1	6.6	5.7
200.	22.9	29.1	31.1	27.9	22.5	17.8	14.3	11.3	9.5	8.3	6.6
300.	17.1	22.1	23.5	22.5	20.2	17.4	14.4	11.5	9.9	9.0	7.2
400.	10.6	15.2	17.3	17.5	16.2	14.3	12.2	10.0	8.6	7.9	6.6
500.	7.0	11.3	13.3	13.7	13.0	11.7	10.2	8.4	7.1	6.3	5.1
700.	1.8	5.2	6.9	7.6	7.3	6.8	6.2	5.1	4.2	3.5	2.6
850.	-1.2	1.1	2.5	3.6	4.1	3.8	3.4	2.7	2.1	1.8	1.2
900.	-2.4	-0.4	1.3	3.0	3.7	3.4	2.7	1.8	1.1	0.9	0.5
950.	-2.7	-1.3	0.4	2.3	3.1	2.8	2.1	1.1	0.4	0.3	0.0
1000.	-3.1	-2.1	-0.4	1.4	2.1	2.0	1.3	0.7	0.3	0.1	-0.3

TABLE A3. AS IN A1. FOR JULY.

LATITUDE (N) =	20	25	30	35	40	45	50	55	60	65	70
PRESSURE (MB)											
0.10	-20.0	-30.0	-38.0	-38.0	-38.0	-38.0	-37.0	-37.0	-38.0	-40.0	-40.0
0.20	-22.0	-30.0	-52.0	-62.0	-61.0	-60.0	-60.0	-61.0	-50.0	-45.0	-35.0
0.50	-37.0	-44.0	-52.0	-54.0	-48.0	-48.0	-52.0	-50.0	-37.0	-32.0	-27.0
1.00	-52.0	-50.0	-48.0	-46.0	-44.0	-42.0	-40.0	-38.0	-30.0	-26.0	-23.0
2.00	-47.0	-43.0	-40.0	-37.0	-35.0	-33.0	-31.0	-28.0	-22.0	-19.0	-17.0
5.00	-36.0	-30.0	-27.0	-24.0	-22.0	-21.0	-19.0	-18.0	-17.0	-15.0	-13.0
10.00	-30.0	-27.0	-24.0	-20.0	-18.0	-17.0	-16.0	-14.0	-13.0	-11.0	-9.0
2.		-44.2		-31.7		-26.6		-20.5		-15.3	
5.		-27.7		-23.2		-18.4		-16.5		-15.0	
10.		-21.3		-16.2		-15.1		-13.8		-9.3	
100.		-4.1		5.1		8.2		3.0		2.3	
10.	-32.5	-24.9	-20.0	-17.0	-14.9	-13.3	-12.0	-10.9	-9.9	-9.0	-7.7
30.	-26.4	-20.5	-15.5	-11.9	-9.4	-7.7	-6.7	-6.2	-5.9	-5.4	-4.7
50.	-23.3	-16.9	-11.7	-7.9	-5.1	-3.3	-2.4	-2.3	-2.5	-2.6	-2.4
100.	-10.7	-7.1	-1.8	3.9	8.1	9.3	7.8	5.3	3.3	2.1	1.5
150.	-5.5	-3.3	3.0	11.4	17.8	18.4	14.2	8.9	5.4	3.6	3.1
200.	-2.3	-0.7	4.8	13.2	20.4	21.6	17.0	11.2	7.5	5.9	5.4
50.	-17.0	-14.8	-11.4	-7.6	-4.0	-0.6	-0.5	-0.2	-1.2	-1.3	-1.2
100.	-13.4	-9.7	-5.8	3.1	8.0	8.6	6.9	4.0	2.1	1.3	1.4
200.	-4.2	-1.9	3.5	12.7	20.0	20.0	15.7	9.7	6.0	5.0	5.0
300.	-3.2	-1.6	3.2	10.8	16.4	16.6	13.1	8.9	6.2	5.7	6.1
400.	-3.1	-1.7	2.1	7.8	12.1	12.7	10.5	7.1	4.8	4.4	5.0
500.	-3.5	-1.8	1.6	5.9	9.2	10.0	8.4	5.8	3.8	3.4	3.8
700.	-1.5	-0.9	0.8	3.0	4.6	5.6	5.3	3.6	2.1	1.8	2.2
850.	-1.9	-1.6	-0.4	1.2	2.4	3.2	3.2	2.1	1.0	0.8	1.1
900.	-2.1	-2.0	-0.8	0.9	2.2	2.9	2.8	1.8	0.8	0.5	0.6
950.	-2.2	-2.1	-1.0	0.7	1.8	2.3	2.2	1.3	0.6	0.3	0.3
1000.	-2.6	-2.1	-1.0	0.2	1.0	1.5	1.4	1.0	0.4	0.1	-0.1

TABLE A4. AS IN A1, FOR OCTOBER.

LATITUDE (N) =	20	25	30	35	40	45	50	55	60	65	70
PRESSURE (MB)											
0.10	15.0	25.0	40.0	47.0	60.0	65.0	63.0	60.0	25.0	5.0	0.0
0.20	20.0	30.0	43.0	50.0	60.0	67.0	67.0	63.0	43.0	10.0	5.0
0.50	30.0	37.0	43.0	47.0	53.0	53.0	54.0	55.0	52.0	27.0	17.0
1.00	22.0	32.0	34.0	36.0	44.0	44.0	44.0	46.0	46.0	28.0	30.0
2.00	13.0	23.0	25.0	28.0	34.0	34.0	34.0	36.0	38.0	26.0	18.0
5.00	0.0	11.0	15.0	20.0	24.0	24.0	22.0	21.0	27.0	23.0	16.0
10.00	-7.0	-1.0	4.0	8.0	11.0	13.0	16.0	18.0	20.0	20.0	13.0
2.		24.6		25.6		29.1		30.9		28.8	
5.		6.8		11.0		18.4		21.7		23.1	
10.		1.6		6.2		10.8		14.9		17.4	
100.		11.2		15.8		14.8		12.0		10.5	
10.	-8.9	-1.7	3.7	7.5	10.5	13.3	16.0	18.5	20.6	21.6	21.0
30.	-8.8	-4.2	0.0	3.5	6.4	8.9	10.8	12.2	13.5	14.3	14.0
50.	-7.0	-2.7	1.4	4.9	7.8	9.9	11.2	11.8	12.3	12.5	11.9
100.	3.3	7.7	12.3	15.9	17.8	17.7	16.2	14.4	13.0	11.8	10.6
150.	8.2	13.2	18.9	23.4	25.0	23.7	20.3	16.5	13.6	11.7	10.4
200.	9.0	14.5	20.4	24.8	26.9	25.9	22.1	17.9	14.5	12.2	10.8
50.	-6.3	-3.4	0.5	4.1	6.7	8.7	8.9	9.9	10.3	10.3	9.9
100.	0.3	5.3	10.3	13.6	14.8	14.3	13.4	11.9	10.4	9.3	8.2
200.	7.5	13.8	19.5	22.1	22.1	20.6	18.6	15.3	12.0	9.5	7.9
300.	5.0	10.6	15.4	17.9	18.6	18.8	17.6	14.7	11.5	9.3	8.0
400.	2.2	7.0	11.1	13.5	14.8	15.7	15.3	12.9	10.0	8.1	6.9
500.	0.3	4.2	7.6	9.9	11.7	13.1	13.1	11.1	8.4	6.6	5.4
700.	-2.0	0.4	2.8	4.8	6.5	8.1	8.8	7.6	5.6	3.9	2.7
850.	-3.3	-1.9	-0.3	1.6	3.4	4.8	5.6	5.0	3.6	2.3	1.5
900.	-3.6	-2.4	-1.2	0.9	2.8	4.1	4.6	4.0	2.7	1.5	0.6
950.	-3.3	-2.7	-1.3	0.6	2.1	3.2	3.7	3.1	1.9	0.9	0.1
1000.	-2.8	-2.2	-0.9	0.5	1.3	2.1	2.3	2.0	1.1	0.6	0.0

TABLE A5. TEMPERATURE DATA (°K) FOR JANUARY. SOURCES: 50-1000MB, #1, 10-200MB, #2, 2-10MB, #3, .09-11.56MB, #4. SEE SECTION IV-3 FOR A DESCRIPTION OF THE DATA SOURCES.

LATITUDE(N)=	20	25	30	35	40	45	50	55	60	65	70
PRESSURE (MB)											
0.09	231.		229.		232.		236.		238.		237.
0.20	243.		242.		243.		244.		246.		249.
0.45	262.		259.		260.		256.		251.		250.
1.02	270.		266.		263.		254.		244.		238.
2.28	260.		260.		254.		241.		228.		226.
5.14	245.		244.		240.		228.		221.		216.
11.56	231.		230.		226.		220.		214.		208.
2.		259.6		254.7		248.8		245.6		247.0	
5.		241.4		239.1		236.2		232.4		227.7	
10.		231.1		229.3		225.5		220.1		214.2	
100.		203.7		210.7		216.5		217.4		213.9	
10.	230.1	229.5	228.3	227.0	225.9	224.4	222.8	220.9	218.6	215.8	213.0
30.	217.2	217.1	217.0	217.2	217.7	218.0	217.7	216.5	214.5	211.9	208.8
50.	209.2	209.9	211.1	213.0	215.1	216.7	217.4	216.9	214.5	212.2	209.1
100.	197.9	201.0	205.3	210.2	214.4	217.1	218.3	218.1	216.6	214.4	212.1
150.	209.2	210.5	212.6	215.0	217.2	218.8	219.4	218.9	217.8	216.2	214.6
200.	217.9	217.5	217.3	217.1	217.2	217.8	218.1	217.7	216.8	215.7	214.8
50.	207.0	208.8	211.2	213.6	215.7	217.4	217.8	217.3	216.0	214.5	213.1
100.	199.1	202.4	206.9	211.6	215.5	217.7	218.4	217.7	216.3	214.4	212.6
200.	219.0	218.8	218.1	217.1	216.6	216.6	216.6	215.9	215.2	214.0	213.1
300.	239.3	236.9	233.1	228.6	224.9	223.0	221.2	220.1	218.9	218.2	217.4
400.	253.9	250.8	246.5	241.7	237.7	234.8	232.6	230.8	229.5	228.1	226.7
500.	265.0	261.8	257.7	253.2	249.0	245.8	243.3	241.3	239.6	238.0	236.3
700.	280.2	276.8	273.0	268.8	264.5	260.9	258.1	255.9	253.9	252.1	250.3
850.	287.0	283.7	280.0	275.9	271.5	267.5	264.2	261.5	259.2	256.8	254.7
900.	289.5	286.0	282.2	278.2	273.9	269.3	265.4	262.7	259.9	256.8	254.0
950.	292.1	288.6	285.0	281.0	276.2	271.3	267.1	264.0	260.6	256.6	253.2
1000.	294.8	291.4	287.9	283.7	278.6	273.4	269.4	266.1	261.5	256.4	252.0

TABLE A6. AS IN A5, FOR APRIL.

LATITUDE (°)=	20	25	30	35	40	45	50	55	60	65	70
PRESSURE (MB)											
0.09	225.		227.		229.		232.		232.		231.
0.20	240.		240.		241.		245.		246.		245.
0.45	263.		262.		262.		263.		262.		263.
1.02	272.		271.		273.		272.		272.		270.
2.28	262.		262.		262.		260.		257.		254.
5.14	250.		249.		247.		244.		242.		240.
11.56	237.		236.		233.		231.		229.		229.
2.		266.6		266.5		265.4		263.2		260.0	
5.		247.5		247.1		246.1		244.6		242.9	
10.		233.6		231.5		229.6		229.2		230.3	
100.		202.5		209.2		214.8		219.2		223.0	
10.	234.0	233.9	233.0	231.9	230.7	229.2	228.2	228.0	228.3	228.9	229.7
30.	218.9	219.1	219.1	219.0	219.0	219.2	219.7	220.3	221.2	222.2	223.2
50.	210.3	211.4	212.6	214.2	215.9	217.5	218.9	220.0	221.0	222.0	222.6
100.	198.3	202.0	206.1	210.2	213.8	216.6	218.7	220.0	221.0	221.7	222.1
150.	207.3	209.1	211.2	213.6	216.0	218.3	220.0	221.1	221.7	221.5	222.4
200.	217.2	216.6	215.9	215.4	216.0	217.2	218.5	219.7	220.5	221.0	221.2
50.	208.3	209.8	211.9	214.0	216.0	218.0	219.5	220.8	221.9	223.2	224.4
100.	199.2	203.1	207.2	211.2	214.8	217.7	219.8	221.2	222.4	223.2	224.1
200.	219.0	218.2	216.8	215.6	215.8	217.1	218.8	219.9	221.2	221.8	222.6
300.	239.2	236.8	233.8	230.5	226.0	226.2	224.6	223.6	222.5	222.2	221.8
400.	254.1	251.9	249.0	245.6	242.2	239.5	237.2	235.0	233.1	231.3	229.8
500.	265.4	263.4	260.8	257.5	254.0	251.0	248.3	245.9	243.7	241.5	239.5
700.	281.8	279.9	277.2	273.7	270.2	266.8	263.7	261.0	258.5	256.1	253.9
850.	290.5	288.1	284.9	281.4	277.9	274.6	271.5	268.6	265.6	262.6	259.6
900.	293.1	290.3	286.6	283.2	279.9	276.7	273.8	270.9	267.6	263.9	260.2
950.	295.3	292.4	288.5	285.3	281.9	278.7	275.9	273.0	269.3	265.0	260.5
1000.	297.1	294.3	290.7	287.5	283.8	280.4	277.5	274.7	270.6	265.8	260.7

TABLE A7. AS IN A5, FOR JULY.

LATITUDE(N)=	20	25	30	35	40	45	50	55	60	65	70
PRESSURE (MB)											
0.09	218.		218.		218.		221.		226.		230.
0.20	240.		238.		239.		240.		247.		252.
0.45	262.		262.		262.		262.		265.		270.
1.02	264.		268.		272.		273.		276.		283.
2.28	260.		261.		264.		270.		272.		277.
5.14	245.		245.		247.		250.		258.		263.
11.56	235.		235.		236.		237.		240.		245.
2.		266.3		270.0		273.4		276.1		278.0	
5.		244.2		247.2		250.5		253.5		256.3	
10.		233.3		234.5		236.4		238.6		241.3	
100.		201.3		207.0		214.6		221.2		225.6	
10.	233.6	234.1	234.5	235.1	236.0	237.0	237.9	238.8	239.5	240.1	240.7
30.	220.1	220.9	221.4	222.0	222.9	224.1	225.3	226.6	228.0	229.2	230.4
50.	212.3	213.4	214.4	215.7	217.5	219.8	222.1	224.2	226.2	228.0	229.5
100.	200.0	201.5	203.3	206.0	210.1	215.0	219.2	222.3	224.6	226.4	228.0
150.	206.2	207.6	208.9	210.7	213.9	217.7	221.1	223.6	225.4	227.0	228.5
200.	219.8	220.0	220.3	220.6	220.9	221.0	221.0	221.9	223.4	225.0	226.8
50.	211.4	212.5	213.8	215.6	217.7	220.1	222.8	224.9	226.9	228.7	230.4
100.	201.8	203.2	205.0	207.7	212.0	217.2	220.9	223.6	225.6	227.3	229.1
200.	220.4	221.1	221.5	221.7	221.8	221.8	222.2	222.6	223.6	224.8	226.4
300.	242.2	242.6	242.4	241.1	238.7	235.9	233.5	232.0	230.7	230.1	229.5
400.	256.9	257.2	256.9	255.3	252.9	250.3	248.0	246.2	244.8	243.4	242.1
500.	267.5	267.8	267.6	266.3	264.3	261.9	259.7	257.9	256.5	255.1	253.8
700.	283.5	283.7	283.5	282.6	280.8	277.9	275.1	273.1	271.7	270.4	269.0
850.	292.0	292.1	291.9	290.9	288.9	286.3	283.7	281.7	280.3	279.0	277.0
900.	294.4	294.4	293.7	292.6	290.6	288.2	285.9	283.9	282.5	281.2	279.1
950.	296.7	296.2	295.2	294.0	292.1	289.5	287.2	285.5	284.2	283.0	280.8
1000.	299.4	298.8	297.6	295.8	293.2	290.5	287.9	286.5	285.3	284.2	281.7

TABLE A8. AS IN A5, FOR OCTOBER.

LATITUDE (°) =	20	25	30	35	40	45	50	55	60	65	70
PRESSURE (MB)											
0.09	221.		225.		227.		229.		232.		232.
0.20	242.		242.		242.		243.		243.		248.
0.45	258.		256.		257.		260.		256.		253.
1.02	270.		267.		268.		260.		254.		250.
2.28	262.		258.		253.		248.		242.		236.
5.14	245.		242.		239.		236.		230.		226.
11.56	232.		231.		229.		227.		223.		219.
2.		260.7		256.6		251.2		245.6		240.0	
5.		242.9		239.0		235.3		231.3		227.5	
10.		230.0		228.9		226.7		223.5		219.6	
100.		200.8		207.2		213.5		217.6		219.9	
10.	232.0	231.6	230.7	229.7	228.9	227.8	226.4	224.7	222.8	220.8	218.8
30.	218.8	219.1	219.0	218.8	218.7	218.6	218.2	217.6	216.8	215.8	214.5
50.	211.5	212.3	213.0	213.9	215.1	216.2	216.9	217.3	217.4	217.1	216.3
100.	197.9	200.0	202.8	206.7	210.6	214.0	216.6	218.3	219.4	219.8	219.7
150.	205.9	207.0	208.7	210.6	212.9	215.5	217.6	219.2	220.3	220.8	221.0
200.	218.6	218.3	217.9	217.3	216.9	217.2	217.8	218.6	219.4	219.9	220.3
50.	210.7	211.5	212.7	214.1	215.5	216.7	217.9	218.7	219.1	219.4	219.2
100.	199.9	201.7	204.4	208.0	211.8	215.2	217.4	219.1	220.2	220.7	220.7
200.	219.4	219.5	219.2	218.5	217.7	217.8	218.6	219.2	220.0	220.0	220.1
300.	241.0	240.0	238.1	234.9	231.7	229.5	227.5	225.8	223.9	222.8	221.6
400.	256.1	255.0	252.8	249.5	246.1	243.2	240.5	237.9	235.7	233.8	232.0
500.	266.9	266.1	264.2	261.2	257.9	254.8	251.7	248.9	246.5	244.5	242.5
700.	282.4	281.5	279.7	277.1	273.8	270.3	266.8	263.8	261.4	259.1	256.9
850.	291.3	289.8	287.6	284.7	281.3	277.6	274.0	270.9	268.1	265.3	262.6
900.	293.7	292.1	289.7	286.8	283.3	279.7	276.2	273.1	270.0	266.6	263.3
950.	296.3	294.6	292.3	289.4	285.8	281.9	278.5	275.4	272.0	268.0	264.2
1000.	298.7	297.1	294.9	291.8	287.9	284.0	280.7	277.7	273.9	269.7	265.3

ACKNOWLEDGEMENTS

Support for this thesis was in part from the National Aeronautics and Space administration under grants NSG 5113 and NGR 22-009-727, and in part from the United states Department of Transportation under Grant AT(11-1)-2249.

The list of those who helped and inspired me in the course of my education is indeed very long, and, for that reason, could not be comprehensive. Nevertheless, I want to thank those to whom I am most indebted.

First, my advisor Professor Peter Stone has always been a source of inspiration and encouragement. He has been very understanding in times of slow progress, and always constructive in his criticism. I also want to thank Professor Edward Lorenz for his good friendship and deep inspiration both as a scientist and a true gentleman. I acknowledge Professor Reginald Newell's guidance in the early years of my study at M.I.T.. Miss Isabelle Kole and Mr. Sam Ricci are to be thanked for their friendship and excellent work of drafting the figures. I am indebted to Ginny (Powell) Siggia for typing the text, and wish her and her husband love in their marriage which took place during the time in which she typed my thesis. I am grateful to Diana Lees Spiegel for her many kind words and competent assistance in coding and running my programs. To Professor Eugenia Rivas I give thanks for her warm friendship and helpful discussions. Revisions and extensions of the thesis were suggested by Professor Jule Charney. I am thankful for the interesting discussions I have had with my fellow students, in particular: Brett Mullan, Gary Moore, Lin Ho, Ron Errico, Minoru Tanaka, Long Chiu, and Bijoy Misra. Administrative assistance was cheerfully given by Jane McNabb and Virginia Mills. I wish to thank Susan Ary, David Nergaard, and Kathy Huber of the Department for their good friendship. And I wish many broken (meteorological) records to the weather station at Saugus Mass. in return for the countless bits of practical advice and ceaseless wit of its operator, Eddie Nelson.

My gratitude for my educational experience extends beyond the Department of Meteorology first of all to my parents, my earliest educators, James Fullmer and Antonine Fullmer. The instilled in me the importance of a good education and made that education available. To them this thesis is lovingly dedicated. My gratitude in addition extends to Sr. Patricia Margaret who also helped start me out on my academic journey, to Mr. Philip Hart who gave me excellent and inspirational instruction in mathematics, to all my mentors at St. Joseph's Prep from whom I received the priceless gift of a broad education, to Professor Leonard Cohen for his friendship and guidance at my undergraduate school, Drexel University, and to Wade Rockwood and Fr. Bob Moran for their kind and good advice.

Very special thanks go to my longest and closest friend, Ted Kuklinski. Ted has helped me in every way a good friend could. His caring and encouragement have always been there to sustain me. I have had the rare and wounderful experience of being in school with this kind and selfless man for no less than SIXTEEN years.

I also want to express my deep gratitude to the many members of the Paulist Center Community who have touched my life in a myriad of different and beautiful ways. They have supported me in rough times and shared the joy of good times. From them I have learned much about the meaning and beauty of life. Just a small fraction of these good people do I mention here: Bill Dougherty, Loretta Jordan, Mary Lou Doran, Blair, Joe, James, and Jennifer Mergel, Bob Paine, Vinny and Elaine Adams, Jim McCarthy, Elanor Morrissey, Linda Jeffrey, Jane Vincent, Nancy O'Brien, Bev Eder, Paula Ripple, Rich Zablocki, Dick and Kathy Noonan, David and Kathy Konkel, Kathie Voigt, Kathi Connors, Cathy Wright, Mary Hardigan, Janet Gawle, and especially Glen Hoffman.

Finally, I want to give my greatest thanks to God who has given me my life, my talents, and my friends, and without whom this thesis could not have been written.

References

Boyd, J.P., 1976: The noninteraction of waves with the zonally averaged flow on a spherical earth and the interrelationships of eddy fluxes of energy, heat, and momentum. J. Atmos. Sci., 33, 2285-2291.

Burger, A.P., 1962: On the non-existence of critical wavelengths in a continuous baroclinic stability problem. J. Atmos. Sci., 19, 30-38.

Cardelino, C.A., 1978: A study on the vertical propagation of planetary waves and the effects of upper boundary condition. M.S. Thesis, Department of Meteorology, M.I.T., Cambridge, Mass.

Charney, J.G., 1947: The dynamics of long waves in a baroclinic westerly current. J. Meteor., 4, 135-162.

Charney, J.G., and M.E. Stern, 1962: On the stability of internal baroclinic hets in a rotating atmosphere. J. Atmos. Sci., 19, 159-172.

Dahlquist, G., and A. Björck, 1974: Numerical Methods. Prentice-Hall, Englewood Cliffs, N.J., 573 pp.

Dickinson, R.E., 1973: Baroclinic instability of an unbounded zonal shear flow in a compressible atmosphere. J. Atmos. Sci., 30, 1520-1527.

Eady, E.T., 1949: Long waves and cyclone waves. Tellus, 1, 33-52.

Eliassen, A., and E. Palm, 1960: On the transfer of energy in stationary mountain waves. Geof. Pub., No. 3, pp. 1-23.

Gall, R., 1976: Structural changes of growing baroclinic waves. J. Atmos. Sci., 33, 374-390.

Gall, R.L., and R.J. Blakeslee, 1977: Comments on "A note on the wavelength of maximum baroclinic instability". J. Atmos. Sci., 34, 1479-1480.

Geisler, J.E., and R.R. Garcia, 1977: Baroclinic instability at long wavelengths on a beta-plane. J. Atmos. Sci., 34, 311-321.

Green, J.S.A., 1960: A problem of baroclinic instability. Quart. J. Roy. Met. Soc., 86, 237-251.

Green, J.S.A., 1970: Transfer properties of large-scale eddies and the general circulation of the atmosphere. Quart. J. Roy. Met. Soc., 96, 157-185.

Green, J.S.A., 1972: Large-scale motion in the upper stratosphere and mesosphere: an evaluation of data and theories. Phil. Trans. Roy. Soc. Lond., A 271, 577-583.

Held, I.M., 1978: The vertical scale of an unstable baroclinic wave and its importance for eddy heat flux parameterizations. J. Atmos. Sci., 35, 572-576.

Holton, J.R., 1974: Forcing of mean flows by stationary waves. J. Atmos. Sci., 31, 942-945.

Holton, J.R., 1975: The dynamic meteorology of the stratosphere and mesosphere. Meteor. Monogr., No. 47, Amer. Meteor. Soc.

Houghton, J., 1978: The stratosphere and mesosphere. Quart. J. Roy. Met. Soc., 104, 1-29.

Kuo, H.-L., 1956: Forced and free meridional circulation in the atmosphere. J. Meteor., 13, 561-568.

Leovy, C.B., and P.J. Webster, 1976: Stratospheric long waves: Comparison of thermal structure in the Northern and Southern hemispheres. J. Atmos. Sci., 33, 1624-1638.

Lindzen, R.S., E.S. Batten, and J.W. Kim, 1968: Oscillations in atmospheres with tops. Mon. Wea. Rev., 96, 133-140.

Lorenz, E.N., 1951: Computations of the balance of angular momentum and the poleward transport of heat. Report No. 6, Contract No. AF 19(122) -153 between Geophys. Res. Direct. and Mass. Inst. Tech.

Lorenz, E.N., 1967: The nature and theory of the general circulation of the atmosphere. World Meteorological Society, Geneva, 161 pp.

McIntyre, M.E., 1972: Baroclinic instability of an idealized model of the polar night jet. Quart. J. Roy. Met. Soc., 98, 165-174.

M.I.T. Information Processing Services Center. Applications Program #42. "EISPACK", 1973.

Molla, A.J., and C.J. Loisel, 1962: On the hemispheric correlations of vertical and meridional wind components. Geofis. pura e appl., 51, 166.

Morel, P. (ed.), 1973: Dynamic Meteorology. D. Reidel, Boston, 622 pp.

Moura, A.D., and P.H. Stone, 1976: The effects of spherical geometry on baroclinic instability. J. Atmos. Sci., 33, 602-616.

Murgatroyd, R.J., 1969: The structure and dynamics of the stratosphere. The Global Circulation of the Atmosphere, G.A. Corby, Ed. London Roy. Meteor. Soc., 159-195.

Murray, F.W., 1960: Dynamic stability in the stratosphere. J. Geophys. Res., 65, 3273-3305.

Newell, R.E., 1964a: The circulation of the upper atmosphere. Scientific American, 210, No. 3, 62-74.

Newell, R.E., 1964b: Further ozone transport calculations and the spring maximum in ozone amount. Pure Appl. Geophys., 59, 191-206.

Newell, R.E., and W.R. Tahnk, Energetics and dynamics of the stratosphere. (Unpublished manuscript) 1976.

Newell, R.E., D.G. Vincent, T.G. Dopplick, D. Ferruzza, and J.W. Kidson, 1969: The energy balance of the global atmosphere. The Global Circulation of the Atmosphere, G.A. Corby, Ed. London Roy. Meteor. Soc., 42-90.

Newell, R.E., G.F. Herman, J.W. Fullmer, W.R. Tahnk, and M. Tanaka, 1974: Diagnostic studies of the general circulation of the stratosphere. Proc. Int'l Conf. on structure, composition, and general circulation of the upper and lower atmospheres and possible anthropogenic perturbations; held in Melbourne, Australia, January, 1974. Office of the Secretary, IAMAP, Atmospheric Environment Service, Canada. Vol. 1, pp. 17-82.

Oort, A., 1971: The observed annual cycle in the meridional transport of atmospheric energy. J. Atmos. Sci., 28, 325-339.

Oort, A.H., and E.M. Rasmusson, 1971: Atmospheric Circulation Statistics, Prof. Paper No. 5, N.O.A.A., U.S. Department of Commerce, Rockville, Maryland. 323 pp.

Palmén, E., and C.W. Newton, 1969: Atmospheric Circulation Systems. New York, Academic Press, 603 pp.

Pedlosky, J., 1964: The stability of currents in the atmosphere and the ocean. Part I. J. Atmos. Sci., 21, 201-219.

Peng, L., 1965a: A simple numerical experiment concerning the general circulation in the lower stratosphere. Pure Appl. Geophys., 61, 197-218.

Peng, L., 1965b: Numerical experiments on planetary meridional temperature gradients contrary to radiational forcing. Pure Appl. Geophys., 62, 173-190.

Phillips, N.A., 1954: Energy transformations and meridional circulations associated with simple baroclinic waves in a two-level, quasi-geostrophic model. Tellus, 6, 273-286.

Simmons, A.J., 1972: Baroclinic instability and planetary waves in the polar stratosphere. Ph.D. Thesis, University of Cambridge, England.

Simmons, A.J., 1974: Planetary scale disturbances in the polar winter stratosphere. Quart. J. Roy. Met. Soc., 100, 76-108.

Staley, D.O., and R.L. Gall, 1977: On the wavelength of maximum baroclinic instability. J. Atmos. Sci., 34, 1679-1688.

Stone, P.H., 1972: A simplified radiative-dynamical model for the static stability of rotating atmospheres. J. Atmos. Sci., 29, 405-418.

Stone, P.H., 1978: Baroclinic adjustment. J. Atmos. Sci., 35, 561-571.

Tahnk, W.R., and R.E. Newell, 1975: Climatology and energy budget of the Northern Hemisphere Middle Stratosphere during 1972. Geofisica Internacional, 15(3), 205-292, Mexico.

U.S. Committee on Extension to the Standard Atmosphere (COESA), U.S. Standard Atmosphere, 1962, prepared under sponsorship of N.A.S.A., U.S. Air Force, and U.S. Weather Bureau and printed by U.S. Government Printing Office, Washington, D.C., Dec. 1972, 278 pp.

Vincent, D.G., 1968: Mean meridional circulation in the Northern Hemisphere during 1964 and 1965. Quart. J. Roy. Met. Soc., 94, 333-349.

Wallace, J.M., 1978: Trajectory slopes, countergradient heat fluxes, and mixing by lower stratospheric waves. J. Atmos. Sci., 35, 554-558.

Andrews, D.G., and McIntyre, M.E., 1976: Planetary waves in horizontal and vertical shear; the generalized Eliassen-Palm relation and the mean zonal acceleration. J. Atmos. Sci., 33, 2031-2048.

Charney, J.G., 1959: On the theory of the general circulation of the atmosphere. The atmosphere and the sea in motion. B. Bolin, Ed., New York, Rockefeller Inst. Press, pp. 178-193.

Charney, J.G., and P.G. Drazin, 1961: Propagation of planetary scale disturbances from the lower into the upper atmosphere. J. Geophys. Res., 66, 83-109.

Charney, J.G., and J. Pedlosky, 1963: On the trapping of unstable planetary waves in the atmosphere. J. Geophys. Res., 68, 6441-6442.

Klein, W.D., 1974: Ozone kinematics and transports in unstable waves. Ph.D. thesis, Department of Meteorology, MIT, Cambridge, Mass.

Pedlosky, J., 1970: Finite-amplitude baroclinic waves. J. Atmos. Sci., 27, 15-30.

Pedlosky, J., 1971: Finite-amplitude baroclinic waves with small dissipation. J. Atmos. Sci., 28, 587-597.